CONTROLLING PROTEIN PERMEABILITY IN HYDROGELS FOR DRUG DELIVERY APPLICATIONS

By

Erik Van Kampen

Submitted to the graduate degree program in Chemical & Petroleum Engineering and the Graduate Faculty of the University of Kansas School of Engineering in partial fulfillment of the requirements for the degree of Doctor of Philosophy

Committee members

Dr. Stevin Gehrke,
Committee Chair

Dr. Cory Berkland

Dr. Michael Detamore

Dr. Prajna Dhar

Dr. David Volkin

Date Defended

Acceptance Page

The dissertation Committee for Erik Van Kampen certifies that this is the approved version of the following dissertation:

CONTROLLING PROTEIN PERMEABILITY IN HYDROGELS FOR DRUG DELIVERY APPLICATIONS

Committee members

_____
Dr. Stevin Gehrke,
Committee Chair

_____
Dr. Cory Berkland

_____
Dr. Michael Detamore

_____
Dr. Prajna Dhar

_____
Dr. David Volkin

_____
Date Defended

ABSTRACT

Extending the release of therapeutic proteins is an area of study that has received a lot of attention of late due to the increasing use of antibodies in treating cancer, autoimmune diseases, viral infections, and even asthma. In many cases, long-term, local delivery systems are preferred over parenteral routes in order to reduce systemic exposure and avoid frequent injections. Hydrogels offer a promising potential for many drug delivery applications because they can be formed into a variety of shapes and sizes using biocompatible materials, while at the same time exhibiting a wide range of permeabilities. However, one of the challenges of developing an effective hydrogel delivery device is in controlling the diffusion of proteins within the hydrogel in order to provide the correct release rate and profile. The objective of this dissertation, therefore, was to investigate the permeability of therapeutic proteins in hydrogels to aid the development of long-term drug delivery vehicles. The work presented in this dissertation includes the study of protein partitioning in hydrogels, the development and modeling of a prototype release system, and the advancement of a hydrogel crosslinking method in an effort to expand the use of hydrogels for extended release applications.

One particular area in which a long-term delivery system is needed is ocular drug delivery, where retinal diseases such as age related macular degeneration and diabetic macular edema require frequent injections into the vitreous in order to deliver drugs to the retina and prevent major vision loss. These diseases affect an estimated 16 million Americans and are the leading cause of blindness and vision loss in people over the age of 50. A hydrogel implant that could deliver sustained release to the retina would offer a number of advantages including convenience, safety, and financial benefits when compared to the current intravitreal dosing regimen.

One of the difficulties in developing a hydrogel delivery device is achieving a significant protein concentration within the hydrogel. A method for loading proteins into monolithic hydrogels using the thermodynamic principles of aqueous two-phase extraction was investigated. By using a

variety of polymers and partitioning salts, significant increases were seen in the partitioning of ovalbumin and IgG in PEG and dextran hydrogels. The results demonstrate the versatility of a method to overcome size exclusion of proteins, even as large as monoclonal antibodies, into many types of hydrogels, thus opening the door to new delivery strategies for therapeutic proteins using hydrogels.

A successful hydrogel delivery device must be small enough to be implanted in the eye, yet carry a large enough drug load to achieve long-term release. Therefore, hollow mini cylinders were chosen as the structure for the intravitreal implants instead of a monolithic device. Achieving these goals requires a hydrogel with a very low diffusion coefficient (values below 10^{-10} cm^2/s), an area of study that has received little attention in the literature yet has major implications in situations where long term, local delivery systems are needed to deliver therapeutic proteins such as ocular delivery. The swelling degrees required to achieve this target diffusion coefficient in a hydrogel were predicted using a free volume theory for protein diffusion in hydrogels, and were estimated to be in the range of 4-6 (g/g). In order to achieve such low swelling degrees, the cylinders were made from HA hydrogels that were highly crosslinked using a base-catalyzed Michael addition and the difunctional crosslinker divinyl sulfone (DVS). HA-DVS hydrogels with swelling degrees as low as 2.7 were achieved using HA concentrations that ranged from 15-30% (w/w) and HA:DVS ratios that ranged from 3:1–1:1. Using a custom mold, prototype cylinders were developed and proved capable of successfully releasing an antigen-binding fragment (Fab) for over 4 months *in vitro* with a maximum release rate of 4 micrograms a day. The results showed that a hollow cylinder made from hydrogels can achieve 3-6 months release of anti-vascular endothelial growth factors to the retina.

In an effort to determine the target diffusion coefficients and cylinder dimensions required for ocular delivery the release of proteins from hollow cylinders was modeled using the physics software COMSOL. The largest size cylinders that were studied (1mm outer diameter) were able to load the largest amount of drug and provide the longest release. These cylinders were capable of

delivering over 1 mg of drug while achieving a release rate of 2.5 micrograms a day for over 4.5 months. Moving to smaller cylinders makes the insertion process faster, safer, and less painful, yet it comes at the expense of smaller drug loading and shorter release times. The results indicated that the small dimensions required for an intravitreal implant leads to a narrow range of diffusion coefficients (1-3 x 10^{-11} cm^2/s) that are capable of producing an effective delivery device, highlighting the importance of being able to tune the diffusion coefficient of hydrogels.

Being able to control the network structure and the diffusion coefficient of a hydrogel was the main motivation for modifying HA with pentenoic anhydride and crosslinking it into hydrogels using the dithiol crosslinker dithiothreitol via a photoinitiated thiol-ene reaction. This crosslinking reaction is hypothesized to allow for greater control of the hydrogel network structure, while at the same time providing a way to quickly and efficiently tune the mechanical properties of the hydrogel. Evidence of a more uniform network included gelation at lower polymer concentrations and higher fracture strains (>85%) when compared with hydrogels crosslinked via the chain polymerization of methacrylated HA. The hydrogel network can also be controlled simply by varying the ratio of thiols:ene, which can increase the crosslinking and reduce the swelling degree. Additionally, in most cases the photoinitiated reaction was completed after only 60 seconds of irradiation with UV light using initiator concentrations of only 0.1 mM, indicating a more efficient crosslinking reaction when compared to HA-DVS and methacrylated HA. The reaction can also occur under physiological conditions, a necessary requirement for the encapsulation of cells and proteins.

ACKNOWLEDGEMENTS

I gratefully acknowledge the funding from the Madison and Lila Self Graduate Fellowship, which allowed me to pursue and explore certain areas in my research that I felt most passionate amount. I would also like to acknowledge my committee members Drs. Stevin Gehrke, Cory Berkland, Michael Detamore, Prajnaparamita Dhar, and David Volkin for their valuable support and guidance in my research project and throughout my years as a graduate student. I would also like to thank all those who have assisted me throughout this research project: Dr. Amir Fakhari and Dr. Jian Qian for all of their help in developing and testing hollow cylinders, Dr. Russ Middaugh for the valuable advice and the use of lab equipment, Dr. David Moore and Heather Shinogle for helping with all of the confocal microscopy experiments, Devany West and Bradley Harris for their help in acquiring data on thiol-ene hydrogels, and Craig Vandevelden for his indispensable help with COMSOL.

I would also like to thank the other members of Dr. Gehrke's lab: Tiffany Suekama, Tricia Sprouse, Anahita Khanlari, and Linda Steele who not only pushed me and challenged me as a scientist but also provided support and encouragement along the way. To my good friends and fellow scientists of Burt Hall: Travis Wentworth, Luke Silvey, and Griffin Roberts, thank you for your friendship, encouragement, and advice throughout the ups and downs of graduate life. I want to also thank the directors, staff, and other graduate students in the Self Graduate Fellowship, thank you for inspiring me and teaching me to be not only a better scientist but a better leader, communicator, and person.

I want to also thank the many people outside of the scientific community at KU who helped make Lawrence feel like home. Thank you to Chad Donohoe, Ryan Mayo, Tyler Clements, Bill Vogler and the community at Grace EPC for supporting me and treating me like

family. For my roommates and good friends John Intfen, Collin Edwards, Aaron Boehmler, Garrett Neiss, and Charles Neiss, thank you for all of your help and support and for putting up with the late nights and my general "nerdiness". I couldn't have done it without your friendship and support.

I want to especially thank my advisor and mentor, Dr. Stevin Gehrke. Thank you for your constant guidance and support, and for taking me in and showing me how to become a scientist. Thank you for providing such a wonderful example of what it means to be passionate about research, teaching, and those you work with. Thank you especially for having the patience and willingness to work with me even as I got married and moved to Chicago. I deeply admire you not only as a professor, but also as a person and friend, and you will always be my mentor.

Finally, I would like to give a special thanks to my wife, Laura, for her love and support throughout this long journey. You inspire me every day to be a better scientist and husband. Thank you to my parents, Steve and Pam, my siblings, my grandparents, and my in-laws, for their constant encouragement, love, and support through my journey from Chicago to Kansas and back to Chicago. Finally, thanks most of all to my faithful Savior, Jesus Christ. I hope that as I continue this scientific journey I will always live by the words of Colossians 3:23, "Whatever you do, work at it with all your heart, as working for the Lord".

TABLE OF CONTENTS

Chapter 1: Introduction

The primary objective of this dissertation was to investigate the permeability of therapeutic proteins in hydrogels to aid the development of effective long-term drug delivery devices. Hydrogels have long been used as drug delivery vehicles as they can be designed to exhibit a wide range of permeabilities using a number of biocompatible materials and crosslinking methods. In these drug delivery systems, controlling the diffusion of proteins within a hydrogel is crucial for providing the correct release rate and profile required to be therapeutically effective. Because of its importance, the diffusion of solutes in hydrogels is a subject that has been well-studied in the literature and has led to an increased understanding of how the diffusion coefficient is affected by key parameters of a hydrogel and solute size. However, one area that has received little attention in the literature is when the diffusion coefficient in hydrogels is very small (100 times lower than in solution), which occurs as the polymer volume fraction of the gel increases, or as the size of the solute increases. Despite the limited amount of work in literature, the diffusion of solutes in hydrogels with low diffusion coefficients is an important area of study that has major implications in situations where long term, local delivery systems are needed to deliver these therapeutic proteins.

One of the motivations for this work was a specific area in which the long term, local delivery of therapeutic proteins is required: ocular drug delivery. Specifically, the need to deliver high molecular weight drugs to the vitreous humor to treat retinal diseases such as age related macular degeneration and diabetic macular edema, two of the leading causes of blindness and vision loss in the elderly. While recent treatments have allowed patients to successfully manage the symptoms and vision loss of retinal diseases, these treatments consist of intravitreal injections that are administered to the patient every 4-8 weeks. A hydrogel implant that could

offer long term, sustained delivery would offer a number of advantages when compared to the current intravitreal dosing regimen. The difficulty in developing a successful ocular implant is that the device must be small enough to be implanted in the eye, yet carry a large enough drug load to achieve long-term release at the desired level. Accomplishing this requires a highly crosslinked hydrogel that has a low swelling degree in order to produce the diffusion coefficients required to achieve extended release.

Therefore, the work presented in this thesis addresses two major aims: 1) to develop a better understanding of the partitioning and diffusion of solutes in hydrogels with low diffusion coefficients and 2) to examine the feasibility of developing a hydrogel delivery device that can be implanted in the vitreous and is capable of delivering therapeutic proteins for 3-6 months. The two aims are closely related and are explored together throughout many of the chapters in this dissertation.

Chapter 2 contains the essential background material on hydrogels, which introduces the reader to the key concepts and terminology that will be used throughout this dissertation. The chapter begins with a brief description of the materials that are used to form hydrogels, including both biological polymers such as hyaluronic acid which is used in Chapters 5 and 7, as well as the synthetic polymer poly(ethylene glycol) which is used in Chapter 4. The chapter continues with a concise description of the synthesis methods that are used throughout this dissertation to form hydrogels: the copolymerization/crosslinking of monomers, and the crosslinking of linear polymers. Next, a description of the characterization methods that were used to define the network structures of the hydrogels in this dissertation is presented. This section includes an overview of the swelling theory, mechanical properties, and mesh size of hydrogels as well as the partition coefficient. The chapter concludes with a brief review of the use of hydrogels as

drug delivery vehicles and the different mechanisms that are often used to control the release rate of drugs in a variety of biomedical applications.

Chapter 3 continues with an in depth review of the current state of the art on the diffusion of solutes in hydrogels, an important area of study that is directly relevant to a number of research fields, including drug delivery, tissue engineering, and separation processes. The first goal of the chapter is to introduce the reader to the theoretical models that have been developed that attempt to relate the diffusion coefficient to the key parameters of a hydrogel. The models are separated into three separate categories that each uses a different phenomenon to describe the hindered diffusion of solutes through hydrogels:

1) Free volume theories that suggest the solutes only diffuse by jumping into the voids, or free volume, within the solvent.

2) Obstruction models that suggest diffusion is restricted due to the polymer chains acting as physical obstructions that increase the length the drug has to travel.

3) Hydrodynamic models which suggest that both the solvent and the polymer chains within the hydrogel increases the hydrodynamic drag on the molecule and slows the diffusion.

While these three models use different approaches for modeling the diffusion of solutes through hydrogels, they all depend primarily on water content and solute size, which leads to similar predictions for hydrogels with high water contents. Where the models differ, however, is in the ways in which the network structure is represented using various parameters. Therefore, the second goal of the chapter is to examine how well these models perform under conditions where the diffusion coefficient in hydrogels is projected to be very small, where the effect of network structure increases. Throughout this dissertation, a central theme is being able to control

and predict the diffusion of large solutes in hydrogels with low swelling degrees. Developing models for hydrogels that accurately describe the diffusion in this region is important not only for making predictions, but also in developing an understanding of how the key parameters such as swelling degree, solute size, and the various parameters that represent the hydrogel network structure play a role in diffusion.

Chapter 4 is the first chapter in this dissertation in which hydrogels are examined for their use as a drug delivery system. The chapter builds on previous work that was performed by Gehrke's research group in which a method for loading proteins into hydrogels was developed using the thermodynamic principles of aqueous two-phase extraction (ATPE) to overcome size exclusion. They developed the method and showed that proteins such as ovalbumin, bovine serum albumin (BSA), and α-amylase could be loaded into dextran hydrogels at significantly higher concentrations when compared with normal equilibration techniques with the addition of poly(ethylene glycol) and salts to the loading solution. It had been hypothesized to be thermodynamically general, but this had not been demonstrated. Therefore, the main goal of Chapter 4 was to test the hypothesis that the thermodynamic principles of this method could be generalized to any type of hydrogel and loading system, including proteins as large as monoclonal antibodies. The results showed that multiple hydrogels and loading systems follow the ATPE heuristics, including both polymer/polymer systems and polymer/salt systems. Additionally, substantial increases in the partitioning of IgG in dextran hydrogels with the addition of PEG in the loading solution were observed, while IgG was completely excluded from the gel in buffer alone. The results provide a much needed and useful way to load antibodies into hydrogels and enables loading systems and drugs that have been successfully demonstrated in literature to be quickly extended to hydrogel drug delivery devices.

While Chapter 4 focuses on the general question of how to increase the partitioning of proteins into preformed gels, Chapter 5 examines a more specific problem and investigates the use of hyaluronic acid (HA) hydrogels for the sustained release of therapeutic proteins to the eye. Hyaluronic acid is natural component of the eye, and a HA hydrogel delivery system would make an excellent device that could be implanted in the eye for long periods of time, where low toxicity is necessary for success. The goal for the chapter was to develop an actual prototype implant that is capable of delivering proteins of similar size to the treatments currently on the market proteins for 3-6 months release at rates that would be therapeutically effective if the device were to be injected or surgically implanted in the back of the eye. Achieving this goal required first investigating whether or not an implantable device of this size and shape (hollow cylinder) could be fabricated using HA hydrogels as well as determining if these hydrogels could be made with a swelling degree low enough to produce the diffusion coefficients required to achieve extended release. HA-DVS hydrogels were made using HA concentrations that ranged from 15-30% (w/w) and HA:DVS ratios that ranged from 3:1–1:1. Using a custom mold, prototype cylinders were developed and loaded with both bovine serum albumin (BSA) and an antigen-binding fragment (Fab). The results showed that a hollow cylinder made from hydrogels can achieve 3-6 months release of anti-vascular endothelial growth factors to the retina.

Having successfully developed a prototype that was able to achieve over 3 months release, Chapter 6 directly follows up the work presented in Chapter 5 by using the physics software COMSOL to model the release of therapeutic proteins from hollow cylinders. The main goal of the chapter was to understand how the diffusion coefficient and cylinder dimensions affect the release rate and profile. The chapter focused on hydrogel implants with three different outer diameters: a 1mm implant that would have to be implanted and had similar dimensions to the

prototypes in Chapter 5, a 0.45 mm implant that could be injected using a 22-gauge microinjector, and a 0.21 mm implant that could be injected using a 27-gauge needle. By modeling the release rate and profile of each implant size, a better idea of the range of the diffusion coefficients and dimensions required for a successful hollow cylinder intravitreal implant were determined.

The results from Chapter 6 revealed that precise control over the diffusion coefficient is required. Therefore, Chapter 7 introduces an alternative way to crosslink HA hydrogels using the thiol-ene reaction, which is hypothesized to allow for greater control of the hydrogel network, an important feature that would be useful for controlling the diffusion in hydrogels while also improving the mechanical properties of the hydrogel. The chemistry of the thiol-ene reaction is also hypothesized to provide many advantages when compared to traditional crosslinking reaction such as the Michael-type addition used in Chapter 5. These advantages include higher selectivity and reactivity, an increase in reaction rate, and milder reaction conditions that will lead to benefits in both drug delivery and tissue engineering. The results showed that the crosslinking reaction occurs within seconds of irradiation, using very little initiator. The network structure of the hydrogel was shown to be easily controlled by varying the ratios of thiol:ene groups, providing a simple way to tune the crosslink density and swelling degree. The hydrogels can be synthesized using physiological conditions, which allowed for the encapsulation and release of the model proteins ovalbumin and BSA.

The final chapter summarizes the key results and presents possibilities for future work.

CHAPTER 2: AN INTRODUCTION TO HYDROGELS

2.1 INTRODUCTION

The purpose of this chapter is to introduce the reader to the key concepts and terminology that will be used throughout this dissertation. In Section 2.2, a brief description of the materials that are used to form hydrogels is given, and includes biological polymers such as hyaluronic acid and dextran, as well as the synthetic polymer poly(ethylene glycol). Section 2.3 provides a concise description of the synthesis methods that are used throughout this dissertation to form hydrogels. The chapter finishes up with a description of the characterization methods that were used to define the network structures of the hydrogels in Section 2.4. This section includes an overview of the swelling theory, mechanical properties, and mesh size of hydrogels as well as the partition coefficient. Excellent articles that contain more information on the materials, synthesis methods, mechanical properties, and uses of hydrogels in biomedical applications are available for a more detailed review.[1-5]

2.2 HYDROGEL MATERIALS

Hydrogels are hydrophilic polymer networks that are crosslinked into a permanent three-dimensional network. These networks are capable of absorbing many times their weight of water, and often contain more than 90% water by weight. They can be made from any hydrophilic polymers, both biological and synthetic, and can be formed using a variety of crosslinking methods. Hydrogels can be made into any size or shape and can even be made to respond to a number of external stimuli, including light, temperature, and pH.[6]

The large number of hydrogel materials and synthesis methods available allow for gels to be made that exhibit a wide range of swelling degrees, mechanical properties, and permeabilities. Of these properties, the most important is the water content of the gel, or the swelling degree (explained in Section 2.4.1). The swelling degree of a hydrogel has a direct influence on the other properties of the hydrogel, as changes in water content can lead to changes in the mechanical properties of the hydrogel such as moduli and crosslink density.[7] The swelling degree can also play a role in determining the rate at which a gel degrades and can influence the permeability of the hydrogel to both water and larger solutes such as proteins and antibodies.

The ability to produce a wide range of properties has led to the use of hydrogels in a number of industries and applications. Hydrogels are used as additives in the food and cosmetic industry, as superabsorbents in the hygiene and agriculture industries, and have even been used to improve oil recovery. However, due to their ability to absorb water and their potential to be biocompatible, a lot of the research in hydrogels has been in the fields of biology and medicine. In fact, some of the earliest work on hydrogels was done in the 1950's when Lim and Wichterle were investigating the use of poly(2-hydroxyethyl methacrylate) hydrogels as contact lenses.[8] Since that time, a large amount of research has been done on the preparation, structure, and properties of hydrogels for use in biomedical applications.[9] Hydrogels have been used as coatings for both pills and catheters, as wound adhesives, burn dressings, and implants. Certain hydrogels also have the ability to safely encapsulate cells, which has led to the extensive use of hydrogels in repairing and regenerating tissues and organs in the rapidly expanding field of tissue engineering.[10]

The widely adjustable properties of hydrogels make them ideal for drug delivery applications. The high water content allows for the safe encapsulation of bioactive molecules

such as proteins, carbohydrates, DNA and antibodies.[11] The loading and release of small molecules and macromolecules through the network structure can be tuned by controlling the swelling degree and crosslink density of the hydrogels.[4] They also have the advantage of being synthesized under relatively mild conditions, as the most common hydrogels are formed in water at ambient temperatures.[12] Because of these many advantages, the use of hydrogels in drug delivery systems has increased over the past few decades and hydrogels are being used as drug delivery systems in ocular, oral, nasal, buccal, rectal, vaginal, nasal and parenteral applications.

One of the key requirements of a hydrogel in drug delivery and biomedical applications is biocompatibility. While this word is often used within the field of biomaterials, there is still a degree of uncertainty as to how biocompatibility is actually defined as well as the assumptions that come along with it.[13] Early work was focused on long term implants, where the goal of the material was to have as little interaction with the cells and tissue as possible. Under these circumstances, a biocompatible material was one that was non-immunogenic, non-toxic, non-carcinogenic, non-irritant, and so on. However, the development of degradable implants along with the rise of tissue engineering presented a need to revisit the definition of biocompatibility.[13] A material could no longer be described as biocompatible by simply being bioinert, but had to take into account how the host area responded to the biodegradation process. Furthermore, in tissue engineering, the biomaterial that is used as a scaffold or matrix is often selected because it can interact with encapsulated cells via molecular or mechanical signals. Biocompatibility is therefore dependent on both the absence of undesirable local or systemic effects as well as the ability to support the desired cellular activity.[13] Hydrogels can be made to exhibit a high degree of biocompatibility, not only because of their high water content, but also because they can be

synthesized so that they have a mechanical and compositional similarity to the extracellular matrix.[1]

There are a number of materials that can be used to form hydrogels for drug delivery and biomedical applications, and these materials play a large role in determining the biocompatibility and mechanical properties of the hydrogel. They are often classified based on where the material is derived, such as biological (e.g. alginic acid, dextran, hyaluronic acid (HA)), synthetic (e.g. poly(ethylene glycol), poly(vinyl alcohol)), and even modified biological or semisynthetic (e.g. cellulose ether, methacrylated HA (MHA)) polymers.[7] Hydrogels formed from biopolymers have a number of advantages, including the inherent ability to be biocompatible and biodegradable. They can also contain biologically recognizable moieties that can participate in cell signaling and other cellular activities.[12] Biopolymers often need to be modified in order to crosslink and form hydrogels, which can lead to a reduction in biocompatibility and cellular interaction. While synthetic materials may not have the same cell signaling capabilities that biological hydrogels have, the enormous amount of monomers and polymers that are available to polymerize or crosslink provide an endless amount of hydrogels with a wide range of physical properties. Hydrogels formed from synthetic materials can produce well-defined and controllable structures, and the degradation rate can be tuned to fit the given application.[12] Many of these synthetic hydrogels have been shown to have very few undesirable local and systemic effects, and have proved to be very useful in drug delivery applications.

Choosing the right material and properties of a hydrogel often depends on the application and the administration site. In some cases, the chemical composition is the key factor for choosing a certain hydrogel material. For example, in Chapters 5 and 6 we investigate the use of hydrogel implants that are implanted into the vitreous humor of the eye in order to deliver drugs

to the retina for 3-6 months. An ideal implant would have a chemical composition that is similar to the vitreous of the eye (hyaluronic acid) in order to decrease the potential for any cellular or inflammatory responses. In other cases, the way the hydrogel material interacts with tissue is the most important criteria.

An example of this is the development of drug delivery systems to remove fungal infections in the oral cavity. The biggest challenge is the fast elimination of any topically applied drugs due to the movement of saliva in the mouth. To overcome this challenge, bioadhesive polymers like chitosan and poly(methyl methacrylate) are used in gel form to extend the residence time in the mouth and increase the amount of drug that can be delivered[14,15]. In other cases, the mechanical properties of the hydrogel are critical for achieving clinical success. For example, in tissue engineering, the hydrogels often fill a void that was once occupied by natural tissue and will be exposed to mechanical loads. In order to maintain stability, the hydrogel must have adequate mechanical properties such as compressibility, elasticity, tensile strength, and failure strain.[16] Selecting the right material and physical properties is often the first step in developing a successful hydrogel drug delivery system.

This dissertation is focused on the synthesis of both biologically and synthetically based hydrogels. The goal is to understand how the synthesis conditions affect the diffusion and partitioning of solutes within the hydrogel. In Chapter 4 both dextran and poly(ethylene glycol) are used to synthesize gels. Chapters 5 and 7 are dedicated to studying the use of hyaluronic acid as a drug delivery vehicle using two different crosslinking methods. In the next section, these polymers are reviewed in greater detail.

2.2.1 Poly(ethylene glycol) (PEG)

Poly(ethylene glycol) (PEG) is one of the most widely used polymers for biomedical applications. PEG is a polymer made up of repeating units of (CH_2CH_2O) and can range in size from 400 Da to over 100 kDa. At low molecular weights, PEG appears as a colorless liquid and at higher molecular weights PEG becomes a solid that is waxy and white in color.[17] PEG is soluble in both water and organic solvents. While the ability to dissolve in water is crucial for biological applications, the fact that it also dissolves in organic solvents allows for easy modification to the end groups of PEG. This, coupled with the commercial significance of PEG, has led to an abundance of PEGs including monofuctional, homobifunctional, heterobifunctional, and even multi-arm PEG.[18]

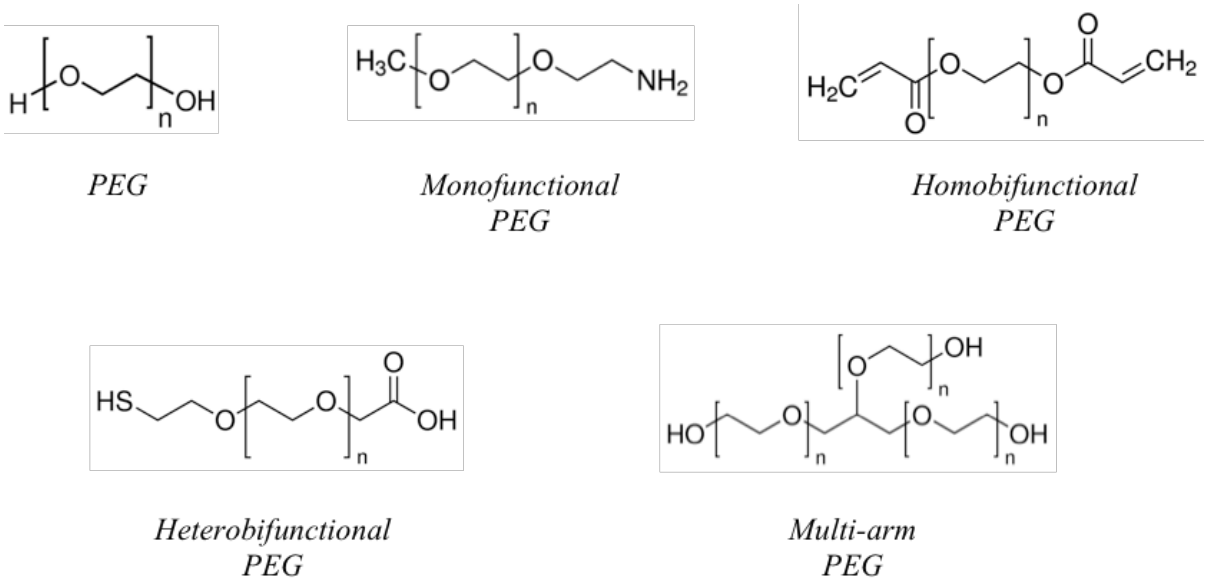

Figure 2.1 The chemical structure of poly(ethylene glycol) and examples of several of the modifications that can be made.

One of the advantages of PEG is that it is one of the most bioinert polymers available and has been approved by the FDA for use in pharmaceutical, cosmetic and even food applications. PEG is eliminated from the body by either the kidney or in the feces (depending on the molecular weight of the PEG), and is considered non-toxic.[19] This has led to widespread use in biomedical applications. One of the most popular uses of PEG in the pharmaceutical industry is to conjugate PEG with proteins and peptides, also known as PEGylation. PEGylation increases the molecular mass of the conjugated drug and reduces renal clearance, which prolongs the circulation in the blood. PEGylation also increases the water solubility of the drug and shields the drug from proteolytic degradation and adverse immunological effects.[20] This leads to a longer half-life and increases the probability that the drug will reach its intended target.[21] The shielding effect of PEG is useful for applications beyond PEGylation, as PEG is used as a coating on implant surfaces, medical devices, and even poly(vinylchloride) bags to prevent interactions with components in the surrounding blood and tissue and to reduce protein adsorption.[22-24] PEG is used as a common excipient in many pharmaceutical applications and is also the main ingredient in a number of commercially available laxatives.[21,25] PEG has also been used extensively in drug delivery to produce liposomes, micelles, and polymersomes and extend the circulation times of these drug delivery vehicles.[26-29]

PEG has also been used to make hydrogels that are well suited for biomedical applications. The many sizes, shapes, and functionalities of PEG that are available can create hydrogels with a wide range of physical and chemical properties. There are a number of methods that can be used to form hydrogels from PEG. Linear or branched PEG polymers can be crosslinked directly by gamma irradiation.[30,31] The end groups of PEG can also be modified with acrylates or methacrylates, which allow it to be polymerized via a number of reaction

mechanisms including free radical polymerization and thiol-ene reactions. Free radical polymerization can be initiated by radiation, however chemical initiators are used more often to generate free radicals. These chemical initiators provide versatility as they can be activated by light, heat, and in some cases even by certain solvents.

This versatility can lead to a number of useful applications. For example, the commercially available Focalseal is a solution containing modified PEG that is used as a surgical sealant to prevent air leaks in lungs after chest surgeries and the removal of lung tumors.[32] Focalseal is applied to the target tissue area as a liquid and is then photoinitiated, forming a hydrogel network that is waterproof. Over time, segments of the gel degrade, leading to eventual dissolution and clearance through the kidneys. Another method to crosslink PEG is through Michael-type addition reactions, and this method has been used in tissue engineering to crosslink four and eight arm PEG molecules into hydrogels that were successfully used to culture chondrocytes for cartilage repair.[33,34] In this dissertation functionalized PEG is used to form hydrogels for use as drug delivery vehicles in Chapter 4. Linear, unmodified PEG is also used in Chapter 4 to create an aqueous two-phase system that is used for loading proteins and antibodies into dextran hydrogels.

2.2.2 Dextran

Dextran is another material that can be easily crosslinked into hydrogels and is used in a number of biomedical applications due to its high solubility and biocompatibility. Dextran is a naturally occurring polysaccharide that is made up of D-glucose molecules that are connected through α(1,6)-linkages. This naturally occurring polysaccharide is synthesized from sucrose by a number of bacteria, including *Leuconostoc*, *Streptococcus*, and *Lactobacillus*.[35,36] The amount of branching, the weight average molecular weight (M_W), and the M_W distribution can change depending on the species.

These key factors play a large role in determining the properties of dextran and can have a direct influence on the way dextran is used in clinical applications. For example, one of the most important uses of dextran is as a blood flow enhancer and plasma volume expander. Dextran solutions are injected and used as a blood plasma substitute in times when plasma is scarce due to their high water solubility and low antigenicity.[37] The dextran provides osmotic pressure and can pull fluid from the interstitial space into the plasma, acting as a substitute for blood proteins.[38] Natural dextran is known to have a very high M_W that generally ranges from 9×10^6 – 5×10^8 Da, with a large M_W distribution.[39] When dextran with this high of M_W is injected into the bloodstream it can disrupt the coagulation process of the blood.[40] At the same time, dextran with a very low molecular weight is quickly cleared by the kidneys, losing its therapeutic effect.[41] Therefore, dextran with a M_W between 40-80 kDa is used clinically, and is produced by partial hydrolysis and fractionation of native dextran in order to produce the M_W and M_W distributions that are needed.[42]

Although the majority of the links occur through α(1,6)-linkages, dextran can also contain a large number of side chains or branches that can stem from α(1,2)-, α(1,3)-, and α(1,4)-

linkages. The amount of branching can range from between 0.5-50% of the total gylcosidic bonds, and plays a large role in the properties of dextran. Dextran that contains a high number of α(1,6)-linkages tend to have both increased chain flexibility and water solubility. Alternatively, if the amount of branching exceeds a certain percentage (> 43%), dextran can become insoluble in water. The amount of branching also affects the pharmacokinetic properties of dextran, as α(1,4)-linkages are broken down in the body much faster than α(1,6)-linkages, and dextran with higher proportions of non α(1,6)-linkages often lead to more occurrences of allergic reactions.

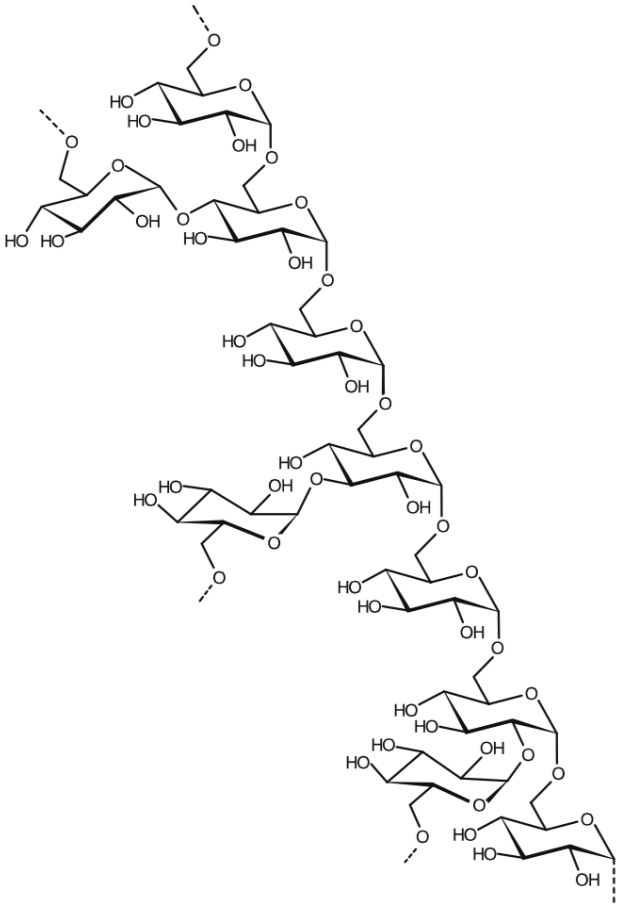

Figure 2.2 The chemical structure of dextran. The main chain consists of D-glucose molecules connected with α(1,6)-linkages. Branching is shown in the α(1,2)-, α(1,3)-, and α(1,4)-positions[38].

Dextran is used in a number of biomedical applications. As mentioned earlier, the high water solubility and low antigenicity of dextran allows it to provide osmotic pressure in physiological environments. These advantages of dextran are also utilized in ophthalmic formulations of eye drops and artificial tears.[43] Dextran has also been used as macromolecular carriers of proteins and drugs, similar to PEGylation, to increase the half-lives of these therapeutic agents in the blood and reduce immunogenicity.[44] Dextran is also used in combination with PEG to create aqueous two-phase systems that are capable of purifying and separating a wide range of biomolecules including cells, proteins, nucleic acids, and viruses.[45]

Dextran hydrogels have received a lot of attention in drug delivery and tissue engineering due to their biocompatibility and their ability to biodegrade. There are a number of ways that dextran can be formed into hydrogels, by both physical and chemical crosslinks. A commonly used chemical crosslinker is epichlorhydrin, which can crosslink dextran in alkaline aqueous solutions to form hydrogels. These hydrogels, known commercially as Sephadex®, are used in separation and purification membranes and act as molecular sieves for important biochemical molecules such as polysaccharides, proteins, and nucleic acids.[39] Another commercially known hydrogel product, Debrisan®, is made using the same crosslinking method and is used as a wound healing agent to speed up the recovery time.[46] Dextran can also be crosslinked from a number of bifunctional reagents including phosphorous oxychloride, diisocyanates, and divinyl sulfone.[47,48] Additionally, dextran can be modified with acrylate or methacrylate groups and polymerized via free radical polymerization. These gels have been used as protein releasing matrices and as scaffolding for tissue engineering and show biocompatibility with native tissue.[49,50]

In this dissertation dextran hydrogels are formed under alkaline conditions using the crosslinker divinyl sulfone. This is done in Chapter 4 and is used to investigate the partitioning of proteins and antibodies in dextran under various loading conditions. Linear, unmodified dextran is also used in Chapter 4 to create an aqueous two-phase system that is used for loading proteins and antibodies into PEG hydrogels.

2.2.3 Hyaluronic Acid

Hyaluronic acid (HA) is another naturally occurring polysaccharide that is used extensively in biomedical applications. Hyaluronic acid is a linear, unbranched polysaccharide that is composed of repeating units of the disaccharide glucoronic acid and N-acetylglucosamine. Unlike dextran, HA is found in all living organisms. It plays a key role in the extracellular matrix of tissues, acting as a scaffold and providing mechanical properties to tissues.[51] HA participates in a number of important biological functions, including the manipulation of cell differentiation and proliferation, and the regulation of cell motility and cell adhesion.[52] HA is negatively charged under physiological conditions due to the presence of the carboxyl group, and electrostatic interactions can have large effects on the rheological and hydrodynamic properties. Under physiological conditions HA forms a stiff twisted ribbon structure due to distinct charged and hydrophobic faces that are formed from the hydrogen atoms and the carboxyl groups of glucoronic acid. This structure, along with the association of counter ions with ionized groups on the HA, causes it to occupy a large volume and leads to a large amount of water trapped inside the structure.[53,54] The structure also provides viscoelasticity to biological fluids and tissue such as synovial fluid and the vitreous humor of the eye.[53]

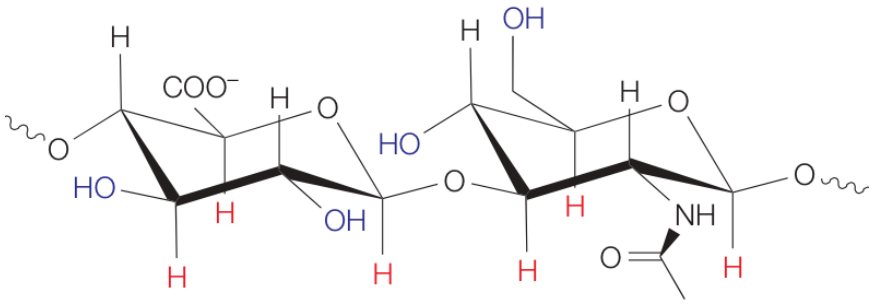

Figure 2.3 The chemical structure of hyaluronic acid. The axial hydrogen atoms are shown in red and form a relatively hydrophobic face. The equatorial hydroxyl groups are shown in blue and, along with the carboxyl group, form a charged hydrophilic face. These two faces are responsible for the stiff backbone in solution and HA's viscoelastic properties[54].

The unique combination of properties of HA, including its biocompatibility, viscoelasticity, and non-immunogenicity has made it a useful material for use in biomedical applications. Unmodified HA has been used as a vitreous replacement during eye surgeries, as a viscosupplementation in arthritis treatments, and in the regeneration and healing of surgical wounds.[53] Despite the many intrinsic benefits of unmodified HA, it has a high turnover and elimination rate in vivo.[55,56] To overcome these disadvantages HA is often crosslinked and formed into hydrogels. HA hydrogels can be synthesized by two routes. The first route is to crosslink unmodified HA directly using bifunctional crosslinkers such as divinyl sulfone or bis-epoxides.[57] The second route is to modify HA with any number of chemical groups including bromoacetate,[58] hydrazides,[59] tyramines,[60] thiols,[61] and methacrylates.[62] These HA derivatives can then be formed into hydrogels by addition reactions, condensation reactions, and radical polymerizations.

HA hydrogels have been used in a number of biomedical and drug delivery applications.[57] HA hydrogels have been studied for their use in tissue applications as scaffolding

for cells.[52,63,64] They have also been used to deliver a wider range of drugs including peptides for chronic wound therapy,[65] anti-inflammatory drugs for coatings of implants,[66]and proteins such as erythropoietin and human growth hormone.[67,68]

In this dissertation, HA was used to synthesize drug delivery vehicles that were capable of providing extended release of proteins and antibodies. HA hydrogels were formed using divinyl sulfone (DVS) as a crosslinker in Chapter 5, and in Chapter 6 the gels were synthesized using the thiol-ene reaction, which will be discussed in Section 2.3.3.

2.3 Hydrogel Synthesis

In this section, the synthesis methods that are used throughout this dissertation to create hydrogels are reviewed. One of the many advantages of hydrogels is that they can be formed using a wide variety of synthesis methods. By definition, a hydrogel is a hydrophilic polymer network that is held in place by crosslinks that support the network's three-dimensional structure. These crosslinks can be formed by any number of methods, including chemical reactions, electrostatic interactions, and even physical entanglements. The synthesis method plays a large role in determining the hydrogel's network structure, which is believed to play a critical factor in drug delivery devices that control the rate at which drugs can be released from the device. The synthesis method is also crucial in deciding whether or not a drug can be incorporated into the network during hydrogel formation. Therefore, because of its importance in the field of drug delivery, a number of synthesis methods have been developed throughout the years to produce hydrogels.

In this dissertation, two types of synthesis methods are used to create hydrogels: the copolymerization/crosslinking of monomers, and the crosslinking of linear polymers. In the

copolymerization/crosslinking of monomers, smaller monofunctional and multifunctional monomers are linked together, usually via free radical polymerization to form a complex network of connected polymer chains. Alternatively, the crosslinking of linear polymers takes long, polymer chains and links them together with multifunctional crosslinks. These methods are described in more detail in the following sections.

2.3.1 Free Radical Polymerization

Free radical chain polymerization is a well-established technique that is used to produce gels from hydrophilic monomers that can be used for pharmaceutical and biomedical applications.[7] The reaction can occur with any monomer that contains double bonds, including vinyl, divinyl, and even 1,3-diene molecules. All free radical chain polymerizations begin with an initiation step that produces a radical species. The radical species can come from a number of sources, including light sensitive, temperature sensitive, or solvent sensitive chemical initiators. These radical species associate with the vinyl groups of the monomer and the reaction continues as more and more vinyl groups are attached to the growing chain. The chain will continue to propagate until the radical species of the chain is terminated by a number of routes including combination, disproportionation, etc. Free radical chain polymerization produces high molecular weight chains that grow quickly and eventually crosslink with other chains to form the hydrogel network.[69] However, even as the reaction is completed, there can still be a number of monomers and even polymer chains that have not incorporated into the network.

Free radical polymerization was used in Chapter 4 to synthesize poly(ethylene glycol) diacrylate (PEGDA) hydrogels. The reaction can be seen in Figure 2.4 in which, following initiation, the acrylate of one PEGDA reacts with the acrylate group of an additional PEGDA.

The reaction produces polyacrylate kinetic chains (zig-zag lines) that link the molecules together. While PEGDA is itself a polymer that has a molecular weight of 700 g/mol, the reaction still undergoes the initiation, propagation, and termination steps that characterize a free radical polymerization.

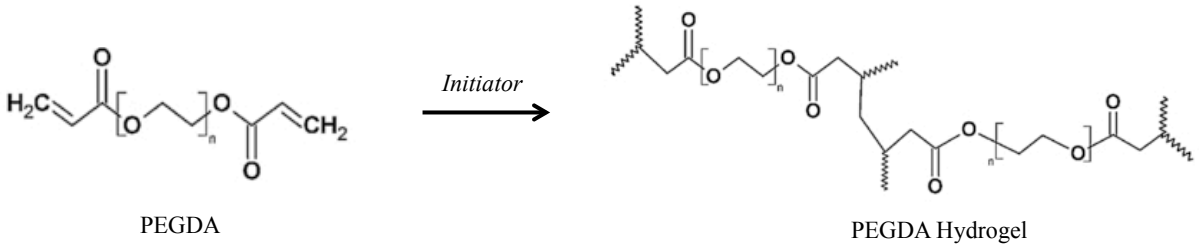

Figure 2.4 The free radical polymerization of poly(ethylene glycol) diacrylate that was used in this dissertation to create hydrogels.

2.3.2 Crosslinking of Linear Polymers

Another way of forming hydrogels is through the crosslinking of linear hydrophilic polymers. These crosslinks can be formed through chemical reactions, physical entanglements, and via ionizing radiation.[2] There are a large number of linear polymers that can be chemically crosslinked into hydrogels and the synthesis method often depends on the chemical groups on the polymers that are available to react.[70] Many hydrophilic polymers contain hydroxyl, carboxyl, or amine groups that can serve as reactive sites for chemical crosslinkers.[7] There are a number of chemical crosslinkers that can be used to react with linear polymers including aldehydes (acetaldehyde, formaldehyde, gluteraldehyde), diepoxides, divinyl sulfone, epichlorohydrin, and diisocyanates to name a few.[70,71] In order to effectively crosslink polymers, these crosslinkers must be difunctional or multifunctional.

In this dissertation, the naturally occurring polysaccharides dextran and hyaluronic acid are crosslinked chemically to form hydrogels. In Chapters 4 and 6, both dextran and hyaluronic acid are crosslinked under basic conditions using the chemical crosslinker divinyl sulfone (DVS) (Figure 2.4). This reaction has been used previously in literature to create hydrogels for biomedical applications due to its ease of use and high degree of crosslinking.[72] They have been investigated for use in tissue engineering, and gels with high molecular weight HA crosslinked with DVS were shown to be bioinert.[73] Further investigation of the hydrogels discovered that by inserting smaller molecular weight HA into the network, cells were able to attach, spread, and proliferate within the hydrogel.[74,75]

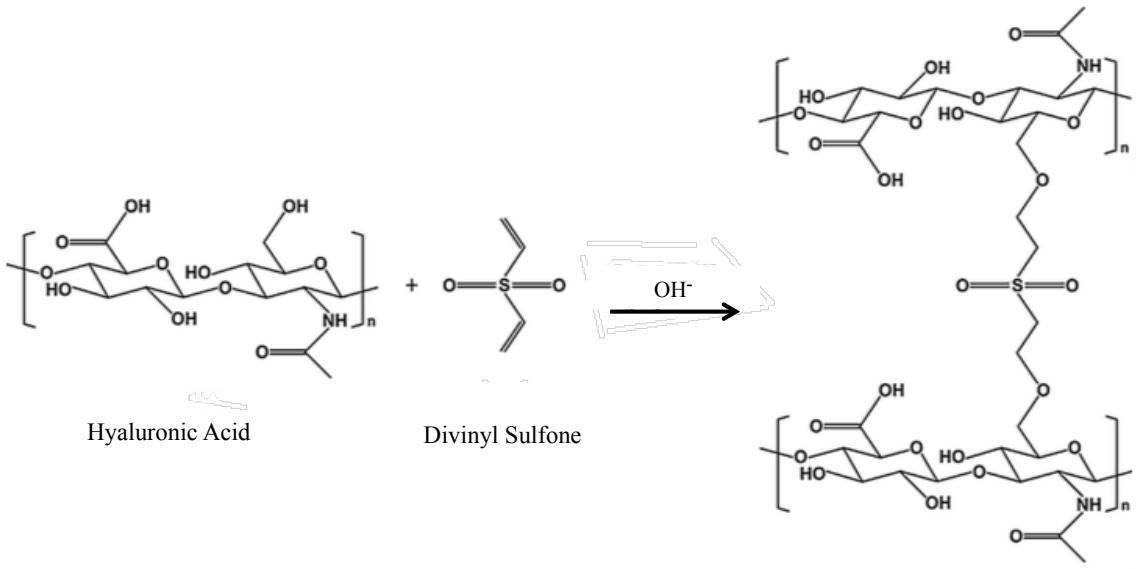

Figure 2.5 The reaction for chemically crosslinking hyaluronic acid (HA) and dextran that was used throughout this dissertation. The reaction occurs through the hydroxyl groups that are present on both dextran and HA and is base catalyzed. Adapted from[76]

2.3.3 Click Chemistry

In 2001 KB Sharpless introduced an approach for a new set of reactions termed "click chemistry" that allowed for the synthesis of new and useful compounds using simple reaction conditions.[77] These reactions were to use materials and reagents that were widely available, proceed to very high yields, be able to be carried out in water and in the presence of oxygen, and give products that are easy to collect and purify. Sharpless realized that in order to achieve these qualities in a reaction, a high thermodynamic driving force would be needed. It is this thermodynamic driving force that causes the reaction to be "spring-loaded" and leads to reactions that proceed rapidly and with high selectivity. Click chemistry is not a single specific reaction, but rather a concept that encompasses a number of possible reactions and mechanisms. Several of the reactions that fit the "click" reaction requirements are seen below in Figure 2.6.[78] Of these reactions, the Cu(I) mediated 1,3-Dipolarcycloaddition of alkynes and azides has been utilized extensively in the literature for drug discovery and material and polymer science due to its orthogonality and near quantitative yields.[78-82] It has become so synonymous with click chemistry that it is often called "the click reaction". While this reaction has been used to create polysaccharide hydrogels of hyaluronic acid[83] and dextran,[84] the toxicity of the copper catalyst prevents it from seeing widespread use in tissue engineering and in vivo applications.[85]

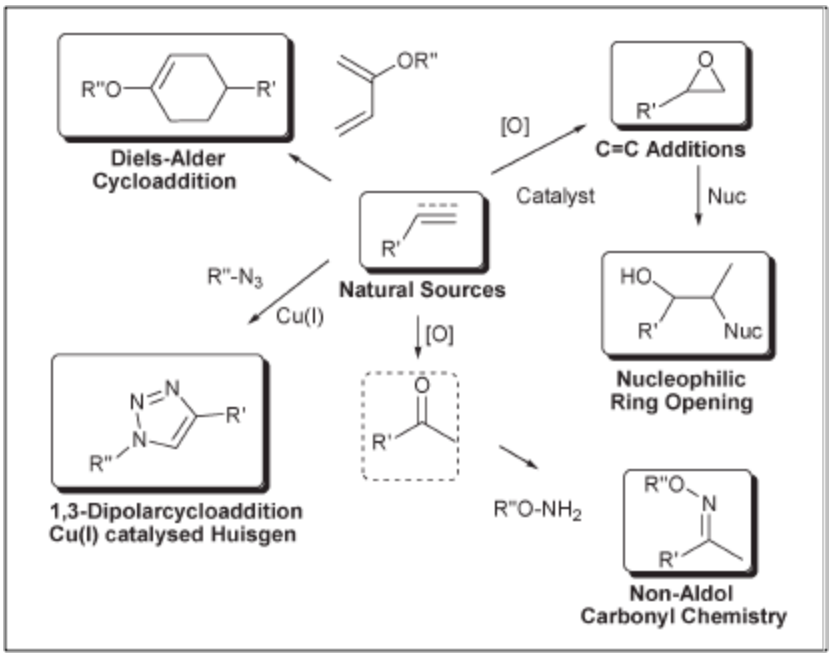

Figure 2.6 Some of the most widely used chemical reactions which fit the requirements of click chemistry. Reproduced from Ref[54]

In Chapter 7 of this dissertation, a relatively new synthesis method called the thiol-ene reaction was developed for crosslinking HA hydrogels. The thiol-ene reaction was studied due to the fact that some of the chemical crosslinking methods used in the earlier chapters were not suitable for the encapsulation of proteins and left behind reactive groups that interacted with proteins and impeded the release from the resulting hydrogels. The thiol-ene reaction, while able to safely encapsulate cells and proteins, is also hypothesized to produce a more homogeneous network structure. A more homogeneous hydrogel network would lead to improved mechanical properties and could also play a role in the diffusion of solutes within the hydrogel. This section will introduce the thiol-ene reaction and give a brief review of the ways in which the reaction has been used previously in literature to form HA hydrogels.

The thiol-ene reaction has been used since the early 1900's, and is, at its core, the hydrothiolation of a carbon-carbon double bond.[86] The reaction is carried out in one of two ways and can be seen below in Figure 2.7.[87] The first is a free radical mechanism that is termed the "thiol-ene" reaction. It involves the addition of a thiyl radical (RS•) to a carbon-carbon bond that can be either electron rich or poor. The second is an anionic mechanism that is termed the "thiol Michael addition". It involves the addition of a thiolate (RS-) to an electron deficient carbon-carbon bond. While the reactions produce the same product, the thiol Michael addition is more restrictive, and requires an electron deficient carbon-carbon bond such as an acrylate or a methacrylate group.

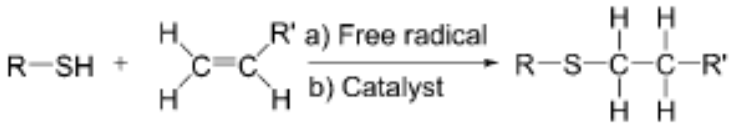

Figure 2.7 The addition of a thiol to an "ene" group by a.) the thiol-ene reaction and b.) the thiol Michael addition reaction. Adapted from Ref [87]

The mechanism of the reaction was first proposed in 1938[76] and can be seen below in Figure 2.8.[88,89] A thiol is first initiated, either with heat or light, to give a thiyl radical. This thiyl radical then propagates across a carbon-carbon double bond, resulting in an intermediate carbon-centered radical. This radical is then able to pull a hydrogen radical off of a second thiol, which gives the final thiol-ene product and in turn generates a new thiyl radical that is able to react with another vinyl group. The termination step has not been systematically studied, however it is assumed that the termination occurs via the quenching of two radical species. It should be noted

that the mechanism in Figure 2.8 is for an ideal thiol-ene reaction. When an activated carbon-carbon double bond is used, it is possible for the carbon centered radical to homopolymerize with another carbon centered radical, essentialy starting a competing chain reaction. However, the thiol-ene reaction occurs so quickly that under most conditions no homopolymerization is seen.

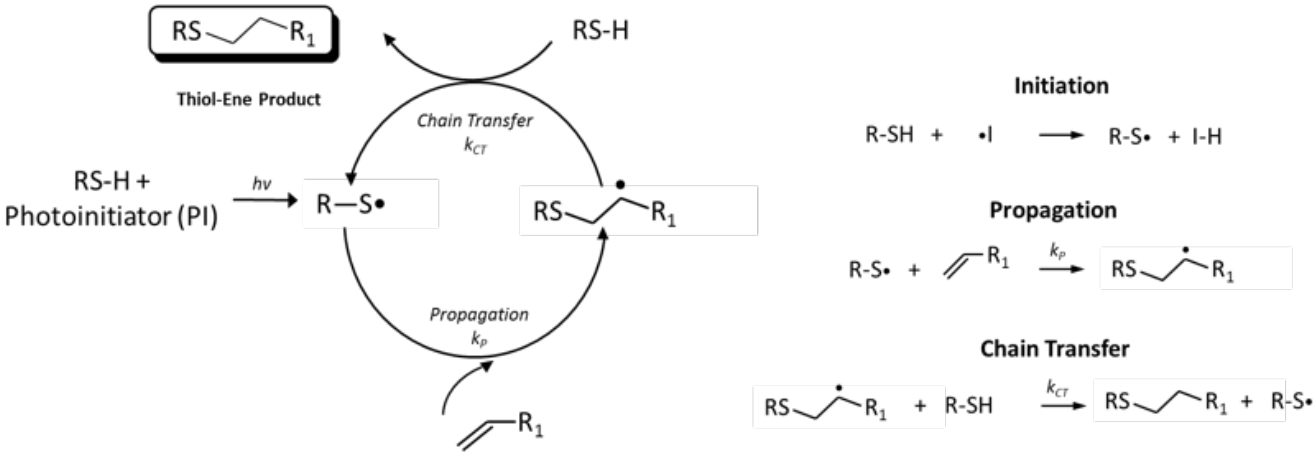

Figure 2.8 The mechanism of the Thiol-Ene reaction including: initiation, propagation, and chain transfer. Adapted from [87,89]

The thiol-ene reaction has many advantages: it is incredibly fast, proceeds to high yields, can be performed in water over a wide range of concentrations, and is insensitive to oxygen.[89-91] The reaction can take place with virtually any carbon-carbon double bond, including terminal, internal, conjugated, substituted, and even cyclic alkenes.[92] At the same time, there are a wide range of thiols that can be used, as any thiol is able to participate in the thiol-ene reaction.

It wasn't until 2012 that a true thiol-ene reaction using a free radical as an initiator was performed using HA. The work was done by Auzély-Velty et al. and it involved attaching a

pentenoate group onto the backbone of HA and dextran by esterification of the hydroxyl groups.[93] The motivation behind the work was mostly to functionalize the polysaccharides with hydrophobic groups, peptides, and oligosaccharides, yet they were also able to form hydrogels using the pentenoate modified dextran and a PEG-dithiol. Similar work was done in 2013 by Burdick who modified HA with a norbornene group.[94] The modified HA was crosslinked using a small disulfide molecule (dithiothreitol), and the compressive moduli was varied with the irradiation time, the ratio of thiols to norbornene, and the weight percent of HA in solution. The focus was on photopatterning the hydrogels to either modify the crosslink density or to couple chemical ligands. This was done by selecting conditions in which after gelation there still existed pendent norbornenes that could undergo further reactions with a variety of thiol containing molecules.

While the use of thiol-ene reactions to create hydrogels is a more recent advance in literature, a number of HA hydrogels have been made using the thiol-Michael addition reaction.[52,95-97] Although the thiol-Michael addition reactions (the addition of a thiolate (RS-) to an electron deficient carbon-carbon bond) are similar to the thiol-ene reaction they lack one of the key advantages of the thiol-ene reaction: the ability to be initiated by a radical species. The ability to be initiated by a radical species enables the thiol-ene reaction to be controlled spatially and temporally via photoinitiation, or by temperature using a thermal initiator. On the other hand, the thiol-michael addition reaction begins immediately when the reactants are mixed together. Not only are thiol-Michael addition reactions spontaneous but they also occur under slightly alkaline conditions that can often lead to disulfide formation and off-stoichiometric reactions of monomers as the hydrogel is being formed.

2.4 Properties of Hydrogels

The swelling degree and mechanical properties of a hydrogel play a large role in determining its usefulness and application as a drug delivery device. In this section, an overview of the equilibrium swelling theory is provided along with the theory for determining the mechanical properties of a hydrogel such as the compressive moduli (Young's and elastic), and crosslink density.

2.4.1 Swelling Theory

One of the most important properties of a hydrogel is the equilibrium swelling degree, as it has a direct influence on the other properties of the hydrogel.[7] The swelling degree is typically expressed as either the mass degree of swelling, q, or the volume degree of swelling, Q, and are defined as:

q = mass of swollen gel/mass of dry polymer (2.1)

Q = volume of swollen gel/volume of dry polymer (2.2)

Unlike polymer chains in solution, the polymer chains of a hydrogel are constrained by crosslinks that serve as elastic junctions. As the chains begin to absorb solvent and swell they become elongated, creating a retractive force that opposes the thermodynamic force of dilution. When these two forces are equal, a state of equilibrium is reached. The physical situation can be described in terms of the Gibbs free energy:

$$\Delta G_{total} = \Delta G_{mixing} + \Delta G_{elastic} \quad (2.3)$$

where ΔG_{mixing} is the change in free energy due to polymer mixing between the solvent and the polymer chains, and $\Delta G_{elastic}$ is the change in free energy due to elastically effective crosslinks in

the hydrogel network. Equation 2.3 can also be described in terms of the osmotic swelling pressure, giving:

$$P_{ext} = \Pi_{mixing} + \Pi_{elastic} \quad (2.4)$$

where:

P_{ext} = the externally applied pressure

Π_{mixing} = the swelling pressure due to the tendency of the polymer to dissolve in the solvent

$\Pi_{elastic}$ = the elastic response of the network due to crosslinking

The model that is used most often used to describe the polymer-solvent mixing term is known as the Flory-Huggins theory, and can be written as:

$$\Pi_{mixing} = \frac{RT}{\tilde{V}_1}\left[\ln(1-\phi_2)+\phi_2+\chi_1\phi_2^2\right] \quad (2.5)$$

in which:

R = gas constant

T = Temperature

$\tilde{V}_1$ = solvent molar volume

ϕ_2 = polymer volume fraction

χ_1 = polymer solvent interaction parameter

The last term in Equation 2.5 represents the enthalpy of mixing using the polymer solvent interaction parameter, and takes into account both the solvent and the material. This interaction parameter is often referred to as the Flory Huggins solubility parameter, and is generally between 0 and 1. Higher values ($\chi > ½$) indicate that polymer-polymer interactions are more prevalent

than polymer-solvent interactions and discourages dissolution. Lower values ($\chi < ½$) indicate that polymer-solvent interactions are more prevalent than polymer-polymer interactions and supports dissolution. Values of χ equal to 1/2 signify that polymers and solvents that have no net interactions.

The elastic contributions in Equation 2.4 can be written as:

$$\Delta\Pi_{elastic} = -\frac{RTv_e}{V_0}\left(\phi_2^{1/3} - \frac{1}{2}\phi_2\right) = -RT\rho_x\left(\phi_2^{1/3} - \frac{1}{2}\phi_2\right) \quad (2.6)$$

where:

v_e = the number of elastically effective chains in the network

V_0 = volume of the undeformed polymer network (network before swelling)

$\rho_x = v_e/V_0$ = effective crosslink density of the hydrogel

For networks made in solution (as is the case for many common hydrogels), Equation 2.6 can be modified to:

$$\Delta\Pi_{elastic} = RT\rho_x\phi_{2,r}\left[\left(\frac{\phi_2}{\phi_{2,r}}\right)^{1/3} - \frac{1}{2}\left(\frac{\phi_2}{\phi_{2,r}}\right)\right] \quad (2.7)$$

in which $\phi_{2,r}$ is the polymer volume fraction at network formation.[98] By combining Equations 2.4, 2.5 and 2.7, the free swelling of a nonionic gel in equilibrium can be defined as:

$$0 = \ln(1-\phi_2) + \phi_2 + \chi_1\phi_2^2 + \tilde{V}_1\rho_x\phi_{2,r}\left[\left(\frac{\phi_2}{\phi_{2,r}}\right)^{1/3} - \frac{1}{2}\left(\frac{\phi_2}{\phi_{2,r}}\right)\right] \quad (2.8)$$

If the gels have ionizable groups, two more terms are added to the equation to take into account the electrostatic and ionic effects that can affect the swelling of the gel, giving:

$$P_{ext} = \Pi_{mixing} + \Pi_{elastic} + \Pi_{ion} + \Pi_{electrostatic} \quad (2.9)$$

where ΔG_{ion} represents the change in free energy due to concentration differences of ions between the hydrogel and solvent, and $\Delta G_{electrostatic}$ represents the change in free energy due to electrostatic interactions between the polymer and the solvent. The ionic term can be represented as:

$$\Delta\Pi_{ion} = RT\left(c - c^{*}\right) \quad (2.10)$$

where c is the molar concentration of mobile ions in the solution inside the gel and c^{*} is the molar concentration of mobile ions in the solution outside the gel. In general, the effects of electrostatics are often much smaller than the osmotic effects in a polyelectrolyte hydrogel, and large changes in the swelling degree of polyelectrolyte gels can be seen as the degree of ionization is altered.

2.4.2 Mechanical Properties

While a number of important properties of the hydrogel network can be determined from the swelling degree, a more complete picture of the hydrogel network is achieved when the mechanical properties of the gel are tested. In this dissertation, all of the gels were tested under compression and a representative stress-strain curve can be seen in Figure 2.9. By using a Gaussian model to describe the chain extensions within the network combined with statistical

thermodynamics, various network properties of the hydrogel can be determined from the stress-strain curve[5].

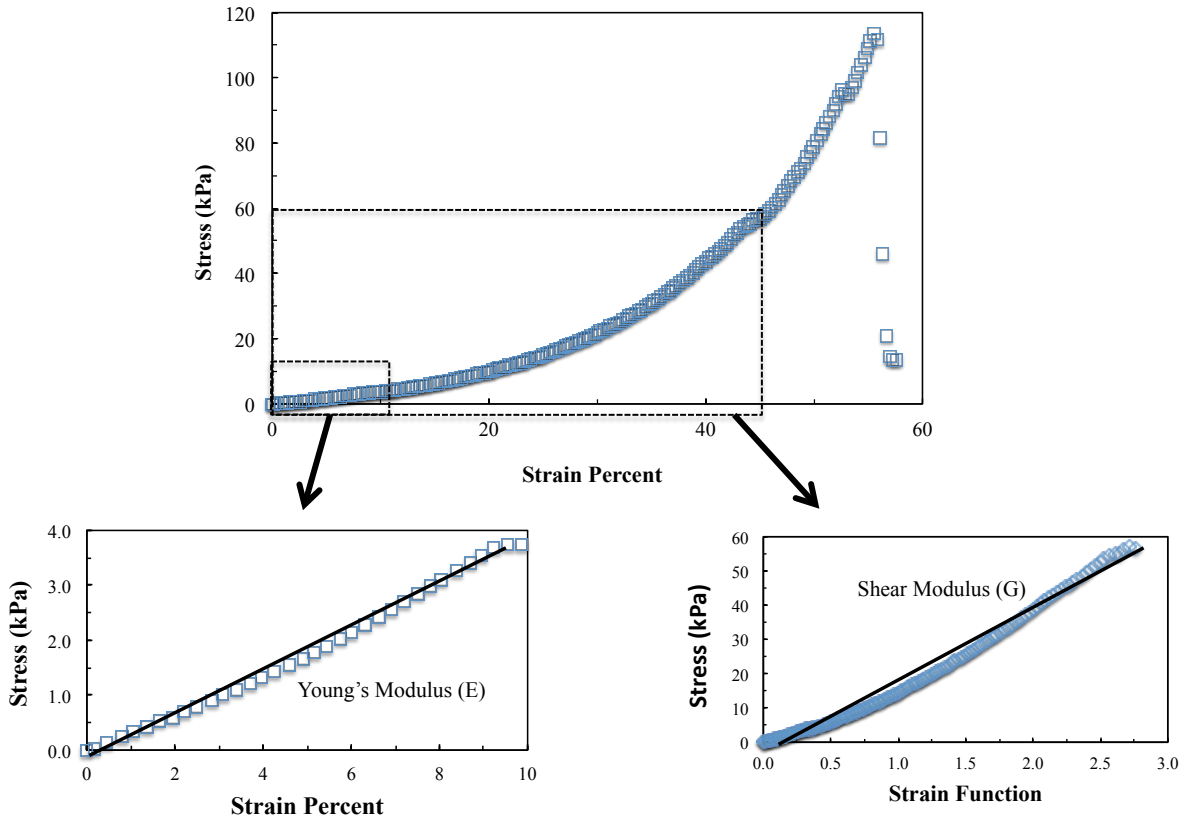

Figure 2.9 A representative sample of the stress-strain curves that were obtained from compression testing of the hydrogels in this dissertation. The curves were used to calculate both the compressive modulus (E) and the shear modulus (G).

When a hydrogel is compressed the work required to deform the network or elastically store a given amount of free energy per unit volume is expressed as:

$$W = -T\Delta S \tag{2.11}$$

When under compression, assuming a uniaxial force and no volume changes, the change in entropy of the chains in the network can be written as:

$$\Delta S = -\frac{1}{2}NkT\left(\lambda^2 + \frac{2}{\lambda} - 3\right) \tag{2.12}$$

where N is the number of crosslinked chains present in the network, k is Boltzmann's constant, and T is the temperature in Kelvin. λ is the extension ratio, and is defined as:

$$\lambda = \frac{L}{L_0} \tag{2.13}$$

When the shear modulus (G) of the network is included in Equation 2.12 and inserted into Equation 2.11, the resulting equation is:

$$W = \frac{1}{2}\,G\,\left(\lambda^2 + \frac{2}{\lambda} - 3\right) \tag{2.14}$$

and, σ, the nominal stress can be expressed as:

$$\sigma = \frac{dW}{d\lambda} = G\,\left(\lambda - \frac{1}{\lambda^2}\right) \tag{2.15}$$

The shear moduli of the hydrogels in this dissertation were calculated using Equation 2.15 and the stress strain data collected. When the stress is plotted against the strain function $\left(\lambda - \frac{1}{\lambda^2}\right)$, a hydrogel that is considered an ideal elastomer and follows neo-Hookean behavior will have a linear slope. The shear modulus can also be expressed in terms of the number average molecular weight between crosslinks ($\overline{M}_c$),

$$G = \frac{\rho RT}{\overline{M}_c} \tag{2.16}$$

Where ρ is the density of the polymer and R is the gas constant per mole. From this equation we see that the shear modulus is directly related to the number of crosslinks per unit volume, as larger number of crosslinks result in lower values of $\overline{M}_c$. The shear modulus can also be used to calculate the crosslink density using the affine model, written as:

$$\rho_x = \frac{G}{RT\, v_2^{1/3}\, v_{2r}^{2/3}} \tag{2.17}$$

in which v_{2r} is the polymer volume fraction during hydrogel formation. There are other models that exist other than the affine model. One of these models, the phantom model, is also commonly used for hydrogels and can be used to calculate the crosslink density as well. The crosslink density calculated from the phantom model is twice the value of the crosslink density calculated from the affine model. The crosslink density and the number average molecular weight between crosslinks are important properties of the hydrogel network and are often used in drug delivery applications to compare network properties between different gels and to calculate the average mesh size, which will be shown in Section 2.4.3.

The compressive modulus, E, can be calculated directly from the stress-strain curve. At low strain percent, the curve follows Hooke's law:

$$\sigma = E\varepsilon = E\,(\lambda - 1) \tag{2.18}$$

The compressive modulus was calculated by using the data up to strains of 10%. The relationship between the compressive modulus and shear modulus can be written by:

$$E = 2G\,(1 + \upsilon) \tag{2.19}$$

in which v is known as Poisson's ratio. For an ideal elastomer, the value of v = 0.5 and therefore, if the ratio of E/G = 3 it is often a good indication that the hydrogel is following the Gaussian statistics and is an ideal elastomer.[99,100] Certain hydrogels do not exhibit a Gaussian chain distribution, which can lead to errors in the calculation of meaningful structural parameters of the gel. For these hydrogels, a different model (such as the Gent model[101]) might more accurately account for the non-Gaussian chain effects.[102]

2.4.3 Hydrogel Mesh Size

One network parameter that is frequently used in drug delivery literature is the hydrogel mesh size. The mesh size is the space between the molecular chains in a hydrogel network. Characterizing these spaces is difficult in a hydrogel due to their heterogeneous nature of hydrogels and the fact that most of the relevant structural features in a hydrogel range from 1-100 nm.[103] The most accurate method in determining the average mesh size in a hydrogel is small-angle X-ray scattering (SAXS), however this method is time consuming and generally requires a synchrotron radiation source.[103,104] Two alternative methods have been developed to estimate the average mesh size within a hydrogel.

The first method was introduced by Peppas[105] and was developed from Flory's classical derivation. The mesh size is based on the swelling and mechanical properties of the hydrogel and is normally represented as the distance between two adjacent crosslinks (ξ). This distance, also known as the correlation length, is calculated using the equation:[105]

$$\xi = \alpha\left(\bar{r}_0^2\right)^{1/2} \tag{2.20}$$

where α is the elongation ratio of the polymer chains in any direction and $\bar{r}_0^2$ is the root-mean-square, unperturbed, end to end distance of the polymer chains between two adjacent crosslinks.[106]

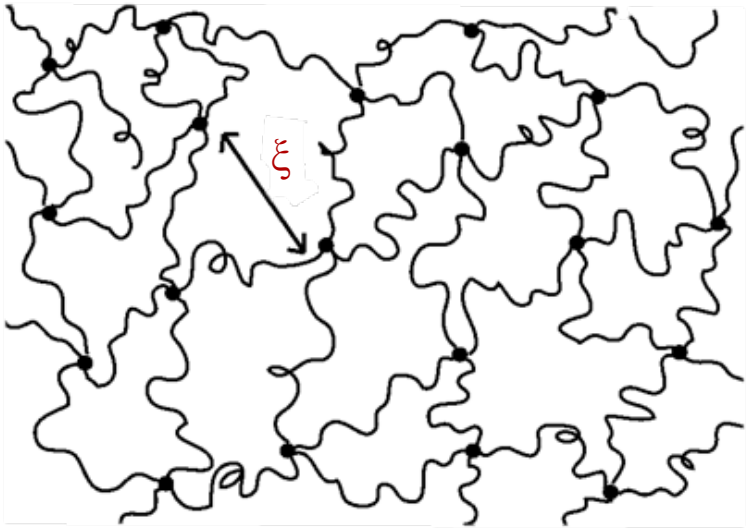

Figure 2.10 Graphical representation of an idealized hydrogel network. The arrow represents the correlation length (ξ), a parameter that is often used to define the mesh size of the network.

For hydrogels that swell isotropically, the elongation ratio of the polymer chains is related to the swollen polymer volume fraction (v_{2s}) as follows:

$$\alpha = v_{2s}^{-1/3} \tag{2.21}$$

and $\left(\bar{r}_0^2\right)^{1/2}$ can be calculated using the equation:

$$\left(\bar{r}_0^2\right)^{1/2} = l(C_n N)^{1/2} \tag{2.22}$$

in which l is the length of the bond along the polymer backbone, C_n is the Flory characteristic ratio, and N is the number of links between two crosslinks calculated as:

$$N = \frac{2\bar{M}_c}{M_r} \tag{2.23}$$

where:

$\bar{M}_c$ = the molecular weight between crosslinks

M_r = the molecular weight of the repeating units from which the chain is composed

By combining Equations 2.20 through 2.23, a final equation is produced that allows for the calculation of the distance between two adjacent crosslinks:

$$\xi = v_{2s}^{-1/3}\left(\frac{2C_n\bar{M}_c}{M_r}\right)^{1/2} l \tag{2.24}$$

While this method for calculating the average mesh size of a hydrogel is much simpler and faster when compared to SAXS, it does have limitations. The theory is highly dependent on an accurate value of $\bar{M}_c$, which is based off of elastic models and can vary in value depending on the model used (affine vs. phantom). Additionally, these models are developed under the assumption that the hydrogel exhibits a Gaussian chain distribution, and there are situations where this assumption is not valid.[2]

The second model for determining the average mesh size of a hydrogel is based on the De Gennes' scaling theory. This model is often known as the "blob" model and calculates the mesh size based on the precursor polymer solution. This model assumes that for polymers in the semidilute state, there are certain entanglement points on the polymer chains where the polymers can interact with each other. The rest of the chain is contained within a region known as a blob,

and is free to move and does not interact with other chains.[107,108] Therefore, crosslinking is assumed to occur at the entanglement points where the polymer chains interact. The blob size, $\xi_{b,}$, can then be estimated by the concentration of the precursor polymer solution:[109,110]

$$\xi_b = R_g \left(\frac{c}{c^*}\right)^{-\upsilon/(3\upsilon-1)} \tag{2.25}$$

where R_g is the radius of gyration, c is the concentration of the polymer, c* is the overlapping concentration of the polymer, and ν is Flory's exponent. As the hydrogel swells, the mesh size of the gel will increase and can be calculated from the blob size by:

$$\xi_m = Q_r^{1/3}\xi_b = Q_r^{1/3} R_g \left(\frac{c}{c^*}\right)^{-\upsilon/(3\upsilon-1)} \tag{2.26}$$

in which Q_r is the volumetric swelling ratio of the gel from the relaxed state to its equilibrium swollen state. In gels that undergo very little swelling from the relaxed state to the equilibrium state, the mesh size of the gel approaches the blob size of precursor polymer solution.

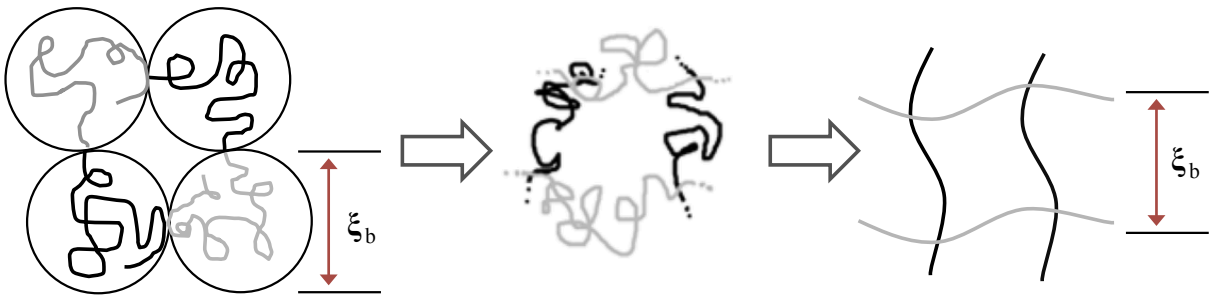

Figure 2.11 Schematic showing the blob size in a semidilute solution and how it is related to the mesh size in an idealized hydrogel. Adapted from Ref[111]

One of the advantages of the blob model is that values of R_g, c^*, and ν can be found in literature for most polymers, making it very easy to calculate the mesh size a priori. However, the model is rather simple and assumes that polymer chains can only be crosslinked at the entanglement points. The model assumes that increasing the degree of modification of the polymers does not affect the mesh size and only increases the density of the polymer chains between entanglement points. The blob model is also only valid when hydrogels are synthesized via the crosslinking of linear polymers and not via the polymerization of multifunctional monomers. Because of this, the Peppas model is utilized much more frequently in literature.

2.4.4 Partition Coefficients of Solutes in Hydrogels

One of the most important properties of a hydrogel is the ability to control the movement of solutes within the hydrogel network and to provide a wide range of permeabilities. This ability to control or restrict the movement of solutes is crucial in many applications including biosensors, chromatography for separation processes, the encapsulation of cells, and especially drug delivery.[112-118] The permeability is highly dependent on the hydrogel network and is influenced by the crosslink density and mesh size of the network, the swelling degree, the size of the solute molecule, and interactions that may occur between the solute and the polymer chains.[10] The permeability is often defined as the product of the diffusion coefficient (D_g), a kinetic term, and the partition coefficient (K), a thermodynamic term.[119] In this section, the focus will be on the partition coefficient, while the diffusion coefficient is discussed in greater detail in Chapter 3.

When a hydrogel is placed in a solution containing a solute, the chemical potential of the solute must be equal in both phases (the gel and the external solution), and results in the solute being distributed between the external solution and the hydrogel.[119] The partition coefficient is

used to describe this distribution that occurs, and is defined as the ratio of the solute concentration within the gel to the concentration of the solute in the external solution:

$$K = \frac{C_{Gel}}{C_{Solution}} \tag{2.27}$$

The partitioning of a solute within a hydrogel will vary depending on a number of factors, including physical parameters such as the size and shape of the solute molecule, but also any chemical interactions that may occur between the hydrogel and the solute such as electrostatic, hydrophobic, and even biospecific interactions. These factors all contribute to the overall partition coefficient, and can be separated into individual partition coefficients as follows:

$$\ln K = \ln K_0 + \ln K_{size} + \ln K_{conf} + \ln K_{hphob} + \ln K_{electr} + \ln K_{biosp} \tag{2.28}$$

where the subscripts *size, conf, hphob, electr* and *biosp* indicate size and conformational effects, hydrophobic interactions, electrostatic interactions, and biospecific interactions, respectively.[119,120] K_0 is often used to describe any other interactions that may occur including hydrogen bonding, van der Waals forces, and even the effects of polymer concentration. The value of K can range from zero (meaning the solute is completely excluded from the hydrogel) to values well over 100. Large values of K are often a result of favorable interactions between the hydrogel and the solute, such as charged solutes that are attracted to an oppositely charged hydrogel network or solutes that are designed to interact with ligands built into the hydrogel network. When K =1, the solute concentration is equal in both of the phases.

One simple case of solute partitioning that is of particular interest in this dissertation is when there are no interactions between the gel and the solute and the partitioning is determined

based only on the size of the molecule. When this situation occurs it is often referred to as ideal size exclusion.[119] Size exclusion occurs due to entropic effects. As the size of the solutes increase or the pores between the polymer chains become smaller, a solute within the gel becomes more restricted and has fewer orientations available relative to free solution.[121] Because of this, solutes that might be small enough to enter into the hydrogel network may no longer partition into the hydrogel. Therefore, in ideal size exclusion, the partitioning is always between 0 and 1, and the value will depend on the size of the solute and the size of the pores in the network.

While the concept of size exclusion is relatively straightforward, it is often wrongly interpreted in drug delivery literature. Authors often make the assumption that because a large molecule is unable to partition into a hydrogel, the mesh size of the hydrogel must be smaller than the diameter or cross sectional area of the solute. In reality, the solute may actually be able to enter the pores of the hydrogel but does not only because of the reduction in orientational freedom that it would experience. At the same time, a hydrogel that has a calculated mesh size that is smaller than a given solute does not mean that the solute will be completely excluded from the hydrogel. Hydrogels are inherently heterogeneous and will have regions of higher and lower crosslink densities and mesh sizes. Additionally, under certain conditions the chemical potential of the solution outside of the hydrogel may change and affect the partitioning of the solute within the hydrogel. The partitioning and size exclusion of solutes in hydrogels is studied in Chapter 4, where the partitioning of ovalbumin and IgG is investigated in dextran and PEGDA hydrogels.

2.5 Hydrogels as Drug Delivery Vehicles

One of the most important applications of hydrogels is their use as drug delivery vehicles. Their high water content and mechanical properties are similar to that of the extracellular matrix, which provides a high degree of biocompatibility while at the same time allowing for the safe encapsulation of bioactive molecules.[1,11] They can be synthesized using a wide range of synthetic or biological materials and can be formed under mild conditions. Because of these many advantages, hydrogel based delivery devices have become a major area of research and have seen commercial success in ocular,[122,123] vaginal,[124-126] buccal,[127] and subcutaneous[128] applications.[129,130]

Controlling the rate of drug release from the gel is essential for a successful delivery device. The release of drugs from hydrogels can be controlled by a number of mechanisms that are often classified as:[12]

1) Chemically-controlled

2) Swelling-controlled

3) Diffusion-controlled

Drug delivery devices that are made up of chemically-controlled hydrogels release drugs at a rate that is dependent on the enzymatic or hydrolytic degradation of the hydrogel network. While this often involves bulk erosion of the hydrogel, it can also include a change of the binding equilibrium between the drug and drug-binding moiety of the hydrogel.[131] Hydrogels consisting of varying formulations of the polymers PEG and poly(lactic acid) have degradation rates that allow them to be used in several biomedical applications including the prevention of

postsurgical adhesion, and the controlled release of a number of proteins and oligonucleotides.[132,133]

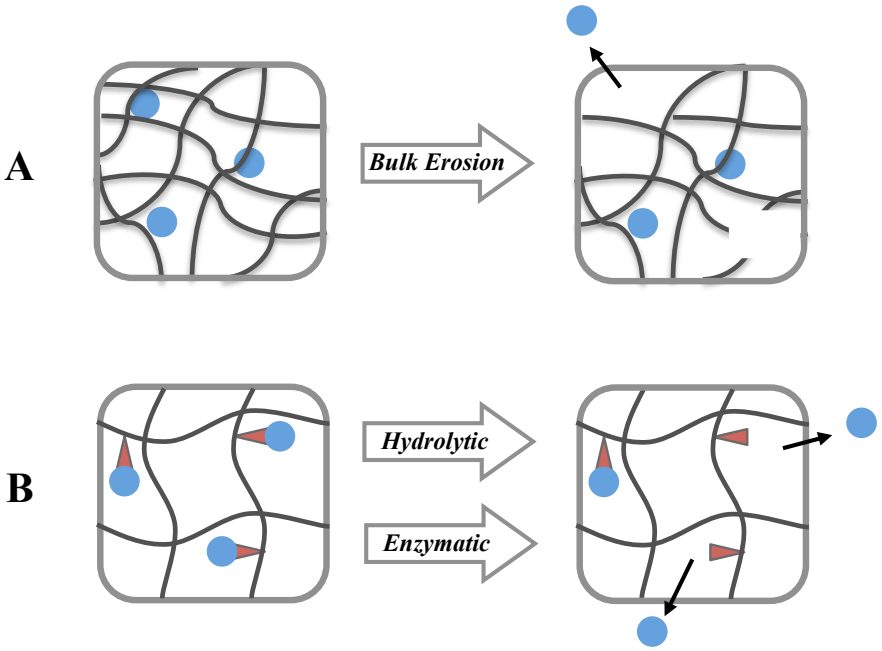

Figure 2.12. Chemically-controlled hydrogels can release drug through A) the bulk erosion of the hydrogel, and B) the hydrolytic or enzymatic degradation of drug-binding moieties that are attached to the network.

In swelling-controlled delivery devices, the release is controlled by the rate at which solvent molecules can penetrate the polymer matrix.[3] As the solvent penetrates the hydrogel, the network begins to swell which allows the drug to diffuse out of the hydrogel. Since the drug diffusion rate occurs at a faster rate than the rate of hydrogel swelling, a broad range of delivery times can be achieved by tuning the swelling rate of the hydrogel matrix. Swelling-controlled hydrogels have been used in a number of biomedical applications. Methocel®, a commercially available hydrogel that consists of hydroxypropyl methylcellulose and methylcelluluse, has been used to prepare swelling-controlled systems for oral drug delivery.[129] Another swelling-

controlled drug delivery system is Cervidil®, a hydrogel vaginal insert that releases the labor inducing drug dinoprostone.[124-126] The moist environment causes the hydrogel to swell and triggers the release.[130]

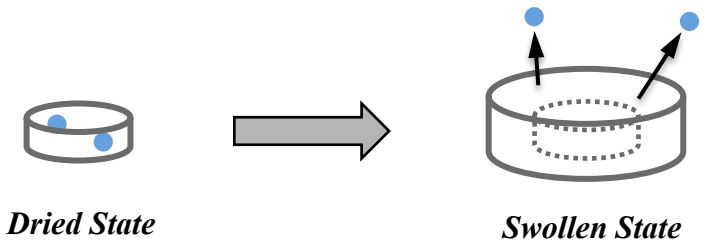

Figure 2.13 Schematic of a swelling-controlled hydrogel delivery device that releases drug as solvent molecules penetrate the gel and swell the network.

In diffusion-controlled devices, the release occurs due to the diffusion of drug through the hydrogel matrix. This movement of drug molecules can be described by Fick's law of diffusion:

$$j = -D\left(\frac{dC}{dx}\right) \tag{2.29}$$

where j is the flux, or rate of transfer per unit area of section, dC/dx is the concentration gradient of the diffusing drug, and D is the diffusion coefficient. The diffusion coefficient is a parameter that represents the transport of drug through the hydrogel network, and takes into account the size of the drug and the physical properties of the system through which it is diffusing. For a drug in solution, diffusion occurs as a result of the random motion of molecules (Brownian motion) in the absence of an external driving force.[119] This is often referred to as D_0, the diffusion coefficient of a drug in solution at infinite dilution. Values of D_0 for solutes in solution

can range from as high as 1.8×10^{-5} cm^2/s for smaller solutes like urea to as low as 4.0×10^{-7} cm^2/s for larger drugs like antibodies.[134,135]

In a hydrogel, the diffusive movement of drugs is restricted. There are several factors that affect the movement of drugs in a hydrogel network including the size of the solute, the amount of water in the network, the polymer concentration, and the polymer chain mobility. In certain cases, the existence of charged groups in the gel may also interact with the drug and reduce the mobility. In some cases, the diffusion coefficient within the hydrogel, D_g, will be so low that drugs are effectively trapped inside the hydrogel network. On the other hand, in highly swollen hydrogels the values of D_g will often approach values of D_0.

Out of the three mechanisms, the one that is most often applicable in hydrogel drug delivery devices is diffusion-controlled release.[131] Diffusion is almost always involved in controlling the release of drug from hydrogel delivery vehicles. In many hydrogels, drug diffusion is the only mechanism in which drug is released from the device. In other cases, diffusion plays a major role in combination with either polymer swelling or the degradation/erosion of the hydrogel network.[129,131,136-140] Much of the work in this dissertation focuses on hydrogel delivery vehicles where the release is controlled predominantly by diffusion. The diffusion of solutes in hydrogels is the primary focus of next chapter, where it discussed in greater detail.

REFERENCES

1. Hoare TR, Kohane DS 2008. Hydrogels in drug delivery: progress and challenges. Polymer 49(8):1993-2007.

2. Peppas NA. 1987. Hydrogels in medicine and pharmacy. ed.: CRC press Boca Raton, FL.

3. Peppas NA, Bures P, Leobandung W, Ichikawa H 2000. Hydrogels in pharmaceutical formulations. European Journal of Pharmaceutics and Biopharmaceutics 50(1):27-46.

4. Gupta P, Vermani K, Garg S 2002. Hydrogels: from controlled release to pH-responsive drug delivery. Drug Discovery Today 7(10):569-579.

5. Anseth KS, Bowman CN, BrannonPeppas L 1996. Mechanical properties of hydrogels and their experimental determination. Biomaterials 17(17):1647-1657.

6. Qiu Y, Park K 2001. Environment-sensitive hydrogels for drug delivery. Adv Drug Deliv Rev 53(3):321-339.

7. Gehrke SH. 2000. Synthesis and properties of hydrogels used for drug delivery. ed.: Marcel Dekker: New York.

8. Wichterle O, Lim D 1960. HYDROPHILIC GELS FOR BIOLOGICAL USE. Nature 185(4706):117-118.

9. Peppas NA, Hilt JZ, Khademhosseini A, Langer R 2006. Hydrogels in biology and medicine: From molecular principles to bionanotechnology. Advanced Materials 18(11):1345-1360.

10. Hoffman AS 2002. Hydrogels for biomedical applications. Adv Drug Deliv Rev 54(1):3-12.

11. Oh JK, Drumright R, Siegwart DJ, Matyjaszewski K 2008. The development of microgels/nanogels for drug delivery applications. Progress in Polymer Science 33(4):448-477.

12. Lin C-C, Metters AT 2006. Hydrogels in controlled release formulations: Network design and mathematical modeling. Adv Drug Deliv Rev 58(12-13):1379-1408.

13. Williams DF 2008. On the mechanisms of biocompatibility. Biomaterials 29(20):2941-2953.

14. Remunan-Lopez C, Portero A, Vila-Jato JL, Alonso MJ 1998. Design and evaluation of chitosan/ethylcellulose mucoadhesive bilayered devices for buccal drug delivery. Journal of Controlled Release 55(2-3):143-152.

15. Senel S, Ikinci G, Kas S, Yousefi-Rad A, Sargon MF, Hincal AA 2000. Chitosan films and hydrogels of chlorhexidine gluconate for oral mucosal delivery. International Journal of Pharmaceutics 193(2):197-203.

16. Drury JL, Mooney DJ 2003. Hydrogels for tissue engineering: scaffold design variables and applications. Biomaterials 24(24):4337-4351.

17. Bailey FJ. 2012. Poly (ethylene oxide). ed.: Elsevier.

18. Sedlak M 2005. Recent advances in chemistry and applications of substituted poly(ethylene glycol)s. Collect Czech Chem Commun 70(3):269-291.

19. Yamaoka T, Tabata Y, Ikada Y 1994. DISTRIBUTION AND TISSUE UPTAKE OF POLY(ETHYLENE GLYCOL) WITH DIFFERENT MOLECULAR-WEIGHTS AFTER INTRAVENOUS ADMINISTRATION TO MICE. Journal of Pharmaceutical Sciences 83(4):601-606.

20. Harris JM, Chess RB 2003. Effect of pegylation on pharmaceuticals. Nature Reviews Drug Discovery 2(3):214-221.

21. Knop K, Hoogenboom R, Fischer D, Schubert US 2010. Poly(ethylene glycol) in Drug Delivery: Pros and Cons as Well as Potential Alternatives. Angewandte Chemie-International Edition 49(36):6288-6308.

22. Tosatti S, De Paul SM, Askendal A, VandeVondele S, Hubbell JA, Tengvall P, Textor M 2003. Peptide functionalized poly(L-lysine)-g-poly(ethylene glycol) on titanium: resistance to protein adsorption in full heparinized human blood plasma. Biomaterials 24(27):4949-4958.

23. Balakrishnan B, Kumar DS, Yoshida Y, Jayakrishnan A 2005. Chemical modification of poly(vinyl chloride) resin using poly(ethylene glycol) to improve blood compatibility. Biomaterials 26(17):3495-3502.

24. Suggs LJ, West JL, Mikos AG 1999. Platelet adhesion on a bioresorbable poly(propylene fumarate-co-ethylene glycol) copolymer. Biomaterials 20(7):683-690.

25. Zurad EG, Johanson JF 2011. Over-the-counter laxative polyethylene glycol 3350: an evidence-based appraisal. Current Medical Research and Opinion 27(7):1439-1452.

26. Blume G, Cevc G 1990. LIPOSOMES FOR THE SUSTAINED DRUG RELEASE INVIVO. Biochimica Et Biophysica Acta 1029(1):91-97.

27. Kabanov AV, Chekhonin VP, Alakhov VY, Batrakova EV, Lebedev AS, Meliknubarov NS, Arzhakov SA, Levashov AV, Morozov GV, Severin ES, Kabanov VA 1989. THE

NEUROLEPTIC ACTIVITY OF HALOPERIDOL INCREASES AFTER ITS SOLUBILIZATION IN SURFACTANT MICELLES - MICELLES AS MICROCONTAINERS FOR DRUG TARGETING. Febs Letters 258(2):343-345.

28. Klibanov AL, Maruyama K, Torchilin VP, Huang L 1990. AMPHIPATHIC POLYETHYLENEGLYCOLS EFFECTIVELY PROLONG THE CIRCULATION TIME OF LIPOSOMES. Febs Letters 268(1):235-237.

29. Kwon GS, Kataoka K 1995. BLOCK-COPOLYMER MICELLES AS LONG-CIRCULATING DRUG VEHICLES. Adv Drug Deliv Rev 16(2-3):295-309.

30. Keys KB, Andreopoulos FM, Peppas NA 1998. Poly(ethylene glycol) star polymer hydrogels. Macromolecules 31(23):8149-8156.

31. Peppas NA, Keys KB, Torres-Lugo M, Lowman AM 1999. Poly(ethylene glycol)-containing hydrogels in drug delivery. Journal of Controlled Release 62(1-2):81-87.

32. Gillinov AM, Lytle BW 2001. A novel synthetic sealant to treat air leaks at cardiac reoperation. Journal of Cardiac Surgery 16(3):255-257.

33. Park Y, Lutolf MP, Hubbell JA, Hunziker EB, Wong M 2004. Bovine primary chondrocyte culture in synthetic matrix metalloproteinase-sensitive poly(ethylene glycol)-based hydrogels as a scaffold for cartilage repair. Tissue Eng 10(3-4):515-522.

34. Metters A, Hubbell J 2005. Network formation and degradation behavior of hydrogels formed by Michael-type addition reactions. Biomacromolecules 6(1):290-301.

35. Chludzin.Am, Germaine GR, Schachte.Cf 1974. PURIFICATION AND PROPERTIES OF DEXTRANSUCRASE FROM STREPTOCOCCUS-MUTANS. Journal of Bacteriology 118(1):1-7.

36. Leathers TD 2002. Dextran. Biopolymers Online.

37. Long DM, Sanchez L, Varco RL, Lillehei CW 1961. THE USE OF LOW MOLECULAR WEIGHT DEXTRAN AND SERUM ALBUMIN AS PLASMA EXPANDERS IN EXTRACORPOREAL CIRCULATION. Surgery 50(1):12-&.

38. Heinze T, Liebert T, Heublein B, Hornig S. 2006. Functional polymers based on dextran. Polysaccharides II, ed.: Springer. p 199-291.

39. Naessens M, Cerdobbel A, Soetaert W, Vandamme EJ 2005. Leuconostoc dextransucrase and dextran: production, properties and applications. Journal of Chemical Technology and Biotechnology 80(8):845-860.

40. de Belder D 1996. Medical application of dextran and its derivatives. Polysaccharides in Medicinal Applications New York, NY: Marcel Dekker:505-524.

41. Guggenheim B, Schroeder H 1967. Biochemical and morphological aspects of extracellular polysaccharides produced by cariogenic streptococci. Helvetica odontologica acta 11(2):131.

42. Zief M, Brunner G, Metzendor J 1956. Fractionation of partially hydrolyzed dextran. Industrial & Engineering Chemistry 48(1):119-121.

43. Holly FJ, Esquivel ED 1985. Colloid osmotic pressure of artificial tears. Journal of ocular pharmacology 1(4):327-336.

44. Mehvar R 2000. Dextrans for targeted and sustained delivery of therapeutic and imaging agents. Journal of controlled release 69(1):1-25.

45. Hatti-Kaul R 2001. Aqueous two-phase systems. Molecular biotechnology 19(3):269-277.

46. Jacobsson S, Jonsson L, Rank F, Rothman U 1976. Studies on healing of Debrisan-treated wounds. Scandinavian Journal of Plastic and Reconstructive Surgery and Hand Surgery 10(2):97-101.

47. Denizli BK, Can HK, Rzaev ZM, Guner A 2004. Preparation conditions and swelling equilibria of dextran hydrogels prepared by some crosslinking agents. Polymer 45(19):6431-6435.

48. Can HK, Denizli BK, Güner A, Rzaev ZM 2005. Effect of functional crosslinking agents on preparation and swelling properties of dextran hydrogels. Carbohydrate polymers 59(1):51-56.

49. Cadee JA, van Luyn MJA, Brouwer LA, Plantinga JA, van Wachem PB, de Groot CJ, den Otter W, Hennink WE 2000. In vivo biocompatibility of dextran-based hydrogels. Journal of Biomedical Materials Research 50(3):397-404.

50. Franssen O, van Ooijen RD, de Boer D, Maes RAA, Hennink WE 1999. Enzymatic degradation of cross-linked dextrans. Macromolecules 32(9):2896-2902.

51. Garg HG, Hales CA. 2004. Chemistry and biology of hyaluronan. ed.: Elsevier.

52. Shu XZ, Liu Y, Palumbo FS, Luo Y, Prestwich GD 2004. In situ crosslinkable hyaluronan hydrogels for tissue engineering. Biomaterials 25(7):1339-1348.

53. Necas J, Bartosikova L, Brauner P, Kolar J 2008. Hyaluronic acid (hyaluronan): a review. Veterinarni medicina 53(8):397-411.

54. Toole BP 2004. Hyaluronan: from extracellular glue to pericellular cue. Nature Reviews Cancer 4(7):528-539.

55. Fraser J, Laurent T, Laurent U 1997. Hyaluronan: its nature, distribution, functions and turnover. Journal of internal medicine 242(1):27-33.

56. Laurent TC, Fraser J 1992. Hyaluronan. The FASEB Journal 6(7):2397-2404.

57. Burdick JA, Prestwich GD 2011. Hyaluronic acid hydrogels for biomedical applications. Advanced materials 23(12):H41-H56.

58. Serban MA, Prestwich GD 2007. Synthesis of hyaluronan haloacetates and biology of novel cross-linker-free synthetic extracellular matrix hydrogels. Biomacromolecules 8(9):2821-2828.

59. Prestwich GD, Marecak DM, Marecek JF, Vercruysse KP, Ziebell MR 1998. Controlled chemical modification of hyaluronic acid: synthesis, applications, and biodegradation of hydrazide derivatives. J Control Release 53(1-3):93-103.

60. Darr A, Calabro A 2009. Synthesis and characterization of tyramine-based hyaluronan hydrogels. J Mater Sci-Mater Med 20(1):33-44.

61. Shu XZ, Liu YC, Luo Y, Roberts MC, Prestwich GD 2002. Disulfide cross-linked hyaluronan hydrogels. Biomacromolecules 3(6):1304-1311.

62. Burdick JA, Chung C, Jia XQ, Randolph MA, Langer R 2005. Controlled degradation and mechanical behavior of photopolymerized hyaluronic acid networks. Biomacromolecules 6(1):386-391.

63. Park KM, Yang JA, Jung H, Yeom J, Park JS, Park KH, Hoffman AS, Hahn SK, Kim K 2012. In Situ Supramolecular Assembly and Modular Modification of Hyaluronic Acid Hydrogels for 3D Cellular Engineering. ACS Nano 6(4):2960-2968.

64. Leach JB, Bivens KA, Patrick CW, Schmidt CE 2003. Photocrosslinked hyaluronic acid hydrogels: natural, biodegradable tissue engineering scaffolds. Biotechnology and bioengineering 82(5):578-589.

65. Barros SC, Martins JA, Marcos JC, Cavaco-Paulo A 2012. Influence of secretory leukocyte protease inhibitor-based peptides on elastase activity and their incorporation in hyaluronic acid hydrogels for chronic wound therapy. Biopolymers 98(6):576-590.

66. Hahn SK, Jelacic S, Maier RV, Stayton PS, Hoffman AS 2004. Anti-inflammatory drug delivery from hyaluronic acid hydrogels. J Biomater Sci-Polym Ed 15(9):1111-1119.

67. Motokawa K, Hahn SK, Nakamura T, Miyamoto H, Shimoboji T 2006. Selectively crosslinked hyaluronic acid hydrogels for sustained release formulation of erythropoietin. Journal of Biomedical Materials Research Part A 78A(3):459-465.

68. Kim MR, Park TG 2002. Temperature-responsive and degradable hyaluronic acid/Pluronic composite hydrogels for controlled release of human growth hormone. Journal of Controlled Release 80(1-3):69-77.

69. Colombani D 1997. Chain-growth control in free radical polymerization. Progress in Polymer Science 22(8):1649-1720.

70. Finch CA. 2013. Chemistry and technology of water-soluble polymers. ed.: Springer Science & Business Media.

71. Kulicke W, Nottelmann H 1989. Structure and swelling of some synthetic, semisynthetic, and biopolymer hydrogels. Adv Chem Ser 223:15-44.

72. Collins MN, Birkinshaw C 2008. Physical properties of crosslinked hyaluronic acid hydrogels. Journal of Materials Science: Materials in Medicine 19(11):3335-3343.

73. Ramamurthi A, Vesely I 2002. Smooth muscle cell adhesion on crosslinked hyaluronan gels. Journal of biomedical materials research 60(1):195-205.

74. Ibrahim S, Kang QK, Ramamurthi A 2010. The impact of hyaluronic acid oligomer content on physical, mechanical, and biologic properties of divinyl sulfone‐crosslinked hyaluronic acid hydrogels. Journal of Biomedical Materials Research Part A 94(2):355-370.

75. Ramamurthi A, Vesely I 2003. Ultraviolet light‐induced modification of crosslinked hyaluronan gels. Journal of Biomedical Materials Research Part A 66(2):317-329.

76. Lai JY 2014. Relationship between structure and cytocompatibility of divinyl sulfone cross-linked hyaluronic acid. Carbohydrate Polymers 101:203-212.

77. Kolb HC, Finn MG, Sharpless KB 2001. Click chemistry: Diverse chemical function from a few good reactions. Angew Chem-Int Edit 40(11):2004-+.

78. Moses JE, Moorhouse AD 2007. The growing applications of click chemistry. Chemical Society reviews 36(8):1249-1262.

79. Binder WH, Sachsenhofer R 2007. 'Click' Chemistry in Polymer and Materials Science. Macromolecular Rapid Communications 28(1):15-54.

80. Kolb HC, Sharpless KB 2003. The growing impact of click chemistry on drug discovery. Drug Discov Today 8(24):1128-1137.

81. Nandivada H, Jiang XW, Lahann J 2007. Click chemistry: Versatility and control in the hands of materials scientists. Adv Mater 19(17):2197-2208.

82. van Dijk M, Rijkers DTS, Liskamp RMJ, van Nostrum CF, Hennink WE 2009. Synthesis and Applications of Biomedical and Pharmaceutical Polymers via Click Chemistry Methodologies. Bioconjugate Chem 20(11):2001-2016.

83. Crescenzi V, Cornelio L, Di Meo C, Nardecchia S, Lamanna R 2007. Novel hydrogels via click chemistry: Synthesis and potential biomedical applications. Biomacromolecules 8(6):1844-1850.

84. Pahimanolis N, Vesterinen AH, Rich J, Seppala J 2010. Modification of dextran using click-chemistry approach in aqueous media. Carbohydr Polym 82(1):78-82.

85. Chang PV, Prescher JA, Sletten EM, Baskin JM, Miller IA, Agard NJ, Lo A, Bertozzi CR 2010. Copper-free click chemistry in living animals. Proc Natl Acad Sci U S A 107(5):1821-1826.

86. Posner T 1905. Information on unsaturated compounds II The addition of mercaptan to unsaturated hydrocarbon. Berichte Der Deutschen Chemischen Gesellschaft 38:646-657.

87. Hoyle CE, Bowman CN 2010. Thiol–ene click chemistry. Angewandte Chemie International Edition 49(9):1540-1573.

88. Kharasch M, MAY EM, MAYO FR 1938. The peroxide effect in the addition of reagents to unsaturated compounds. Xviii. The addition and substitution of bisulfite*. The Journal of Organic Chemistry 3(2):175-192.

89. Lowe AB 2010. Thiol-ene "click" reactions and recent applications in polymer and materials synthesis. Polymer Chemistry 1(1):17-36.

90. Hoyle CE, Lee TY, Roper T 2004. Thiol–enes: chemistry of the past with promise for the future. Journal of Polymer Science Part A: Polymer Chemistry 42(21):5301-5338.

91. Hoyle CE, Lowe AB, Bowman CN 2010. Thiol-click chemistry: a multifaceted toolbox for small molecule and polymer synthesis. Chemical Society Reviews 39(4):1355-1387.

92. Roper TM, Guymon C, Jönsson E, Hoyle C 2004. Influence of the alkene structure on the mechanism and kinetics of thiol–alkene photopolymerizations with real‐time infrared spectroscopy. Journal of Polymer Science Part A: Polymer Chemistry 42(24):6283-6298.

93. Mergy J, Fournier A, Hachet E, Auzely-Velty R 2012. Modification of polysaccharides via thiol-ene chemistry: A versatile route to functional biomaterials. J Polym Sci Pol Chem 50(19):4019-4028.

94. Gramlich WM, Kim IL, Burdick JA 2013. Synthesis and orthogonal photopatterning of hyaluronic acid hydrogels with thiol-norbornene chemistry. Biomaterials 34(38):9803-9811.

95. Shu XZ, Liu Y, Luo Y, Roberts MC, Prestwich GD 2002. Disulfide cross-linked hyaluronan hydrogels. Biomacromolecules 3(6):1304-1311.

96. Vanderhooft JL, Mann BK, Prestwich GD 2007. Synthesis and characterization of novel thiol-reactive poly (ethylene glycol) cross-linkers for extracellular-matrix-mimetic biomaterials. Biomacromolecules 8(9):2883-2889.

97. Shu XZ, Ahmad S, Liu Y, Prestwich GD 2006. Synthesis and evaluation of injectable, in situ crosslinkable synthetic extracellular matrices for tissue engineering. Journal of Biomedical Materials Research Part A 79(4):902-912.

98. Peppas NA, Merrill EW 1976. Poly (vinyl alcohol) hydrogels: Reinforcement of radiation‐crosslinked networks by crystallization. Journal of Polymer Science: Polymer Chemistry Edition 14(2):441-457.

99. Sanabria-DeLong N, Crosby AJ, Tew GN 2008. Photo-cross-linked PLA-PEO-PLA hydrogels from self-assembled physical networks: mechanical properties and influence of assumed constitutive relationships. Biomacromolecules 9(10):2784-2791.

100. Urayama K, Takigawa T, Masuda T 1993. POISSON RATIO OF POLY(VINYL ALCOHOL) GELS. Macromolecules 26(12):3092-3096.

101. Horgan CO 2015. The remarkable Gent constitutive model for hyperelastic materials. International Journal of Non-Linear Mechanics 68:9-16.

102. Li J, Suo Z, Vlassak JJ 2014. A model of ideal elastomeric gels for polyelectrolyte gels. Soft matter 10(15):2582-2590.

103. Mansur HS, Oréfice RL, Mansur AA 2004. Characterization of poly (vinyl alcohol)/poly (ethylene glycol) hydrogels and PVA-derived hybrids by small-angle X-ray scattering and FTIR spectroscopy. Polymer 45(21):7193-7202.

104. Lin-Gibson S, Jones RL, Washburn NR, Horkay F 2005. Structure-property relationships of photopolymerizable poly (ethylene glycol) dimethacrylate hydrogels. Macromolecules 38(7):2897-2902.

105. Canal T, Peppas N. Proceed Intern Symp Control Rel Bioactiv Mater, 1988, pp 19-20.

106. Canal T, Peppas NA 1989. Correlation between mesh size and equilibrium degree of swelling of polymeric networks. Journal of Biomedical Materials Research 23(10):1183-1193.

107. De Gennes P-G. 1979. Scaling concepts in polymer physics. ed.: Cornell university press.

108. Teraoka I. Polymer solutions: An introduction to physical properties 2002. ed.: Wiley-Interscience.

109. Liu R, Gao X, Oppermann W 2006. Dynamic light scattering studies on random cross-linking of polystyrene in semi-dilute solution. Polymer 47(26):8488-8494.

110. Seiffert S, Oppermann W 2008. Diffusion of linear macromolecules and spherical particles in semidilute polymer solutions and polymer networks. Polymer 49(19):4115-4126.

111. Yu Y, Chau Y 2015. Formulation of In Situ Chemically Cross-Linked Hydrogel Depots for Protein Release: From the Blob Model Perspective. Biomacromolecules 16(1):56-65.

112. Cruise GM, Scharp DS, Hubbell JA 1998. Characterization of permeability and network structure of interfacially photopolymerized poly(ethylene glycol) diacrylate hydrogels. Biomaterials 19(14):1287-1294.

113. Ratner B 1989. Biomedical applications of synthetic polymers. Pergamon Press plc, Comprehensive Polymer Science 7:201-247.

114. Okay O 2000. Macroporous copolymer networks. Progress in Polymer Science 25(6):711-779.

115. Feil H, Bae YH, Feijen J, Kim SW 1991. MOLECULAR SEPARATION BY THERMOSENSITIVE HYDROGEL MEMBRANES. Journal of Membrane Science 64(3):283-294.

116. Dai WS, Barbari TA 1999. Hydrogel membranes with mesh size asymmetry based on the gradient crosslinking of poly(vinyl alcohol). Journal of Membrane Science 156(1):67-79.

117. Hwang CM, Sant S, Masaeli M, Kachouie NN, Zamanian B, Lee SH, Khademhosseini A 2010. Fabrication of three-dimensional porous cell-laden hydrogel for tissue engineering. Biofabrication 2(3).

118. Nguyen KT, West JL 2002. Photopolymerizable hydrogels for tissue engineering applications. Biomaterials 23(22):4307-4314.

119. Gehrke SH, Fisher JP, Palasis M, Lund ME 1997. Factors determining hydrogel permeability. Annals of the New York Academy of Sciences 831(1):179-184.

120. Walter H. 2012. Partitioning In Aqueous Two–Phase System: Theory, Methods, Uses, And Applications To Biotechnology. ed.: Elsevier.

121. Amidon GL, Lee PI, Topp EM. 1999. Transport processes in pharmaceutical systems. ed.: CRC Press.

122. Sawhney AS, Jarrett P, Bassett M, Blizzard C. 2013. Drug delivery through hydrogel plugs. ed.: Google Patents.

123. Masket S, Hovanesian JA, Levenson J, Tyson F, Flynn W, Endl M, Majmudar PA, Modi S, Chu R, Raizman MB, Lane SS, Kim T 2014. Hydrogel sealant versus sutures to prevent fluid egress after cataract surgery. Journal of Cataract and Refractive Surgery 40(12):2057-2066.

124. Mozurkewich EL, Chilimigras JL, Berman DR, Perni UC, Romero VC, King VJ, Keeton KL 2011. Methods of induction of labour: a systematic review. Bmc Pregnancy and Childbirth 11.

125. Almomen A, Cho S, Yang C-H, Li Z, Jarboe EA, Peterson CM, Huh KM, Janat-Amsbury MM 2015. Thermosensitive Progesterone Hydrogel: A Safe and Effective New Formulation for Vaginal Application. Pharmaceutical Research 32(7):2266-2279.

126. Ewert K, Powers B, Robertson S, Alfirevic Z 2006. Controlled-release misoprostol vaginal insert in parous women for labor induction: a randomized controlled trial. Obstetrics & Gynecology 108(5):1130-1137.

127. Halliday JA, Robertson S 2008. Pilocarpine Buccal Insert. DRUGS AND THE PHARMACEUTICAL SCIENCES 183:75.

128. Miller BS, Shukla AR 2010. Sterile Abscess Formation in Response to Two Separate Long-Acting Gonadotropin-Releasing Hormone Agonists, Supprelin LA (R) and Lupron Depot-Ped (R). Endocrine Reviews 31(3).

129. Colombo P 1993. Swelling-controlled release in hydrogel matrices for oral route. Advanced Drug Delivery Reviews 11(1):37-57.

130. Caló E, Khutoryanskiy VV 2015. Biomedical applications of hydrogels: a review of patents and commercial products. European Polymer Journal 65:252-267.

131. Siepmann J, Siepmann F 2012. Modeling of diffusion controlled drug delivery. Journal of Controlled Release 161(2):351-362.

132. Hill-West JL, Dunn RC, Hubbell JA 1995. Local release of fibrinolytic agents for adhesion prevention. Journal of Surgical Research 59(6):759-763.

133. Anseth KS, Metters AT, Bryant SJ, Martens PJ, Elisseeff JH, Bowman CN 2002. In situ forming degradable networks and their application in tissue engineering and drug delivery. Journal of controlled release 78(1):199-209.

134. Tyn MT, Gusek TW 1990. Prediction of diffusion coefficients of proteins. Biotechnology and bioengineering 35(4):327-338.

135. White ML, Dorion GH 1961. Diffusion in a crosslinked acrylamide polymer gel. Journal of Polymer Science 55(162):731-740.

136. Siepmann J, Podual K, Sriwongjanya M, Peppas N, Bodmeier R 1999. A new model describing the swelling and drug release kinetics from hydroxypropyl methylcellulose tablets. Journal of pharmaceutical sciences 88(1):65-72.

137. Hoffman AS 2012. Hydrogels for biomedical applications. Advanced drug delivery reviews 64:18-23.

138. Jeong B, Bae YH, Kim SW 2000. Drug release from biodegradable injectable thermosensitive hydrogel of PEG–PLGA–PEG triblock copolymers. Journal of controlled release 63(1):155-163.

139. Franssen O, Vandervennet L, Roders P, Hennink W 1999. Degradable dextran hydrogels: controlled release of a model protein from cylinders and microspheres. Journal of controlled release 60(2):211-221.

140. Peppas NA, Khare AR 1993. Preparation, structure and diffusional behavior of hydrogels in controlled release. Advanced drug delivery reviews 11(1):1-35.

Chapter 3: Modeling The Diffusion Of Solutes In Hydrogels

3.1 Introduction

The diffusion of solutes in hydrogels is an important area of study that is directly relevant to a number of research fields, including drug delivery, tissue engineering, and separation processes. In drug delivery, understanding the diffusive properties of solutes within a hydrogel is crucial for designing controlled release devices that are able to provide the correct release rate and profile to be therapeutically effective.[1,2] The diffusion of solutes in hydrogels is also critical in tissue engineering and in the development of artificial organs, where the survival of encapsulated cells requires the diffusion of oxygen, glucose, and nutrients while minimizing the diffusion of immunoglobulins and cytokines that might trigger an immune response.[3-5] Hydrogels are also used as membranes in many biological and biomedical applications, such as plasmapheresis, where the diffusion of solutes is critical in achieving accurate separations.[6,7] In all of these applications, a fundamental understanding of the diffusion of solutes through hydrogels and the important variables that govern this diffusion is essential.

Given how essential it is to control the release of solutes from a hydrogel, a number of theoretical models have been developed that attempt to relate the diffusion coefficient to the key parameters of a hydrogel. The majority of these models compare the relationship between the diffusivity of drugs in hydrogels to the diffusivity in solution, taking the general form:

$$\frac{D_g}{D_0} = f(r_s, \phi) \tag{3.2}$$

where D_g is the diffusion coefficient within the hydrogel, D_0, the diffusion coefficient of a drug in solution at infinite dilution, r_s is the size of the drug that is being delivered, and ϕ is the polymer volume fraction of the hydrogel. Various models also include more specific parameters related to the hydrogel network, including the molecular weight between crosslinks, the correlation length, and the fiber radius of the polymer chains.

In all of the models the normalized diffusion coefficient, D_g/D_0, decreases as the radius of the solute increases, and as the polymer volume fraction decreases.[8-10]

While all of the models share this same trend, the models differ in exactly how or why D_g/D_0 changes as the radius of the solute changes or hydrogel network changes. The models can be separated into three separate categories that each uses a different phenomenon to describe the hindered diffusion of solutes through hydrogels. Free volume theories suggest that the diffusion of solutes is restricted in hydrogels due to a reduction in free volume within the polymer space. On the other hand, obstruction models suggest that diffusion is restricted due to the polymer chains acting as physical obstructions that increase the length the drug has to travel.[11] Lastly, hydrodynamic models suggest that the tight pores that the solutes must diffuse through increases the hydrodynamic drag on the molecule and slows the diffusion.

The majority of these models have been around for over 20 years. The models were first reviewed by Muhr and Blanshard in 1981.[12] Amsden then expanded upon this work in 1998 where he reviewed the most recent work and tested the various models against literature data.[11] Since that time, very few models have been developed and the focus in literature has shifted to determining which models are best suited to use for a given hydrogel. This has proven to be difficult, as the large number of materials and synthesis methods available to form hydrogels has led to a wide range of properties and network structures.

In both of the reviews mentioned earlier, the authors separate hydrogels into two distinctive groups depending on their structure. The first group was classified as homogenous hydrogels and is made up of hydrogels whose chains have a high degree of mobility and exhibit a more random distribution within the network. Examples of hydrogels that the authors classified as homogenous included poly(ethylene glycol) (PEG), poly(acrylamide), poly(vinyl alcohol) (PVA), dextran, and hydroxypropyl methycellulose. The second group, classified as heterogeneous hydrogels, involves hydrogels whose chains are often assumed to be completely immobile and exhibit a high degree of inter-polymer interactions such as calcium alginate and agarose hydrogels.[13] One of the assumptions made in the reviews is that the chain mobility of the hydrogel determines which models are more suitable in predicting the diffusion coefficient. This is due to the fact that in many of the diffusion models, the gel structure is often assumed to have some idealized defined geometry such as a series of random impenetrable fibers, or tortuous cylindrical rods that connect the two surfaces.

However, recent research has shown that not only do many hydrogels not fit neatly into these two categories, but also that many of the models have proven to be effective at modeling the diffusion of solutes in both homogeneous and heterogeneous hydrogels. For example, Zhang

and Amsden have shown that for polymer solutions, the polymer chains can actually be considered immobile when the time frame of solute diffusion is considered, an assumption that is made into many of the obstruction models.[14] Waters and Frank followed up on this work and showed that these obstruction models were in fact accurate in modeling the diffusion of solutes from PEG/poly(acrylic acid) hydrogels, a network that is believed to contain polymer chains with a high degree of mobility.[15] Recent modeling work performed by Quesada-Pérez also explored how the stiffness of chains affected an obstruction model. By using Monte Carlo simulations, they showed that the model was unaffected by chain stiffness and gave identical results for polymer chains that were rigid, semi-rigid, and even flexible. They concluded that even though the model was developed around rigid fibers, the model is suitable for hydrogels with flexible polymer chains.[16]

Despite this recent work, one area that has received little attention in the literature is how the models perform under conditions where the diffusion coefficient in hydrogels is projected to be very small, with values below 10^{-10} cm^2/s. These low values are achieved as the polymer volume fraction of the gel increases, or as the size of the solute increases. Under these conditions, it is hypothesized that the size of the solute approaches the average mesh size of the hydrogel, causing a dramatic reduction in the diffusion coefficient. In this dissertation, this hypothesized reduction is referred to as the screening effect. Unfortunately, there are very few studies with hydrogels that display these screening effects. Figure 3.1 shows the diffusion of bovine serum albumin (BSA) within various types of hydrogels that have been reported in literature. Only one study, the release of BSA from dextran hydrogels, includes hydrogels with a polymer volume fraction above 0.15. In all of the other studies, the diffusion was studied in hydrogels with polymer volume fractions less than 0.1, and resulted in diffusion coefficients that

were all higher than 6.0 x 10^{-10} cm^2/s. The diffusion of IgG, an even larger solute, in hydrogels produces a similar figure, as few studies have been done at polymer volume fractions above 0.10.

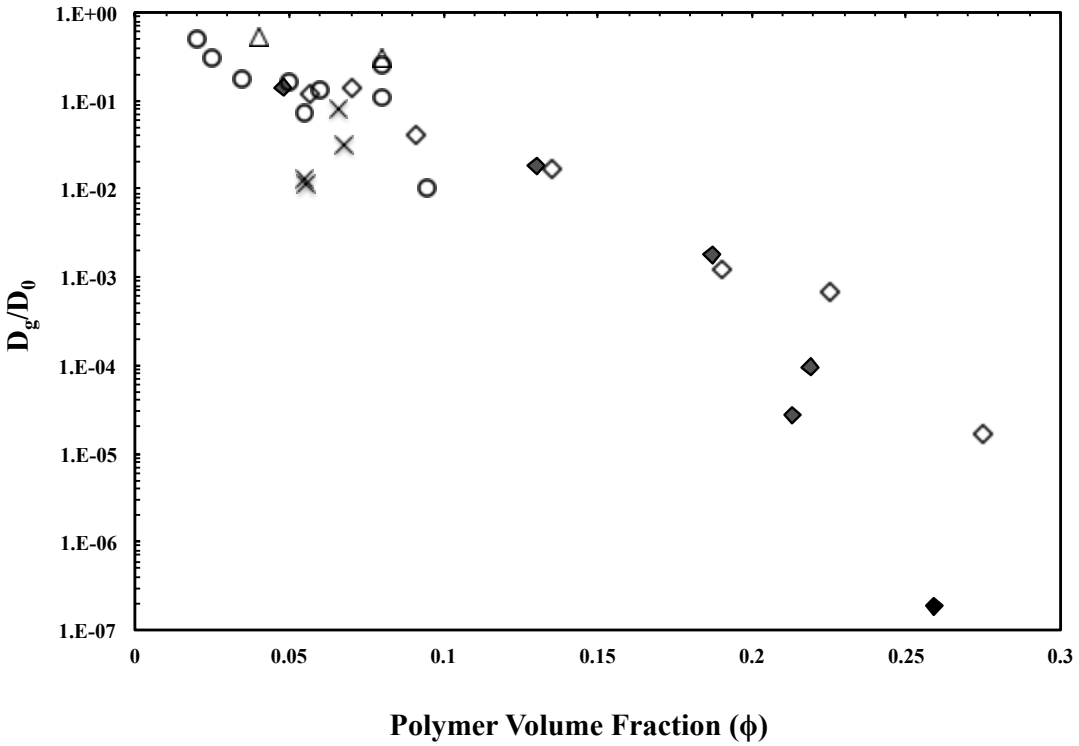

Figure 3.1. The diffusion coefficients of BSA in various hydrogels over a range of polymer volume fractions. (O) = polyacrylamide hydrogels[17], (Δ) = agarose hydrogels[18], (◇) = dextran hydrogels (◆ - represents dextran gels with a higher degree of substitution)[19], (X) = PEG hydrogels[20]

There are a number of reasons for the limited amount of work seen in literature on solute diffusion in hydrogels with low diffusion coefficients. In order to achieve this hypothesized screening effect, either the radius of the solute must be large, the polymer volume fraction must be high (which correlates with a smaller mesh size), or some combination of the two. The larger the solute size, the lower the polymer volume fraction needed to observe the screening effect. As

the solute size decreases, a larger polymer volume fraction is needed to observe the screening effect. Evidence of this is seen in the release of solutes from dextran gels. The screening effects of IgG (r_s = 5.35 nm[21]) were observed at polymer volume fractions as low as 0.17, while the screening effects in BSA (r_s = 3.63 nm[22]) were seen at 0.20, and lysozyme (r_s = 2.05 nm[22]) was as high as 0.29.[19] For some small solutes, such as caffeine (r_s = 0.525[23]), screening effects are not seen in hydrogels, even with polymer volume fractions as high as 0.48.[23] In some cases, the solubility of the polymers,[15] the polymer's degree of functionalization,[24] or the crosslinking method[25,26] limits the ability to produce hydrogels with a polymer volume fraction that is high enough to observe the screening effect. Another reason for the limited amount of work seen in literature is the difficulty in measuring diffusion coefficients at such low values in hydrogels. The small diffusion coefficient lowers the release rates from hydrogels, making measurements difficult as concentrations are often below the detection limit[27] or take too long to build up to the detection limit within the time period studied.[19,27]

Despite the limited amount of work in literature, the diffusion of solutes in hydrogels with low diffusion coefficients is an important area of study that has major implications in drug delivery and tissue engineering. The development of recombinant protein technology has introduced a number of large protein and peptide therapeutics that are used in the treatment of cancer, autoimmune diseases, and viral infections. There are a number of situations where long term, local delivery systems are needed to deliver these therapeutic proteins. A number of researchers have examined the use of hydrogels for sustained delivery of therapeutics to the eye,[28,29] in the treatment of chronic arthritic pain,[30,31] and for delivering chemotherapeutics to tumors.[32-34] In all of these applications achieving a low diffusion coefficient requires a hydrogel

with a low swelling degree. The large size of the therapeutics being delivered will begin to approach the mesh size of the hydrogel where the screening effect is hypothesized to occur.

Developing models for hydrogels that accurately describe the diffusion in this region is important not only for making predictions, but also in developing an understanding of how the key parameters such as swelling degree, solute size, and crosslink density play a role in diffusion. Therefore, because of its importance in this dissertation and the literature, this chapter reviews a number of theories that describe the diffusion of solutes within hydrogels, specifically focusing on how the models predict the diffusion of large solutes in hydrogels with low swelling degrees.

3.2 Diffusion Models

In this section three main categories of diffusion models are reviewed: free volume theories, hydrodynamic models, and obstruction models. While these theories have been reviewed extensively before, the focus in those reviews was on hydrogels with a lower polymer volume fraction and diffusion coefficients greater than 10^{-10} cm^2/s. Therefore, this section focuses on diffusion of large solutes at low swelling degrees where the screening effect is hypothesized to occur. The models are displayed with data from literature that comes from a study by Hennink et al. on the diffusion of BSA in dextran hydrogels.[19] This data set was used because:

1) It provided the largest range of polymer volume fractions
2) It is one of the only papers in literature with values of $D < 10^{-10}$ cm^2/s
3) Dextran hydrogels (and similar polysaccharide hydrogels) are used throughout this dissertation and the physical properties of the polymer are well known.

The goal of this section was not to determine how accurate each of the models are in fitting the selected data but rather to examine how these models predict diffusion coefficients at low swelling degrees and determine the key parameters that influence each of the models in this region.

3.2.1 Free Volume Theory

The free volume theory used to describe the diffusion in hydrogels is based on the theory developed by Cohen and Turnbull to explain the diffusion of molecules in solution. The theory assumes that solutes diffuse by jumping into the voids, or free volume, within the liquid.[35] These voids are formed at a molecular level due to packing irregularities, excluded volume effects, and the movement of neighboring liquid molecules due to Brownian motion. The diffusion can only occur if the solute has enough energy to overcome the translational barrier required to jump to the new void. The diffusion also hinges on the probability that there is a space large enough for the solute to jump, and the distance needed to jump to this new space. This can be expressed mathematically by the equation:

$$D_0 = V \lambda \exp\left(-\frac{\gamma v^*}{v_f}\right) \tag{3.3}$$

where V is the average thermal velocity, λ is the jump length that is roughly equivalent to the diameter of the solute, v^* is the required amount of free volume required for the solute to jump into a new hole, defined as $v^* = \lambda \pi r_s^2$, γ is a geometric correction factor that takes into account

the overlap of free volume for multiple solvent molecules, and v_f is the average free volume that is available in the liquid.[11]

This model was then applied by Yasuda et al. to describe the diffusion of solutes within a hydrogel.[36] The free volume in the gel is the sum of the free volumes of both the polymer itself, and the water within the polymer, given as:

$$v_f = (1-\phi)\, v_{f,w} + \varphi v_{f,p} \tag{3.4}$$

in which ϕ is the volume fraction of polymer in the gel ($\phi = 1/Q$), $v_{f,w}$ is the free volume per molecule of the water, and $v_{f,p}$ is the free volume per molecule of polymer. One of the assumptions in developing the model was that the free volume per molecule of polymer was very small, leading to:

$$v_f = (1-\phi)\, v_{f,w} \tag{3.5}$$

In other words, the diffusion was assumed to occur only within the water-filled regions of the hydrogel. The model also has to take into account the fact that a jump can only be made if there is an opening in the polymer network that is large enough for the solute to pass through. When this is taken into consideration, the diffusion of a solute within a hydrogel can be written as:

$$\frac{D_g}{D_0} = P_0 \exp\left(-\frac{Ba^*}{v_{f,w}}\left(\frac{\phi}{1-\phi}\right)\right) \tag{3.6}$$

wherein $B = \gamma \lambda$, and a* is the effective cross-sectional area of the solute molecule. P_0 is the sieving probability and represents the chances of finding an opening within the polymer chains. Essentially, P_0 is the way in which the model takes into consideration the screening effect. The

sieving probability can range in value from zero to one. When the solute is much smaller than the openings in the polymer chains P_0 can be taken as unity. Yasuda et al. mentions that, on the other hand, in certain cases large molecules might be rejected from the network because there are no appropriate sized holes within the network, meaning $P_0 = 0$. In the original paper,[36] this sieving function is described as:

$$P_0(a) = \int_{a^*}^{\infty} f(a)\, da \tag{3.7}$$

where $P_0(a)$ is the probability of a solute passing through a given hole in the mesh, and f(a) is the hole area distribution function. In other words, the probability of a solute of size a* diffusing into the hydrogel is based on how many holes are available in the mesh that are large enough for it to pass through. The difficulty in this approach is determining the hole area distribution function, f(a), for a given hydrogel. As the polymer volume fraction increases, the average hole size will decrease and there will be a smaller number of holes that are large enough to diffuse through. Yasuda presented a number of simple distribution functions that might accurately describe f(a) for a hydrogel, yet none of them were based on data.

In Figure 3.2 the Yasuda free volume theory is plotted against data from literature in which the diffusion coefficient of BSA was released from dextran hydrogels.[19] The dashed line represents Equation 3.6 when P_0 is equal to one and no sieving effects are taken into consideration. Under these conditions the model does an excellent job of correlating the data at high swelling degrees. This is due to the fact that the constant, $Ba^*/v_{f,w}$, was set at a value of 26.2 that has been shown by Amsden to give the best fit to the data at polymer volume fractions below 0.2.[11] However, as ϕ approaches 0.2, the data begins to deviate from the model's predictions. The difficulty in using the sieving probability function developed by Yasuda et al. is

in determining how to represent f(a). While many simple functions are available it is difficult to relate this function to measurable properties of a hydrogel.

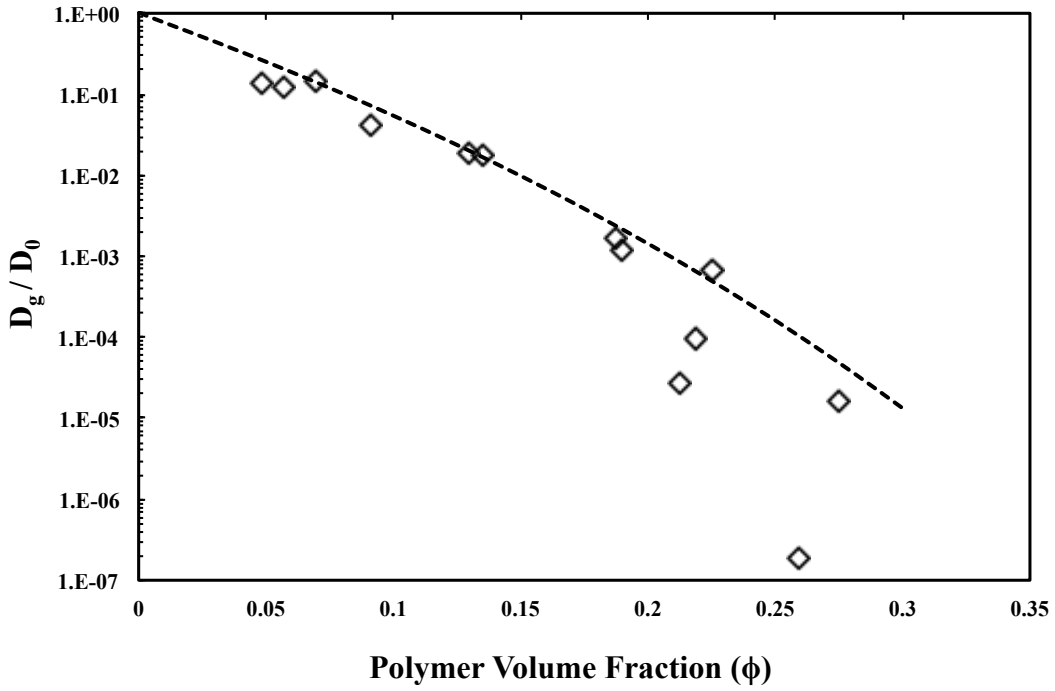

Figure 2. The application of the Yasuda free volume theory to literature data on the diffusion of BSA in dextran hydrogels. The dashed line represents the condition in which $P_0 = 1$ and $Ba^*/v_{f,w} = 26.2$

A number of variations of the Yasuda free volume theory have been developed. The most commonly used variation is the model developed by Reinhart and Peppas, which is given as:

$$\frac{D_g}{D_0} = k_1 \left(\frac{\bar{M}_c - \bar{M}_c^*}{\bar{M}_n - \bar{M}_c^*} \right) \exp\left(- k_2 r_s^2 \left(\frac{\phi}{1-\phi} \right) \right) \qquad (3.7)$$

in which k_1 is a fitting parameter that depend on the polymer-solvent system being used, $k_2 = \gamma \lambda \pi/v_{f,w}$, r_s is the radius of the solute, $\overline{M}_c$ is the number average molecular weight between the polymer crosslinks, $\overline{M}_c^*$ is the critical molecular weight between crosslinks that occurs at the point where the solute is no longer allowed to pass through, and $\overline{M}_n$ is the number average molecular weight of the uncrosslinked polymer.[37]

Similar to Yasuda's original model, the sieving effect is determined by the probability of finding holes within the hydrogel mesh that are large enough for a solute to pass through. This probability is represented by the sieving term, which is defined as:

$$p(r_s) = \left(\frac{\overline{M}_c - \overline{M}_c^*}{\overline{M}_n - \overline{M}_c^*} \right) \tag{3.8}$$

Despite using this model to describe the diffusion within poly(vinyl alcohol)/poly(acrylic acid) interpenetrating networks,[38] they have also suggested that the sieving term might be more accurately expressed as:[39]

$$p(r_s) = \left(\frac{\overline{M}_c - \overline{M}_c^*}{\overline{M}_n - \overline{M}_c^*} \right)^2 \tag{3.9}$$

Unlike Yasuda et al., Reinhart and Peppas relate this probability to physical parameters of the hydrogel. They assume that the cross sectional area of the holes within a hydrogel is proportional to the mesh size of an ideal tetrafunctional mesh.[37] This area is directly related to the number average molecular weight between the polymer crosslinks, $\overline{M}_c$, a parameter that can be determined from either swelling or mechanical testing. In Equation 3.8, the value of $\overline{M}_c$ is compared to both $\overline{M}_c^*$ and $\overline{M}_n$. $\overline{M}_n$ is the number average molecular weight of the uncrosslinked polymer and represents the largest mesh size that is possible for a given hydrogel. When $\overline{M}_c$ =

$\bar{M}_n$, the sieving function should be equal to 1, as the mesh size of the hydrogel is large and no screening effects should be seen. $\bar{M}_c^*$ is the critical molecular weight that represents the point at which the mesh size is so small that solutes are unable to pass through. When $\bar{M}_c \leq \bar{M}_c^*$, the solute is no longer able to penetrate the mesh and the sieving function is equal to 0.

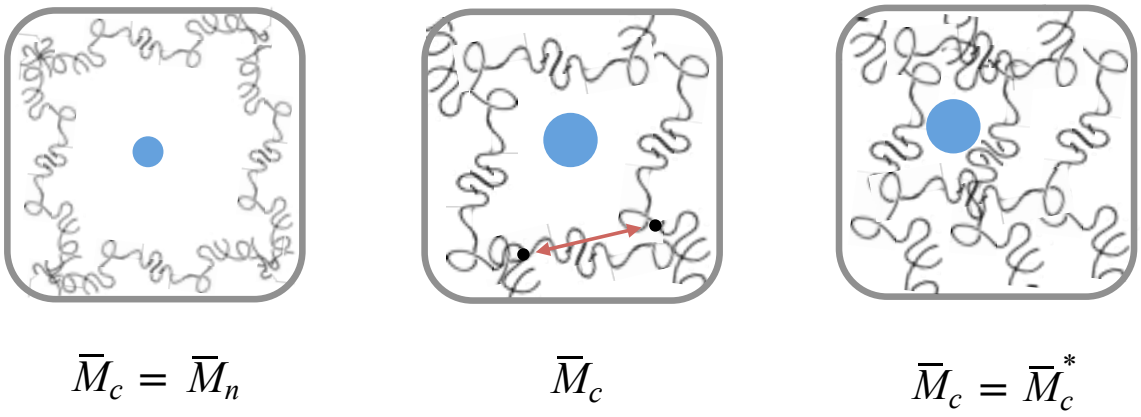

Figure 3.3. A schematic representing the range of sizes for $\bar{M}_c$, the number average molecular weight between crosslinks in a hydrogel that are used to calculate the sieving term in Equations 3.8 and 3.9. $\bar{M}_n$ is the number average molecular weight of the uncrosslinked polymer and represents the largest mesh size that is possible for a given hydrogel. $\bar{M}_c^*$ is the critical molecular weight at which point the mesh size is so small that solutes are unable to pass through.

The Reinhart and Peppas model using Equation 3.7 is shown in Figure 3.4. The constant k_2 was at 0.017, a value that Amsden determined fit the data best in his review.[11] In that review, Amsden did not use the sieving terms, so the fitting parameter k_1 was set at 2.0. Varying k_1 shifts the data set up or down, and at a k_1= 2.0 the normalized diffusion coefficient was equal to zero at a polymer volume fraction of zero. In Figure 3.4, $\bar{M}_c^*$ was varied from 800-

2000 g/mol. In each of the curves, at the point when $\overline{M}_c^*$ reaches the $\overline{M}_c$ of the gel, the diffusion coefficient is predicted to be to zero. This is due to the fact that, as $\overline{M}_c$ drops below $\overline{M}_c^*$, the value of $\left(\frac{\overline{M}_c - \overline{M}_c^*}{\overline{M}_n - \overline{M}_c^*}\right)$ becomes negative. In Equation 3.7, this causes the normalized diffusion coefficient to also become negative, a limitation of the model. The assumption was made that at this point the sieving term effectively goes to zero and that solutes are no longer able to diffuse into the hydrogel.

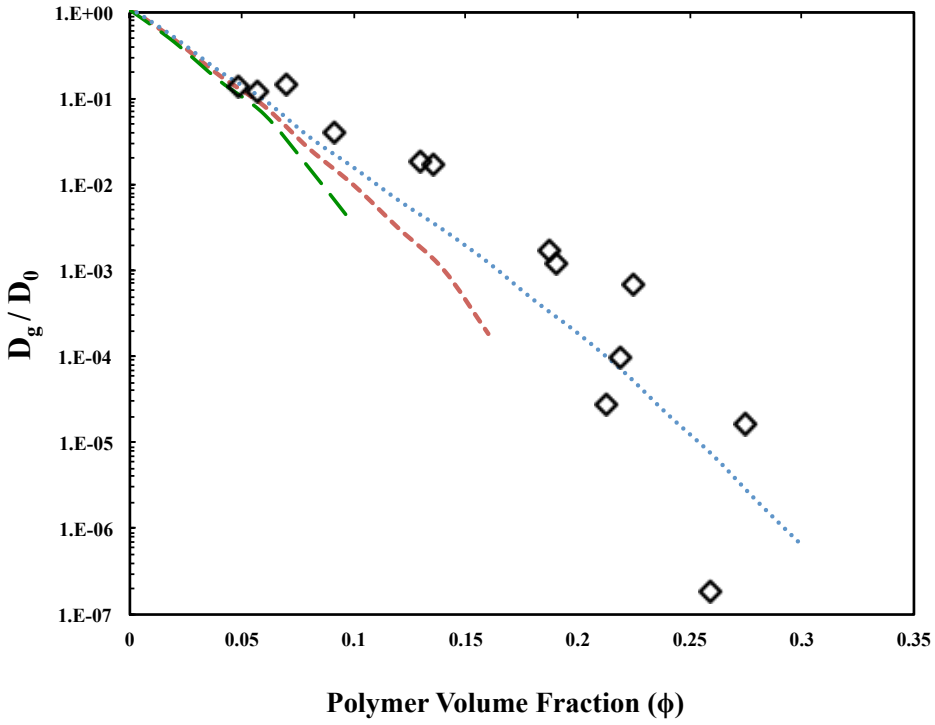

Figure 3.4. The application of the Reinhart Peppas model to literature data on the diffusion of BSA in dextran hydrogels. The value of $\overline{M}_c$ was calculated based on data from ref[19]
k_1 =2, k_2 =0.017, M_n =16,700, (·····) $\overline{M}_c^*$ = 2000, (— –) $\overline{M}_c^*$ = 1400, (-----) $\overline{M}_c^*$ = 800.

Figure 3.4 shows that the Reinhart and Peppas model is heavily reliant on an accurate value of $\overline{M}_c^*$. Because of the way the model is set up, as soon as $\overline{M}_c$ drops below $\overline{M}_c^*$ the diffusion coefficient instantly goes to zero. The value of $\overline{M}_c^*$ will depend on both the hydrogel and the solute being studied, and must be determined experimentally before making any predictions. The theory also makes the large assumption that the holes within the mesh of the hydrogel are all uniform and have a single relevant length scale. In reality, there will be a distribution of hole sizes and a distribution of values for $\overline{M}_c$. Because of this distribution, sharp drops like the one seen in Figure 3.4 are unrealistic.

The Reinhart and Peppas model using Equation 3.9 is shown in Figure 3.5. By using Equation 3.13 the sharp drop-off that is seen in Figure 3.4 is eliminated. This is due to the fact that, as $\overline{M}_c$ drops below $\overline{M}_c^*$, the value of $\left(\frac{\overline{M}_c - \overline{M}_c^*}{\overline{M}_n - \overline{M}_c^*}\right)$ becomes negative. Unlike in Equation 3.7, in Equation 3.9, this negative term is squared which allows the normalized diffusion coefficient to remain positive. This is a limitation in the model, as the sieving term actually increases once the value of $\overline{M}_c$ drops below $\overline{M}_c^*$. In reality, when $\overline{M}_c$ drops below $\overline{M}_c^*$ the theory predicts that the sieving term should decrease, yet this is not reflected in the model.

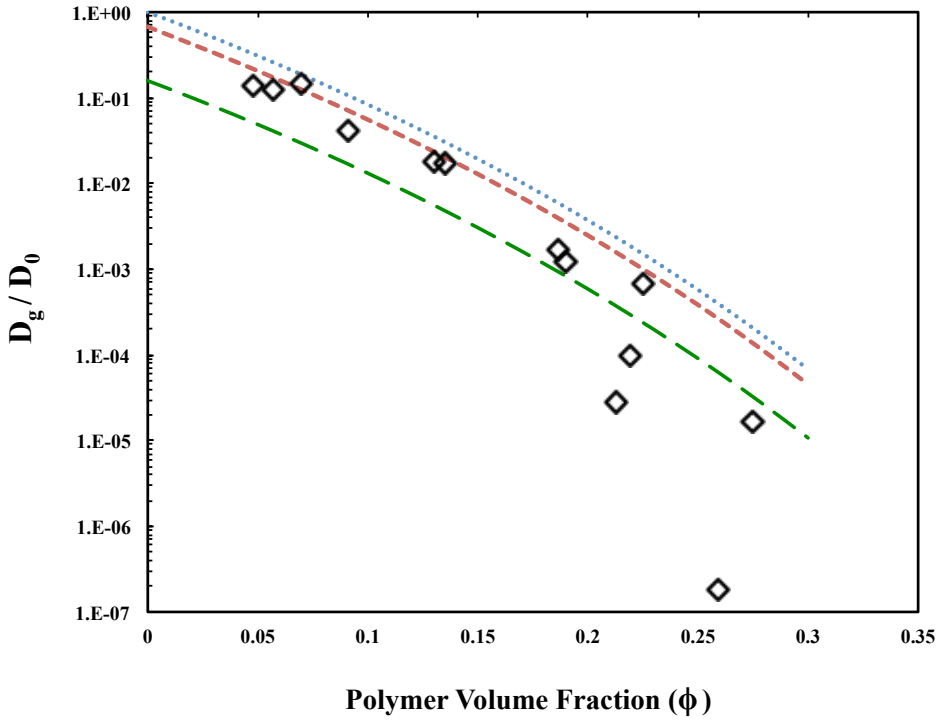

Figures 5. The application of the Reinhart Peppas model (using Equation 3.13 to describe the sieving effect) to literature data on the diffusion of BSA in dextran hydrogels. $k_1 = 3$, $k_2 = 0.017$, $M_n = 16{,}700$, (— –) $\bar{M}_c^* = 2000$, (----) $\bar{M}_c^* = 1400$, (·····) $\bar{M}_c^* = 800$.

A similar model based on the free volume theory was modified by Lustig and Peppas in which the screening effect is again determined by the probability of finding mesh sizes within the hydrogel that are large enough for a solute to pass through. The sieving factor was changed to take into account the correlation length between crosslinks, ξ.[40] This model expresses the sieving term as:

$$p(r_s) = 1 - \frac{r}{\xi} \tag{3.12}$$

However the authors have also used the form:

$$p(r_s) = 1 - \left(\frac{r}{\xi}\right)^2 \tag{3.13}$$

to describe the sieving term in a number of papers.[41,42] The correlation length defines the space that is available between network chains in a hydrogel network, and can be defined as the distance between two adjacent crosslinks. In Equations 3.12 and 3.13, r represents the size of the solute and is defined as the diameter of an equivalent sphere that represents the solute. The equations differ in that Equation 3.12 uses the ratio of the radii to calculate the probability, whereas Equation 3.13 uses the ratio of the areas. The authors concluded that, as Figure 3.6 illustrates, the probability is best represented by the ratio of the radii.

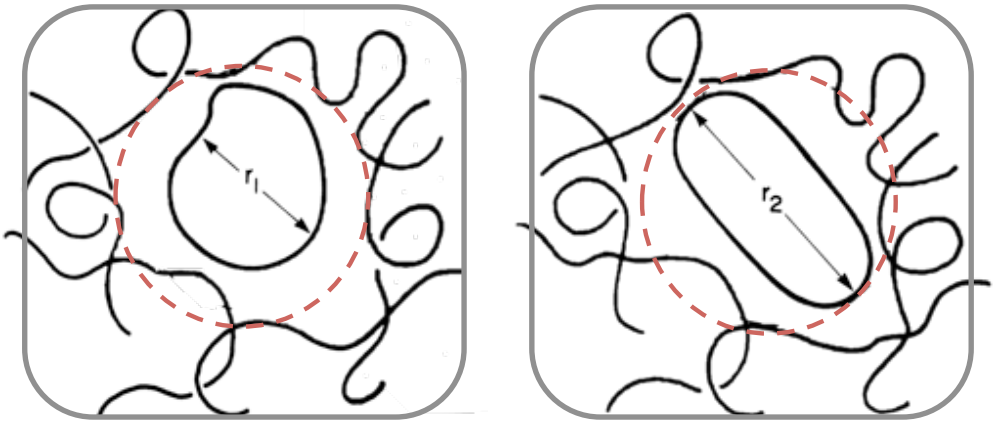

Figure 3.6. A schematic showing the diffusion of two different solutes through a crosslinked hydrogel network. The red circle represents the average mesh of the hydrogel network that the solutes must pass through. While the two solutes have the same cross-sectional area, the different shapes and values of r make it more probable for solute 1 to pass through the hydrogel mesh. Adapted from ref [43]

The Lustig and Peppas model using Equations 3.12 and 3.13 are shown in Figure 3.7. As expected, both models show a dramatic reduction in the diffusion coefficient as soon as the diameter of the solute approaches the mesh size. For the given conditions, the two models are

very similar through the entire range of the polymer volume fractions, with Equation 3.12 predicting slightly lower values until the diffusion coefficient begins to drop sharply. Equations 3.12 and 3.13 follow the same trend of the Reinhart and Peppas model that is seen in Figure 3.4. This was expected, as the model has the same function and only differs in the parameters that are used to describe the hydrogel network. The model also shares the same assumption as the Reinhart and Peppas that the hydrogel mesh is uniform and can be represented by a single value.

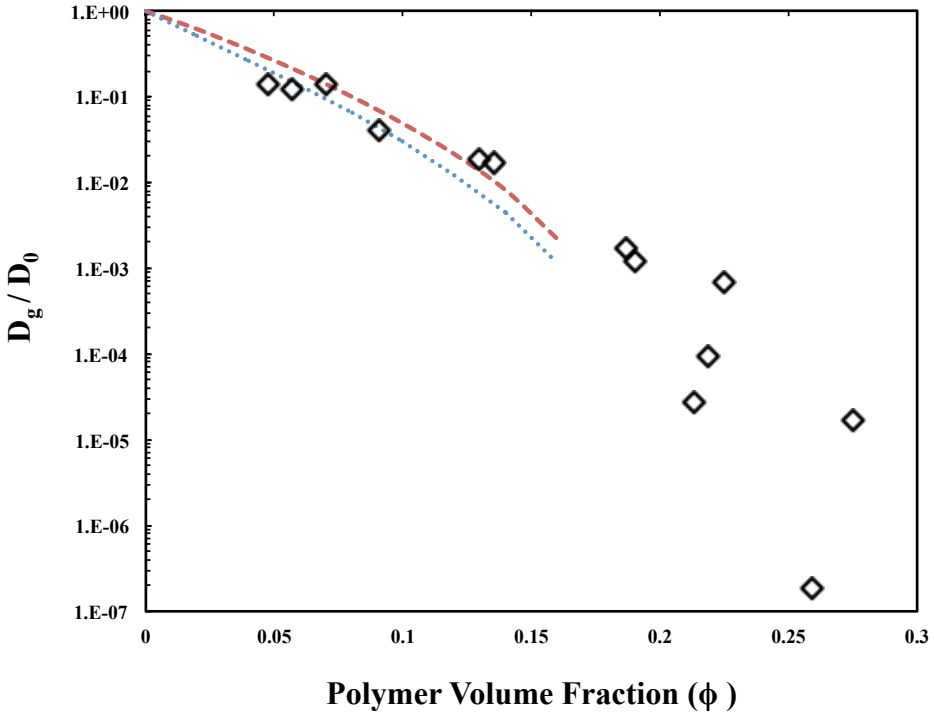

Figure 3.7. The application of the Lustig and Peppas model to literature data on the diffusion of BSA in dextran hydrogels. ξ is the correlation length of a hydrogel and is calculated according to ref [44]. k_2 =0.017, r_s =3.63nm, (.....) = r / ξ , (_ _ _ _) = $(r / \xi)^2$

One criticism of these free volume theories is that they rely too much on undefined structural parameters. While they can be accurately fitted to data, these undefined parameters make it very difficult to make predictions a priori when only hydrogel characteristics are known. Developing a better understanding of these parameters and the ranges in which they are suitable are critical in developing accurate models, especially at high polymer volume fractions where the screening effect is predicted to occur.

3.2.2 Hydrodynamic Theory

Hydrodynamic theories are based on the idea that as a solute moves through a gel, it will experience frictional drag from both the solvent and the polymer chains within the hydrogel. The theories were developed from the Stokes-Einstein equation, which describes the diffusion of a hard spherical solute through a continuum of much smaller solvent molecules as:

$$D = \frac{k_B T}{f} = \frac{k_B T}{6\pi\mu r_s} \tag{3.11}$$

where k_B is Boltzmann's constant, T is the temperature in Kelvin, f is the friction coefficient of the solute, and μ is the solvent viscosity.[45]

In a hydrogel, the polymer chains are modeled as fixed centers of hydrodynamic resistance that slow down the solvent molecules nearest to the polymer chains and increase the frictional drag on the solute moving through the hydrogel[11]. Cukier was one of the first to use this thinking in describing the diffusion of solutes through a hydrogel. He modeled the diffusion of spherical solutes through a solution made up of rod-like polymers and a solution made up of

random coils.[46] In a network comprised of random coils, the diffusion of solutes can be described by:

$$\frac{D_g}{D_0} = \exp\left(-k_c r_s \phi^{0.75}\right) \tag{3.12}$$

wherein k_c is an undefined proportionality constant. The diffusion coefficient within the hydrogel decreases exponentially as r_s and φ increase, similar to the free volume theory models. Unlike the free volume theory models, there is no sieving factor. While there have been a number of diffusion models that have been developed based on hydrodynamic theories, it was demonstrated that a majority of them are mathematically equivalent.[47] Therefore, we have chosen to focus on the Cukier model, as it is one of the most widely cited models in literature for describing the diffusion of solutes in hydrogels.[11,48-51]

Equation 3.12 has shown to correlate well with data at moderate swelling degrees (ϕ <0.15)[11], despite the fact that it does not contain any sort of sieving factor. For a given solute molecule, any reduction in D_g that is seen is the result of an increase in polymer volume fraction. Therefore, significant decreases in the diffusion coefficient due to screening effects are not expected based on the model. This is evident in Figure 3.8, which displays the Cukier model to the release of BSA from dextran hydrogels. Changes in k_c shift the curve downwards, but do not cause the model to predict any noticeable screening effects at high polymer volume fractions. Similar to the free volume theory models, the model hinges on an undefined parameter. Unlike the free volume theories, k_c is a parameter that is based on solvent-polymer interactions and has been shown to be consistent in cases where multiple solutes are studied for a given polymer-solvent system.[11]

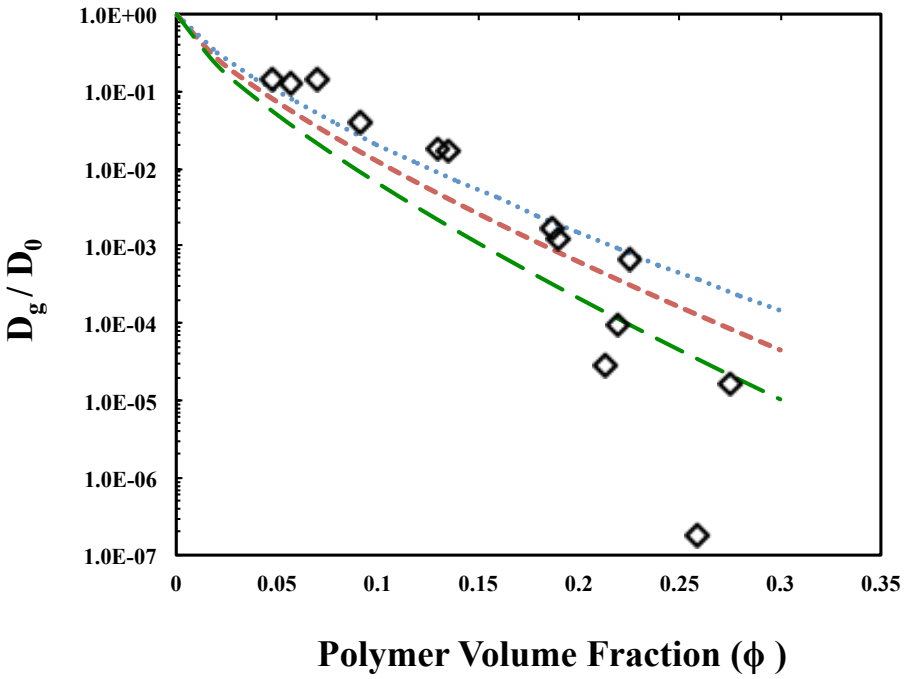

Figure 8. The application of the Cukier model to literature data on the diffusion of BSA in dextran hydrogels. r_s =3.63nm, (— —) k_C = 0.8, (- - - -) k_C = 0.7, (·····) k_C = 0.6.

3.2.2 Obstruction Theory

A number of models have been developed based on the obstruction theory. This theory suggests that the polymer chains of a hydrogel act as a barrier that obstructs the diffusion of solutes within the gel and increase the path length that these solutes must travel. Mackie and Meares developed one of the earliest models in which they used a lattice model to express the diffusion of solutes in a hydrogel.[52] The reduction in solute diffusivity is given by

$$\frac{D_g}{D_0} = \left(\frac{1 - \phi}{1 + \phi}\right)^2 \tag{3.13}$$

The model is based on several assumptions including the assumption that the solute molecule is equal in size to the polymer segments and that the diffusion can occur only in the spaces that are unoccupied by polymer chains. The model is rather simple, only including the volume fraction of polymer in the gel and not including any other properties of the hydrogel or the size of the solute. Relative to the other models described in this chapter, Equation 3.13 (shown in Figure 3.10a) predicts a much higher diffusion coefficient and the normalized diffusion coefficient displays very little curvature.

Another model based on the obstruction theory was developed by Ogston and assumes that the diffusion of solutes occurs through hydrogels that are modeled as a network of straight cylindrical fibers (Figure 3.9).[53]

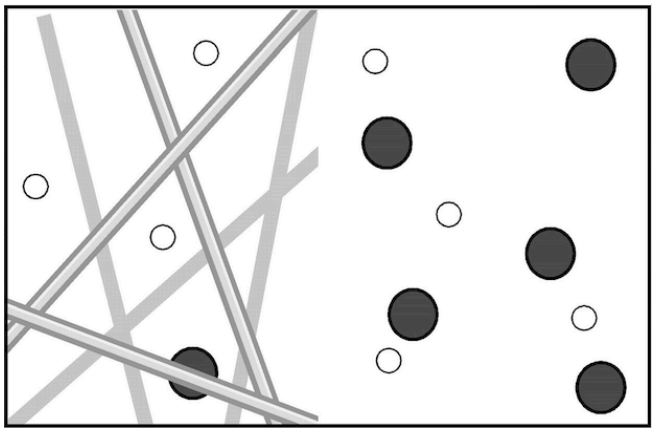

Figure 3.9. Schematic of the random cylindrical fibers that are used to describe the diffusion of solutes through hydrogels in the Ogston model[54].

These fibers have a given radius, r_f, and the diffusion hinges on the probability that a molecule with a certain radius can find a space between the fibers large enough to diffuse through. The expression for the reduction in diffusivity is given as

$$\frac{D_g}{D_0} = \exp\left(-\frac{(r_s+r_f)}{r_f}\sqrt{\phi}\right) \tag{3.14}$$

The models based on the obstruction theory assume that the polymer chains are straight, rigid, and motionless. Because of these assumptions, the models are mostly used when attempting to describe the diffusion of solutes through gels with a very rigid network that has well defined pores. Initially it would seem that applying the same models to gels in which the polymers are semi-flexible or flexible coils would lead to large errors. However, as mentioned early, when compared to some of the available data, an obstruction-scaling model was shown to fit quite well with the diffusion of solutes in flexible hydrogels such as dextran and poly(ethylene

oxide),[55] and recent modeling showed that the model was unaffected by chain stiffness and gave identical results for polymer chains that were rigid, semi-rigid, and even flexible.

The sieving effect of these obstruction models is directly built in due to the theory and so there are no additional terms that need to be added. However, as can be seen in Figure 3.10, the obstruction models like the one developed by Mackie and Meares and Ogston do not always provide the best fit.

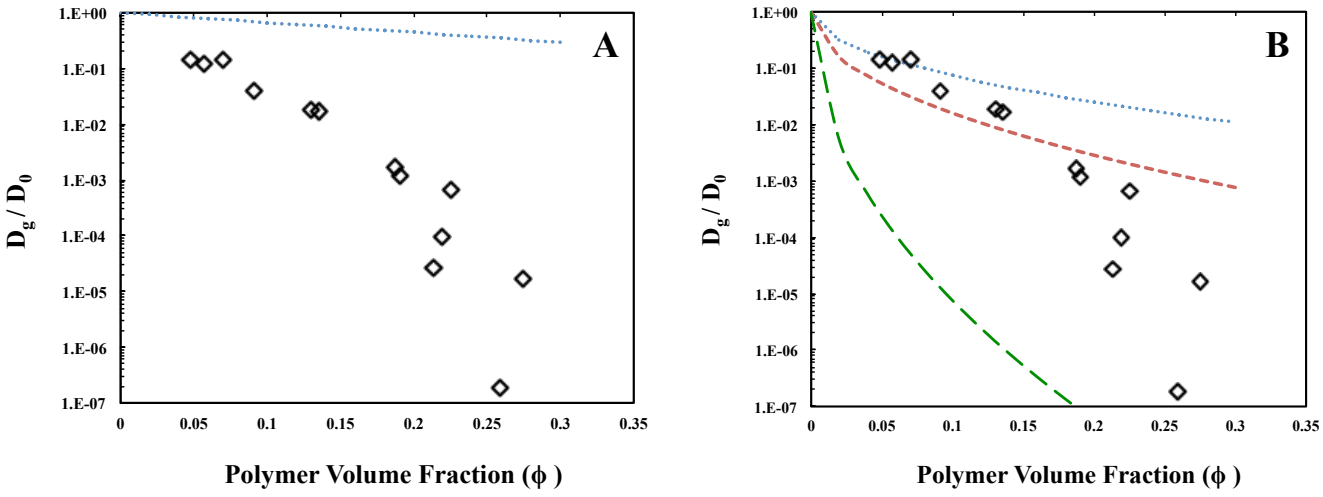

Figures 3.10a and 3.10b. The application of the Mackie and Meares model (A) and the Ogston model (B) to literature data on the diffusion of BSA in dextran hydrogels. (B) r_s =3.63nm, (— —) r_f = 1, (– – –) r_f = 3, (·····) r_f = 5. The r_f of dextran in literature ranges from 0.25 – 1.0 nm[56,57].

Another obstruction model was developed by Amsden and is based on the Ogston model. Similar to the Ogston model, the diffusion is predicted based on the probability of a solute finding an opening between polymer chains in the hydrogel network. However, in the Amsden model scaling relationships are used to describe the size of spaces between flexible polymer

chains instead of using rigid cylindrical fibers.[15] When this is taken into consideration, the diffusion of a solute within a hydrogel can be written as:

$$\frac{D_g}{D_0} = \exp\left(-\pi\left(\frac{(r_s + r_f)}{\xi + 2r_f}\right)^2\right) \tag{3.15}$$

where ξ represents the average mesh size within the hydrogel based on the De Gennes' scaling theory, or blob model. The model can be seen in Figure 3.11, and shows that decreasing the fiber radius reduces the curvature of the line. Similar to the Ogston model, at large fiber radii the model predicts higher diffusion coefficients when compared with lower fiber radii.

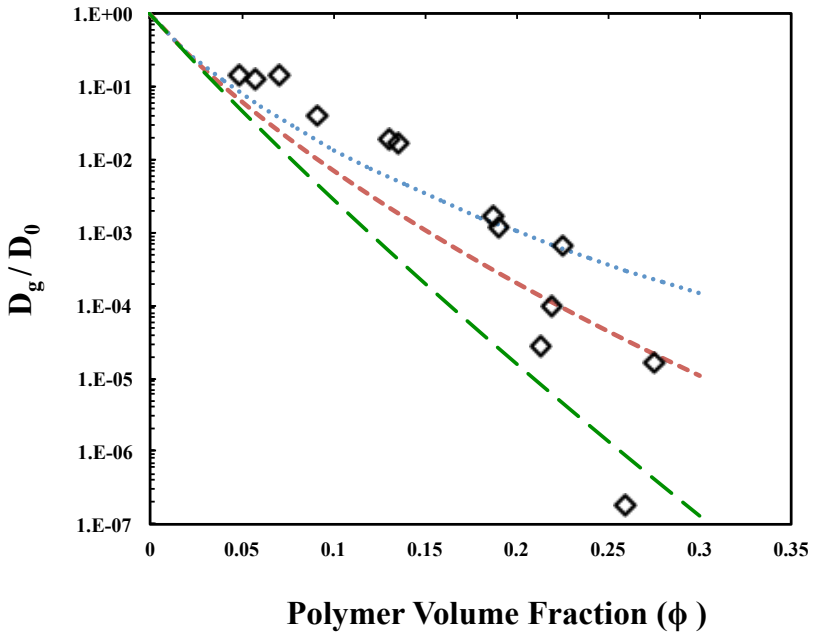

Figure 3.11 The application of the Amsden model to literature data on the diffusion of BSA in dextran hydrogels. r_s =3.63nm, (— - —) r_f = 1, (- - - -) r_f = 3, (·····) r_f = 5. The r_f of dextran in literature ranges from 0.25 – 1.0 nm[56,57].

3.3 CONCLUSIONS

The goal of this chapter was to review the current state of art on the diffusion of large solutes in hydrogels with a focus on low swelling degrees where the screening effect is expected to occur. While the models use different approaches for modeling the diffusion of solutes through hydrogels, they all depend primarily on water content and solute size, which leads to similar predictions for hydrogels with high water contents. Where the models differ, however, is at these low swelling degrees.

A number of free volume theories were reviewed in this chapter. A number of these, such as the Lustig and Peppas model and the Reinhart and Peppas model, include a sieving factor that under certain circumstances can cause a dramatic drop in the diffusion coefficient. In these models the predictions are highly dependent on the accuracy of calculated parameters such as $\overline{M}_c$, $\overline{M}_c^*$, and ξ that are derived from idealized theory. These models also rely heavily on undefined fitting parameters that need to be defined in order to be predictive.

The hydrodynamic theory of Cukier was also reviewed this chapter. Unlike the free volume theories, the model does not contain any parameters that can account for possible screening effects and reductions in D_g are based only on increases in the polymer volume fraction of the hydrogel. The model does contain a parameter that is based on solvent-polymer interactions, however it has been shown to be physically consistent in cases in multiple polymer-solvent systems.

A few obstruction theories were reviewed in this chapter including the model developed by Mackie and Meares and the model developed by Ogston and Amsden. These models are based on the idea that polymer chains in the hydrogel network act as obstructions and increase the solute diffusion path length. Models like the one developed by Mackie and Meares only take

into account the volume fraction of polymer in the gel. It does not include any other properties of the hydrogel or the size of the solute, and is therefore quite limited in its usefulness for predicting the diffusion of solutes in gels. The Ogston and Amsden models take into account the radius of the solute and the radius of the polymer chains, which are modeled as either long straight fibers or flexible chains. The models were shown to be highly dependent on the radius of the fibers, and exhibited the most noticeable declines in the diffusion coefficient at high swelling degrees. While this is the opposite of the trend than what would be expected from a hypothesized screening effect, the models have been shown to be useful in predicting the diffusion of solutes in hydrogels with higher swelling degrees ((ϕ <0.15).[15,58]

Overall, the results show that models based on the free volume theory are the only ones that contain a specific parameter (the sieving factor) that can cause a dramatic drop in the predicted diffusion coefficient. Despite its limitations, the free volume theory is used in this dissertation to predict the diffusion of various solutes through hydrogels due to the fact that they provide a number of variable sieving terms that can be used to describe possible screening effects. This may be one of the reasons why free volume models are widely used in drug delivery. However, the results also highlight the need for additional data in order to rigorously test the models and any undefined parameters and see how they perform under a wide range of hydrogels and solutes. All of the models in this chapter were reviewed using a single hydrogel/solute data set. Unfortunately, accurately measuring the diffusion coefficients at such low values becomes increasingly difficult and time consuming, which has led to a limited amount of data available in the literature. With the rise in popularity and usage of therapeutic proteins, obtaining more data on the diffusion of these large molecules in hydrogels and how it is impacted by the screening effect is critical in developing successful drug delivery devices.

The diffusion coefficients of solutes within hydrogels is a central theme throughout this dissertation, especially in the region where the size of the solute approaches the mesh size of the hydrogel and the screening effect is hypothesized to occur. One of the goals of Chapter 5 is to obtain long-term delivery from a hydrogel delivery vehicle. In order for this to be achieved a very low diffusion coefficient is needed. While this is normally achieved by increasing the polymer volume fraction of the hydrogel, there are certain situations where this is either not possible or simply undesired due to unwanted side reactions or reductions in biocompatibility. If the screening effect does exist, it would provide a useful way to significantly lower the diffusion coefficient while maintaining higher swelling degrees. Additionally, one of the hypotheses of Chapter 7 is that the hydrogel synthesis method and resulting network structure could impact the diffusion of solutes through the network and under certain conditions cause a screening effect. Understanding the diffusion coefficients of solutes within hydrogels and the factors that determine when the screening effect is an important area of study that will be discussed throughout this dissertation.

REFERENCES

1. Lin C-C, Metters AT 2006. Hydrogels in controlled release formulations: Network design and mathematical modeling. Adv Drug Deliv Rev 58(12-13):1379-1408.

2. Hoare TR, Kohane DS 2008. Hydrogels in drug delivery: progress and challenges. Polymer 49(8):1993-2007.

3. Kang J, Erdodi G, Kennedy JP, Chou H, Lu L, Grundfest-Broniatowski S 2010. Toward a Bioartificial Pancreas: Diffusion of Insulin and IgG Across Immunoprotective Membranes with Controlled Hydrophilic Channel Diameters. Macromolecular Bioscience 10(4):369-377.

4. Orive G, Santos E, Pedraz J, Hernandez R 2014. Application of cell encapsulation for controlled delivery of biological therapeutics. Advanced drug delivery reviews 67:3-14.

5. Drury JL, Mooney DJ 2003. Hydrogels for tissue engineering: scaffold design variables and applications. Biomaterials 24(24):4337-4351.

6. Matsuyama H, Teramoto M, Urano H 1997. Analysis of solute diffusion in poly(vinyl alcohol) hydrogel membrane. Journal of Membrane Science 126(1):151-160.

7. Yang Q, Adrus N, Tomicki F, Ulbricht M 2011. Composites of functional polymeric hydrogels and porous membranes. Journal of Materials Chemistry 21(9):2783-2811.

8. Peppas N, Bures P, Leobandung W, Ichikawa H 2000. Hydrogels in pharmaceutical formulations. European journal of pharmaceutics and biopharmaceutics 50(1):27-46.

9. Yasuda H, Lamaze C, Ikenberry L 1968. Permeability of solutes through hydrated polymer membranes. Part I. Diffusion of sodium chloride. Die Makromolekulare Chemie 118(1):19-35.

10. Johansson L, Skantze U, Loefroth JE 1991. Diffusion and interaction in gels and solutions. 2. Experimental results on the obstruction effect. Macromolecules 24(22):6019-6023.

11. Amsden B 1998. Solute diffusion within hydrogels. Mechanisms and models. Macromolecules 31(23):8382-8395.

12. Muhr AH, Blanshard JM 1982. Diffusion in gels. Polymer 23(7):1012-1026.

13. Wong JY, Bronzino JD, Peterson DR. 2012. Biomaterials: Principles and practices. ed.: CRC Press.

14. Zhang Y, Amsden BG 2006. Application of an obstruction-scaling model to diffusion of vitamin B12 and proteins in semidilute alginate solutions. Macromolecules 39(3):1073-1078.

15. Waters DJ, Frank CW 2009. Hindered diffusion of oligosaccharides in high strength poly (ethylene glycol)/poly (acrylic acid) interpenetrating network hydrogels: Hydrodynamic vs. obstruction models. Polymer 50(26):6331-6339.

16. Quesada-Perez M, Adroher-Benitez I, Maroto-Centeno JA 2014. Size-exclusion partitioning of neutral solutes in crosslinked polymer networks: A Monte Carlo simulation study. Journal of Chemical Physics 140(20).

17. Tong J, Anderson JL 1996. Partitioning and diffusion of proteins and linear polymers in polyacrylamide gels. Biophys J 70(3):1505-1513.

18. Kosto KB, Deen WM 2004. Diffusivities of macromolecules in composite hydrogels. Aiche J 50(11):2648-2658.

19. Hennink WE, Talsma H, Borchert JCH, De Smedt SC, Demeester J 1996. Controlled release of proteins from dextran hydrogels. Journal of Controlled Release 39(1):47-55.

20. Engberg K, Frank CW 2011. Protein diffusion in photopolymerized poly (ethylene glycol) hydrogel networks. Biomedical Materials 6(5):055006.

21. Burczak K, Fujisato T, Hatada M, Ikada Y 1994. Protein permeation through poly (vinyl alcohol) hydrogel membranes. Biomaterials 15(3):231-238.

22. Merrill EW, Dennison KA, Sung C 1993. Partitioning and diffusion of solutes in hydrogels of poly (ethylene oxide). Biomaterials 14(15):1117-1126.

23. Graham N, Zulfiqar M, MacDonald B, McNeill M 1987. Caffeine release from fully swollen poly (ethylene oxide) hydrogels. Journal of controlled release 5(3):243-252.

24. Shu XZ, Liu Y, Luo Y, Roberts MC, Prestwich GD 2002. Disulfide cross-linked hyaluronan hydrogels. Biomacromolecules 3(6):1304-1311.

25. Chang C, Lue A, Zhang L 2008. Effects of crosslinking methods on structure and properties of cellulose/PVA hydrogels. Macromolecular Chemistry and Physics 209(12):1266-1273.

26. Van Tomme SR, De Geest BG, Braeckmans K, De Smedt SC, Siepmann F, Siepmann J, van Nostrum CF, Hennink WE 2005. Mobility of model proteins in hydrogels composed of oppositely charged dextran microspheres studied by protein release and fluorescence recovery after photobleaching. Journal of controlled release 110(1):67-78.

27. Cruise GM, Scharp DS, Hubbell JA 1998. Characterization of permeability and network structure of interfacially photopolymerized poly(ethylene glycol) diacrylate hydrogels. Biomaterials 19(14):1287-1294.

28. Wang XH, Li S, Liang L, Xu XD, Zhang XZ, Jiang FG 2013. Evaluation of RGD peptide hydrogel in the posterior segment of the rabbit eye. Journal of Biomaterials Science-Polymer Edition 24(10):1185-1197.

29. Xie BB, Jin L, Luo ZC, Yu J, Shi S, Zhang ZL, Shen MX, Chen H, Li XY, Song ZM 2015. An injectable thermosensitive polymeric hydrogel for sustained release of Avastin (R) to treat posterior segment disease. International Journal of Pharmaceutics 490(1-2):375-383.

30. Kim KS, Park SJ, Yang JA, Jeon JH, Bhang SH, Kim BS, Hahn SK 2011. Injectable hyaluronic acid-tyramine hydrogels for the treatment of rheumatoid arthritis. Acta Biomaterialia 7(2):666-674.

31. Dhal PK, Gianolio DA, Miller RJ. 2012. Polymer based therapies for the treatment of chronic pain. ed.: INTECH Open Access Publisher.

32. Konishi M, Tabata Y, Kariya M, Suzuki A, Mandai M, Nanbu K, Takakura K, Fujii S 2003. In vivo anti-tumor effect through the controlled release of cisplatin from biodegradable gelatin hydrogel. Journal of controlled release 92(3):301-313.

33. Jeyanthi R, Nagarajan B, Rao KP 1991. Solid tumour chemotherapy using implantable collagen‐poly (HEMA) hydrogel containing 5‐fluorouracil. Journal of pharmacy and pharmacology 43(1):60-62.

34. Konishi M, Tabata Y, Kariya M, Hosseinkhani H, Suzuki A, Fukuhara K, Mandai M, Takakura K, Fujii S 2005. In vivo anti-tumor effect of dual release of cisplatin and adriamycin from biodegradable gelatin hydrogel. Journal of controlled release 103(1):7-19.

35. Cohen MH, Turnbull D 1959. Molecular transport in liquids and glasses. The Journal of Chemical Physics 31(5):1164-1169.

36. Yasuda H, Peterlin A, Colton C, Smith K, Merrill E 1969. Permeability of solutes through hydrated polymer membranes. Part III. Theoretical background for the selectivity of dialysis membranes. Die Makromolekulare Chemie 126(1):177-186.

37. Peppas NA, Reinhart CT 1983. SOLUTE DIFFUSION IN SWOLLEN MEMBRANES .1. A NEW THEORY. Journal of Membrane Science 15(3):275-287.

38. Peppas NA, Wright SL 1996. Solute diffusion in poly(vinyl alcohol) poly(acrylic acid) interpenetrating networks. Macromolecules 29(27):8798-8804.

39. Reinhart CT, Peppas NA 1984. SOLUTE DIFFUSION IN SWOLLEN MEMBRANES .2. INFLUENCE OF CROSSLINKING ON DIFFUSIVE PROPERTIES. Journal of Membrane Science 18(MAR):227-239.

40. Lustig SR, Peppas NA 1988. SOLUTE DIFFUSION IN SWOLLEN MEMBRANES .9. SCALING LAWS FOR SOLUTE DIFFUSION IN GELS. Journal of Applied Polymer Science 36(4):735-747.

41. Peppas NA, Lustig SR 1985. THE ROLE OF CROSS-LINKS, ENTANGLEMENTS, AND RELAXATIONS OF THE MACROMOLECULAR CARRIER IN THE DIFFUSIONAL RELEASE OF BIOLOGICALLY-ACTIVE MATERIALS - CONCEPTUAL AND SCALING RELATIONSHIPS. Annals of the New York Academy of Sciences 446:26-41.

42. Ende MTA, Peppas NA 1997. Transport of ionizable drugs and proteins in crosslinked poly(acrylic acid) and poly(acrylic acid-co-2-hydroxyethyl methacrylate) hydrogels .2. Diffusion and release studies. Journal of Controlled Release 48(1):47-56.

43. Peppas NA. 1987. Hydrogels in medicine and pharmacy. ed.: CRC press Boca Raton, FL.

44. Canal T, Peppas NA 1989. Correlation between mesh size and equilibrium degree of swelling of polymeric networks. Journal of Biomedical Materials Research 23(10):1183-1193.

45. Bird RB, Stewart WE 1960. Lightfoot transport phenomena. John & Sons, New York 647.

46. Cukier RI 1984. DIFFUSION OF BROWNIAN SPHERES IN SEMIDILUTE POLYMER-SOLUTIONS. Macromolecules 17(2):252-255.

47. Kosar TF, Phillips RJ 1995. Measurement of protein diffusion in dextran solutions by holographic interferometry. Aiche J 41(3):701-711.

48. Kwak S, Lafleur M 2003. Self-diffusion of macromolecules and macroassemblies in curdlan gels as examined by PFG-SE NMR technique. Colloids and Surfaces a-Physicochemical and Engineering Aspects 221(1-3):231-242.

49. Valente AJM, Polishchuk AY, Burrows HD, Miguel MG, Lobo VMM 2003. Sorption/diffusion behaviour of anionic surfactants in polyacrylamide hydrogels: from experiment to modelling. European Polymer Journal 39(9):1855-1865.

50. Valente AJM, Polishchuk AY, Lobo VMM, Geuskens G 2002. Diffusion coefficients of lithium chloride and potassium chloride in hydrogel membranes derived from acrylamide. European Polymer Journal 38(1):13-18.

51. Masaro L, Zhu X 1999. Physical models of diffusion for polymer solutions, gels and solids. Progress in polymer science 24(5):731-775.

52. Mackie JS, Meares P 1955. THE DIFFUSION OF ELECTROLYTES IN A CATION-EXCHANGE RESIN MEMBRANE .1. THEORETICAL. Proceedings of the Royal Society of London Series a-Mathematical and Physical Sciences 232(1191):498-509.

53. Ogston AG, Preston BN, Wells JD, Ogston AG, Preston BN, Snowden JM, Wells JD 1973. TRANSPORT OF COMPACT PARTICLES THROUGH SOLUTIONS OF CHAIN-POLYMERS. Proceedings of the Royal Society of London Series a-Mathematical Physical and Engineering Sciences 333(1594):297-316.

54. Lazzara MJ, Deen WM 2001. Effects of plasma proteins on sieving of tracer macromolecules in glomerular basement membrane. American Journal of Physiology-Renal Physiology 281(5):F860-F868.

55. Amsden B 1999. An obstruction-scaling model for diffusion in homogeneous hydrogels. Macromolecules 32(3):874-879.

56. Saltzman WM. 2001. Drug delivery: engineering principles for drug therapy. ed.: Oxford University Press, USA.

57. White JA, Deen WM 2002. Agarose-dextran gels as synthetic analogs of glomerular basement membrane: water permeability. Biophys J 82(4):2081-2089.

58. Hadjiev NA, Amsden BG 2015. An assessment of the ability of the obstruction-scaling model to estimate solute diffusion coefficients in hydrogels. Journal of Controlled Release 199:10-16.

Chapter 4: High Efficiency Loading Of Therapeutic Proteins Into Hydrogel Delivery Vehicles Using Thermodynamics Of Aqueous Two-Phase Polymer Systems

4.1 Abstract

A versatile and effective method for loading therapeutic proteins and antibodies into crosslinked PEG and dextran hydrogels is developed using the thermodynamic principles of aqueous two-phase extraction (ATPE) to overcome size exclusion. The partitioning of the model protein ovalbumin in a PEG/dextran system corresponded with ATPE heuristics, and the effects of salt and pH matched the data trends found in literature. ATPE heuristics correctly predicted the observed trends using a PEG-salt system, and the addition of 0.13 M phosphate caused the partition coefficient to double compared to buffer alone. ATPE thermodynamics could even overcome size exclusion of proteins as large as antibodies, thus demonstrating the potential of the method to load monoclonal antibodies into pre-formed gels. This was demonstrated by loading IgG into both PEG and dextran hydrogels by adding a polymer into the solution along with the appropriate salt. Partition coefficients as high as 18 were achieved in a dextran hydrogel with the addition of only 6% PEG. These results demonstrate the versatility of a method using FDA-GRAS additives to overcome size exclusion of proteins, even as large as monoclonal antibodies, into many types of hydrogels, thus opening the door to new delivery strategies for therapeutic proteins using hydrogels.

4.2 INTRODUCTION

The release of a therapeutic dose of a drug from a drug delivery system (DDS) over an extended period of time is an important topic in drug delivery. The use of hydrogels as a rate-controlling barrier in such a DDS is a common approach. Because of their hydrophilic nature, they are particularly compatible with protein therapeutics. There are few protein therapeutics that have as great a demand and as wide range of use as monoclonal antibodies (mAbs). Because mAbs have such high molecular weights (150 kDa), post-loading into monolithic hydrogels or microgels may be impossible due to steric size exclusion of the mAbs from the hydrogel mesh. We have previously shown that the thermodynamics of aqueous two-phase polymer systems can be used to overcome steric exclusion for proteins on the order of 50,000 Da in dextran gels by adding PEG and salts to the loading solution.[1-3] This chapter investigates the hypothesis that the thermodynamic principles of this method can be generalized to any type of hydrogel and that it can work even for proteins as large as mAbs. It also sets out to prove the versatility of the systems and the ability to quickly adapt the systems and theories already developed in literature.

In the past 25 years the discovery and use of monoclonal antibodies (mAbs) has significantly changed the pharmaceutical industry and has increased the need for effective methods to incorporate them into drug delivery systems. In 2009 monoclonal antibodies reached 38 billion dollars in total sales which accounted for almost 40 percent of all biopharmaceutical sales worldwide[4]. In 2009 alone there were 240 mAbs in clinical trials[5], and seven new monoclonal antibodies were approved to come to market for the first time in the United States and Europe.[4] Since then, the sale of monoclonal antibodies has shown major growth every year, and in 2013 the total global sales of mAbs was nearly 75 billion dollars.[6-8] With the surge in sales of monoclonal antibodies comes the increased need to effectively and safely deliver them in

correct doses to target areas of the body. Because of their large size and complex structure, monoclonal antibodies can often be challenging to incorporate into a drug delivery device.[9] Hydrogels have many suitable properties that would make them a very successful drug delivery device if a high concentration of antibodies could be achieved within a hydrogel.[10]

Hydrogels are hydrophilic polymer networks that can be designed to exhibit a wide range of permeabilities.[11] As a result, hydrogels have long been used as drug delivery vehicles for controlling and extending the release of therapeutic proteins. There are many ways to release proteins from hydrogels: release due to polymer degradation and swelling, release due to hydrogel responses to stimuli such as pH or temperature, and even the hydrolytic or enzymatic cleavage of proteins that are either covalently or non-covalently attached.[12-14] In drug delivery systems, release that occurs primarily through diffusion is one of the most widely used and studied release mechanisms.[15] In most of these systems the protein is either placed in a hydrogel reservoir or loaded evenly throughout a monolithic hydrogel. Monolithic hydrogels, which is the approach followed in this chapter, can be loaded in in two ways: by encapsulating the drug within the gel during formation, or by synthesizing the gel and then absorbing the drug by equilibrating it with a drug solution. The first method is useful for loading a high concentration of drug into a hydrogel, yet is generally limited to physically gelling polymers because of the possible chemical reactions that can take place between the drug and the hydrogel precursors as well as any of the reagents that are used during synthesis. Furthermore, any impurities that might accumulate in the hydrogel network during synthesis due to incomplete reaction or side reactions will be difficult to leach away without also removing the drug itself. Loading a gel by soaking it in a drug solution eliminates these two obstacles, yet at the same time it introduces new difficulties. Depending on the dimensions of the device and the diffusion rate of the protein,

post-loading a gel can be significantly limited by the time it takes for diffusion into the gel. Even more significantly, large molecules may be partially excluded based on the entropic size exclusion phenomenon and some large molecules, such as antibodies, might even be completely excluded from the hydrogel network.

Overcoming these difficulties is crucial to achieving an effective delivery device with high loading and protein that is still functional upon release. While a lot of research has been done to decrease the problems associated with protein encapsulation,[16-18] our group described a method to overcome the exclusion constraint that plagues most post-loading methods. In a series of papers, it was demonstrated that the protein partitioning in hydrogels closely follows the aqueous two-phase extraction (ATPE) heuristics. ATPE is a well-developed technique that uses the immiscibility of two aqueous polymer phases to purify proteins. Proteins selectively partition into one of the two polymer phases due to the additional thermodynamic contributions that the protein experiences from the polymers in solution. The partitioning is measured using the partition coefficient, K, which is defined as the concentration of solute inside the gel divided by the concentration of the solute in the loading solution.

$$K = \frac{C_{Gel}}{C_{Solution}} \tag{4.1}$$

The partitioning can be controlled by a number of factors including polymer type and molecular weight, salt type and concentration, and pH.[19] The same thermodynamics that controls partitioning when two polymers are in solution also apply when of the phases is crosslinked to form a hydrogel, an advantage that can be manipulated when loading large molecules. Using the thermodynamic principles of ATPE, proteins such as ovalbumin, bovine serum albumin (BSA), and α-amylase were loaded into hydrogels at significantly higher concentrations when compared

with normal equilibration techniques.[1-3] Using these loading systems, partition coefficients as high as 80 and loadings as high as 450 mg protein per gram of polymer were reported while maintaining bioactivity.[2] The concept was further exploited to manufacture protein-loaded dextran microspheres by using an aqueous two-phase system by Hennink.[20] In his initial paper, a water-in-water emulsion was prepared with PEG and methacrylated dextran and when an initiator was added, dextran microspheres were formed. In later papers, proteins such as IgG were also added to the solution, and the use of ATPE principles were exploited to improve the partitioning of the protein within the microspheres during gelation.[21,22]

One of the goals of the previous work in the literature was trying to achieve the highest possible partition coefficient however, there are two aspects that control the loading of a solute into a hydrogel: the partition coefficient and the swelling degree. The total amount of solute that can be loaded into a hydrogel is given by the following:

$$\frac{M_s}{M_p} = QKx \qquad (4.2)$$

Where M_s is the total mass of solute absorbed by the gel; M_p is the mass of polymer in the gel; Q is the gel swelling degree (mass of loaded hydrated mass/mass of dry, unloaded gel); K is the partition coefficient of the solute; and x is the mass fraction of solute in the loading solution. Equation 4.2 shows that in order to maximize the loading a system should be chosen that maximizes both the partitioning and the swelling degree. While a lot of work has focused on how the partitioning is affected by the loading solution, very little has been done to explore how the loading conditions affect the swelling degree. The swelling is hypothesized to be indicated by the slope of the tie lines of the ternary phase diagram for the given aqueous two-phase system (see Figure 4.1).[19] In almost every aqueous PEG-dextran systems, the tie lines indicate that the

PEG phase will contain a greater percentage of water compared with the dextran phase. Therefore, a PEG hydrogel in aqueous dextran is hypothesized to swell much more than a dextran gel in aqueous PEG. If partitioning values are similar, a higher drug loading could actually be achieved with a PEG hydrogel if the swelling degree is in fact higher, yet the partitioning and swelling of PEG hydrogels in these ATPE loading systems has never been investigated.

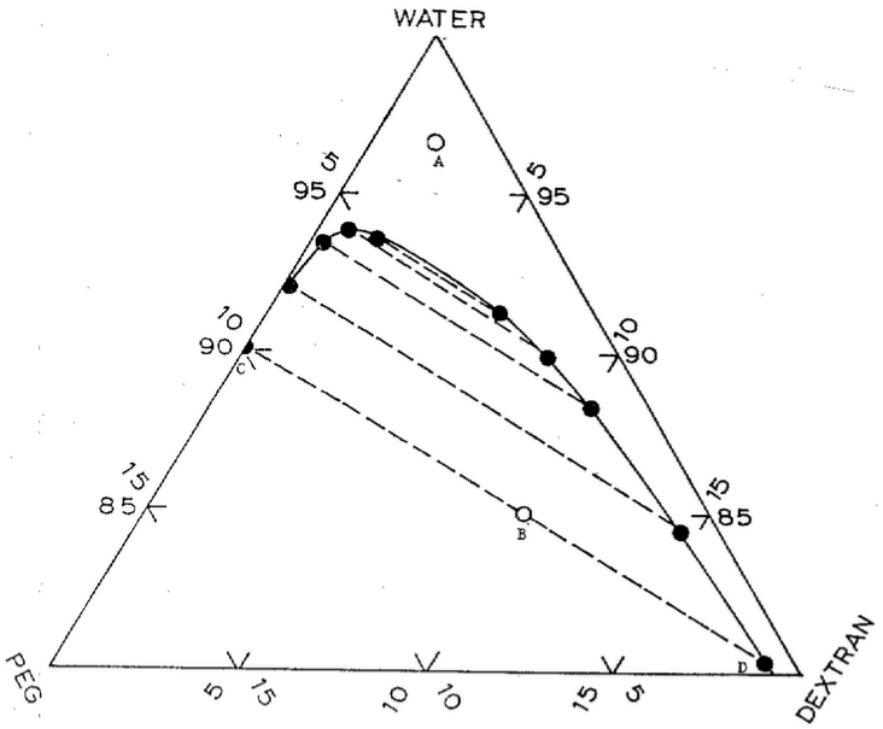

Figure 4.1 Tertiary phase diagram of a representative PEG-dextran two-phase system.[19] A solution containing 85% water, 10% dextran, and 5% PEG (Point B) will split into two distinct phases. The compositions of these phases are determined by the tie lines (dashed lines). One phase (Point C) will be predominantly PEG, while the other phase (Point D) will be predominantly dextran.

The focus of this chapter is on two hypotheses. The first is that the aqueous two-phase driven gel loading phenomenon should be generally applicable to any hydrogel. While there is quite a large amount of research that has been done on ATPE using linear polymers in solution, in all of the studies on using these principles for drug loading, dextran gel has been used.[1-3] If alternative systems using hydrogels other than dextran can be shown to follow the ATPE heuristics found in literature it would greatly expand the material options for drug delivery. It would allow selection of loading systems and drugs that have been successfully demonstrated in literature and quickly extend them to hydrogel drug delivery devices. Systems could be chosen that maximize both K and Q and have a polymer that is best suited for a given application in terms of biocompatibility, degradability, etc. The second hypothesis is that the systems that are studied in this first section of the chapter can be used to load molecules as large as mAbs into hydrogels. While size exclusion can be overcome with ATPE principles, it would seem reasonable that at some size this will no longer be possible. And although the literature has shown that large molecules such as BSA and ovalbumin can partition into hydrogels, antibodies have an even larger hydrodynamic radius (5.3m vs. 3.55 and 2.78nm).[23-25] Given the increasing demand for monoclonal antibodies and efficient ways to deliver them, if ATP systems are shown to work, it would provide a much needed and useful way to load antibodies into hydrogel delivery devices.

4.3 Materials And Methods

4.3.1 Hydrogel Synthesis

Poly(ethylene glycol) diacrylate (PEGDA) hydrogels were synthesized by mixing an aqueous solution of 10 w/w% PEGDA polymer 700 MW (Sigma-Aldrich, St. Louis, MO) with 0.3% wt/wt of the initiator Irgacure 2959 (Ciba, Tarrytown, NY).[26] The solution was then stirred for 15 minutes and loaded into silicon rubber molds that were 2 mm thick and had precut holes 5 mm in diameter. These molds were clamped between two thin glass plates (1 mm thick) and irradiated in a Spectronics Spectrolinker XL-1000 (Westbury, NY) at 312 nm for 10 minutes at an intensity of 3 mW cm^{-2}. The gels kept in the molds at room temperature for 24 hours before being removed and placed into an excess of D.I. water. The gels were leached in D.I. water multiple times a day for three days to remove unreacted monomer and initiator and to allow the gels to swell to equilibrium.

Dextran hydrogels were synthesized by mixing 10 w/w% dextran polymer (40k MW, Amersham Bioscience, Uppsala, Sweden) with the crosslinker divinyl sulfone (Sigma Aldrich, St. Louis, MO) in an aqueous solution of 0.02 M NaOH [3]. The solution was vigorously stirred and then quickly loaded into the molds described previously. The dextran gels were allowed to react for 24 hours and then leached in the same manner as the PEG gels.

4.3.2 Loading Experiments

The loading solutions were made by mixing a 10 mM sodium citrate buffer at a pH of either 3.3 or 5.9 with various partitioning salts and polymers. The partitioning salts used were potassium chloride and tetrabutylammonium fluoride trihydrate at a concentration of 0.22 M and were both purchased from Sigma (St. Louis, MO). The polymers in solution were poly(ethylene

glycol) (Sigma, St. Louis, MO) and dextran 40k at a 10 w/w% concentration. The model proteins used were ovalbumin (lyophilized powder, ≥ 98%, Sigma, St. Louis, MO) and human IgG (lyophilized powder, ≥ 98%, MP Biomedicals, Solon, OH).

To ensure gel volume was constant, before the gels were placed in loading solutions containing protein they were pre-equilibrated in 1 mL of protein-free loading solution and allowed to soak for 24 hours. The gels were then added to 1 mL of the same loading solution that contained 1 mg/mL of either ovalbumin or IgG. The gels were equilibrated by placing the vials in a shaking incubator (60 rpm) for 24 hours at 4° C.

4.3.3 Protein Recovery and Analysis

To determine the amount of protein absorbed during the loading step, the protein was leached from the gels by soaking them in 1 mL of protein and polymer free buffer in a shaking incubator at 4° C for 24 hours. The protein concentration of the leached solution was then determined by using a Bradford assay (Thermo Scientific, Rockford, Illinois) according to the procedure provided by the manufacturer. To confirm that all of the protein had been leached from the hydrogels they were then soaked in 1 mL of protein and polymer free buffer for an additional 48 hours and the protein content was measured once again. In all of the samples, 100% recovery occurred in the first 24 hours and no additional protein was detected after that.

4.3.4 Release Kinetics

The release study was done using dextran gels synthesized in the same manner as the loading experiments except that instead of using a disc-shaped mold, the pre-gel solution was injected into a glass capillary tube with an inner diameter of 1.1 mm. The hydrogels were removed from the capillary tubes and loaded using the same procedures described earlier, and

were then placed in 1 mL of pure buffer. For each data point the entire release volume was removed and a fresh allotment of pure buffer was added. The sampled volume was then analyzed using the Bradford assay. To obtain the diffusion coefficient of the protein in the gel, the data was fit to the analytical solution of diffusion from a long cylinder under sink conditions:[27]

$$\frac{M_t}{M_\infty} = 1 - \sum_{n=1}^{\infty} \frac{4}{a^2 \alpha_n^2} \exp\left(-D\alpha_n^2 t\right) \tag{4.3}$$

where M_t is the mass of the solute that has been released from the cylinder at time t, M_∞ is the total mass released from the cylinder, a is the radius of the cylinder, D is the diffusion coefficient, t is time, and α_ns are the roots of the equation $J_0(a\alpha_n) = 0$ where $J_0(x)$ is the Bessel function of the first kind of order zero.[27] An assumption was made that the total amount of protein loaded was the same as the amount of protein released, based on the assumption that any protein that diffuses into the gel should also be able to diffuse out. All the calculations were done on a Microsoft Excel spreadsheet and the least squares method was used to determine the best-fit diffusion coefficient.

4.4 Results

4.4.1 Ovalbumin Partitioning in Hydrogel Systems

In this section, the partitioning of the model protein ovalbumin is studied in both PEG and dextran hydrogels using aqueous two-phase partitioning. Using a variety of loading systems, the protein loading and gel swelling measurements are compared with trends seen in ATPE literature. The concept is then further extended from gel-soluble polymer two-phase systems to a PEG-phosphate two-phase system.

4.4.1.1 Ovalbumin in PEG-Dextran Systems

PEG-dextran systems are the most widely studied aqueous two-phase systems. While previous work by our group focused on the partitioning of proteins in dextran hydrogels, in this chapter the partitioning of proteins in PEG hydrogels was studied under similar conditions in order to make direct comparisons. There are two main sub-hypotheses to be addressed upon looking at the partitioning in PEG hydrogels. The first is that switching from a dextran to a PEG gel, should cause opposite trends be seen in protein partitioning. In our previous work, we saw that the ovalbumin tended to favor the dextran gels over the PEG in solution as predicted by ATPE literature but that the dextran gel deswelled significantly in the PEG solution. When switching to a PEG gel, the hypothesis is that the ovalbumin should now favor the dextran solution, and that this effect can be enhanced by adding KCl to the solution and suppressed by adding tetrabutylammonium fluoride. The second hypothesis is that the swelling degree of PEG hydrogels should be less affected by the addition of dextran to the system than dextran gels are to

the addition of PEG into the system, based on the tie lines seen in PEG-dextran aqueous two phase systems. Confirming these hypotheses increases the versatility of the loading method and proves that the swelling can successfully be predicted from ternary diagrams in ATPE literature.

Table 4.1 summarizes the results of the PEG-dextran loading experiments at three different conditions in order to compare the swelling degree, partition coefficient, and percent loading. As mentioned earlier, the hypothesis is that for a PEG-dextran system, a PEG hydrogel in aqueous dextran will swell more than a dextran gel does in aqueous PEG. Dextran hydrogels have a swelling degree of 7.79 in pure buffer, yet when 10% PEG is added to the system the swelling drops sharply to 3.14, a 60% decrease. PEG hydrogels have a swelling degree of about 10 in pure buffer, yet the addition of 10% dextran only decreases the swelling degree to 7.5, a 25% decrease. The swelling results confirm the hypothesis that the slope of the tie lines in the ternary diagrams seen in literature for aqueous two-phase systems comprised of PEG and dextran directly relate to gel deswelling.[28]

Table 4.1. Swelling Degrees and Ovalbumin Partitioning of PEGDA and Dextran Hydrogels in PEG-Dextran ATP Systems

Hydrogel	Loading Solution	Swelling Degree (g/g)	Partition Coefficient	Percent Loading*
10% Dextran	Buffer, pH 5.9	7.79 ± 0.16	0.29 ± 0.01	0.23 ± 0.01
	Buffer, pH 5.9, PEG	3.14 ± 0.03	2.37 ± 0.12	0.74 ± 0.04
	Buffer, pH 5.9, PEG, KCl	3.28 ± 0.04	5.03 ± 0.89	1.09 ± 0.20
	Buffer, pH 5.9, PEG, Bu_4NF	3.05 ± 0.02	0.80 ± 0.05	0.21 ± 0.01
10% PEGDA	Buffer, pH 5.9	9.57 ± 0.16	0.38 ± 0.02	0.30 ± 0.01
	Buffer, pH 5.9, Dextran	7.55 ± 0.08	0.47 ± 0.04	0.28 ± 0.02
	Buffer, pH 5.9, Dextran, KCl	7.71 ± 0.18	0.40 ± 0.02	0.26 ± 0.01
	Buffer, pH 5.9, Dextran, Bu_4NF	7.39 ± 0.15	0.50 ± 0.03	0.25 ± 0.02
10% PEGDA	Buffer, pH 3.3	10.45 ± 0.21	0.30 ± 0.02	0.29 ± 0.01
	Buffer, pH 3.3, Dextran	8.09 ± 0.22	0.56 ± 0.04	0.43 ± 0.04
	Buffer, pH 3.3, Dextran, KCl	7.59 ± 0.36	0.59 ± 0.03	0.43 ± 0.02
	Buffer, pH 3.3, Dextran, Bu_4NF	7.65 ± 0.19	0.46 ± 0.04	0.33 ± 0.03

*Percent Loading = protein loaded (g) / polymer content (g)
Ovalbumin concentration is 1 mg/mL; Salt concentrations are 0.22 M
Polymer concentrations are 10% (w/w); PEG = 10 kDa, Dextran = 40 kDa
Bu_4NF = tetrabutylammonium fluoride

To clearly demonstrate the trends, the partition coefficients in the dextran gel-PEG solution and PEG gel-dextran solution from Table 4.1 have been plotted in Figures 4.2a (dextran gels) and 4.2b (PEG gels). The results of the partitioning in dextran hydrogels using PEG as the soluble polymer can be seen in Figure 4.2a. When 10% PEG is added, the partition coefficient is increased by a factor of 8 when compared to buffer alone, which is consistent with predictions and our prior work. Additional salts were then added to test the predictions of ATPE regarding the ability of salts to increase or decrease the partition coefficient. Based on heuristics developed for ATPE, KCl should amplify the partitioning into the dextran phase while Bu_4NF should diminish the partition coefficient. KCl and Bu_4NF were both used due to their predicted ability to substantially impact the partition coefficient in opposite manners. It should be noted that there are a wide range of partitioning salts that have been used in literature. The results shown in Figure 4.2a validate heuristics, as the partition coefficient is doubled when KCl is added, from 2.37 to 5.03, while the addition of Bu_4NF causes the partitioning to drop from 2.37 to 0.80, a 66% decrease. The partitioning results in dextran hydrogels show that ovalbumin generally favors the dextran phase over the PEG phase.

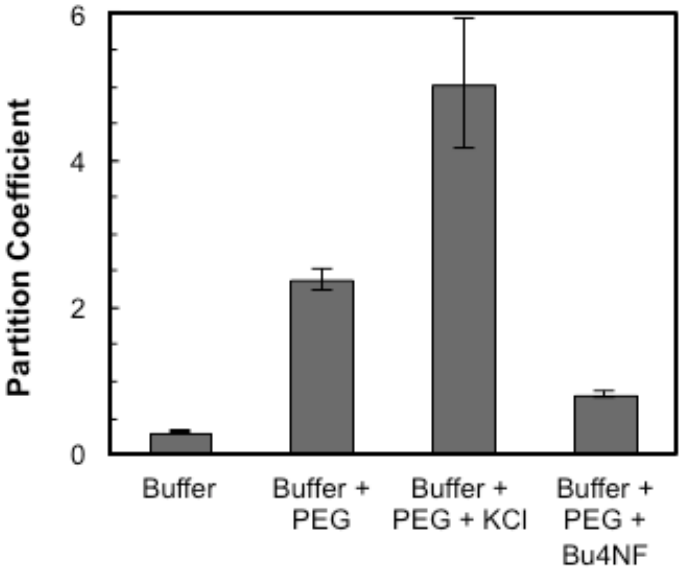

Figure 4.2a. Effect of PEG and salt on the partition coefficients of ovalbumin in dextran hydrogels. The data show that soluble PEG increases the partition coefficient, and salts can be used to amplify or suppress the effect of PEG, consistent with ATPE heuristics. Buffer: 0.01 M Sodium citrate (pH = 5.9). Salt concentrations: 0.22 M. PEG (10kDa) Concentration: 10% (w/w). All differences were statistically significant ($p < .007$)

In switching over to PEG hydrogels, the hypothesis is that the partition coefficients would be lower compared to dextran (since ovalbumin favors the dextran phase), yet that the partition coefficients can still be manipulated using the different salts in a manner predicted by the heuristics. Specifically, it is expected from theory that the partitioning salts would have the opposite effect on ovalbumin partitioning in PEG hydrogels than with dextran hydrogels.[2] The results at pH 5.9, shown in Figure 4.2b, confirm these hypotheses. Although the partition coefficients in buffer alone are similar, the addition of 10% dextran doesn't have nearly the effect that the addition of 10% PEG had on dextran hydrogels. The addition of dextran still causes the partition coefficient to increase, from 0.38 to 0.47. The addition of KCl results in a

decrease in partitioning, which is what was predicted since KCl causes the ovalbumin to favor the dextran phase in this system. However, the addition of Bu_4NF did not result in a statistically significant change in partition coefficient. ($p > 0.05$). Taken as a whole, the results confirm that the while the partitioning in PEG is lower than in dextran, the partitioning still follows the predictions of heuristics and can be increased with the addition of a polymer and even further with the addition of KCl. The partitioning with polymer and Bu_4NF was inconclusive and requires more testing in order to prove a statistically significant increase in partitioning when compared to polymer alone.

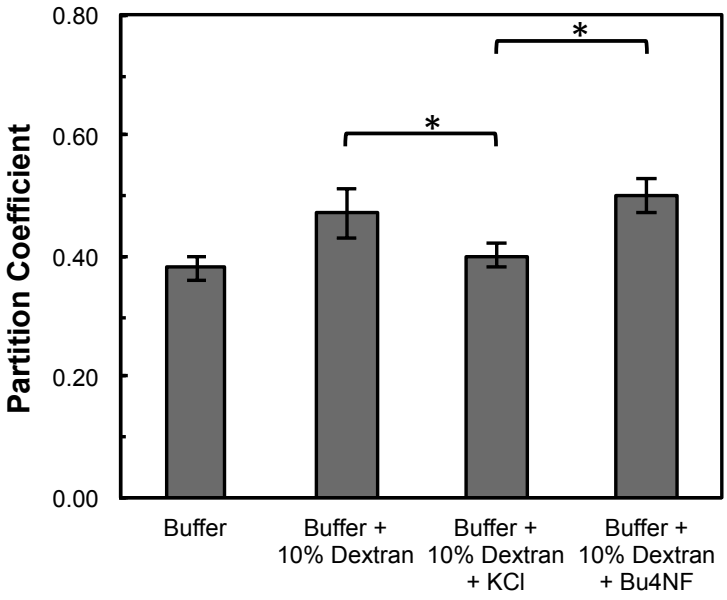

Figure 4.2b. Partitioning of ovalbumin in PEG hydrogels show the effects of dextran and partitioning salts on the partition coefficient. Buffer: 0.01 M Sodium citrate (pH = 5.9). Salt concentration = 0.22M. Dextran (40kDa) concentration = 10% (w/w). *$p<0.05$

The next hypothesis that was tested is the important observation seen in aqueous two-phase systems where switching from above the isoelectric point to below the isoelectric point produces opposite effects in the partitioning. The isoelectric point of ovalbumin is 4.6, and the data presented in Figures 4.2a and 4.2b had been conducted at pH 5.9 where the protein had a net negative charge.[29] The literature heuristics indicate that partitioning salts should affect positively and negatively charged proteins in opposite manners, so at a low pH KCl would be expected to favor the partitioning of ovalbumin into the PEG phase and Bu_4NF to would be expected to favor the partitioning into the dextran phase[2]. The results, shown in Figure 4.3, are consistent with this hypothesis. Once again, the addition of 10% soluble dextran increased the partition coefficient, as the partition coefficient nearly doubles when compared to pure buffer. The addition of KCl did not cause a statistically significant change in partitioning ($p > 0.05$) however the addition of Bu_4NF decreased the partitioning from 0.56 to 0.46, a statistically significant drop that matched predictions ($p=0.04$). The results from these experiments show that the partitioning trends exhibited in ATPE systems can be directly applied to a system containing either a dextran hydrogel or a PEG hydrogel and that these trends are valid both above and below the isoelectric point of the protein.

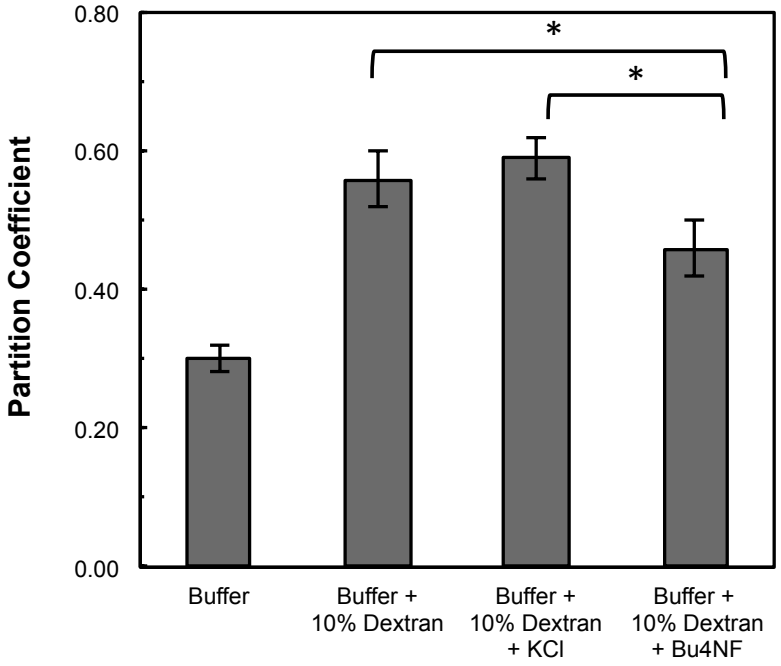

Figure 4.3. Partitioning of ovalbumin in PEG hydrogels at pH 3.3 show the contrasting effects of partitioning salts below the isoelectric point of ovalbumin when compared to Figure 4.1b.
Buffer: 0.01 M Sodium citrate (pH = 3.3). Salt concentration = 0.22M.
Dextran (40kDa) concentration = 10% (w/w). *$p<0.05$

4.4.1.2 Ovalbumin in PEG-Phosphate and Dextran-Phosphate Systems

Although much of the research in literature on aqueous two-phase systems has been focused on polymer-polymer systems there is also a great deal that focuses on polymer-salt systems. One of the most common polymer-salt systems used for ATPE is the PEG-phosphate system, and it is hypothesized that this same system can be used as a successful loading method when, instead of using a soluble PEG phase, PEG hydrogels are used to form the second phase of the system with phosphate. To prove this, the partitioning of ovalbumin into a PEG-phosphate

system as well as a dextran-phosphate system was studied. It is well documented in literature that PEG and phosphate form two separate phases, which should provide a suitable system for loading ovalbumin into PEG hydrogels. On the other hand, due to the fact that phosphate does not induce a phase separation with dextran in solution, no additional thermodynamic driving force from the phosphate is expected. Following this hypothesis, the swelling degrees of PEG hydrogels in a salt solution would be expected to decrease based on the PEG-phosphate phase diagram tie lines if there is phase separation, as was observed with PEG-dextran systems, while the swelling of dextran hydrogels in similar salt solutions would not be affected by the addition of salts since the swelling of nonionic gels is not typically significantly affected by salt.[30]

Figure 4.4a shows the swelling degrees of PEG and dextran hydrogels in the polymer-phosphate system. In buffer alone the PEG hydrogels swell significantly more (13.2 vs. 8.8) than the dextran hydrogels. The addition of phosphates causes the swelling of PEG to drop from 13.2 to 7.0, and the addition of sodium chloride caused an additional decrease in swelling to 4.8. The same addition of phosphates and sodium chloride had very little effect on the dextran hydrogels, which remain at a swelling degree around 10. The partition coefficients of ovalbumin in the polymer-phosphate systems can be seen in Figure 4.4b. In buffer alone, ovalbumin has a partition coefficient of about 0.20 in both dextran and PEG hydrogels, reflecting size exclusion which is primarily a function of water content. When the concentration of phosphate in the loading system is increased to 0.132 M the partition coefficient doubles to 0.43 for the PEG gels, while remaining at 0.20 with the dextran gels. The addition of NaCl further increases the partitioning of ovalbumin into the PEG gels, giving a value of 0.52, yet the partitioning in the dextran gels remains unchanged at 0.2.

The overall trend confirms the hypothesis quite well, although the partition coefficients

for both hydrogels are small in magnitude. The swelling results and the partitioning of ovalbumin in the PEG loading system give clear evidence of two distinct thermodynamic phases that causes the ovalbumin to prefer the PEG phase. The partition coefficient increases with the addition of NaCl as predicted by ATPE heuristics. On the other hand, in the dextran loading system a change is not observed in partitioning or swelling despite the addition of phosphate or NaCl. This confirms the hypothesis that the protein partitioning effect is only seen in systems that contain two thermodynamically distinct phases.

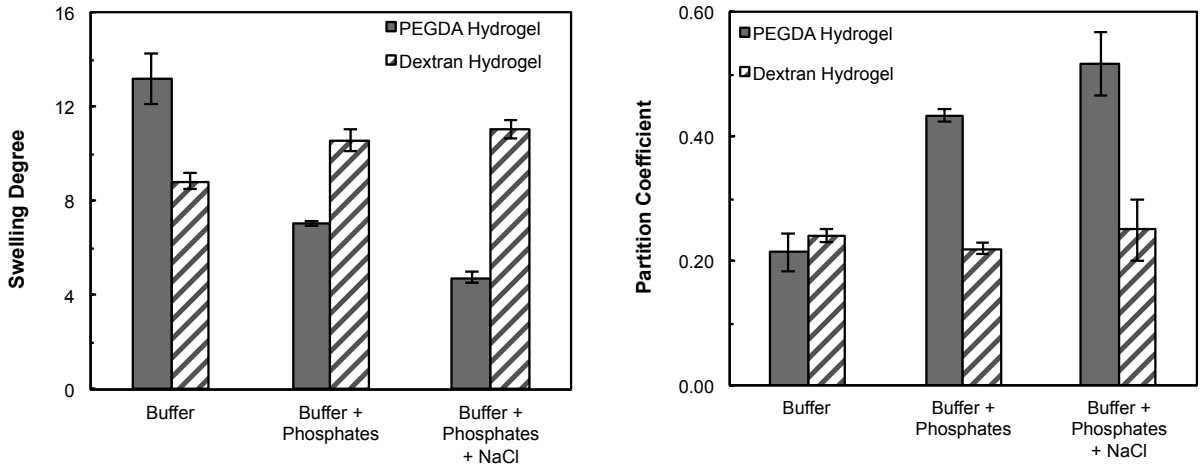

Figures 4.4a & 4.4b. Swelling and partitioning of ovalbumin in a PEG-phosphate system and a dextran-phosphate system. The swelling degrees in Figure 4.3a are consistent with the fact that there is a phase separation in the soluble PEG-salt system but not in the dextran-salt system. Figure 4.3b shows that the partitioning in PEG increases with the addition of salts, while the partitioning in dextran remains unchanged. Buffer: 0.01 M potassium phosphate (pH = 6.0). Phosphate concentration = 0.132 M. NaCl concentration = 1.39 M

4.4.1.3 Release Kinetics

In order to confirm that the protein was distributed throughout the gel and not simply adsorbed onto the surface, a release kinetics study was performed. The results in Figure 4.5 show an example data set for the release of ovalbumin from dextran hydrogels cylinders loaded with a PEG-dextran aqueous two-phase system. The release profile is initially linear with the square root of time, providing visual evidence of Fickian release. Additionally, the curve fit of the release profile based on Equation 4.3 corresponds with the data throughout the entire range and provides further evidence of Fickian diffusion. The calculated diffusion coefficient is 8.1 ± 0.2 x 10^{-8} cm^2/sec (n = 3) which is consistent with values reported in literature for ovalbumin diffusion in hydrogels with similar swelling degrees.[3] The data confirms that ovalbumin is being released in a manner consistent with Fickian diffusion from a uniformly loaded gel.

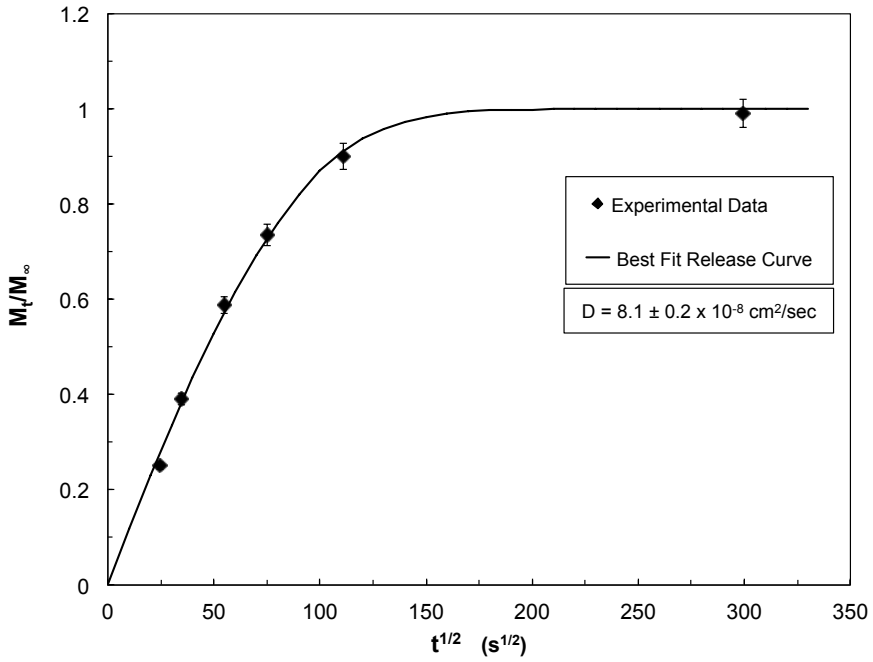

Figure 4.5. Fickian release of ovalbumin from 10% dextran gels confirms protein is distributed within the gel. Buffer: 0.01 M Sodium citrate (pH = 5.9). PEG (10kDa) concentration: 10% (w/w).

4.4.2 IgG Partitioning in Hydrogel Systems

The key motivation for undertaking this research was to determine the feasibility of loading mAbs into hydrogels using the aqueous two-phase system loading concept. With the hypothesis that this loading mechanism is applicable to any polymer system with phase separation, the demonstration of the potential of the technique was undertaken using the partitioning of IgG as the model immunoglobulin for mAbs. This was done by testing the partitioning of IgG in a PEG-phosphate system and the IgG in a PEG-dextran system.

4.4.2.1 IgG in a PEG-Dextran System

In ATPE literature, it has been observed that IgG strongly preferred the dextran phase over the PEG phase, and thus based on the work presented to this point, it is expected that similar trends should be observed with a hydrogel-based aqueous two-phase system comprised of a dextran gel and a PEG loading solution.

For this experiment, the loading and leaching times were increased, and the experiment was run with 50, 100, and 200 hours of loading and leaching times. Although the diffusion of antibodies in hydrogels at very low swelling degrees has not been extensively researched in literature, it was estimated using data from literature and the free volume theory described in Chapter 3[31] that the diffusion coefficient of IgG is about 10,000 times slower than ovalbumin in a dextran hydrogel under these experimental conditions ($D = 7 \times 10^{-12}$ cm^2/s).[31] However, due to concerns about degradation, the experiments were not carried out to equilibrium given the fact that during the length of the entire experiment the IgG would be in solution for a total time of 100, 200, and 400 hours. The amount of linear PEG in solution was also reduced to 6% due to precipitation that occurs at higher concentrations of PEG.[32,33]

The results were as predicted. While IgG is completely excluded from the gel in buffer alone, the partition coefficient increases substantially with the addition of just 6% PEG, as shown in Figure 4.6. The amount of IgG absorbed by the dextran gel increased as the loading time was extended from 50, to 100 and then to 200 hours and resulted in partition coefficients of 5.29 ± 0.16, 8.96 ± 2.71, 17.96 ± 6.40 respectively.

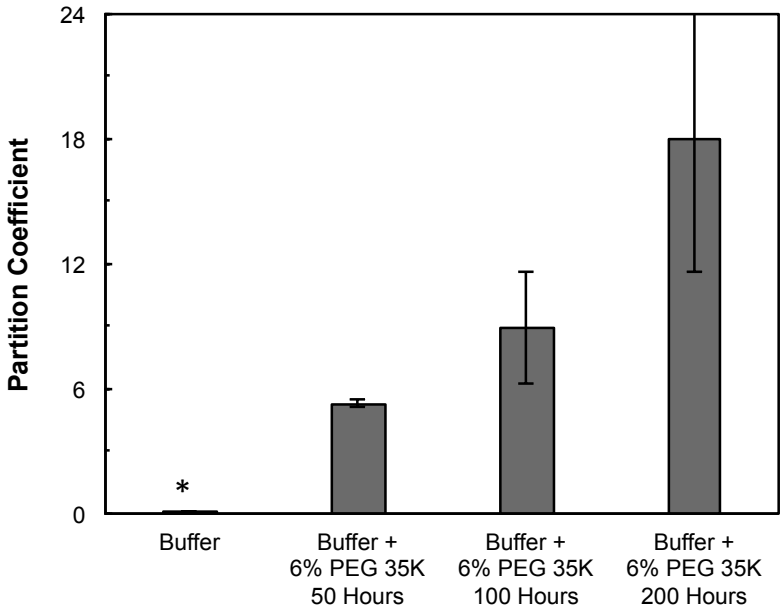

Figure 4.6. Partitioning of IgG into 10% dextran hydrogels show that by adding only 6% PEG to the loading solution, size exclusion can be overcome and a partition coefficient of 18 can be achieved. Buffer = .01 M Potassium Phosphate (pH = 6.6). PEG (35kDa) Concentration: 6% (w/w). *K = 0.06 ± 0.02 All values were statistically significant ($p < 0.05$)

The large partition coefficients of IgG in a dextran hydrogel illustrate the potential for the use of the PEG-dextran system as a mAb hydrogel loading method. While virtually all of the IgG was excluded in buffer alone, the loading percentages were at 3.5% after 200 hours. This is evidence that large amounts of IgG can be selectively partitioned into a hydrogel using only buffer and PEG.

4.4.2.2 IgG in a PEG-Phosphate System

The PEG-phosphate system was examined because the literature predicts a favorable partitioning of IgG into the PEG phase, and PEG gels are widely used in drug delivery. In the ATPE literature, a PEG-phosphate system was successfully used to separate IgG from a hybridoma cell culture supernatant, and the work was followed up on and optimized using pure IgG in a PEG-phosphate system.[34,35] With two aqueous phases, a partition coefficient of 10 or higher was common and in some cases the partition coefficient was measured at over 100.[34,36] The results from the hydrogel loading system can be seen in Figure 4.7 and show that in buffer alone IgG is almost completely excluded (0.06 ± 0.06) from the PEG hydrogel, presumably due to entropically-driven steric size exclusion from the gel mesh. When phosphates are added the partition coefficient jumps up only slightly to 0.12, and as seen in the literature for ATPE, it isn't until sodium chloride is added that a large jump in partitioning to 0.77 is seen.[34]

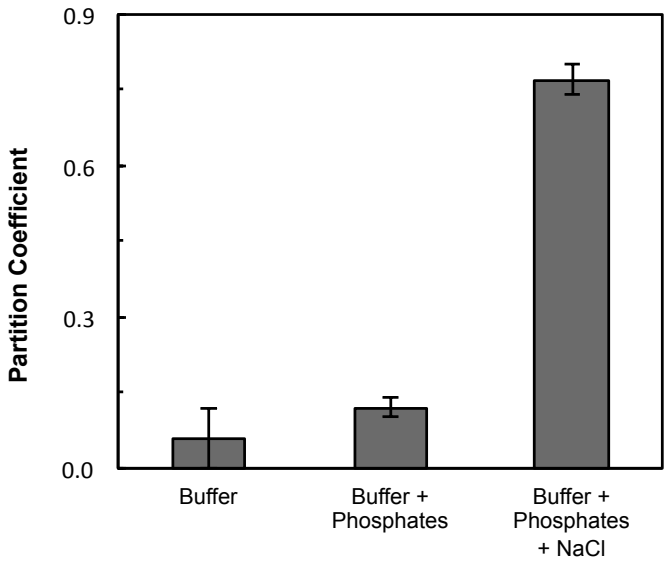

Figure 4.7. Partitioning of IgG into 10% PEGDA hydrogels shows that the addition of phosphates can increase partitioning and overcome size exclusion. Buffer = 0.01 M Potassium Phosphate (pH = 6.0). Phosphate concentration = .132 M NaCl concentration = 1.39 M

The identical experiment was also run using various molecular weights of PEGDA, ranging from 700 Da to 6000 Da. By changing the molecular weight of the PEG it was hypothesized that the structure of the hydrogel network would change, leading to a change in the partitioning. Studies have shown that increasing the molecular weight of the PEG leads to a larger average mesh size which leads to an increase in the diffusivity of proteins within PEG hydrogels.[37,38]

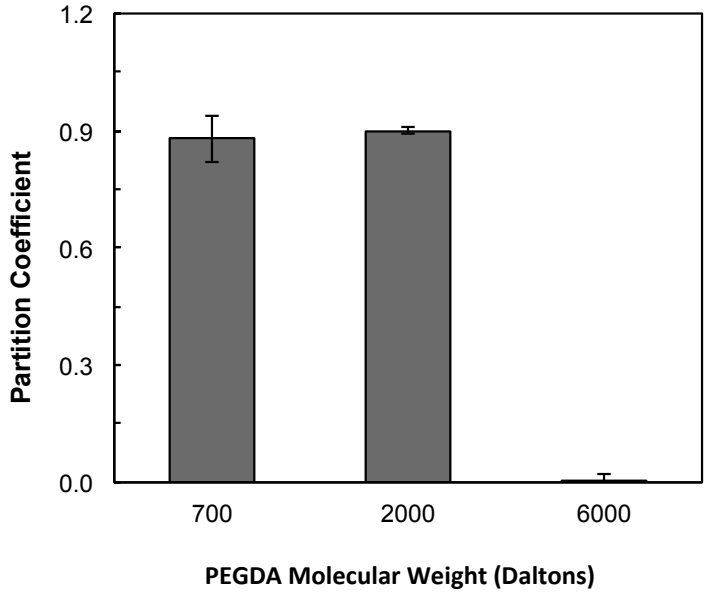

Figure 4.8. Partitioning of IgG into 10% PEGDA hydrogels with varying molecular weights using buffer, phosphates, and NaCl as the loading solution. Buffer = 0.01 M Potassium Phosphate (pH = 6.0). Phosphate Concentration = .132 M NaCl Concentration = 1.39 M

The partitioning of IgG in PEG can be seen in Figure 4.8 along with the corresponding swelling degrees in Figure 4.9. While the partitioning is almost identical at molecular weights of 700 and 2000, when 6000 molecular weight PEG is used to form hydrogels IgG is completely excluded from the gel, despite the fact that all three gels have similar swelling degrees. The

results run counter to the predictions, as a larger mesh size should cause an increase in partitioning. However, the mesh size is a bulk property, and PEG hydrogels are known to have a heterogeneous structure. Despite having a smaller predicted average mesh size, the PEG hydrogels made with 700 and 2000 molecular weight PEG may be more heterogeneous and contain regions in the gel that have a much higher mesh size and allow partitioning.

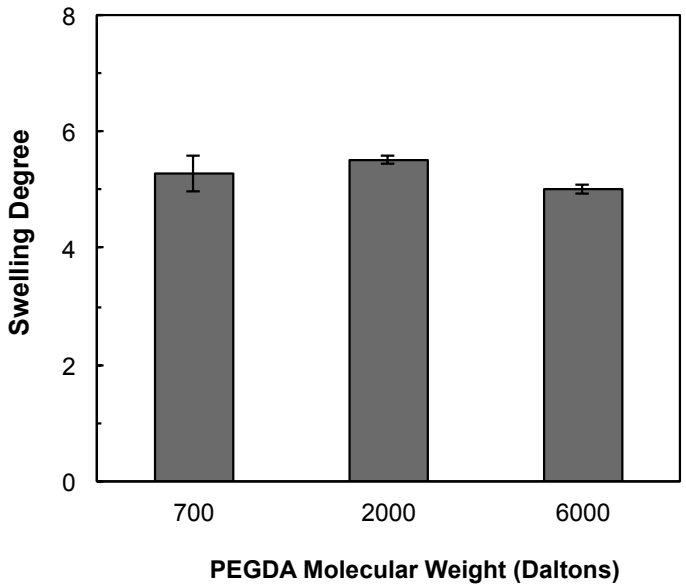

Figure 4.9. Swelling degrees of 10% PEGDA hydrogels with varying molecular weights in phosphate and sodium chloride loading solution. phosphates, and NaCl as the loading solution. Buffer = 0.01 M Potassium Phosphate (pH = 6.0). Phosphate Concentration = .132 M NaCl Concentration = 1.39 M

To further understand the effects of hydrogel network structure on the partitioning, the network structure was altered by changing the solvent in which the polymerization occurred. Previous studies have shown that altering the solvent composition by using various ratios of ethanol and water can significantly affect the network structure of PEG hydrogels. By increasing

the ethanol content of the solvent, the solvent-polymer interaction becomes less favorable and leads to a decrease in the polymer coil's hydrodynamic volume, an increase in heterogeneity, and a decrease in the reaction rate. [39,40] As the ethanol content in the solvent increases, certain PEG hydrogels have been shown to exhibit a significant increase (up to 5-fold) in swelling, as well as a significant (~ 150 fold) decrease in the shear modulus of the gel.[40] However, the swelling degrees of 10% PEGDA hydrogels (seen in Figure 4.10) do not display a significant change as the ethanol content of the solvent is increased. In fact, the swelling degrees only range from 8.35 to 9.86 as the ethanol content in the solvent is changed from 0 to 50% by volume. While the average standard deviation for a given batch is relatively low (0.16), the batch-to-batch variation was higher, as three separate batches synthesized using 20% ethanol produced a range of swelling degrees from 8.54 - 9.86.

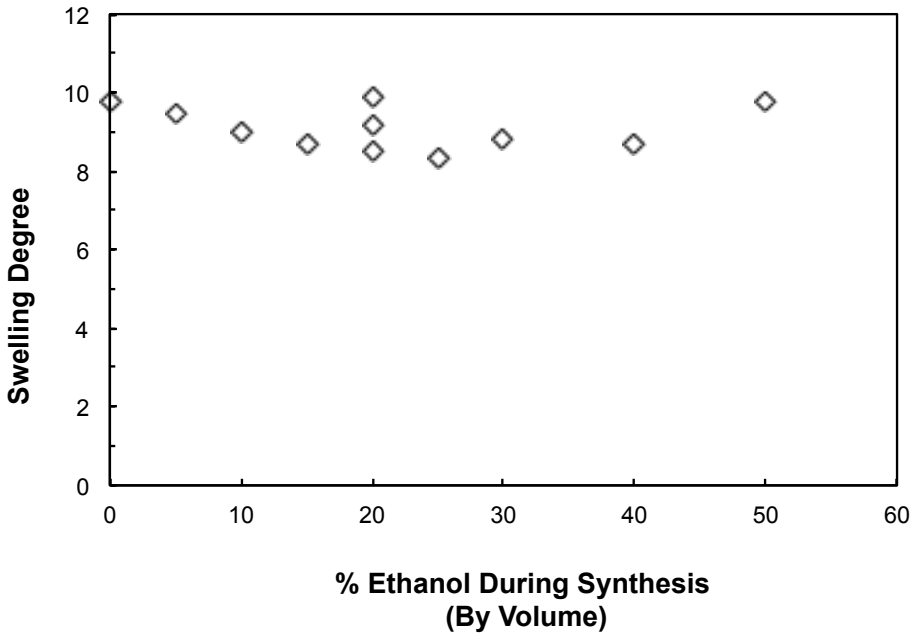

Figure 4.10 Swelling degrees of 10% PEGDA hydrogels synthesized in a water-ethanol solvent. The size of the markers represents the average standard deviation (0.16) that was observed. n=5.

The partitioning of IgG in 10% PEG hydrogels is also not affected by the amount of ethanol present during hydrogel synthesis. The results in Figure 4.10 show that hydrogels synthesized with 25% ethanol in the solvent exhibited similar partitioning results to hydrogels synthesized in pure water. Hydrogels synthesized with 25% ethanol in the solvent displayed a partitioning of 0.72 ± 0.08, while gels synthesized in pure water had a partitioning of 0.76 ± 0.10. While the presence of ethanol in the solvent may result in more heterogeneous PEG hydrogels, the results of Figure 4.11 in combination with Figure 4.10, show that it does not affect the swelling or partitioning.

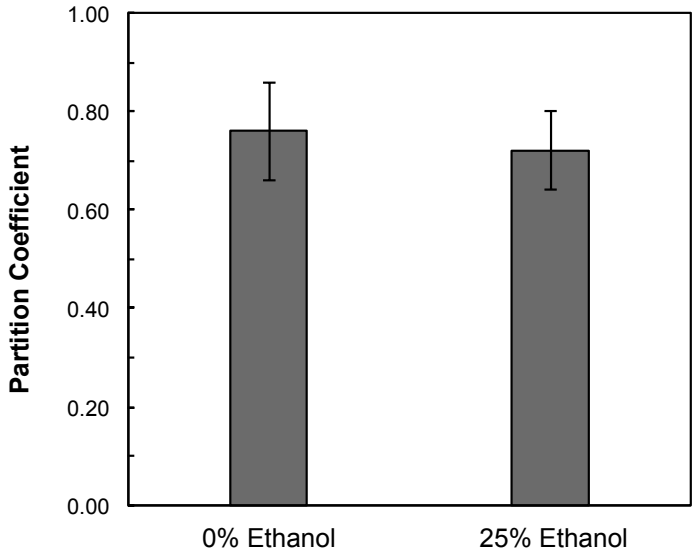

Figure 4.11. Partitioning of IgG into 10% PEGDA hydrogels synthesized in a water-ethanol solvent. Buffer = 0.01 M Potassium Phosphate (pH = 6.0). Phosphate Concentration = .132 M NaCl Concentration = 1.39 M

4.5 Discussion

The results in the previous section confirm the two hypotheses that this chapter set out to test. The loading method used in this chapter for proteins is thermodynamically general and can be extended to a variety of polymer systems where phase separation occurs including both polymer-polymer and polymer-salt systems. In all of the cases the trends match up well with the heuristics that are available from ATPE literature, making the selection of promising formulations for drug loading quick and efficient. The results also show that this drug loading method works very well for mAbs, removing the size exclusion restraints that tend to plague most post loading methods.

The results also show potential for future drug delivery applications that hope to incorporate therapeutic proteins and antibodies into hydrogels. With the addition of only 6% PEG, partition coefficients of up to 18 were reached for IgG in dextran hydrogels, with room for potential improvement. The experiment was not run to equilibrium, no loading salts were used, and only two systems and hydrogels were studied. Future work that focused on maximizing the loading of antibodies into the gels, either by increasing the concentration of antibody in solution or by changing some of the parameters of the loading solution, would further increase the potential of this loading system. A higher partition coefficient leads not only to higher loading concentrations, but it also leads to higher amounts of the protein in the loading solution being absorbed, something that is commercially important when dealing with antibodies that can be incredibly expensive.

Although the magnitude of the partition coefficient of IgG in PEG hydrogels is lower than in the dextran gels the results nevertheless demonstrate the potential of the approach. With the addition of only NaCl and phosphates the partitioning can be increased by almost an order of

magnitude. Regardless, the partitioning may not be high enough to have useful drug loading capabilities in a PEG gel. Looking back at Equation 4.2, in order to effectively use this system for loading antibodies in hydrogels, high swelling degrees would be needed along with a large concentration of antibodies in the loading solution. Unfortunately, the solubility of IgG is limited at high salt concentrations, and precipitation was seen at concentrations above 1 mg/mL. This, combined with the low swelling degrees seen in the loading solution, significantly limits the ability to load high amounts of antibodies into the hydrogels, suggesting that for practical application the PEG-phosphate system may not be suitable for mAb loading.

The results also lay out a roadmap for developing a hydrogel mAb loading system. First, a hydrogel of interest is chosen based on the target application and any safety or biocompatibility restraints. Then, the ATPE literature can be used to identify a thermodynamically incompatible polymer or salt that will create a phase separation and provide a driving force. Ideally a system would be chosen in which the tie lines slope in a favorable direction and would lead to high swelling degrees and a higher loading capacity. And finally, based on the mAb or protein of interest, a loading buffer at a certain pH can be selected along with additional partitioning salts to increase the partition coefficient and maximize loading. The results from this chapter show that the ability to use the extensive amounts of ATPE literature available becomes a significant advantage in developing an effective hydrogel mAb loading system.

However, the experiments also illustrate some of the challenges and limitations of the method. As was mentioned earlier, due to concerns about degradation, the experiment was not run longer than 200 hours. The diffusion of IgG in dextran is much slower than that of ovalbumin in dextran, limiting the practical ability of a drug loading method. In order to load enough IgG into a hydrogel delivery device that is therapeutically useful, a long loading time

might be needed which lowers the effectiveness of the method and could also lead to stability issues. One simple way around this disadvantage would be to use a shorter characteristic diffusion length. The most practical use for the loading system would be in hydrogels systems that could be quickly loaded, such as nanogels and microgels. The small diffusion length would allow for loading times on the order of a few hours, and would help maintain the stability and activity of any therapeutic protein that would be loaded. While larger monolithic devices have their usefulness in drug delivery, there are a lot of advantages that would make nanogels and microgels the preferred route to deliver antibodies and therapeutic proteins.[41-43] One of the potential drawbacks of using an aqueous two-phase system to load proteins into hydrogels previously noted in the literature is the when the system is used to simultaneously crosslink and load microspheres at the same time, it is difficult to wash the microspheres without the protein also leaching out.[44] However, many of the two-phase systems are compromised of common excipients used in drug formulations such as buffers, salts, and polymers that are recognized by the FDA as GRAS (generally recognized as safe), so rinsing the surface may not be required. Additionally, the slow diffusion of antibodies out of the microspheres would allow most of the low molecular weight excipients to rinse out without losing too much of the loaded drug product. Nevertheless, the main advantage of the loading method is in its ability to overcome size exclusion constraints, and this advantage could be used in a number of applications that extend beyond simple monolithic devices.

4.6 Conclusions

The results from the experiments in this chapter confirm that the loading method for proteins is thermodynamically general and can be applied to a number of hydrogels. Systems using hydrogels other than dextran were shown to follow the ATPE heuristics found in literature, greatly expanding the material options for drug delivery. The results also show that both a polymer-polymer and polymer-salt system can be utilized as an effective loading method as long as systems are chosen that contain two thermodynamically distinct phases that induce a phase separation. And most importantly, the results present clear evidence that the loading method can be used to successfully load mAbs into hydrogels.

The results show the potential utility of the method for drug delivery applications. The large amount of ATPE literature available allows a system to be chosen that uses the ATPE heuristics to zero in on promising formulations quickly and efficiently. This greatly reduces the amount of time and experiments needed to develop a successful loading method. The experiments performed in this chapter display how to maximize the loading by increasing the partition coefficient, the swelling degree, and the concentration of protein in the loading solution. While the work presented here was focused on monolithic, diffusion based drug delivery systems, the method can be easily applied to nanogel or microgel based systems. Additionally, by showing that the method works for molecules as large as antibodies, the method provides a much needed and beneficial way to load antibodies into a variety of hydrogel delivery systems at a time when antibodies are being produced and utilized more than ever.

ACKNOWLEDGEMENTS

This work was supported in part by Grant DMR 0805264 from the National Science Foundation. Any opinions, findings and conclusions or recommendations expressed in this article are those of the authors and do not necessarily reflect the views of the National Science Foundation. EVK was generously supported by the Madison and Lila Self Graduate Fellowship.

REFERENCES

1. Gehrke SH, Robeson J, Johnson JF, Vaid N 1991. Protein-Isolation By Solution-Controlled Gel Sorption. Biotechnol Prog 7(4):355-358.

2. Gehrke SH, Vaid NR, McBride JF 1998. Protein sorption and recovery by hydrogels using principles of aqueous two-phase extraction. Biotechnol Bioeng 58(4):416-427.

3. Gehrke SH, Uhden LH, McBride JF 1998. Enhanced loading and activity retention of bioactive proteins in hydrogel delivery systems. J Control Release 55(1):21-33.

4. Walsh G 2010. Biopharmaceutical benchmarks 2010. Nat Biotechnol 28(9):917-924.

5. Sheridan C 2010. Fresh from the biologic pipeline-2009. Nat Biotechnol 28(4):307-310.

6. Rodrigues ME, Costa AR, Henriques M, Azeredo J, Oliveira R 2010. Technological Progresses in Monoclonal Antibody Production Systems. Biotechnol Prog 26(2):332-351.

7. Rader C 2014. Chemically programmed antibodies. Trends Biotechnol 32(4):186-197.

8. Ecker DM, Jones SD, Levine HL 2015. The therapeutic monoclonal antibody market. mAbs 7(1):9-14.

9. Manning MC, Chou DK, Murphy BM, Payne RW, Katayama DS 2010. Stability of Protein Pharmaceuticals: An Update. Pharm Res 27(4):544-575.

10. Vermonden T, Censi R, Hennink WE 2012. Hydrogels for Protein Delivery. Chem Rev 112(5):2853-2888.

11. Gehrke SH, McBride JF, Oconnor SM, Zhu H, Fisher JP 1997. Gel-coated catheters as drug delivery systems. Abstr Pap Am Chem Soc 213:139-PMSE.

12. Censi R, Di Martino P, Vermonden T, Hennink WE 2012. Hydrogels for protein delivery in tissue engineering. J Control Release 161(2):680-692.

13. Peppas NA, Bures P, Leobandung W, Ichikawa H 2000. Hydrogels in pharmaceutical formulations. Eur J Pharm Biopharm 50(1):27-46.

14. Hoare TR, Kohane DS 2008. Hydrogels in drug delivery: Progress and challenges. Polymer 49(8):1993-2007.

15. Siepmann J, Siepmann F 2012. Modeling of diffusion controlled drug delivery. J Control Release 161(2):351-362.

16. McCall JD, Anseth KS 2012. Thiol-Ene Photopolymerizations Provide a Facile Method To Encapsulate Proteins and Maintain Their Bioactivity. Biomacromolecules 13(8):2410-2417.

17. Elbert DL, Pratt AB, Lutolf MP, Halstenberg S, Hubbell JA 2001. Protein delivery from materials formed by self-selective conjugate addition reactions. J Control Release 76(1-2):11-25.

18. Lin CC, Sawicki SM, Metters AT 2008. Free-radical-mediated protein inactivation and recovery during protein photoencapsulation. Biomacromolecules 9(1):75-83.

19. Albertsson PÅ. 1986. Partition of cell particles and macromolecules : separation and purification of biomolecules, cell organelles, membranes, and cells in aqueous polymer two-phase systems their use in biochemical analysis and biotechnology. 3rd ed., New York: Wiley. p 346 p.

20. Stenekes RJH, Hennink WE 2000. Polymerization kinetics of dextran-bound methacrylate in an aqueous two phase system. Polymer 41(15):5563-5569.

21. Franssen O, Vandervennet L, Roders P, Hennink WE 1999. Degradable dextran hydrogels: controlled release of a model protein from cylinders and microspheres. J Control Release 60(2-3):211-221.

22. Franssen O, Stenekes RJH, Hennink WE 1999. Controlled release of a model protein from enzymatically degrading dextran microspheres. J Control Release 59(2):219-228.

23. Armstrong J, Wenby R, Meiselman H, Fisher T 2004. The hydrodynamic radii of macromolecules and their effect on red blood cell aggregation. Biophysical Journal 87(6):4259-4270.

24. West ES, Todd WR, Mascon HS, Van Bruggen JT. 1974. Textbook of biochemistry. ed.: Oxford and IBH Publishing.

25. Jachimska B, Wasilewska M, Adamczyk Z 2008. Characterization of globular protein solutions by dynamic light scattering, electrophoretic mobility, and viscosity measurements. Langmuir 24(13):6866-6872.

26. DeKosky BJ, Dormer NH, Ingavle GC, Roatch CH, Lomakin J, Detamore MS, Gehrke SH 2010. Hierarchically Designed Agarose and Poly(Ethylene Glycol) Interpenetrating Network Hydrogels for Cartilage Tissue Engineering. Tissue Eng Part C-Methods 16(6):1533-1542.

27. Crank J. 1983. The mathematics of diffusion. ed.: Oxford University Press.

28. Zijlstra GM, Michielsen MJF, deGooijer CD, vanderPol LA, Tramper J 1996. Hybridoma and CHO cell partitioning in aqueous two-phase systems. Biotechnol Prog 12(3):363-370.

29. Pezennec S, Gauthier F, Alonso C, Graner F, Croguennec T, Brule G, Renault A 2000. The protein net electric charge determines the surface rheological properties of ovalbumin adsorbed at the air-water interface. Food Hydrocolloids 14(5):463-472.

30. Gehrke SH, Fisher JP, Palasis M, Lund ME. 1997. Factors determining hydrogel permeability. In Prokop A, Hunkeler D, Cherrington AD, editors. Bioartificial Organs: Science, Medicine, and Technology, ed., New York: New York Acad Sciences. p 179-207.

31. Hennink WE, Talsma H, Borchert JCH, DeSmedt SC, Demeester J 1996. Controlled release of proteins from dextran hydrogels. J Control Release 39(1):47-55.

32. Polson A, Potgieter GM, Largier JF, Joubert FJ, Mears GEF 1964. Fractionation Of Protein Mixtures By Linear Polymers Of High Molecular Weight. Biochimica Et Biophysica Acta 82(3):463-&.

33. Gibson TJ, McCarty K, McFadyen IJ, Cash E, Dalmonte P, Hinds KD, Dinerman AA, Alvarez JC, Volkin DB 2011. Application of a High-Throughput Screening Procedure with PEG-Induced Precipitation to Compare Relative Protein Solubility During Formulation Development with IgG1 Monoclonal Antibodies. J Pharm Sci 100(3):1009-1021.

34. Andrews BA, Nielsen S, Asenjo JA 1996. Partitioning and purification of monoclonal antibodies in aqueous two-phase systems. Bioseparation 6(5):303-313.

35. Sulk B, Birkenmeier G, Kopperschlager G 1992. Application Of Phase Partitioning And Thiophilic Adsorption Chromatography To The Purification Of Monoclonal-Antibodies From Cell-Culture Fluid. J Immunol Methods 149(2):165-171.

36. Azevedo AM, Rosa PAJ, Ferreira IF, Aires-Barros MR 2007. Optimisation of aqueous two-phase extraction of human antibodies. J Biotechnol 132(2):209-217.

37. Cruise GM, Scharp DS, Hubbell JA 1998. Characterization of permeability and network structure of interfacially photopolymerized poly (ethylene glycol) diacrylate hydrogels. Biomaterials 19(14):1287-1294.

38. Lee S, Tong X, Yang F 2014. The effects of varying poly (ethylene glycol) hydrogel crosslinking density and the crosslinking mechanism on protein accumulation in three-dimensional hydrogels. Acta biomaterialia 10(10):4167-4174.

39. Mehrdad A, Akbarzadeh R 2009. Effect of temperature and solvent composition on the intrinsic viscosity of poly (ethylene glycol) in water− ethanol solutions. Journal of Chemical & Engineering Data 55(7):2537-2541.

40. Ravi N, Mitra A, Hamilton P, Horkay F 2002. Characterization of the network properties of poly (ethylene glycol)–acrylate hydrogels prepared by variations in the ethanol–water solvent composition during crosslinking copolymerization. Journal of Polymer Science Part B: Polymer Physics 40(23):2677-2684.

41. Bysell H, Mansson R, Hansson P, Malmsten M 2011. Microgels and microcapsules in peptide and protein drug delivery. Adv Drug Deliv Rev 63(13):1172-1185.

42. Hamidi M, Azadi A, Rafiei P 2008. Hydrogel nanoparticles in drug delivery. Adv Drug Deliv Rev 60(15):1638-1649.

43. Oh JK, Drumright R, Siegwart DJ, Matyjaszewski K 2008. The development of microgels/nanogels for drug delivery applications. Prog Polym Sci 33(4):448-477.

44. Schillemans JP, Verheyen E, Barendregt A, Hennink WE, Van Nostrum CF 2011. Anionic and cationic dextran hydrogels for post-loading and release of proteins. J Control Release 150(3):266-271.

Chapter 5: Hyaluronic Acid Hydrogel Implants For The Ocular Delivery Of Therapeutic Proteins

5.1 Abstract

A prototype intravitreal implant was developed with the goal of providing 3-6 months release of anti-vascular endothelial growth factors to the retina for the treatment of retinal diseases such as diabetic macular edema and age-related macular degeneration. The focus of chapter was in developing a hollow cylinder made from a hyaluronic acid (HA) hydrogel that could be filled with a concentrated drug solution and then capped. The hollow cylinder structure was chosen in order to provide the required dosage in a device small enough to be implanted in the vitreous. The device was made from an HA hydrogel due to its similarity in composition to the vitreous humor. However, achieving extended release from a polyelectrolyte gel was especially challenging, as it required a hydrogel with a very low swelling degree. In order to achieve such low swelling degrees, the cylinders were made from HA hydrogels that were highly crosslinked using the difunctional crosslinker divinyl sulfone (DVS). HA-DVS hydrogels with swelling degrees as low as 2.7 were achieved using HA concentrations that ranged from 15-30% (w/w) and HA:DVS ratios that ranged from 3:1–1:1 (w/w). The final prototype cylinders were capable of successfully releasing an antigen-binding fragment (Fab) for over 4 months at a maximum release rate of 4 micrograms a day.

5.2 Introduction

In this work, the use of hyaluronic acid (HA) hydrogels was investigated for the sustained release of therapeutic proteins to the eye. While the rise in the number of people affected by retinal diseases has lead to the development of a promising new class of drugs, the current delivery methods highlight the need for a more effective long-term delivery system. Due to its similarity in composition to the vitreous humor, a HA hydrogel is a logical system to deliver drugs to the retina. The goal of this chapter is to develop a prototype HA hydrogel implant that is capable of delivering sustained release to the retina. In order to achieve sustained release from such a device, a very low diffusion coefficient is required and it is hypothesized that this is only possible with a hydrogel that has a very low swelling degree. Achieving such a low swelling degree is particularly challenging using a hydrophilic polyelectrolyte like HA. While there are many examples of hyaluronic acid hydrogels in literature[1], very few are able to achieve release that extends past a few days or even a week.[2-6]

Two of the most frequent causes of blindness and vision loss in the world come from retinal diseases: diabetic macular edema and age-related macular degeneration.[7-9] Diabetic macular edema (DME) is the swelling of the central retina that is caused by the breakdown and leakage of plasma from the blood vessels that surround the retina.[10] DME affects an estimated 21 million people worldwide, and being a diabetic complication, that number is expected to rise as the amount of people with diabetes is predicted to double by 2030.[11,12] Age-related macular degeneration (AMD) affects more than 25-30 million people worldwide. It occurs in two forms termed “wet” and “dry” AMD. Dry AMD accounts for roughly 80% of all AMD cases, and this form is characterized by extracellular depositions called drusen that form under the retina.[8] Wet AMD, while less prevalent than dry AMD, actually causes more severe and sudden vision loss,

and this occurs when blood vessels expand and form directly beneath the retina, leaking fluid and blood which damage the photoreceptor cells that are responsible for vision.[7] As the prevalence of AMD increases with age, incidences of both wet and dry AMD are expected to rise in the next decade as the population ages and the average life expectancy reaches continues to increase.

While there is no cure for AMD and DME, recent development of anti-vascular endothelial growth factor (anti-VEGF) treatments have allowed patients to successfully manage the symptoms and vision loss of retinal diseases. These treatments work by binding to the protein VEGF and inhibiting its ability to bind to receptors on cells that stimulate angiogenesis and vasculogenesis. Anti-VEGF treatments have been shown to stabilize vision in 90% of patients with wet AMD, with 30% of patients even seeing a substantial improvement in vision.[13] The three most common FDA approved medicines used to inhibit VEGF are ranibizumab (Lucentis, Genentech, South San Francsicso, CA/Roche, Basel, Switzerland), aflibercept (Eylea, Regeneron, Tarrytown, NY), and pegaptanib (Macugen, Valeant Pharmaceuticals, Bridgewater, NJ). Although these three molecules all inhibit VEGF, they are quite different molecules and do so in different ways. Ranibizumab is a recombinant humanized IgG1 kappa isotype monoclonal antibody fragment with a molecular weight of 48 kDa. Aflibercept is a fusion protein of the binding domains of human VEGFR1 and VEGF2 combine with a human IgG1 Fc fragment and has a molecular weight of 97 kDa. Pegaptanib is a pegylated aptamer with a molecular weight of 50 kDa.

The current delivery method of each of these anti-VEGF treatments is an intravitreal injection that are administered to the patient every 4-8 weeks, depending on the drug used and the patient's condition.[14] While effective at reducing symptoms, this delivery method is not only unpleasant for the patient but it also requires frequent trips to the doctor's office. Frequent

intravitreal injections drive up the cost of treatment and can also lead to rare but serious complications such as infectious endopthalmitis, increased intraocular pressure, and cataracts.[15,16] In an effort to reduce the number of injections needed per year, much research has been done on less frequent dosing schedules.[17] The two most widely used dosing schedules are the "as needed" and "treat and extend". In the "as needed schedule", three monthly injections are given initially and then the patient is monitored and given more injections only when evidence of disease reoccurs.[18] In the treat and extend schedule, three monthly injections are given initially and the patient continues to receive additional injections that are continuously extended by two weeks as long as symptoms do not reoccur and there are no signs of increased neovascularization.[19,20] While these regimens do reduce the number of injections per year (from 12 to on average 5-8[21]), the overall health benefits and long term impact on the patients are still being debated and studied. It is clear, however, that a long term, sustained delivery device would offer a number of advantages including convenience, safety, and financial benefits when compared to the current intravitreal dosing regimen.

There are a number of drug delivery methods that have been developed to deliver long-term, sustained release to the retina including microspheres, implants, microcatheters, injectable depots, and even microneedles.[22-24] Of these methods, the one that has had the most clinical and regulatory success so far has been implants.[25] Early efforts focused on implants that were non-biodegradable and made from a combination of polymers such as polyvinyl alcohol, ethylene vinyl acetate, and silicone. Vitrasert ® and Retisert ® (Bausch & Lomb, Rochester, NY) were two of the first non-biodegradable implants commercially available and can effectively deliver the small molecule drugs ganciclovir and fluocinolone acetonide (255 and 452 Da) for eight months and three years respectively for the treatment of cytomegalovirus retinitis and chronic

uveitis.[26,27] While these implants are excellent at controlling the release rate of small corticosteroids for an extended period of time they have the downside of having to be surgically implanted and removed once the implant is depleted.[28]

In an effort to reduce the amount of surgery needed, biodegradable implants were developed. The hydrophobic polymers polylactide (PLA) and poly(lactide-co-glycolide) (PLGA) are the most widely used biodegradable materials for ocular implants.[29] In 2009 the FDA approved Ozurdex® (Allergan, Irvine, CA), a biodegradable PLGA implant that is able to deliver 0.7 mg of dexamethasone (392 Da) for up to 6 months for patients who suffer from DME.[30] Despite the success of these implants for small molecule drugs, the heat, pressure, and solvents required to integrate the active substance and form the implant limits the process to small, stable molecules. The anti-VEGF treatments needed for wet AMD are less stable and have a tendency to aggregate when incorporated into a biodegradable implant.[31] Although some recent work has been able to limit this aggregation[32], more work is needed in order to achieve a biodegradable implant that can safely and effectively deliver the anti-VEGF treatments.[25]

An alternative option to hydrophobic polymer implants is hydrogels, which have been shown to be effective at delivering proteins.[33,34] Hydrogels are hydrophilic polymer networks that are crosslinked into a permanent three-dimensional network. These networks have the ability to swell in aqueous solution and take up a considerable amount of water, making them suitable for storing sensitive proteins and antibodies. Hydrogels can be formed into many different shapes and sizes and can be synthesized from a wide variety of biocompatible and biodegradable polymers. Because of their versatility and wide range of properties, hydrogels offer a promising potential for ocular delivery, both as injectable implants and as *in situ*-forming hydrogels.[35-37]

As a natural component of the eye, HA is a logical choice for a hydrogel delivery system that would be implanted in the eye for long periods of time, where biocompatibility and low toxicity are crucial for success.[38] Hyaluronic acid is a negatively charged, linear, unbranched polysaccharide that is composed of repeating units of the disaccharide glucoronic acid and N-acetylglucosamine.[39] It has an unusually high viscosity and this coupled with its ability to hold and retain water gives HA a number of integral roles in the human body, including providing structure in the vitreous of the eye.[40,41] The biocompatible and biodegradable nature of HA along with its unique properties has led to an increase in its use in biomedical applications over the years, including applications in tissue engineering, cardiac repair, valvular engineering, the treatment of osteoarthritis, the prevention of post-surgical adhesions, and even as a dermal filler.[42] HA has also been used extensively in clinical ophthalmology for the treatment of severe dry eyes and as a viscoelastic agent in cataract surgery.[43-45] HA hydrogels crosslinked with adipic acid dihydrazide were tested on retina pigmented epithelium (RPE) cells and were found to be non-toxic, and crosslinked HA hydrogels were also seen to be biocompatible when injected subconjunctivally. [46,47]

Unlike the hydrophobic polymers mentioned earlier, hydrogels have high water contents, which cause proteins diffusing through them to have relatively high diffusion coefficients (10^{-7}-10^{-8} cm^2/s). Because of their high water content, these hydrogels often exhibit the rapid release of drugs by diffusion. [48,49] HA hydrogels that are chemically or physically crosslinked often display release profiles that see complete release in less than a few days, and in limited cases, up to a few weeks.[50] In order to extend the release rate of drugs, a HA hydrogel with a low water content is needed, and it is hypothesized that this can only be achieved with a highly crosslinked HA gel. In this chapter, the feasibility of synthesizing a HA hydrogel with a low water content

was investigated using the crosslinker divinyl sulfone (DVS). While there are a number of ways to crosslink HA, using DVS has a number of advantages for this project. Unlike many other crosslinking methods, crosslinking with DVS requires no prior modification of HA, as the hydroxyls groups of HA react with the vinyl groups of DVS.[51] While this reduces the time and cost needed to prepare the HA, the ability to react with the hydroxyl groups also provides DVS with a large number of possible crosslinking sites. HA gels formed with DVS have also been shown to be bioinert, while polysaccharide gels made with a comparable crosslinker gluteraldehyde have shown cytotoxicity when exposed to retinal pigment epithelial cells.[52,53] While the synthesis method has been used before in literature, all of the resulting HA-DVS gels had high swelling degrees ($q > 20$). [52,54-56]

Despite these advantages, one of the limitations in using DVS to crosslink HA is that proteins cannot be incorporated into the hydrogel during formation. Since the reaction is a base catalyzed Michael addition, the reaction only occurs under alkaline conditions. This, along with the long reaction time required for crosslinking (24 hrs) can cause DVS to react with proteins during hydrogel formation, leading to a potential loss in activity and the possibility of covalently attaching the proteins to the hydrogel network. One of the ways around this problem is to synthesize the hydrogel and then postload the drug into the gel after formation.

In this chapter, the release of model protein was studied using hollow cylinders that were made of HA-DVS hydrogels. Due to its simple design, hollow cylinders have been used before in drug delivery systems, and their principles are well understood. They can be fabricated without the protein, and then subsequently loaded so that degradative conditions are minimized. The ability to load a single drug or multiple drugs, as well as slurries or suspensions makes these very versatile for drug delivery applications. Additionally, the inner and outer diameters can be

easily adjusted to fine-tune the release profile and the amount of drug that can be delivered and the cylindrical shape also makes it very convenient to inject.

There were a number of scientific goals that this chapter set out to achieve in order to develop a prototype HA hydrogel implant that is capable of delivering sustained release to the retina. The first was to determine if hollow mini cylinders could be fabricated using HA hydrogels crosslinked with DVS. The second was to determine if these hydrogels could be made with a swelling degree low enough to produce the diffusion coefficients required to achieve extended release. Whether or not it is possible to achieve such low diffusion coefficients is something that has not been proven in literature to date using HA hydrogels. The final goal of this chapter was to demonstrate that a HA-DVS implant could achieve 3-6 months release at a rate that would be therapeutically effective if injected or surgically implanted in the back of the eye using model proteins of similar size to the anti-VEGF treatments currently on the market.

5.3 Materials And Methods

5.3.1 Materials

Hyaluronic acid (51 kDa Mw, pharmaceutical grade from bacterial fermentation)was obtained from Lifecore Biomedicals (Chaska, MN). Bovine serum albumin (BSA, lyophilized powder, ≥ 98%), divinyl sulfone (DVS >98%), ethylene glycol, and vitamin B_{12} were obtained from Sigma Aldrich (St. Louis, MO) along with an albumin–fluorescein isothiocyanate conjugate (FITC-BSA) and sodium azide (>99.5%). Pierce™ Coomasie Plus Bradford Reagent was obtained from Thermo Fisher Scientific (Waltham, MA). Additionally, an antigen-binding fragment (Fab) with an approximate weight of 50 kDa was donated by a pharmaceutical company and used in this work.

5.3.2 Hydrogel Synthesis

Hyaluronic acid hydrogels were synthesized by mixing various concentrations of hyaluronic acid and the crosslinker divinyl sulfone in an aqueous solution of 0.02M NaOH. The mixture was stirred vigorously by hand using a glass rod and then centrifuged for one minute to remove any air bubbles. It was then pipetted into molds that were 2 mm thick and had precut holes 5 mm in diameter. These molds were clamped between two thin glass plates (1 mm thick) and allowed to react for 24 hours at room temperature. Once formed, the gels were removed from the molds and placed into an excess of D.I. water to remove any unreacted monomer or crosslinker. In some cases, the gels were then placed in 30% (v/v) ethylene glycol (0.02 M NaOH) solution for 48 hours to cap any singly reacted vinyl sulfone groups that might be reactive toward the protein.[57] The gels were rinsed by soaking them in excess D.I. water that was changed every 12 hours.

5.3.3 Swelling Degree

Fully formed gels were soaked in solutions of D.I. water and 0.01 M phosphate buffer saline (PBS, pH =7.4, Sigma Aldrich) until they were fully equilibrated. The gels were lightly blotted to remove excess water and the wet mass was then measured. The gels were then placed in a dessicator for 48 hours and allowed to dry. The gels that were soaked in PBS were first soaked in excess D.I. water to remove any salt before being placed in the dessicator. The dry mass was measured and the swelling degree (q) was defined as:

$$q = \frac{\text{Wet Mass}}{\text{Dry Mass}} \tag{5.1}$$

5.3.4 Mechanical Testing

The compressive modulus (E) and shear modulus (G), fracture stress, and fracture strain, were calculated from stress vs. strain data measured using a RSA-III dynamic mechanical analyzer (TA Instruments, New Castle, DE). Cylindrical gels were tested under uniaxial compression at a rate of 0.05 mm/s until failure. The compressive modulus was calculated from the initial slope of the stress-strain curve. The shear modulus (G) was calculated using the neo-Hookean model for an ideal elastomer as the slope of the stress (σ) versus the strain function $\left(\lambda - \frac{1}{\lambda^2}\right)$ as shown below:

$$\sigma = G\left(\lambda - \frac{1}{\lambda^2}\right) \tag{5.2}$$

where $\lambda = L/L_0$ and L and L_0 are the thickness of the deformed and undeformed specimen, respectively.

The crosslink density was calculated using the swelling degree and the shear modulus according to the affine model of rubber elasticity:

$$\rho_x = \frac{G}{RT\, \upsilon_2^{1/3}\, \upsilon_{2r}^{2/3}} \tag{5.3}$$

Where ρ_x is the crosslink density, R is the ideal gas law constant, T is the absolute temperature, v_2 is the polymer volume fraction at the testing conditions, and v_{2r} is the polymer volume fraction during hydrogel formation.

ρ_x was used to calculate the molecular weight between crosslinks, $\bar{M}_c$, using the equation:

$$\bar{M}_c = \frac{\rho_2}{\rho_x} \tag{5.4}$$

in which ρ_2 is the density of the dry polymer network. The molecular weight between crosslinks was then used in calculating the average mesh size of the gels using the following equation [58]:

$$\xi = v_{2,s}^{1/3} \left[C_n \left(\frac{2\bar{M}_c}{M_r} \right) \right]^{\frac{1}{2}} l \tag{5.5}$$

where C_n is the Flory characteristic ratio for HA, M_r is the molecular weight of the repeating units, and l is the length of bond along the polymer backbone.

5.3.5 Confocal Microscopy Diffusion Study

15% (w/v) 2:1 and 3:1 HA hydrogel discs were placed in vials containing 1 mg/mL of FITC-BSA in 0.01 M PBS (pH 7.4) with 0.01% NaN_3. The vials were gently stirred at 4° C until being tested. At predetermined time points, the samples were removed and 3-dimensional image stacks were taken using a Zeiss Meta 510 upright confocal microscope (Carl Zeiss, Thornwood,

NY). The slices were 5.9 μm thick and the images taken had 512 x 512 pixels with a pixel size of 0.5 μm. FITC-BSA was excited at 488 nm using an argon laser and the fluorescence was collected using a 505 nm long pass filter. At each time point, 3 images were taken from each gel at different locations in order to remove any effects of photobleaching that could occur. The concentration of FITC-BSA was found to have a linear relationship with emission intensity for the range of concentrations in this study and the shallow sample thickness that was being measured minimized any effects of signal attenuation. The discs had a diameter to thickness aspect ratio of 5, which was sufficient to make the assumption that diffusion occurred only in the z direction and that radial diffusion was negligible given the size of the sample and the low diffusion coefficient being measured. All of the images obtained were analyzed using ImageJ software (v1.49), obtained directly from the National Institutes of Health.

5.3.6 Hollow Cylinder Fabrication

In order to form the gels into hollow cylinders, custom molds were machined using polytetrafluoroethylene and stainless steel cylindrical rods of varying diameters. A small glass plate was sealed at the bottom of the base of the mold and the HA-DVS solution was pipetted in. The upper cap was then inserted into the mold and clamped into place. After 24, hours the upper cap and glass plate were removed and the hollow cylinder was carefully ejected from the mold using a custom plunger (shown in Figure 5.1). The cylinders were then placed into an excess of D.I. water to remove any unreacted polymer or crosslinker. All of the cylinders had identical outer dimensions with a height of 10 mm and a width 1 mm in diameter. The inner diameters varied from 0.460 mm to 0.635 mm.

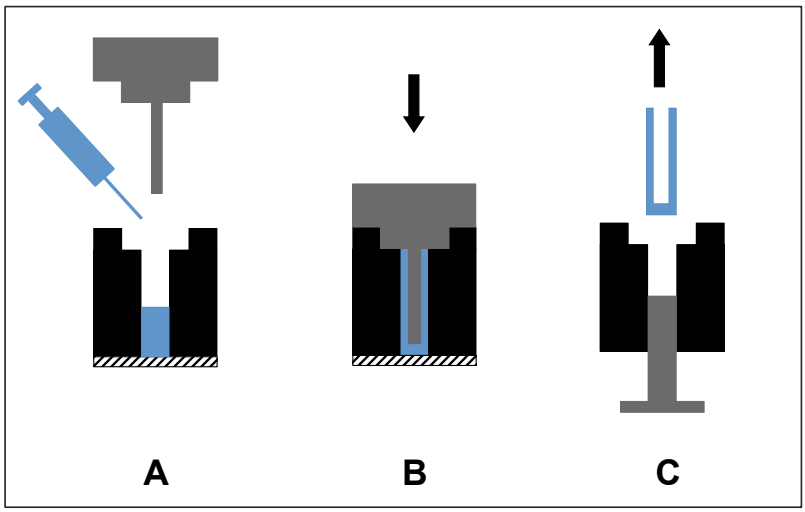

Figure 5.1. Fabrication method used to create HA-DVS hollow cylinders. (A) HA-DVS solution is pipetted into a mold. A glass plate seals the bottom of the mold. (B) Upper cap is inserted into the mold while the crosslinking reaction occurs. (C) Both the upper mold and glass plate are removed and the finished hollow cylinders are removed from the mold using a custom plunger.

5.3.7 In Vitro Release from Hollow Cylinders

Hollow cylinders were loaded with a concentrated solution of either vitamin B_{12}, BSA, or the Fab in 0.01 M PBS (pH 7.4) with 0.01% NaN_3. The cylinders were then carefully capped using cyanoacrylate glue and placed in a vial with 1 mL of buffer. At predetermined time points the buffer was removed and was replaced with fresh buffer in order to maintain sink conditions. The concentration of the proteins were then measured using a Bradford assay, while the concentration of vitamin B_{12} was measured by absorption at 550 nm using a Cary 300 UV-Vis spectrophotometer (Agilent Technologies, Santa Clara, CA). This process was repeated until all of the protein was released. All of the release studies were performed at room temperature and were gently shaken to reduce external mass transfer resistance. The diffusion coefficient was calculated using COMSOL Multiphysics© software, a program that uses a finite element method to model the release from the hollow cylinders. The release of drugs from a hollow cylinder was modeled using Fick's first law:

$$N_i = -D_i \nabla c_i \tag{5.6}$$

where N_i is the flux of solute i, D_i is the diffusion coefficient, and ∇c_i is the concentration gradient of species i. When combined with the continuity equation for mass,

$$\frac{\partial c_i}{\partial t} + \nabla \circ N_i = 0 \tag{5.7}$$

Fick's second law is obtained and is the main equation used to model the unsteady-state diffusion in multiple dimensions:

$$\frac{\partial c_i}{\partial t} = D_i \nabla^2 c_i \tag{5.8}$$

The COMSOL software also includes convection terms into the equations, however these were set to zero due to the fact that the release through the walls of the hydrogel implants occurs only by diffusion. A boundary condition set the diffusion from the top of the cylinder equal to zero, simulating an impermeable cap and the initial concentration outside of the cylinder was set at zero. Diffusion coefficients were calculated for each data set using the software's parameter estimation model.

5.4 Results And Discussion

In this section, the goal was to create a prototype hydrogel implant that could deliver therapeutic proteins for three to six months. Achieving extended release required a hydrogel with a very low swelling degree. A number of concentrations of HA and various ratios of HA:DVS were tested in an effort to produce hydrogels with low swelling degrees and high crosslinking densities. The mechanical and swelling properties of HA hydrogels were examined and used to estimate the diffusion coefficient of various sized solutes. HA hollow mini cylinders were then fabricated and loaded with vitamin B_{12}, BSA, and a model Fab and the release rates were measured. In order to confirm that the diffusion coefficient was in the desired range, 1-D diffusion was also measured through confocal microscopy by using Fickian diffusion models and high molecular weight fluorescent probes.

5.4.1 Designing a Hollow Cylinder

In order to be successful in delivering therapeutic proteins to the retina, a hollow mini cylinder has to meet certain requirements. These include having the proper release rate and total dosage required as well as having the proper diameter, length, and structural integrity to be effective. The most important requirement is to be able to deliver the amount of drug needed to be therapeutically effective when implanted into the eye. The target release rate for this work was 2.5 micrograms per day, which when delivered over a period of 3-6 months, gives a total dosage target of 225-450 micrograms. For comparison, intravitreal injections of ranibizumab and aflibercept are 0.5 mg and 2.0 mg, respectively.

Another important design specification is the size of the hollow cylinder. While the smallest cylinder possible would be best, the cylinder has to be able to hold 450 micrograms of

drug and at the same time have a wall thick enough to slow the release of drug to achieve the extended release needed. Additionally, the cylinder has to have enough structural integrity to be washed, loaded with drug, and inserted in the eye. Some of the early non-biodegradable implants were cylinders that were 0.37 mm in diameter (Iluvien®, Psividia, Watertown, MA) and could be injected with a 25-gauge needle. The biodegradable implants that followed were generally larger, as Ozurdex ® has a diameter of 0.45 mm and is injected into the vitreous using a 22-gauge microinjector. The largest implant available to date is Renexus® (Neurotech, Cumberland, RI), which is currently in Phase II clinical trials[59]. This polymeric hollow cylinder is 6 mm long, has a diameter of 1 mm, and is inserted through a 2 mm incision in the pars plana.

The dimensions of the HA cylinders used in this paper have a diameter of 1 mm and a length of 10 mm. The thickness of the cylinder walls ranged from 0.183 mm to 0.27 mm. Dimensions of this size would certainly require an incision in the pars plana in order to insert the cylinder into the eye, an option that is much less convenient than an injection with a small needle. While the larger dimensions were suitable for carrying out the release experiments and handling the cylinders, the cylinders can theoretically be scaled to any dimension required. Once the diffusion mechanism is well understood, release rates and profiles can be quickly calculated and controlled by varying the dimensions of the cylinder, the formulation of HA hydrogel, and the drug size and concentration as will be discussed in Chapter 6.

Given the total dosage needed and the hollow cylinder dimensions, a target diffusion coefficient was calculated using COMSOL. Based on these calculations, in order for the cylinder to release 450 micrograms for at least three months within the given geometric constraints, a diffusion coefficient of 7×10^{-11} cm^2/s is needed.

5.4.2 Formulating HA-DVS Hydrogels

In order to achieve the desired release rate, an HA hydrogel had to be synthesized that could achieve this very low diffusion coefficient. As discussed in Chapter 3, there are several factors that influence the diffusion rate of solutes in hydrogels, primarily solute size and swelling degree. [60] There are many models used to predict solute diffusion in gels. They invariably include parameters related to solute size and water content, and some even include parameters associated with the polymer gel network. The Yasuda et al. free volume theory yields a simple but widely used equation that determines the diffusion coefficients of solutes in hydrogels using the parameters seen in the equation below:

$$\ln\left(\frac{D_H}{D_0}\right) = \ln(\Phi) - \left(\frac{kr_s^2}{V_f}\right)\left(\frac{1}{H} - 1\right) \qquad (5.9)$$

where, D_h is the diffusion of the solute in the hydrogel, D_0 is the diffusion of the solute in water, k is a constant based on the characteristic of the polymer, r_s is the hydrodynamic radius of the solvent, and V_f is the free volume unoccupied by the solvent or the polymer chains. H is the degree of hydration of the hydrogel and is directly related to the swelling degree $\left(q = \frac{1}{1\text{-}H}\right)$. Φ is a sieving factor that takes into account the screening effect of the network. While the shortcomings of free volume theories were discussed in Chapter 3, this theory and Equation 5.9 were used due to its widespread use in drug delivery literature and because it provided the best fit of the sample data that was available in literature.

There are a large number of studies in literature that measure the diffusion coefficients of solutes of various sizes in highly swollen polysaccharide hydrogels. While there is little

information available on the diffusion in HA hydrogels, work has been done determining the diffusion coefficients of IgG, BSA, and Vitamin B_{12} in dextran hydrogels at a wide range of swelling degrees.[61] Using the Yasuda et al. free volume theory (Equation 5.9) and the data from literature, the slope (kr_s^2/V_f) can be approximated from a plot of $\ln(D_m/D_0)$ vs. (1/H -1) for each solute of radius r (Figure 5.2). This slope is a characteristic of the polymer/water system for dextran hydrogels and, despite differences in the structure of the polysaccharides, it was assumed that HA hydrogels would exhibit a slope similar enough to make an acceptable estimate of the diffusion coefficient.

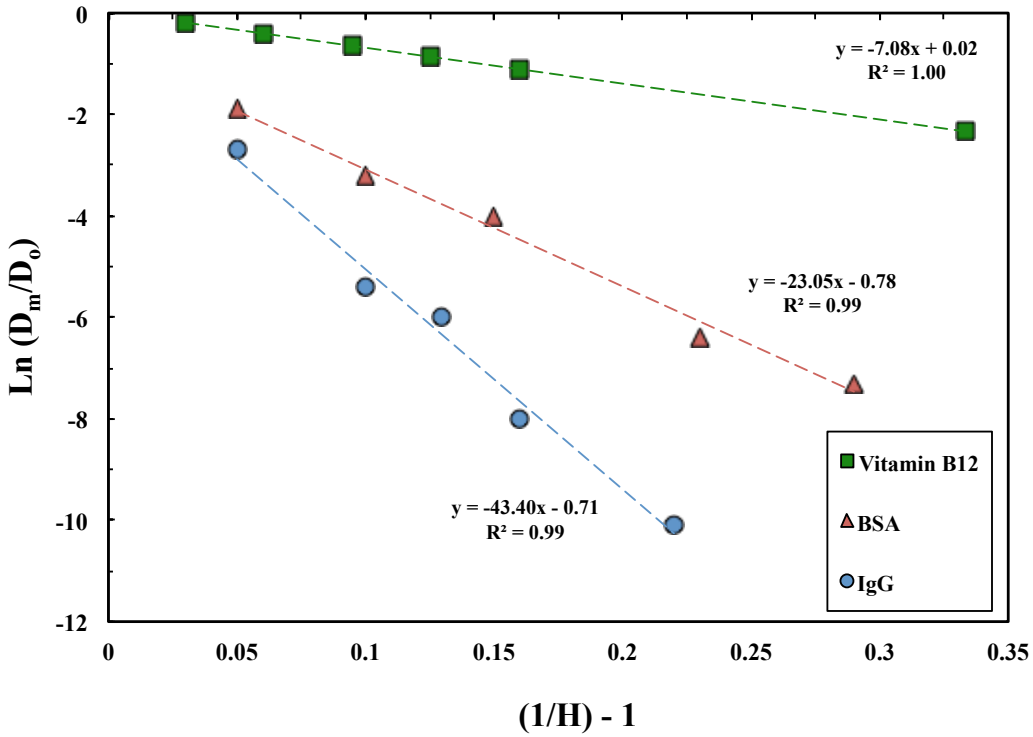

Figure 5.2. The logarithm of the normalized diffusion coefficients of various solutes in dextran hydrogels as a function of the inverse of hydrogel hydration. The data points represent actual diffusion coefficients measured in literature and the dashed lines represent the calculated slopes and equal (kr_s^2/V_f). Adapted from Hennink et al.[62,63]

With this information, a plot of the diffusion coefficient as a function of swelling degree can be created, and the data can be extrapolated down to very low swelling degrees (q<6). This is seen in Figure 5.3 for Vitamin B_{12}, BSA, and IgG. The proteins (BSA, IgG) were chosen because of their similarity in size to a Fab and mAb. Vitamin B_{12} was chosen due to its use as a test marker when working with the prototype cylinders. The data points represent the actual diffusion coefficients measured in literature for dextran gels, and ranged in swelling degrees from 20 to 4. The curve represents the extrapolated projections based on the free volume theory, assuming Φ is equal to 1. In order to reach the target diffusion coefficient of 7×10^{-11} cm^2/s, a swelling degree of roughly 3.5 is needed for a solute with a similar hydrodynamic radius of BSA. If a larger solute is used, such as IgG, a higher swelling degree of 5.8 can achieve the same diffusion coefficient. On the other hand, if a smaller solute is used, such as Vitamin B_{12}, a much lower swelling degree of 1.6 is needed to reach the target diffusion coefficient.

Figure 5.3 illustrates the difficulty in achieving the target diffusion coefficient of 7×10^{-11} cm^2/s. In order to achieve this diffusion coefficient, very low swelling degrees are required, and as was discussed in Chapter 3, it is hypothesized that under these conditions the size of the solute approaches the average mesh size of the hydrogel and can lead to a dramatic reduction in the diffusion coefficient. The free volume theory takes this hypothesized screening effect into account by introducing the sieving factor (Φ) seen in Equation 5.9. For the calculations in Figure 5.3, Φ was set equal to 1, making the initial term go to zero. However, at very low swelling degrees is exactly where the solute size would begin to approach the average hydrogel mesh size and these hypothesized screening effects would begin to take place. In fact, one method used to get a rough measurement of the average mesh size of hydrogels is to determine at what swelling degree the diffusion coefficient begins to stray from the free volume theory[61,62].

Nevertheless, the free volume theory and the extrapolations made in Figure 5.3 are a useful tool to estimate the swelling degree needed to achieve the extended release from a hollow cylinder. Given that the sieving factor ranges from 1 to 0, any additional screening effects that occur would result in a lower diffusion coefficient than predicted in Figure 5.3, and would allow for a hydrogel with a higher swelling degree to be used.

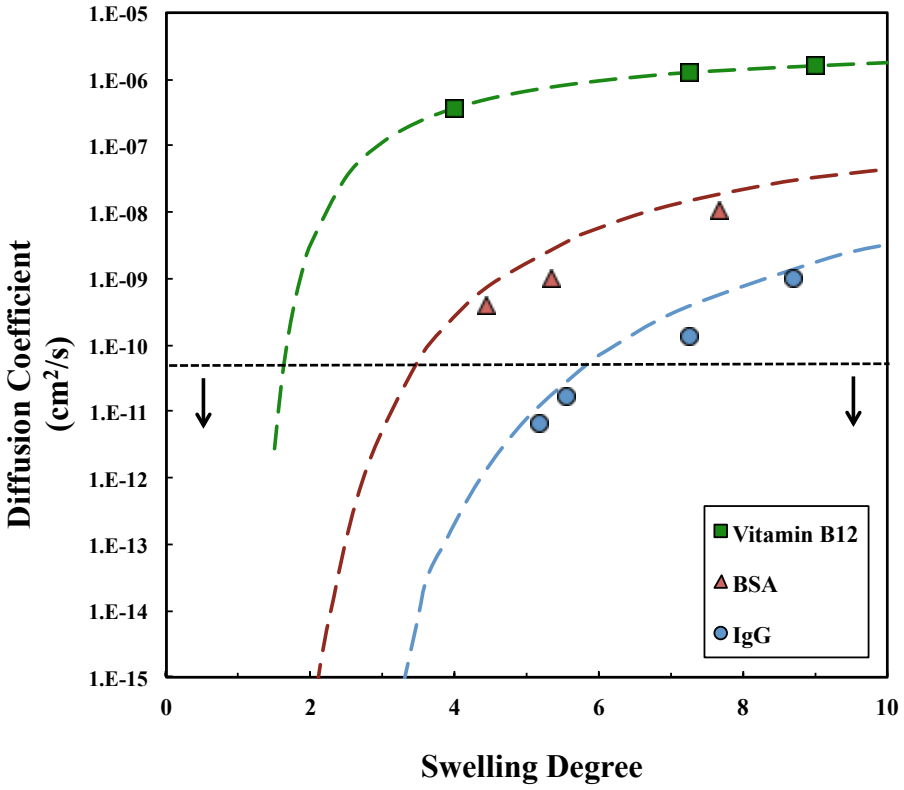

Figure 5.3. The predicted diffusion coefficients of hyaluronic acid hydrogels as a function of the swelling degree. The data points represent actual diffusion coefficients measured in literature[61,62] and the dashed lines represent the extrapolated projections based on the free volume theory, assuming Φ =1. The horizontal dashed line represents the target diffusion coefficient of $D=7x10^{-11}$ cm^2/s. The arrows indicate that all of the values of D below this line will result in release over 3 months for the cylinder dimensions used in this chapter. (□) = Vitamin B_{12}, (Δ) = BSA, (O) = IgG.

5.4.3 Swelling Ratio and Mechanical Properties

HA hydrogels were made using various formulations of HA and DVS. The goal was to not only reach the target swelling degree needed for the desired release profile, but also to determine the range of swelling degrees that could be achieved as very little research has been done with HA hydrogels at very low swelling degrees[63,64]. The concentration of HA ranged from 15 to 30% (w/v) due to the fact that at concentrations higher than 30% the solution became too viscous to work with. The ratio of HA: DVS varied from 3:1 to 1:1. The gels were formed in discs, as seen in Figure 5.4, for ease of handling and in order to run the mechanical testing.

Figure 5.4. Representative image of a HA-DVS disc used to carry out swelling and mechanical testing. The discs were 5 mm in diameter and had a height of 2 mm.

The swelling degree of the hydrogels in both water and PBS can be seen in Figure 5.5. The swelling decreases as the ratio of HA:DVS increases and as the concentration of HA increases. As expected, the highest swelling degree comes from the HA gels at the lowest concentration of HA (15%) and the lowest ratio of HA to crosslinker (3:1). Unexpectedly, the swelling degree seems to be unaffected by the addition of more DVS at the higher concentrations of HA. However, almost all of the gels were below a swelling degree of 5.6, the estimated

swelling degree calculated from Figure 5.3 that is needed to reach the desired diffusion coefficient for a mAb. Only the 30% HA hydrogels were below the target swelling degree of 3.5 needed for a Fab.

Figure 5.5 also shows the swelling degrees of HA-DVS hydrogels in a 0.01 M PBS solution. The swelling degree of a polyelectrolyte gel is described by Flory's classic theory[65], and is a balance of the osmotic forces from the elastically effective junctions (crosslinking), from the polymer-solvent mixing, and from the osmotic pressure of counterions. The swelling of most polyelectrolyte hydrogels are affected by the addition of salt, however these HA hydrogels show very little change in swelling.

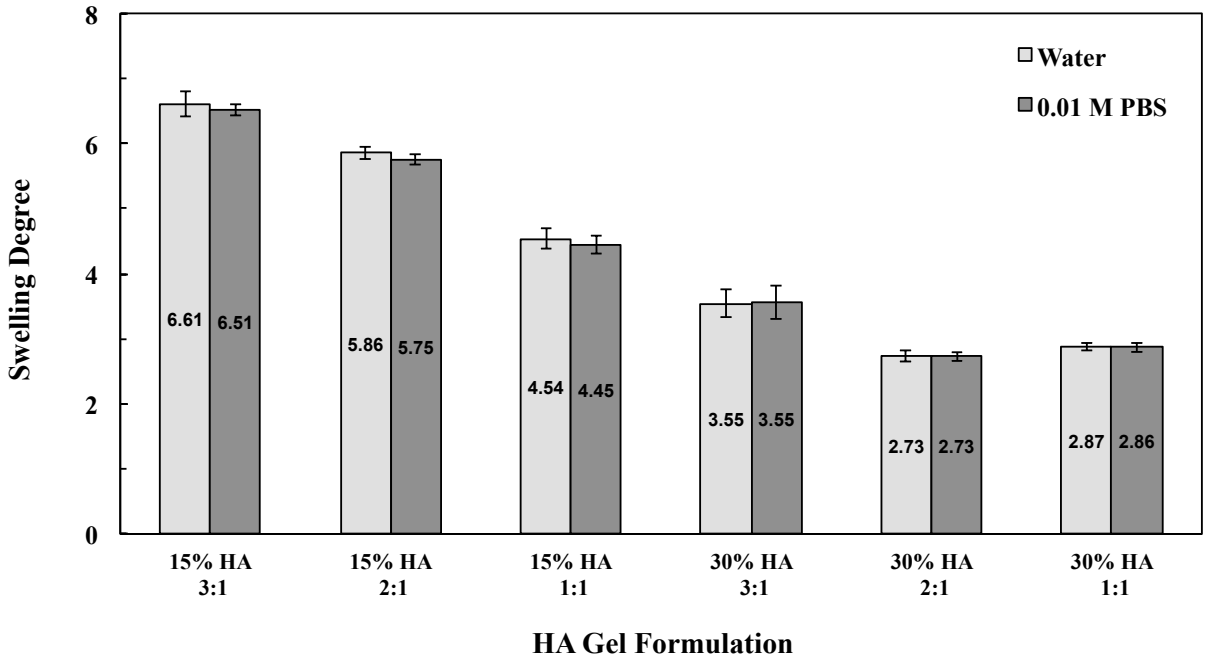

Figure 5.5. Swelling degrees of HA-DVS hydrogels in water and 0.01 M PBS. The swelling degrees of crosslinked HA-DVS gels decreased as a function of HA concentration and as a function of the HA: DVS ratio.

The calculated compressive modulus (E), shear modulus (G), E/G ratio, fracture stress and fracture strain for the HA gels are reported in Table 5.1. The compressive modulus and shear modulus mirror the same general trend seen in the swelling degree, slowly increasing until they reach a plateau at a HA concentration of 30% and a HA:DVS ratio of 2:1. The E/G ratios are close to 3 and validate the assumption that these HA gels are ideal elastomers. While the fracture stress increased with higher concentrations of HA and DVS, in all of the formulations the gel fracture strain remained between 21 to 26%.

Table 5.1. Mechanical properties of HA-DVS hydrogels.

Gel Formulation		Moduli			Compressive Failure Properties	
% HA (wt/v)	HA:DVS Ratio	E (MPa)	G (MPa)	E/G	Stress (MPa)	Strain (%)
15	3:1	2.23 ± 0.16	0.68 ± 0.06	3.2 ± 0.1	0.73 ± 0.23	26.6 ± 6.5
15	2:1	2.57 ± 0.32	0.76 ± 0.10	3.3 ± 0.2	0.76 ± 0.34	23.8 ± 8.5
15	1:1	3.11 ± 0.33	0.84 ± 0.10	3.7± 0.3	0.95 ± 0.24	27.4 ± 4.7
30	3:1	7.45 ± 0.86	2.37 ± 0.28	3.1 ± 0.9	1.93 ± 0.39	22.7 ± 3.1
30	2:1	11.82 ± 2.9	3.71 ± 0.45	3.1 ± 0.8	2.72 ± 0.35	21.0 ± 3.0
30	1:1	9.82 ± 0.93	3.05 ± 0.19	3.2 ± 1.0	2.82 ± 0.63	24.3 ± 3.6

n = 5 for 15% HA and n=6 for 30% HA samples

In an effort to better understand the trends seen in Figure 5.5 and Table 5.1, the sulfur content of the hydrogels were measured and can be seen in Table 5.2 along with the crosslink density, the molecular weight between crosslinks, and the mesh size. For 15% HA hydrogels, the addition of more DVS leads to more DVS reacting with HA and being incorporated into the network, as evidenced by the increase in the sulfur content. Despite the fact that more DVS is reacting with HA and being incorporated into the network, the crosslink density of the 15% HA gels does not seem to be affected, suggesting that the DVS molecules are reacting only once and

not forming elastically effective crosslinks. With similar crosslinking densities, the decrease in swelling seen in Figure 5.5 can be attributed to an increase in hydrophobicity that occurs from the addition of unreacted vinyl groups to the network.

The results in Table 5.2 also reveal that doubling the amount of HA used to formulate the hydrogels from 15% to 30% results in crosslink densities that are twice as high. For the 30% HA gels, the swelling degree and mesh size reach a minimum at a HA: DVS ratio of 2:1. The addition of more DVS at a ratio of 1:1 does not decrease the swelling degree any further. This is hypothesized to be a result of phase separation that is seen when adding excessive amounts of DVS and is evidenced by a steep drop in reaction efficiency. Despite the fact that twice as much DVS is added, the number of DVS molecules that have reacted with HA are roughly identical.

Table 5.2. Network properties and sulfur content of HA-DVS hydrogels

Gel Formulation		Crosslink Density	Molecular Weight Between Crosslinks	Mesh Size	Sulfur Content	N_{DVS}	Reaction Efficiency*
% HA (wt/v)	HA:DVS Ratio	ρ_x (mol/cm^3)	M_c (g/mol)	ξ (nm)	% S (w%)		
15	3:1	1.85E-03	783	7.36	5.6	0.87	81%
15	2:1	1.98E-03	732	6.84	7.3	1.29	81%
15	1:1	2.02E-03	719	6.23	10.0	1.91	60%
30	3:1	3.30E-03	440	4.49	6.6	1.15	107%
30	2:1	4.73E-03	306	3.43	8.2	1.45	91%
30	1:1	3.96E-03	366	3.81	8.0	1.5	47%

N_{DVS}= the number of DVS molecules per HA repeat unit (disaccharide)

* Defined as the percentage of DVS added that reacted with HA

n = 5 for 15% HA and n=6 for 30% HA samples

5.4.4 Diffusion Coefficient Measurement by Confocal Microscopy

Having formulated hydrogels with the desired swelling degrees, the next step was to confirm that the diffusion coefficients of these gels were in fact in the desired range before building the prototype. This was done my measuring the diffusion coefficients of FITC-BSA in HA hydrogel discs using confocal microscopy. 15% HA discs with a HA:DVS ratio of 2:1 and 3:1 were soaked in a 1 mg/mL FITC-BSA solution for 280 hours, and the 1-D diffusion into the discs were examined. Image stacks were captured at three different locations on the hydrogel at 135 and 280 hours and the concentration gradients were calculated from image analysis at each penetration depth. In order to compare the results with theory, the diffusion of FITC-BSA was calculated using the solution to Fick's second law in a semi-infinite slab assuming constant concentration at the surface ($C = C_1$, $x = 0$, $t \geq 0$), an initial condition of zero initial concentration throughout the gel ($C = C_0$, $0 < x < \infty$, $t = 0$), and a constant diffusion coefficient [66].

$$\frac{(C-C_1)}{(C_0-C_1)} = \text{erf}\left(\frac{x}{2\sqrt{Dt}}\right) \tag{5.10}$$

The experimental and theoretical concentration profiles can be seen in Figure 5.6a and Figure 5.6b for 15% 2:1 HA hydrogels. The diffusion coefficient used to calculate the theoretical concentration profile was estimated by fitting the experimentally measured data to the Fickian profile. In general, the experimental data fits the theoretical profile, validating the expectation that a Fickian diffusion mechanism would be present. The largest deviation between the experimental and theoretical profiles occurs at the larger penetration depths and is even more pronounced in Figure 5.6b after 280 hours. This is believed to be a result of the instability of FITC-BSA bond, as has been reported in literature. FITC-BSA incubated in buffer solutions has

been shown to degrade and produce smaller fragments after just four days[67]. Any fragments or free FITC that has a much smaller molecular weight would diffuse much faster into the gel than FITC-BSA. This would lead to higher concentration readings at the large penetration depths, and would also explain why the error is more pronounced at longer time points.

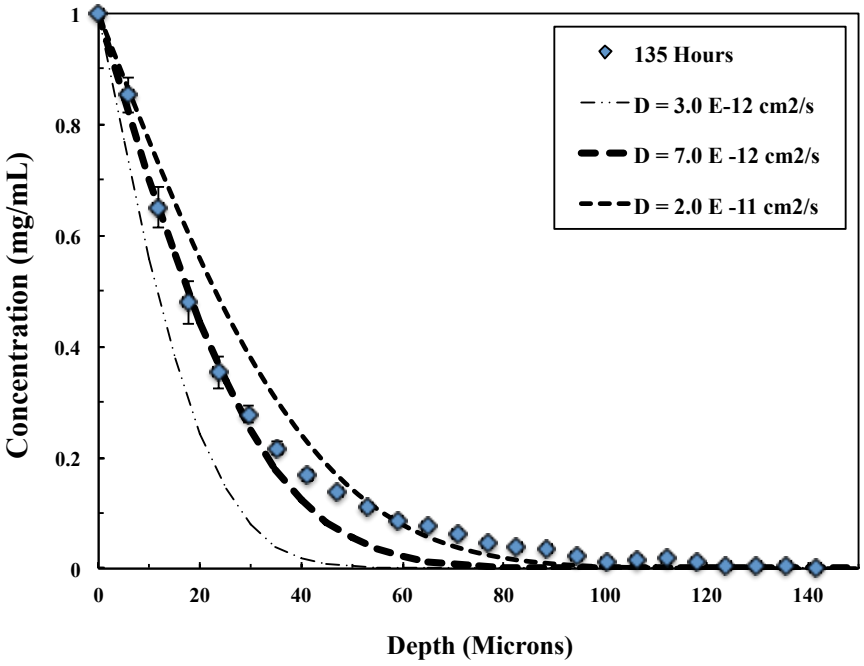

Figure 5.6a. Concentration profiles of FITC-BSA in 15% HA 2:1 hydrogel discs after 135 hours. The dashed lines represent the solution to Fick's law in a thick slab with varying diffusion coefficients from 3.0×10^{-12} - 1.0×10^{-11} cm^2/s.

Even though the data deviates from the theoretical profile, the experiment is still able to provide an estimation of the diffusion coefficient. The dashed lines in Figures 5.6a and 5.6b help provide a range of diffusion coefficients that bracket the data. The estimated diffusion coefficient for a 15% 2:1 hydrogel was 7×10^{-12} cm^2/s. With a swelling degree of 5.75, the expected diffusion coefficient was predicted to be around 4.5×10^{-9} cm^2/s based on the estimates in Figure 5.3 from free volume theory, a much higher number. The estimated diffusion

coefficient for the 15% 3:1 hydrogels (not pictured) was 2 x 10^{-11} cm^2/s. This number was also much lower than expected, as a swelling degree of 6.51 would be expected to have a diffusion coefficient around 8.8 x 10^{-9} cm^2/s. The large discrepancy between the diffusion coefficients predicted from free volume theory and the diffusion coefficients measured by confocal microscopy is possible evidence that screening effect is being observed. Similar observations were seen in literature with BSA in dextran hydrogels. As soon as the swelling degree dropped below 5, screening effects caused significant deviations from the free volume theory, with diffusion coefficients straying up to three orders of magnitude from predicted values[61]. Another possibility is that the free volume model used is not very accurate when extrapolated to such low swelling degrees.

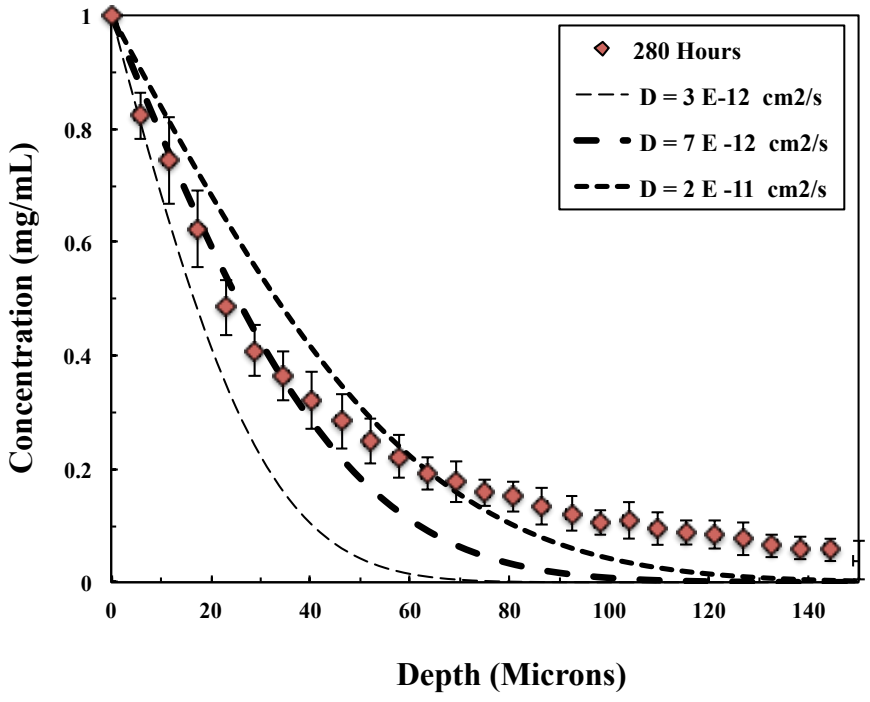

Figure 5.6b. Concentration profiles of FITC-BSA in 15% HA 2:1 hydrogel discs after 280 hours. The dashed lines represent the solution to Fick's law in a thick slab with varying diffusion coefficients from 3.0 x 10^{-12} - 1.0 x 10^{-11} cm^2/s.

5.4.5 Release From Hollow Mini Cylinders

While the prior sections helped provide a better understanding of how the swelling degree affects the diffusion coefficient in HA-DVS gels, the major goal of this work was to fabricate a prototype mini cylinder in order to confirm that extended release of 3-6 months could be achieved. While the main objective of developing a prototype was to show the release of larger molecules (48-97 kDa) from HA mini cylinders, the first solute that was tested in the hollow cylinders was Vitamin B_{12}. Due to its smaller size (1355 Da), the diffusion rate of Vitamin B_{12} is much faster than BSA or the Fab, allowing for complete release to occur in less than a day. Vitamin B_{12} also has the advantage of forming a colored solution when mixed with water, which helps in detecting leaks due to cracks in the cylinder or a faulty cap. The release profile of two different cylinders can be seen in Figure 5.7. The formulation for both cylinders was 30% HA 3:1.

The cylinders exhibit similar release profiles that correspond well with the diffusion model, with 90% of the loaded amount released within 200 minutes and 100% release achieved by 300 minutes. The total amount of Vitamin B_{12} released from cylinder 1 was 0.017 mg, while cylinder 2 released 0.014 mg. The difference is due to an inefficient capping method that can occasionally reduce the effective inner volume inside some of the cylinders. This is taken into account when fitting the data with a diffusion coefficient using the modeling software. A diffusion coefficient of $D = 1.3 \pm 0.1 \times 10^{-8}$ cm^2/s was fit to the data. The diffusion coefficient was calculated for both cylinders separately and then averaged together to get the final estimated diffusion coefficient. This diffusion coefficient is about 2 times lower than the 2.4×10^{-7} diffusion coefficient that was predicted based on free volume theory. Given its small molecular weight and hydrodynamic radius (0.85 nm) any deviations from the theory due to possible

screening effects seem improbable, with a more likely explanation being an error in the diffusion coefficient estimation due to extrapolation.

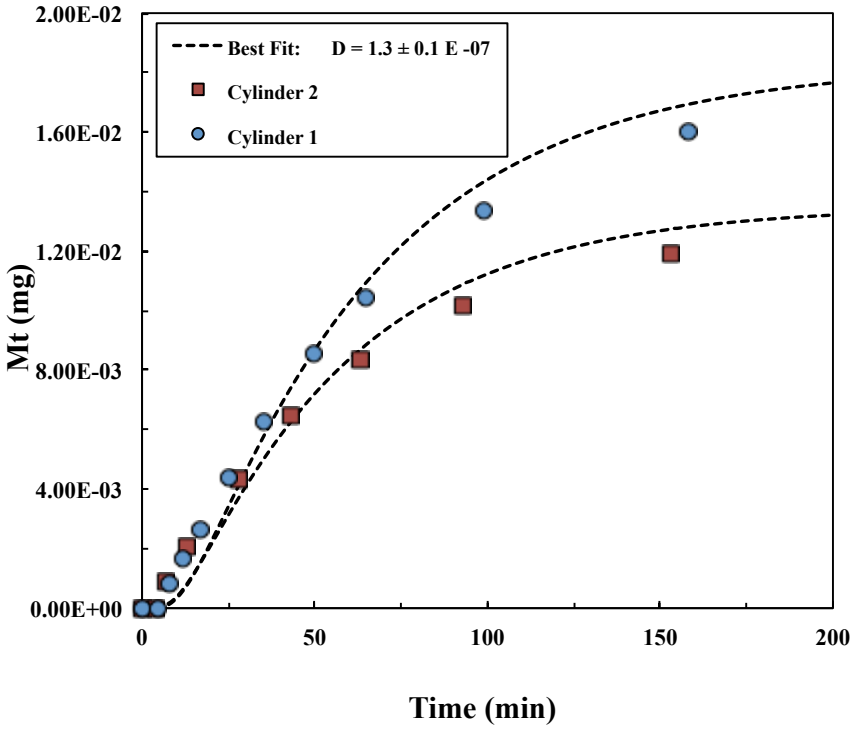

Figure 5.7. The release of Vitamin B_{12} from 30% HA 3:1 hollow mini cylinders. The release data fits the numerical solution to Fick's law when solved for a hollow cylinder (Eq. 5.8), represented by the dashed line with a diffusion coefficient of $1.3 \pm 0.1 \times 10^{-7}$ cm^2/s. All of the Vitamin B_{12} is released within 300 minutes.

Having established a successful method to synthesize, load, and cap HA cylinders using Vitamin B_{12}, the focus shifted to the main goal of demonstrating that larger molecules could be successfully released at the desired rates. BSA and a Fab were used as model proteins, and the cylinders were loaded with solutions that had a concentration of 160 mg/mL. Figure 5.8 shows the release of BSA from 15% HA-DVS 3:1 hollow cylinders that had not been treated with

ethylene glycol. While BSA seemed to be releasing at a normal rate initially, after 15 days the release rate significantly dropped. The experiment was run for 200 days, however the cylinders stopped releasing any protein after 50 days. The total amount of BSA released is about 10 mg, equating to only 2% of the amount of BSA that was loaded into the cylinders. Similar results were seen in cylinders with formulations of 15% 2:1, 15% 1:1, and 30% 3:1 for both BSA and the Fab.

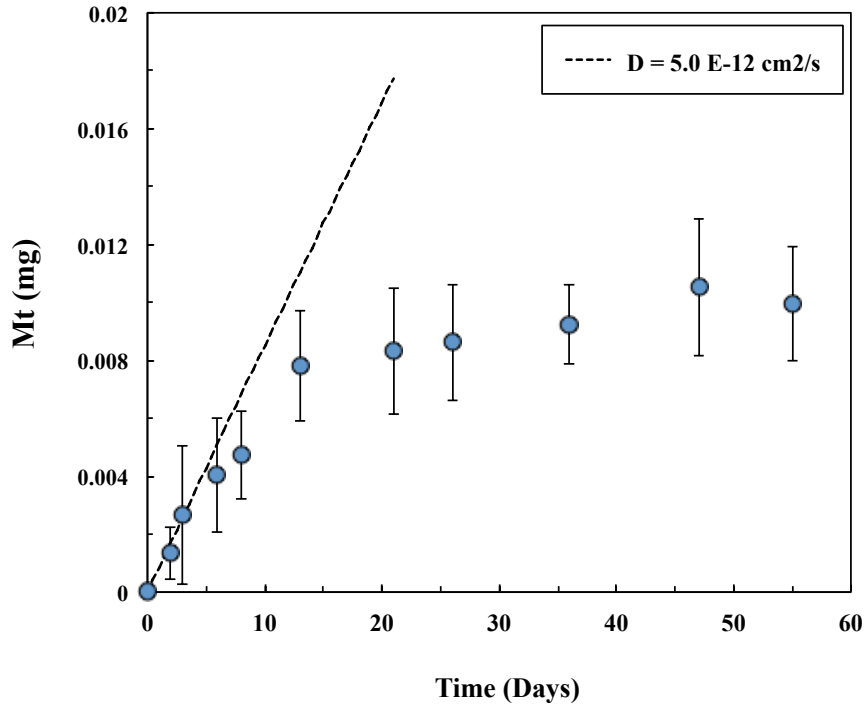

Figure 5.8. Release of BSA from an untreated 15% HA-DVS 3:1 hollow cylinder. After 55 days only 2% of the BSA that was loaded had released from the cylinder. The dashed line represents a Fickian release profile with a D = 5.0x 10^{-12} cm^2/sec. N=5

Figure 5.8 highlights the importance of the crosslinking reaction. While the use of DVS provides an easy synthesis method to crosslink HA and achieve the low swelling degrees needed, it has some drawbacks. While DVS is an excellent difunctional crosslinker, the results from the

mechanical testing and sulfur content of the HA-DVS gels prove that there are a large number of instances in which only one of the vinyl groups reacts with HA, leaving unreacted vinyl groups within the hydrogel networks. These residual vinyl groups have the ability to react with proteins diffusing through the network, covalently attaching them to the hydrogel network and at the same time potentially restricting the diffusion. While this reaction generally occurs at higher pH values (8-9), the reaction has been shown to occur at a pH of 7 at room temperature[57]. Given the hypothesis that the reaction of protein is affecting the diffusion through the network over time, it is difficult to accurately fit the data to a diffusion coefficient. The dashed line represents the Fickian release of BSA from a cylinder with a $D= 5.0 \times 10^{-12}$ cm^2/s. The initial release does, however, seem to be in the correct range (slower by a factor of 4) of what was expected from the confocal microscopy experiments.

The release experiments were thus performed using HA-DVS hollow cylinders in which the residual vinyl groups had been capped with ethylene glycol. It should be noted that the capping procedure with ethylene glycol did not significantly affect the swelling degrees of HA-DVS hydrogels (See Appendix A5.4). The release of BSA from 15% HA DVS 3:1 cylinders can be seen in Figure 5.9. The large variance in the data emphasizes the difficulty in performing extended release studies with hollow mini cylinders. The crude capping method, while effective initially, began to break down after repeated handling, causing some of the cylinders to leak. While these cylinders could easily be recapped, a few cylinders were punctured or cracked accidentally during some of the measurements and had to be discarded. This led to a smaller number of cylinders being tested and contributed to the high variability that is seen in Figure 5.9.

Despite some of the issues with handling and capping the cylinders, the results in Figure 5.9 show that BSA can be released from a hollow cylinder for over 120 days. The cylinders

were loaded with a BSA solution with a concentration of 250 mg/mL in order to achieve the high release rates. The maximum release rate is during the first 5 days, when the cylinders are releasing an average of 8 micrograms a day. The release rate stays above the target release rate of 2.5 micrograms a day for over 50 days. While the release rate slowly decreases over time, the cylinders continued to slowly release BSA after 120 days. The cylinders had released 90% of the total load after 140 days. A diffusion coefficient of $7.1 \pm 3.1 \times 10^{-11}$ cm^2/s was fit to the data using Equation 5.9 and the least squares method. While the deviation is large, the diffusion coefficient is only 3.6 times larger than the measured diffusion coefficient obtained through the confocal microscopy experiments.

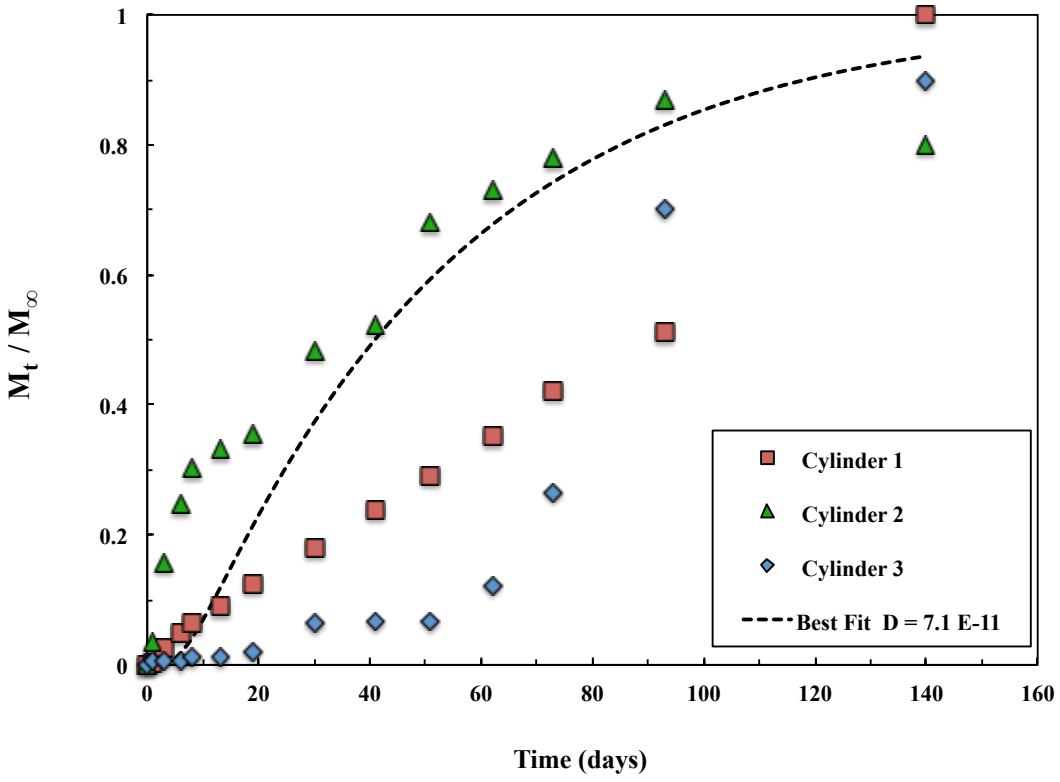

Figure 5.9. Release of BSA from 15% HA-DVS 3:1 hollow cylinders. The release data fits the numerical solution to Fick's law when solved for a hollow cylinder (Eq. 5.8), represented by the dashed line with a diffusion coefficient of $D = 7.1 \times 10^{-11}$ cm^2/sec.

The release of Fab from 15% HA-DVS 3:1 cylinders was also studied and can be seen in Figure 5.10. The results demonstrate that these cylinders are capable of delivering Fabs for 3 months. The release is slightly faster when compared to that of BSA, which is to be expected given the smaller size of the Fab. This is reflected in the measured diffusion coefficient of 1.3 ± 0.5 x 10^{-10} cm^2/s, which is about twice as large as the diffusion coefficient of BSA in the same cylinders. The cylinder releases 90% of the total protein loaded at 120 days. Due to limited amounts of Fab, these cylinders were loaded with a concentration of 90 mg/mL. However, the maximum release rate observed was 4 micrograms a day, which is still above the target release rate. However, the shape of release curve does not change with concentration, and achieving a higher release rate can be easily obtained by simply increasing the concentration.

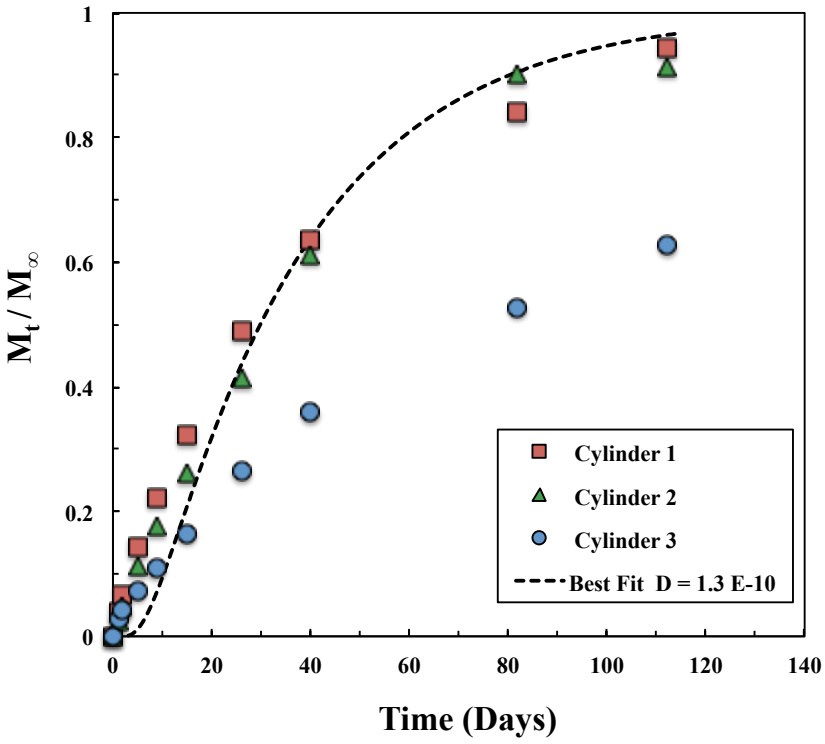

Figure 5.10. Release of Fab from 15% HA-DVS 3:1 hollow cylinders. The release data fits the numerical solution to Fick's law when solved for a hollow cylinder (Eq. 5.8), represented by the dashed line with a diffusion coefficient of D = 1.3x10^{-10} cm^2/sec.

5.5 Conclusions

The results of this chapter demonstrate the potential of HA hollow mini cylinders to deliver therapeutic proteins to the retina for the desired 3-6 months of time. They also present a drug delivery system that is versatile and can be extended to many other applications where long term delivery of proteins is needed. By controlling the concentration of HA and the ratio of HA to DVS, the swelling degrees can be altered, and the results proved that this crosslinking method was capable of achieving very low swelling degrees. The low swelling degrees and high crosslink densities provide a network for reducing the diffusion of solutes of multiple sizes and attaining extended release. The hydrogels exhibited diffusion coefficients that were much lower than predicted using the free volume theory, which was hypothesized to be a result of screening effects, although more testing is needed to confirm this. Furthermore, hollow cylinders with a wide range of dimensions can be easily fabricated with molds. These cylinders can be filled with proteins of any size or molecular weight, demonstrated by the release of Vitamin B_{12}, BSA, and a model Fab that showed release profiles consistent with Fickian diffusion. Release experiments with both BSA and the model Fab showed sustained release of at least 16 weeks. The results show that these HA-DVS hollow cylinders are suitable implants that can provide extended release and could be further investigated for the treatment of retinal diseases.

At the same time, the work in this chapter revealed some of the shortcomings of an HA-DVS hollow cylinder. The hydrogel required a high concentration of DVS in order to get the low swelling degrees that were required for extended release. This led to an excess amount of singly-reacted vinyl sulfone groups that were attached to the HA backbone which required ethylene glycol capping to eliminate unwanted side reactions with the proteins. It is because of these issues that a more efficient crosslinking method is investigated in Chapter 7.

REFERENCES

1. Coviello T, Matricardi P, Marianecci C, Alhaique F 2007. Polysaccharide hydrogels for modified release formulations. J Control Release 119(1):5-24.

2. Barbucci R, Fini M, Giavaresi G, Torricelli P, Giardino R, Lamponi S, Leone G 2005. Hyaluronic acid hydrogel added with ibuprofen‐lysine for the local treatment of chondral lesions in the knee: In vitro and in vivo investigations. Journal of Biomedical Materials Research Part B: Applied Biomaterials 75(1):42-48.

3. Luo Y, Kirker KR, Prestwich GD 2000. Cross-linked hyaluronic acid hydrogel films: new biomaterials for drug delivery. J Control Release 69(1):169-184.

4. Tian W, Zhang C, Hou S, Yu X, Cui F, Xu Q, Sheng S, Cui H, Li H 2005. Hyaluronic acid hydrogel as Nogo-66 receptor antibody delivery system for the repairing of injured rat brain: in vitro. J Control Release 102(1):13-22.

5. Jin Y, Yamanaka J, Sato S, Miyata I, Yomota C, Yonese M 2001. Recyclable characteristics of hyaluronate–polyhydroxyethyl acrylate blend hydrogel for controlled releases. J Control Release 73(2):173-181.

6. Leach JB, Schmidt CE 2005. Characterization of protein release from photocrosslinkable hyaluronic acid-polyethylene glycol hydrogel tissue engineering scaffolds. Biomaterials 26(2):125-135.

7. Holz FG, Schmitz-Valckenberg S, Fleckenstein M 2014. Recent developments in the treatment of age-related macular degeneration. Journal of Clinical Investigation 124(4):1430-1438.

8. Ambati J, Fowler BJ 2012. Mechanisms of Age-Related Macular Degeneration. Neuron 75(1):26-39.

9. Heng LZ, Comyn O, Peto T, Tadros C, Ng E, Sivaprasad S, Hykin PG 2013. Diabetic retinopathy: pathogenesis, clinical grading, management and future developments. Diabetic Medicine 30(6):640-650.

10. Frank RN 2004. Diabetic retinopathy. New England Journal of Medicine 350(1):48-58.

11. Wild S, Roglic G, Green A, Sicree R, King H 2004. Global prevalence of diabetes - Estimates for the year 2000 and projections for 2030. Diabetes Care 27(5):1047-1053.

12. Shen Q, Wu JZ, Wong JC 2013. Potential drug interventions for diabetic retinopathy. Drug discovery today 18(23-24):1334-1341.

13. Velez-Montoya R, Oliver SCN, Olson JL, Fine SL, Mandava N, Quiroz-Mercado H 2013. CURRENT KNOWLEDGE AND TRENDS IN AGE-RELATED MACULAR DEGENERATION Today's and Future Treatments. Retina-the Journal of Retinal and Vitreous Diseases 33(8):1487-1502.

14. Smith AG, Kaiser PK 2014. Emerging treatments for wet age-related macular degeneration. Expert Opinion on Emerging Drugs 19(1):157-164.

15. Sampat KM, Garg SJ 2010. Complications of intravitreal injections. Current Opinion in Ophthalmology 21(3):178-183.

16. Pershing S, Bakri SJ, Moshfeghi DM 2013. Ocular Hypertension and Intraocular Pressure Asymmetry After Intravitreal Injection of Anti-Vascular Endothelial Growth Factor Agents. Ophthalmic Surgery Lasers & Imaging 44(5):460-464.

17. Haller JA 2013. Current Anti-Vascular Endothelial Growth Factor Dosing Regimens Benefits and Burden. Ophthalmology 120(5):S3-S7.

18. Spaide R 2007. Ranibizumab according to need: A treatment for age-related macular degeneration. American Journal of Ophthalmology 143(4):679-680.

19. Gupta OP, Shienbaum G, Patel AH, Fecarotta C, Kaiser RS, Regillo CD 2010. A Treat and Extend Regimen Using Ranibizumab for Neovascular Age-Related Macular Degeneration Clinical and Economic Impact. Ophthalmology 117(11):2134-2140.

20. Engelbert M, Zweifel SA, Freund KB 2009. "TREAT AND EXTEND" DOSING OF INTRAVITREAL ANTIVASCULAR ENDOTHELIAL GROWTH FACTOR THERAPY FOR TYPE 3 NEOVASCULARIZATION/RETINAL ANGIOMATOUS PROLIFERATION. Retina-the Journal of Retinal and Vitreous Diseases 29(10):1424-1431.

21. Schmucker CM, Rücker G, Sommer H, Virgili G, Loke YK, Oeller P, Agostini H, Ehlken C 2015. Treatment as Required versus Regular Monthly Treatment in the Management of Neovascular Age-Related Macular Degeneration: A Systematic Review and Meta-Analysis. PloS one 10(9):e0137866.

22. Del Amo EM, Urtti A 2008. Current and future ophthalmic drug delivery systems. A shift to the posterior segment. Drug discovery today 13(3-4):135-143.

23. Yasukawa T, Ogura Y, Tabata Y, Kimura H, Wiedemann P, Honda Y 2004. Drug delivery systems for vitreoretinal diseases. Progress in retinal and eye research 23(3):253-281.
24. Kang-Mieler JJ, Osswald CR, Mieler WF 2014. Advances in ocular drug delivery: emphasis on the posterior segment. Expert Opinion on Drug Delivery 11(10):1647-1660.
25. Yasin MN, Svirskis D, Seyfoddin A, Rupenthal ID 2014. Implants for drug delivery to the posterior segment of the eye: A focus on stimuli-responsive and tunable release systems. J Control Release 196:208-221.
26. Bourges JL, Bloquel C, Thomas A, Froussart F, Bochot A, Azan F, Gurny R, BenEzra D, Behar-Cohen F 2006. Intraocular implants for extended drug delivery: Therapeutic applications. Advanced Drug Delivery Reviews 58(11):1182-1202.
27. Jaffe GJ, Martin D, Callanan D, Pearson PA, Levy B, Comstock T, Fluocinolone Acetonide Uveitis S 2006. Fluocinolone acetonide implant (Retisert) for noninfectious posterior uveitis - Thirty-four-week results of a multicenter randomized clinical study. Ophthalmology 113(6):1020-1027.
28. Yasukawa T, Ogura Y, Sakurai E, Tabata Y, Kimura H 2005. Intraocular sustained drug delivery using implantable polymeric devices. Advanced Drug Delivery Reviews 57(14):2033-2046.
29. Kimura H, Ogura Y 2001. Biodegradable polymers for ocular drug delivery. Ophthalmologica 215(3):143-155.
30. Haller JA, Kuppermann BD, Blumenkranz MS, Williams GA, Weinberg DV, Chou C, Whitcup SM, Dexamethasone DDSPIISG 2010. Randomized Controlled Trial of an Intravitreous Dexamethasone Drug Delivery System in Patients With Diabetic Macular Edema. Arch Ophthalmol 128(3):289-296.
31. van de Weert M, Hennink WE, Jiskoot W 2000. Protein instability in poly(lactic-co-glycolic acid) microparticles. Pharm Res 17(10):1159-1167.
32. Rajagopal K, Wood J, Tran B, Patapoff TW, Nivaggioli T 2013. Trehalose limits BSA aggregation in spray-dried formulations at high temperatures: Implications in preparing polymer implants for long-term protein delivery. J Pharm Sci 102(8):2655-2666.
33. Qiu B, Stefanos S, Ma J, Lalloo A, Perry BA, Leibowitz MJ, Sinko PJ, Stein S 2003. A hydrogel prepared by in situ cross-linking of a thiol-containing poly (ethylene glycol)-based copolymer: a new biomaterial for protein drug delivery. Biomaterials 24(1):11-18.

34. Hoare TR, Kohane DS 2008. Hydrogels in drug delivery: Progress and challenges. Polymer 49(8):1993-2007.

35. Yin HB, Gong CY, Shi SA, Liu XY, Wei YQ, Qian ZY 2010. Toxicity Evaluation of Biodegradable and Thermosensitive PEG-PCL-PEG Hydrogel as a Potential In Situ Sustained Ophthalmic Drug Delivery System. J Biomed Mater Res Part B 92B(1):129-137.

36. Xu X, Weng YH, Xu L, Chen H 2013. Sustained release of avastin (R) from polysaccharides cross-linked hydrogels for ocular drug delivery. Int J Biol Macromol 60:272-276.

37. Lu CH, Zahedi P, Forman A, Allen C 2014. Multi-arm PEG/Silica Hydrogel for Sustained Ocular Drug Delivery. J Pharm Sci 103(1):216-226.

38. Widjaja LK, Bora M, Chan P, Lipik V, Wong TTL, Venkatraman SS 2014. Hyaluronic acid-based nanocomposite hydrogels for ocular drug delivery applications. J Biomed Mater Res Part A 102(9):3056-3065.

39. Laurent TC, Fraser JRE 1992. HYALURONAN. Faseb J 6(7):2397-2404.

40. Scott JE 1992. THE CHEMICAL MORPHOLOGY OF THE VITREOUS. Eye 6:553-555.

41. Laurent TC, Laurent UBG, Fraser JRE 1995. FUNCTIONS OF HYALURONAN. Ann Rheum Dis 54(5):429-432.

42. Fakhari A, Berkland C 2013. Applications and emerging trends of hyaluronic acid in tissue engineering, as a dermal filler and in osteoarthritis treatment. Acta Biomaterialia 9(7):7081-7092.

43. Jeng BH, Hoyt CS, McLeod SD 2004. Completion rate of continuous curvilinear capsulorhexis in pediatric cataract surgery using different viscoelastic materials. Journal of Cataract & Refractive Surgery 30(1):85-88.

44. McDonald C, Kaye S, Figueiredo F, Macintosh G, Lockett C 2002. A randomised, crossover, multicentre study to compare the performance of 0.1%(w/v) sodium hyaluronate with 1.4%(w/v) polyvinyl alcohol in the alleviation of symptoms associated with dry eye syndrome. Eye 16(5):601-607.

45. Lai J-Y 2014. Relationship between structure and cytocompatibility of divinyl sulfone cross-linked hyaluronic acid. Carbohydrate polymers 101:203-212.

46. Zarembinski TI, Doty NJ, Erickson IE, Srinivas R, Wirostko BM, Tew WP 2014. Thiolated hyaluronan-based hydrogels crosslinked using oxidized glutathione: An injectable matrix designed for ophthalmic applications. Acta Biomaterialia 10(1):94-103.

47. Su W-Y, Chen K-H, Chen Y-C, Lee Y-H, Tseng C-L, Lin F-H 2011. An Injectable Oxidated Hyaluronic Acid/Adipic Acid Dihydrazide Hydrogel as a Vitreous Substitute. Journal of Biomaterials Science-Polymer Edition 22(13):1777-1797.

48. Xu X, Jha AK, Harrington DA, Farach-Carson MC, Jia X 2012. Hyaluronic acid-based hydrogels: from a natural polysaccharide to complex networks. Soft Matter 8(12):3280-3294.

49. Oh EJ, Park K, Kim KS, Kim J, Yang J-A, Kong J-H, Lee MY, Hoffman AS, Hahn SK 2010. Target specific and long-acting delivery of protein, peptide, and nucleotide therapeutics using hyaluronic acid derivatives. J Control Release 141(1):2-12.

50. Motokawa K, Hahn SK, Nakamura T, Miyamoto H, Shimoboji T 2006. Selectively crosslinked hyaluronic acid hydrogels for sustained release formulation of erythropoietin. J Biomed Mater Res Part A 78A(3):459-465.

51. Schante CE, Zuber G, Herlin C, Vandamme TF 2011. Chemical modifications of hyaluronic acid for the synthesis of derivatives for a broad range of biomedical applications. Carbohydrate Polymers 85(3):469-489.

52. Ramamurthi A, Vesely I 2002. Smooth muscle cell adhesion on crosslinked hyaluronan gels. J Biomed Mater Res 60(1):196-205.

53. Lai J-Y, Li Y-T, Wang T-P 2010. In vitro response of retinal pigment epithelial cells exposed to chitosan materials prepared with different cross-linkers. International journal of molecular sciences 11(12):5256-5272.

54. Credi C, Biella S, De Marco C, Levi M, Suriano R, Turri S 2014. Fine tuning and measurement of mechanical properties of crosslinked hyaluronic acid hydrogels as biomimetic scaffold coating in regenerative medicine. J Mech Behav Biomed Mater 29:309-316.

55. Lai JY 2014. Relationship between structure and cytocompatibility of divinyl sulfone cross-linked hyaluronic acid. Carbohydrate Polymers 101:203-212.

56. Sannino A, Madaghiele M, Conversano F, Mele G, Maffezzoli A, Netti PA, Ambrosio L, Nicolais L 2004. Cellulose derivative-hyaluronic acid-based microporous hydrogels cross-linked through divinyl sulfone (DVS) to modulate equilibrium sorption capacity and network stability. Biomacromolecules 5(1):92-96.

57. Morpurgo M, Veronese FM, Kachensky D, Harris JM 1996. Preparation and characterization of poly (ethylene glycol) vinyl sulfone. Bioconjugate chemistry 7(3):363-368.

58. Peppas NA, Merrill EW 1976. POLYVINYL-ALCOHOL) HYDROGELS - REINFORCEMENT OF RADIATION-CROSSLINKED NETWORKS BY CRYSTALLIZATION. Journal of Polymer Science Part a-Polymer Chemistry 14(2):441-457.

59. Kuno N, Fujii S 2012. Ocular drug delivery systems for the posterior segment: a review. Retina Today:54-59.

60. Amsden B 1998. Solute diffusion within hydrogels. Mechanisms and models. Macromolecules 31(23):8382-8395.

61. Hennink WE, Talsma H, Borchert JCH, DeSmedt SC, Demeester J 1996. Controlled release of proteins from dextran hydrogels. J Control Release 39(1):47-55.

62. Hennink WE, Franssen O, vanDijkWolthuis WNE, Talsma H 1997. Dextran hydrogels for the controlled release of proteins. J Control Release 48(2-3):107-114.

63. Ibrahim S, Kang QK, Ramamurthi A 2010. The impact of hyaluronic acid oligomer content on physical, mechanical, and biologic properties of divinyl sulfone‐crosslinked hyaluronic acid hydrogels. J Biomed Mater Res Part A 94(2):355-370.

64. Collins MN, Birkinshaw C 2008. Physical properties of crosslinked hyaluronic acid hydrogels. Journal of Materials Science: Materials in Medicine 19(11):3335-3343.

65. Flory PJ 1953. Principles of polymer chemistry.

66. Crank J. 1983. The mathematics of diffusion. ed.: Oxford University Press.

67. Wischke C, Borchert H-H 2006. Fluorescein isothiocyanate labelled bovine serum albumin (FITC-BSA) as a model protein drug: opportunities and drawbacks. Die Pharmazie-An International Journal of Pharmaceutical Sciences 61(9):770-774.

CHAPTER 6: MODELING THE RELEASE FROM HOLLOW MINI CYLINDERS

6.1 ABSTRACT

The release of therapeutic proteins from hollow cylinders was modeled using the physics software COMSOL for the treatment of retinal diseases. The goal of the chapter was to determine the range of diffusion coefficients that would produce a therapeutically effective ocular delivery device. Hydrogel implants with three different outer diameters were modeled in an effort to understand how the diffusion coefficient and cylinder dimensions affect the release rate and profile: a 1mm implant that would have to be implanted, a 0.45 mm implant that could be injected using a 22-gauge microinjector, and a 0.21 mm implant that could be injected using a 27-gauge needle. Cylinders with a 1mm outer radius were capable of delivering over 1 mg of drug while achieving the target release rate of 2.5 micrograms a day for over 4.5 months. While the smaller cylinders make the insertion process faster, safer, and less painful, the 0.45 mm cylinders were only capable of releasing at the target rate for a full month, while the 0.21 mm cylinders could only achieve the target release rate for one week. The hollow cylinders were most effective at diffusion coefficients between 1.0×10^{-11} and 3.0×10^{-11} cm^2/s, a rather narrow range that highlights the importance of being able to tune the diffusion coefficient of hydrogels.

6.2 Introduction

Extended release of therapeutic proteins is an area of study that has received a lot of attention of late due to the increasing use of antibodies in treating cancer, autoimmune diseases, viral infections, and even asthma.[1] While the number of therapeutic proteins in clinical trials continues to rise, focus is now being shifted on effective ways to deliver these high value drugs for prolonged periods of time. Due to their large size, complex structure, and sensitivity to enzymatic degradation, the majority of proteins cannot be given by the preferred oral route and are instead administered via parenteral routes. While effective, these routes (intravenous, subcutaneous, intramuscular) often require large doses to be therapeutically effective and the systemic exposure and frequent injections required can often lead to unwanted side effects. Alternatively, long term, targeted delivery systems provide local delivery and require lower dosages while at the same time improving patient compliance.[2]

There are a number of chronic illnesses that require a constant level of therapeutic proteins and would benefit from extended release systems. In oncology, injectable implants are able to increase a tumors exposure to chemotherapeutics locally while reducing systemic toxicity. Extended release systems can also be used to treat arthritic pain, release needed hormones like human growth hormone and insulin, and even deliver growth factors for tissue engineering applications.

Another area that emphasizes the need for targeted extended release is retinal diseases, specifically diabetic macular edema (DME) and age-related macular degeneration (AMD). These two diseases affect more than 30 million people worldwide and are the leading cause of blindness and vision loss. Both of these diseases stem from issues within the blood vessels in the retina. Due to its location in the posterior segment of the eye, traditional eye drops and

intravenous injections are ineffective due to restrictions from the blood-retinal barrier.[3] While there are a number of effective treatments that have recently been developed, delivering these molecules to the retina remains a challenge. The current delivery method is intravitreal injections that are administered every 4-8 weeks. These diseases are not curable, and patients have to continually receive these injections to manage the symptoms. These frequent injections are not only unpleasant, but are also expensive and increase the risk of complications. The ideal intravitreal implant would be able to be injected into the vitreous of the eye and release drugs for 3-6 months, reducing the amount of times a patient would need to be injected.

In the previous chapter, an implantable hydrogel implant was introduced that is capable of delivering therapeutic proteins for over three months. The implants are made of hyaluronic acid (HA), a natural component of the eye, and are molded into hollow cylinders. These cylinders can be loaded with therapeutic proteins, capped, and implanted into the eye for sustained release. While many implants control the release rate via degradation, diffusion, pH, temperature, or a combination of these factors, the release from these cylinders are controlled by diffusion alone. By controlling the HA formulation, wall thickness, and concentration of protein within the hollow cylinder, the release profile and rate can be easily controlled.

One of the advantages of a hydrogel implant is that it can be molded and shaped into any size that is needed for a given application. In the previous chapter, hollow cylinders were synthesized that were 1 mm in diameter and 10 mm in length. This size was chosen for the prototype because it is the largest cylinder size known to date that has gone under clinical trials for intravitreal drug delivery.[4,5] The large size made loading, capping, and handling of the cylinders practicable while also providing a large dose that was easy and accurate to measure. However, a cylinder of this size would have to be surgically implanted in the vitreous after

making a 2mm incision in the pars plana. While this method is feasible, cylinders that could be injected using a smaller needle would reduce both time and cost and would be much safer for the patient. One example of a smaller, biodegradable (PLGA) implant that has had clinical success delivering small molecules is Ozurdex ®, which has a diameter of 0.45 mm and is injected into the vitreous using a 22-gauge microinjector. Using a 22-gauge microinjector allows for intravitreal injections that are much faster and safer when compared to implanting the cylinders after incision. However, a 22-gauge needle is still quite large when compared to the needles that are currently used for intravitreal injections. 27-gauge needles are currently the standard option for delivering substances that are more crystalline in nature (e.g. triamcinolone acetonide suspension), while 30 gauge needles or smaller are used to deliver solutions of the anti-vascular endothelial growth factors that are the standard treatment for macular degeneration and diabetic macular edema.[6] In general, both doctors and patients prefer smaller needles, as they have been shown to lower the chances of complications and scleral damage while also reducing discomfort.[7]

The production of smaller hollow cylinders has its fair share of challenges and limitations. Smaller cylinders become increasingly difficult to load and cap. Also, the smaller the cylinder, the less volume there is to load with a concentrated drug solution. This becomes even more challenging with intravitreal implants because most of the drugs that are used have a high molecular weight and the desired duration of release is 3-6 months. One way to increase the amount of volume inside the cylinder is to reduce the wall thickness. However, this not only makes the cylinders more susceptible to breaking, it also increases the rate of release as there is less hydrogel that the drug has to diffuse through. Fabricating such small cylinders and testing all of these variables over the time length required for ocular delivery would be very tedious.

Fortunately, diffusion in a hollow cylinder is a problem that has been well studied. In 1959, Carslaw and Jaeger outlined a number of solutions that accounted for the conduction of heat through a hollow cylinder under a variety of boundary conditions.[8] The mathematical work was then applied by Crank to a few select cases of diffusion in hollow cylinders.[9] This work was extended recently by Huang and Yen to include mathematical solutions that take into account the steady state, transient state, and decay transient states of solutes diffusing within a hollow cylinder.[10] While these mathematical solutions are helpful in understanding the release of drugs from hollow cylinders, almost all of the solutions were developed for cases where the boundary conditions are constant. Crank has solutions for the steady state release from a hollow cylinder where the inner and outer surfaces are kept at a constant concentration.[9] Huang and Yen developed unsteady state solutions for cases where the inner or outer concentrations are kept constant as well as solutions for the case when the walls contain an initial amount of drug and the inner and outer surfaces are kept at zero concentration.[10] In a hydrogel implant, the concentration inside of the hollow cylinder will slowly decline with time, further complicating the analysis. When challenging boundary conditions are involved numerical solutions are often utilized instead of developing complex analytical solutions. The increase of computing power and the large number of software options available has made solving these numerical problems easier than ever.

In this chapter, the diffusion of drugs through intravitreal hollow cylinder hydrogel implants are modeled using COMSOL Multiphysics© software in an effort to understand how the diffusion coefficient and cylinder dimensions affect the release rate and profile. This software is based on a finite element method and has been used to model many biological systems, including transdermal drug delivery, the release of drug from a scleral patch, and even the distribution of

heat within the human eye.[11-13] Hydrogel implants with three different outer diameters are modeled: a 1mm implant that would have to be implanted, a 0.45 mm implant that could be injected using a 22-gauge microinjector, and a 0.21 mm implant that could be injected using a 27-gauge needle. By using a variety of wall thicknesses and diffusion coefficients, a wide range of release rates and profiles can be achieved. While the focus of this chapter is on ophthalmic drug delivery, the delivery devices and release profiles explored in this chapter can be utilized in a number of biomedical applications where sustained, local release is required.

6.3 Model Development

6.3.1 Overview

The release of drugs from a hollow cylinder was modeled using Fick's first law:

$$N_i = -D_i \nabla c_i \tag{6.1}$$

where N_i is the flux of solute i, D_i is the diffusion coefficient, and ∇c_i is the concentration gradient of species i. When combined with the continuity equation for mass,

$$\frac{\partial c_i}{\partial t} + \nabla \circ N_i = 0 \tag{6.2}$$

Fick's second law is obtained and is the main equation used to model the unsteady-state diffusion in multiple dimensions:

$$\frac{\partial c_i}{\partial t} = D_i \nabla^2 c_i \tag{6.3}$$

The COMSOL software also includes convection terms into the equations, however these were set to zero due to the fact that the release through the walls of the hydrogel implants occurs only by diffusion.

6.3.2 Dimensions and Boundary Conditions

The dimensions of the implants that were modeled can be seen in Figure 6.1. While the outer radius (r_o) of the cylinders varied, all of the cylinders were 10 mm long and had a 1 mm base at the bottom. The wall thickness and the inner volume of the cylinders was varied by changing the inner radius (r_i). The parameter K, defined as the ratio of the outer radius to the inner radius ($K=r_o/r_i$), ranged from 1.05 to 5. The volume of the loading cavity ranged from 0.03 to 6.4 microliters, depending on the inner and outer radius of the cylinder.

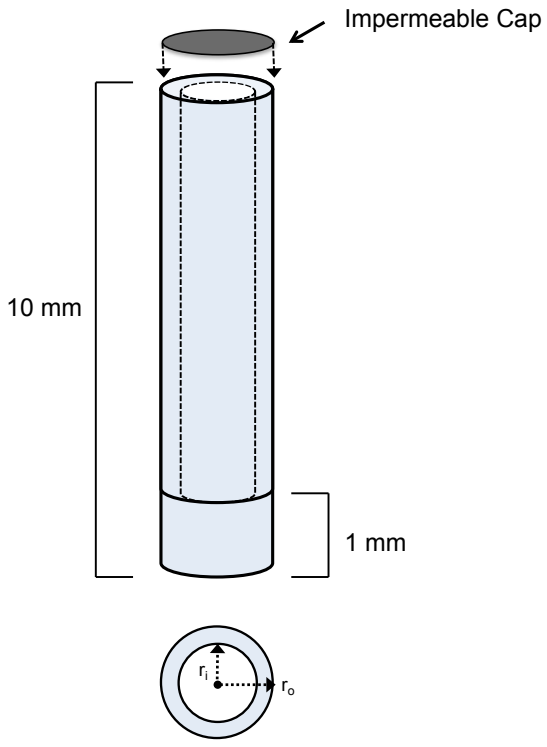

Figure 6.1. Dimensions of the hollow cylinder implants. The outer diameter (r_o) was kept constant and the wall thickness was varied by changing the inner radius (r_i).

The values of the various simulation parameters used in the model are given in Table 6.1. The molecular weight parameter was set at 66 kDa, the molecular weight of bovine serum albumin (BSA) which was chosen due to its similarity in size and molecular weight to the therapeutic proteins on the market that are currently being used to treat retinal diseases. The two most commonly used drugs are ranibizumab (Lucentis, Genentech, South San Francsicso, CA/Roche, Basel, Switzerland) and aflibercept (Eyelea, Regeneron, Tarrytown, NY), and have molecular weights of 48 and 97 kDA, respectively. The initial concentration within the hollow cylinder was set at 160 mg/mL in order to keep consistent with Chapter 5, where 160 mg/mL of was loaded into hollow cylinder implants and used for release experiments. While the solubility limit of BSA is higher than 160 mg/mL, this concentration was chosen to more closely represent the concentration that a therapeutic protein would be administered at. In implants of this size, the drug formulations often range in concentration from 100 – 500 mg/mL in order to achieve extended release.[14] In fact, one advantage of a hollow cylinder implant is the ability to load a supersaturated solution or slurry in order to increase the total dosage of the device. The solubility of therapeutic proteins will vary based on their size, hydrophobicity, and the distribution of charges and electrostatics.[15,16] The current treatment method for AMD and DME consists of intravitreal injections at concentrations that range from 10 mg/mL (ranibizumab) to 40 mg/mL (aflibercept). Given the frequency of the injections, the half-life of these drugs in the vitreous (~ 9-12 days), and the cost of the drugs, the low concentrations were probably chosen in order to achieve the most effective dosage and to limit systemic exposure and do not reflect the solubility limits of these drugs.

Table 6.1. Simulation parameters

Parameter	Description	Value
H	Height of gel	1 cm
R_o	Outer radius of gel	0.105 - 0.5 mm
R_i	Inner radius of gel	0.035 - 0.476 mm
$K = R_o/Ri$	Ratio of outer and inner radii	1 - 5
V_{load}*	Volume of loading cavity	0.03 - 6.4 uL
M_W	Molecular weight of drug	66000 g/mol
C_0	Initial concentration	160 mg/ml
M_t	Mass released at time t	2 - 1026 ug
M_∞	Total mas released	2 - 1026 ug
D_{gel}	Diffusion coefficient in the gel	1×10^{-10} - 1×10^{-12} cm^2/s
D_{inner}	Diffusion coefficient in the inner volume	1×10^{-7} cm^2/s
D_{outer}	Diffusion coefficient outside the implant	1×10^{-7} cm^2/s
L	Length of permeable portion of cylinder	0.9 cm

* Calculated using R_o and R_i

The diffusion coefficient of protein within the hydrogel wall was varied systematically between 1×10^{-10} and 1×10^{-12} cm^2/s. Diffusion occurred both radially through the cylinder walls and through the hydrogel base at the bottom of the cylinder. A boundary condition set the diffusion from the top of the cylinder equal to zero, simulating an impermeable cap. Additionally, the initial concentration outside of the cylinder was set at zero.

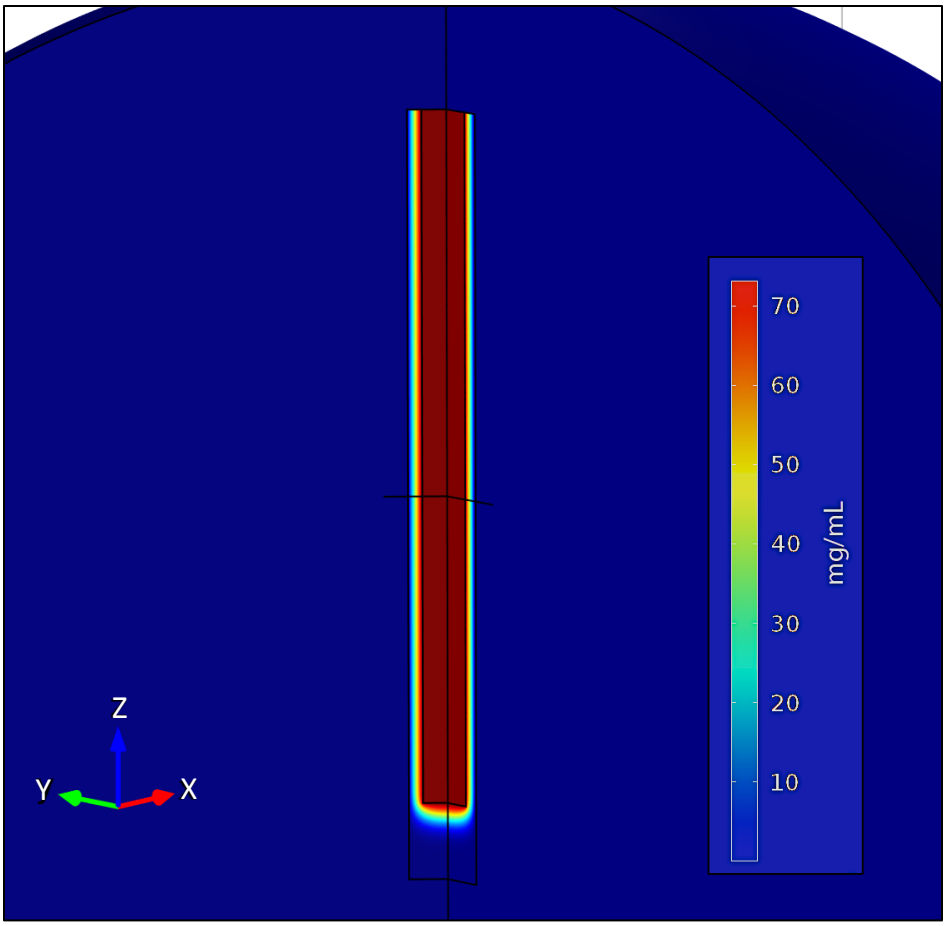

Figure 6.2. Sample concentration profile of a hollow cylinder showing diffusion through the walls and base. The dark red inside the cylinder represents the higher concentration of drug initially loaded, while the blue sphere outside of the cylinder represents the release volume that is set at a concentration of 0 mg/mL in order to model sink conditions.

6.3.3 Finite Element

A three dimensional free triangular mesh was used to define the computational domain. The network was set to be finer in and around the hollow cylinder and broader the further the distance away from the implant. The maximum element size was 0.1 mm and the minimum element size was 2.4 x 10^{-5} mm.

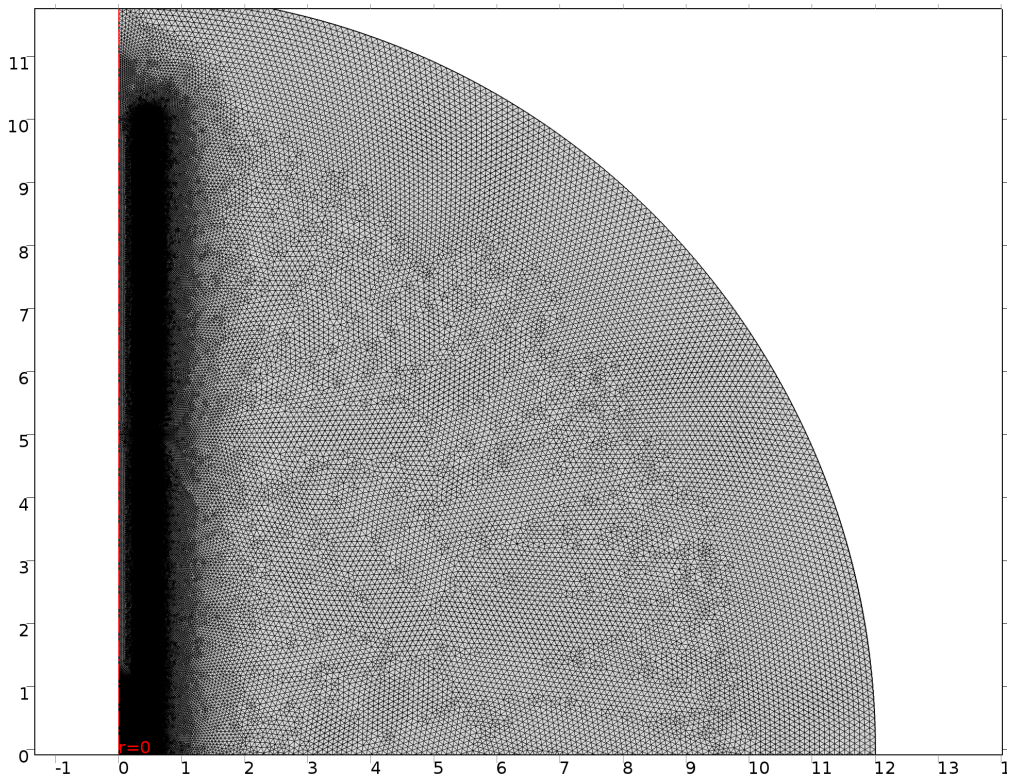

Figure 6.3. Two dimensional mesh of the hollow cylinder used to define the computational domain. The network is much finer in and around the hollow cylinder and increases in size the further the distance away from the implant. All units are in mm.

6.3.4 Release Rate and Profile

In evaluating the performance of the hollow cylinders it is helpful to define some of the terms that are used to characterize the release rate and profile. A sample release profile can be seen in Figure 6.4. The release profile is displayed in terms of the cumulative drug released, defined as the mass released at t = t (M_t) divided by the mass that is released from the cylinder at t = ∞ (M_∞). A distinctive feature of reservoir delivery devices (assuming the wall is unsaturated) is the time it takes for the drug to penetrate the wall and begin releasing, defined as t_{lag}. The lag time will depend on both the wall thickness and the diffusion coefficient of the drug within the wall. $t_{50\%}$ and $t_{90\%}$ are the times it takes for the device to release 50% and 90% of the total drug loaded.

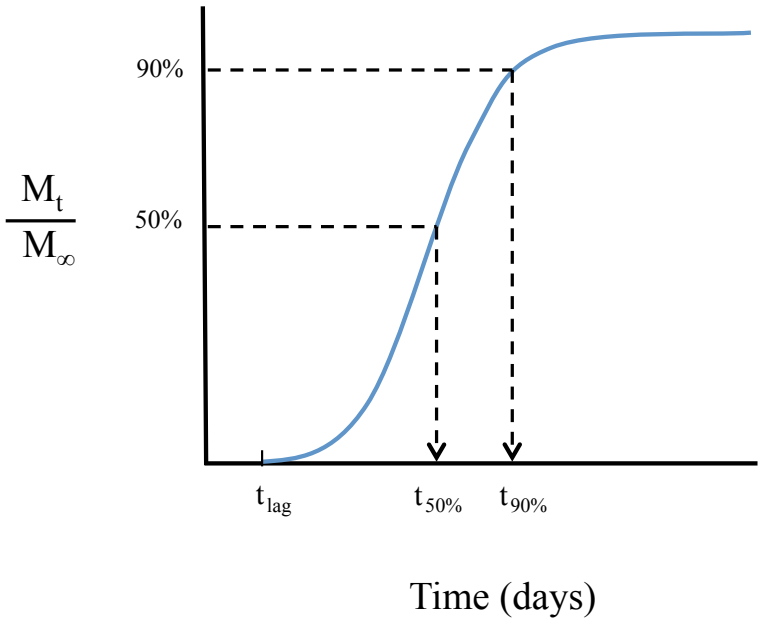

Figure 6.4. Release profile from a hollow cylinder.

Another crucial aspect of any drug delivery device is the rate at which the device releases drug to the intended target area. If the device cannot release drug at a fast enough rate, the concentration at the target area will not be high enough to have a therapeutic effect. If the device releases drug too quickly, the concentration at the target area can become too high and may lead to potentially toxic side effects. The concentration range that provides a safe, yet effective, therapeutic effect is referred to as the therapeutic window in drug delivery applications and can be seen in Figure 6.5. In this chapter, the concept of the therapeutic window is used to describe the release rate that can achieve this concentration range at the retina. The upper and lower boundaries for the release rates of this therapeutic window are defined as $r_{t,max}$ and $r_{t,min}$. r_{max} is defined as the maximum release rate that is achieved from the delivery device and will vary depending on the initial concentration within the implant (C_0), the wall thickness, and the diffusion coefficient.

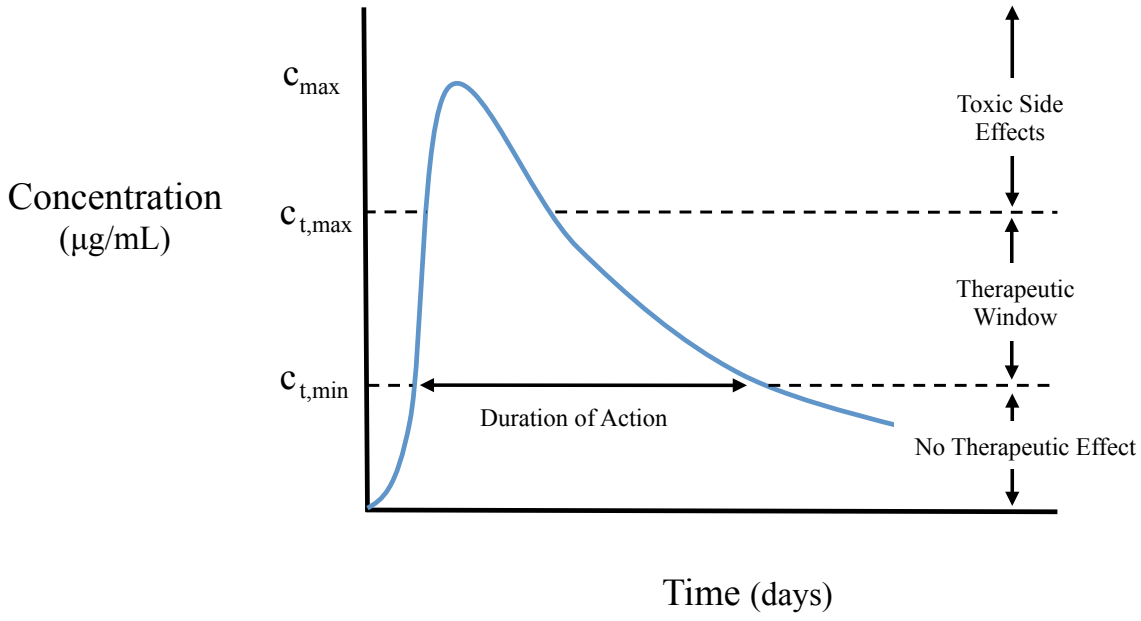

Figure 6.5. The concentration range required for a drug to be effective, yet safe is known as the therapeutic window. This is achieved by controlling the release rates from hollow cylinders.

Defining these upper and lower boundaries for an ocular implant is challenging in large part due to the difficulty of taking frequent samples from the human vitreous. Looking at the current treatment methods for patients who suffer from AMD and DME can help define the target range of concentrations needed for an ocular implant. The current treatment method is intravitreal injections that range in dosage from 0.5 mg (ranibizumab) to 2 mg (aflibercept), giving maximum vitreous concentrations of 0.125 mg/mL to 0.5 mg/mL[17,18]. Although the blood-retinal barrier drastically limits the amount of drug that reaches the serum (approx. 90,000 times lower than vitreous concentrations), increased levels of these inhibitors in the serum can lead to hypertension, and wound complications[19]. The maximum amount of drug loaded in the cylinders modeled in this paper is just over 1 mg. Even if the cylinder would crack or break and release the entire amount instantaneously, it would lead to a concentration in the vitreous of only 0.25 mg/mL, similar to that of the intravitreal injections. Therefore the maximum concentrations and corresponding release rates described in this paper are all below the $c_{t,max}$ for the intended intravitreal application.

The lower boundary that defines the minimum concentration necessary to achieve a therapeutic effect is much harder to define. Both ranibizumab and aflibercept target a signal protein called vascular endothelial growth factor (VEGF). VEGF plays an important role in the development of new blood vessels and elevated levels in the eye can lead to neovascularization that occurs behind the retina.[20] This can lead to abnormal growth and leakage of the choroidal vessels, which leads to macular degeneration and edema.[21] Both ranibizumab and aflibercept can prevent the signaling between VEGF and endothelial cells. Ranibuzumab was shown *in vitro* to specifically inhibit the proliferation of human umbilical vein endothelial cells that were induced by VEGF-A by 50% at concentrations between 11-27 ng/mL.[22] Numerous studies have also

shown that patients with DME and AMD have elevated levels of VEGF in the vitreous that can range from 0.05-2.0 ng/mL.[21,23-25] This wide range of VEGF levels makes it difficult to accurately calculate the concentration needed. In this chapter the $c_{t,min}$ was set at 625 ng/mL. This concentration within the vitreous of the eye is over 20 times the concentration estimated to inhibit cell proliferation and over 300 times the concentration of VEGF in the vitreous. The release rate required to achieve this concentration is 2.5 μg/day and was set as the $r_{t,min.}$ This value was used to calculate the duration of action, defined as the number of days that the release rate of the implant exceeded 2.5 μg/day.

6.4 Results And Discussion

In this section hydrogel implants with three different outer diameters are modeled: a 1mm implant that would have to be implanted, a 0.45 mm implant that could be injected using a 22-gauge microinjector, and a 0.21 mm implant that could be injected using a 27-gauge needle. Using COMSOL, the release rates and release profiles are plotted for each cylinder (similar to Figures 6.4 & 6.5) at varying wall thicknesses. Additionally, the release rates and profiles were also plotted using a wide range of diffusion coefficients. Given the large amount of data produced, this section focuses on a reduced set of parameters such as $t_{50\%}$, $t_{90\%}$, r_{max}, and the duration of action in order to more easily compare the cylinders. The primary goal of this section is to determine the range of diffusion coefficients required for a successful hollow cylinder intravitreal implant.

6.4.1. Implantable Hollow Cylinder – 1mm O.D.

The release of drug from a 1 mm cylinder was modeled with values of K ranging from 1.05 to 3. Table 6.2 shows the physical dimensions, wall thicknesses, inner volume, and the total mass of drug loaded for the cylinders studied. Although a delivery device of this size would have to be implanted, the large inner volumes and high drug loading that can be achieved at this diameter provide the greatest versatility in terms of possible release rates and therapeutic durations when compared to the smaller devices. Using an initial concentration of 160 mg/ml, the total drug loaded at K = 1.05 is just over 1 mg of drug. This is the equivalent dose of two standard intravitreal injections of ranibuzumab while offering the advantage of controlled release that can be tuned by changing the diffusion coefficient within the wall.

Table 6.2. Physical dimensions and loading capacity of 1mm O.D. hollow cylinders

K (b/a)	**Inner Diameter (mm)**	**Wall Thickness (mm)**	**Inner Volume (µL)**	**M_∞* (µg)**
1.05	0.952	0.024	6.41	1026
1.1	0.909	0.045	5.84	935
1.2	0.833	0.083	4.91	785
1.25	0.800	0.100	4.52	724
1.5	0.667	0.167	3.14	503
2	0.500	0.250	1.77	283
5	0.200	0.4	0.28	45

*M_∞ was calculated using 160 mg/mL as the initial loading concentration and assuming 100% release

The release profile from a 1mm hollow cylinder can be seen in Figures 6.6 and 6.7. Figure 6.6 shows how changes in the wall thickness and diffusion coefficient affect $t_{50\%}$. The dashed lines indicate the $t_{50\%}$ required for 3-6 months release. As expected, an increase in the diffusion coefficient causes a decrease in the time it takes for the implant to release 50% of the total load. At the highest diffusion coefficient modeled, D = 1.0 x 10^{-10} cm^2/s, $t_{50\%}$ reaches the required target in only the cylinders with the thickest walls (K = 2-5). On the other hand, at the lowest diffusion coefficient modeled, D = 1.0 x 10^{-11} cm^2/s, even the thinnest wall thickness at K = 1.05, reaches the required target of 45 days ($t_{50\%}$ = 47 days).

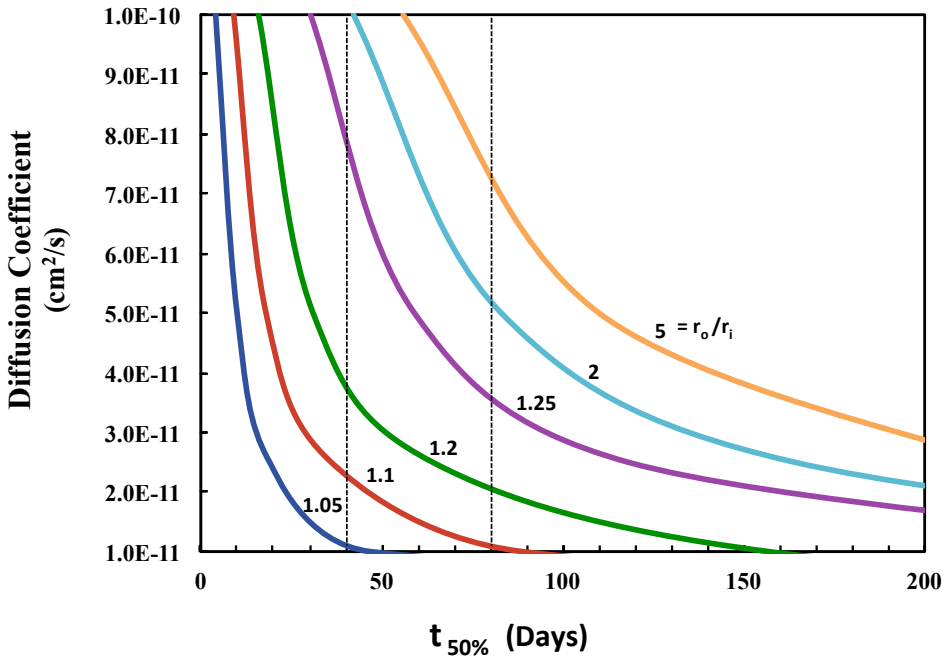

Figure 6.6. The effect of the diffusion coefficient and wall thickness on the release of drugs from a hollow cylinder with an outer diameter of 1 mm. Release was measured in terms of $t_{50\%}$, the time it takes for 50% of the loaded drug to be released from the device. The labels indicate the value of K, which is the ratio of the outer to inner radius of the hollow cylinders. (---) = K = 1.05, (---) = K = 1.1, (---) = K = 1.2, (---) = K = 1.25, (---) = K = 2, (---) = K = 5. The dashed lines represent the target $t_{50\%}$ required for 3-6 months release.

Similar results are seen in Figure 6.7, which shows how changes in the wall thickness and diffusion coefficient affect $t_{90\%}$. At the highest diffusion coefficient modeled, D = 1.0 x 10^{-10} cm^2/s, $t_{90\%}$ reaches the required target in only cylinders in which K > 1.5. At the slowest diffusion coefficients, D = 2.5 x 10^{-11} cm^2/s and D = 1.0 x 10^{-11} cm^2/s, small changes in K lead to large changes in $t_{90\%}$. All of the cylinder dimensions reach the required target for 3-6 months release and as K reaches values larger than 1.5 the cylinders take over a year to release the entire load. At a fixed value of K of 1.05, $t_{90\%}$ ranged from as low as 16 days to as high as 156 days showing the wide range of release times that can be achieved by changing only the diffusion coefficient.

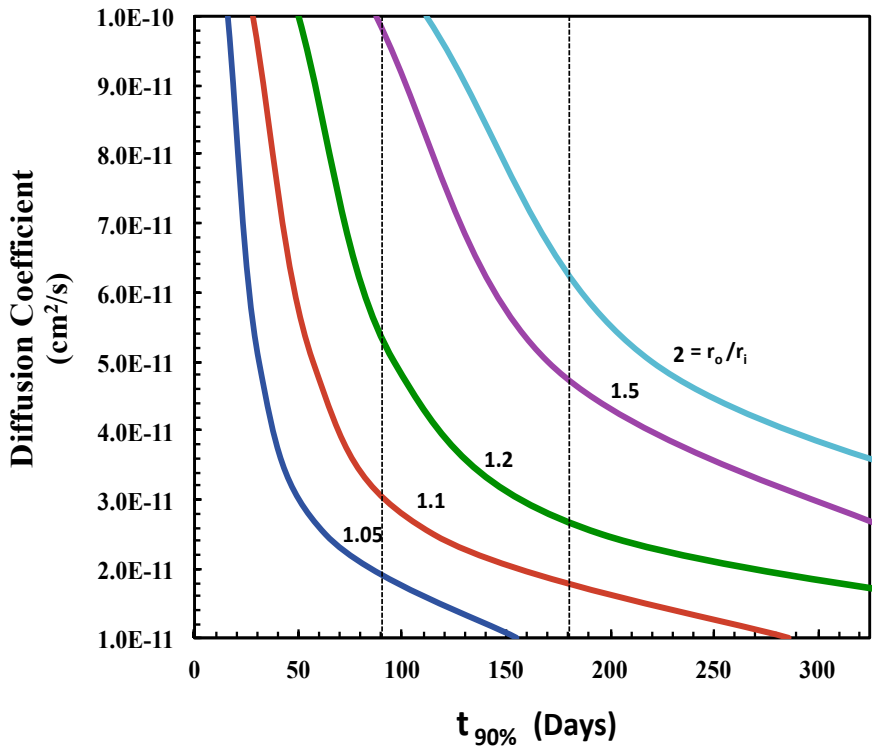

Figure 6.7. The effect of the diffusion coefficient and wall thickness on the release of drugs from a hollow cylinder with an outer diameter of 1 mm. Release was measured in terms of $t_{90\%}$, the time it takes for 90% of the loaded drug to be released from the device. The labels indicate the value of K, which is the ratio of the outer to inner radius of the hollow cylinders. (---) = K = 1.05, (---) = K = 1.1, (---) = K = 1.2, (---) = K= 1.25, (---) = K = 2. The dashed lines represent the target $t_{90\%}$ required for 3-6 months release.

While the time required to release 50 and 90 percent of the drug loaded is helpful for determining the range of diffusion coefficients required, the release rate is necessary in order to get a more accurate range. For example, in Figures 6.6 and 6.7 there were no upper boundaries set on $t_{50\%}$ and $t_{90\%}$. While many of the cylinders in the figure exceed the required 3-6 months release, this extended release may come at the expense of a lower release rate. If the release rate is too low, the concentration at the retina may never reach the $c_{t,min}$ required to be therapeutically effective. Therefore, a closer look at the release rates is required.

The maximum release rate from a 1mm hollow cylinder can be seen in Figure 6.8. It is important to note that, unlike the release times ($t_{50\%}$ and $t_{90\%}$), the maximum release rate is dependent on the initial concentration loaded within the cylinder. In this chapter, this concentration was kept constant at 160 mg/mL. Higher or lower initial concentrations will lead to an increase or decrease in the release rates from the values reported in this chapter. In general, as the wall thickness (K) increases, the release rate decreases, and as the diffusion coefficient increases, the release rate increases. The largest variations in the release rate occur at values of K below 1.2 where the walls are the thinnest. As expected, the maximum release rate occurs at K = 1.05 and ranges from 15 μg/day all the way up to 132 μg/day. These release rates are 7-50 times higher than the target $r_{t,min}$ which was set at 2.5 μg/day (dashed line in Figure 6.8). Alternatively, cylinders with thick walls in which the value of K is greater than 2 fail to reach the target, and at K=2, the cylinder only reaches the target release rate when the diffusion coefficient is higher than 4.5×10^{-11} cm^2/s.

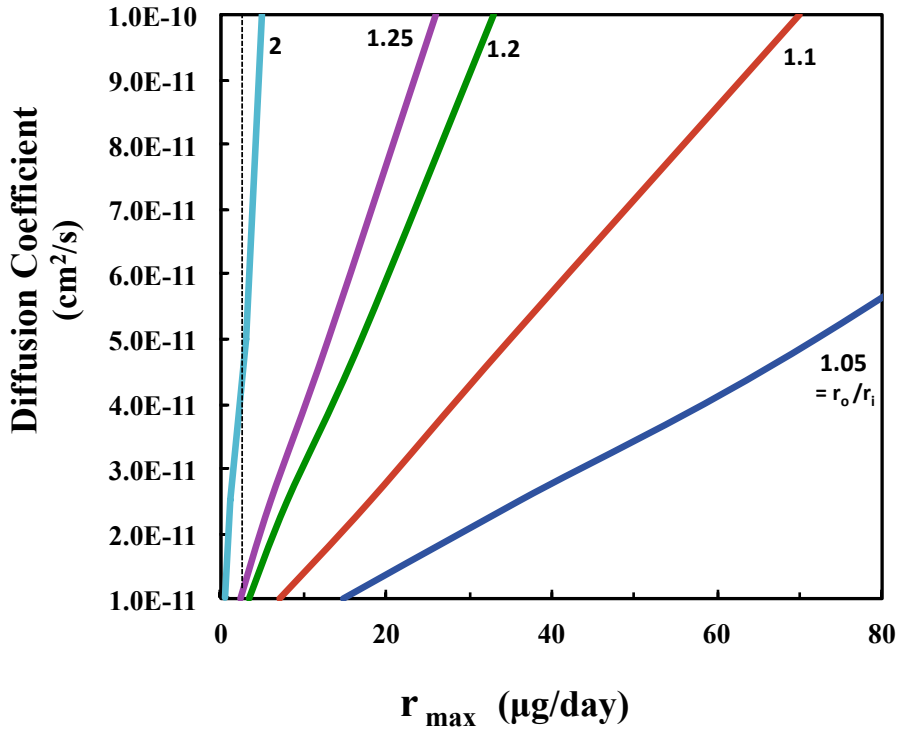

Figure 6.8. The effect of the diffusion coefficient and wall thickness on the maximum release rate of drugs from a hollow cylinder with an outer diameter of 1 mm. The labels indicate the value of K, which is the ratio of the outer to inner radius of the hollow cylinders. (---) = K = 1.05, (---) = K = 1.1, (---) = K = 1.2, (---) = K= 1.25, (---) = K = 2. The dashed line represents the target release rate of 2.5 µg/day that is required in order to reach the therapeutically effective concentration at the retina.

Once again, there is no upper boundary placed on the maximum release rate in Figure 6.8. As mentioned earlier, even if the cylinder would crack or break and release the entire dose instantaneously the concentration at the retina would still not be high enough to elicit any toxic side effects. However, excessively high release rates (r_{max} > 20 µg/day) are not desired as they quickly reduce the extended release that can be achieved without providing any known additional therapeutic benefit. Due to the small size of ocular implants, the drug load is often limited and it is crucial to release the drug as efficiently as possible.

One way to gauge this efficiency is by measuring the time each implant releases above the target release rate, known as the duration of action. Figure 6.9 displays the duration of action that each cylinder can achieve. The longest duration is 139 days at K = 1.1 and D = 1.0 x 10^{-11} cm^2/s. This is just over 4.5 months of release at a rate that is above 2.5 μg/day. Surprisingly, the longest durations do not occur at K = 1.05 for any of the diffusion coefficients. In fact, the longest durations occur at larger values of K the faster the diffusion coefficient is, as evidenced by the fact that at D = 1.0 x 10^{-10} cm^2/s, the longest duration occurs at a K value of 2. This means that as the diffusion coefficient increases, a longer therapeutic duration can be achieved by actually making the walls thicker and decreasing the total volume and load inside the cylinder. This is due to the fact that at the lower values of K, the release rates from the thinner walls is initially so high that it quickly depletes the amount of drug inside the cylinder, reducing the amount of time the release rate is above $r_{t,min}$. Alternatively, at lower diffusion coefficients, having too thick of a wall can lower the release rate so much that it never exceeds $r_{t,min}$. This can be seen for values of K greater than 1.5 for D = 1.0 x 10^{-12} cm^2/s.

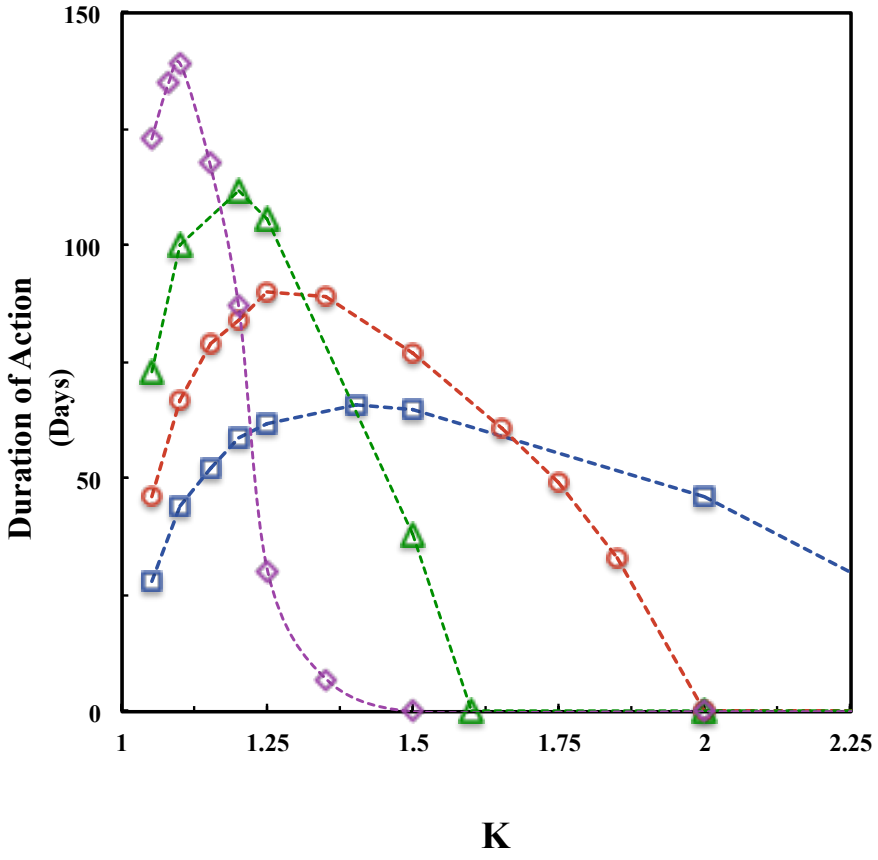

Figure 6.9. The effect of the diffusion coefficient and wall thickness on the duration of action that can be achieved from a hollow cylinder with an outer diameter of 1 mm. (□) = D = 1.0 x 10^{-10} cm^2/s, (O) = D = 5.0 x 10^{-11} cm^2/s, (Δ) = D = 2.5 x 10^{-11} cm^2/s, (◇) = D = 1.0 x 10^{-11} cm^2/s

6.4.2. Microinjected Hollow Cylinder – 0.45mm O.D.

The release of drug from a 0.45 mm cylinder was modeled with values of K ranging from 1.05 to 5. Table 6.3 shows the physical dimensions, wall thicknesses, inner volume, and the total mass of drug loaded for the cylinders studied. The main benefit from a delivery device of this diameter is that it can be inserted into the vitreous using a microinjector, a much safer and faster process than making an incision and implanting the device. However, even though the device is just under half the diameter of the 1 mm cylinders, the inner volume is dramatically reduced. This limits the amount of drug that can be loaded. The total drug loaded at K = 1.05 is 208 micrograms, roughly five times less than the maximum drug that can be loaded in the larger 1mm cylinders. Additionally, the wall thicknesses of the 0.45 mm cylinders are much thinner than those of the 1.0 mm cylinder at similar values of K.

Table 6.3. Physical dimensions and loading capacity of 0.45mm hollow cylinders

K (r_o/r_i)	**Inner Diameter (mm)**	**Wall Thickness (mm)**	**Inner Volume (µL)**	**M_∞ (µg)**
1.05	0.0013	0.011	1.298	208
1.1	0.409	0.020	1.183	189
1.2	0.375	0.038	0.994	159
1.5	0.300	0.075	0.636	102
2	0.225	0.113	0.358	57
3	0.150	0.150	0.159	25
5	0.090	0.169	0.057	9

*M_∞ was calculated using 160 mg/mL as the initial loading concentration and assuming 100% release

The release profile from a 0.45 mm hollow cylinder can be seen in Figures 6.10 and 6.11. Figure 6.10 shows how changes in the wall thickness and diffusion coefficient affect $t_{50\%}$. The trend is very similar to that seen in Figure 6.6 for the 1mm cylinders, however the release is much faster. At D = 1.0 x 10^{-10} cm^2/s, $t_{50\%}$ never reaches more than 12 days, where as the 1 mm cylinders reached a maximum of 56 days. Even though the cylinders are much smaller, the devices are still capable of releasing drug for the target period of 3-6 months, as evidenced by the $t_{50\%}$ of 112 at K = 5 and D = 1.0 x 10^{-11} cm^2/s. However, given the cylinders smaller dimensions, this is only possible with thicker walls (K > 1.5) and at lower diffusion coefficients (D < 3.0 x 10^{-10} cm^2/s).The release can be extended even further by decreasing the diffusion coefficient to D = 1.0 x 10^{-12} cm^2/s. The release profiles of cylinders at this diffusion coefficient are not shown in Figure 6.10, yet the values of $t_{50\%}$ at K = 1.05 and 1.1 are 95 and 180, respectively.

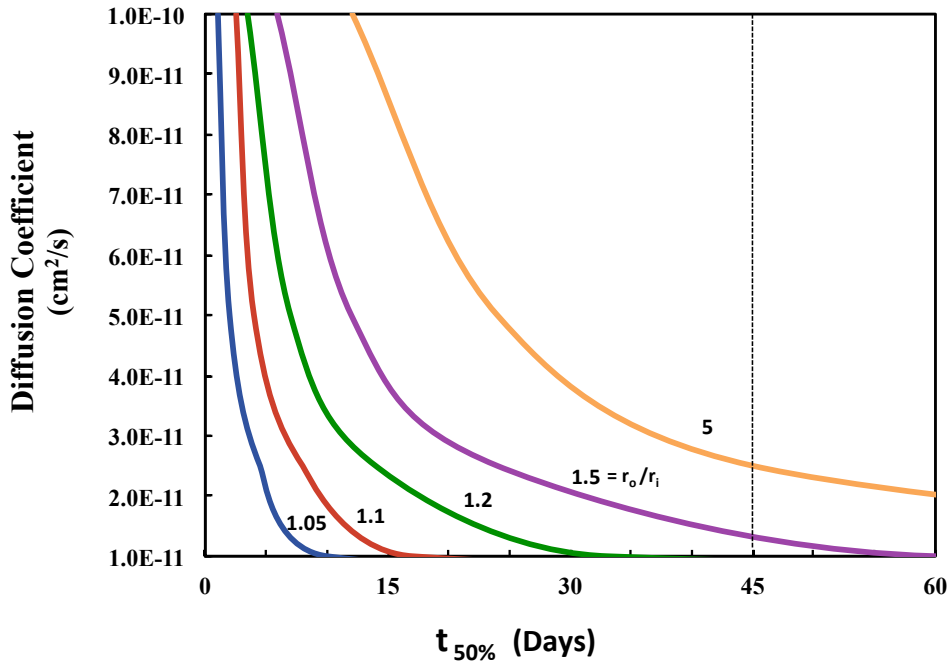

Figure 6.10. The effect of the diffusion coefficient and wall thickness on the release of drugs from a hollow cylinder with an outer diameter of 0.45 mm. Release was measured in terms of $t_{50\%}$, the time it takes for 50% of the loaded drug to be released from the device. The labels indicate the value of K, which is the ratio of the outer to inner radius of the hollow cylinders. (---) = K = 1.05, (---) = K = 1.1, (---) = K = 1.2, (---) = K= 1.25, (---) = K = 5. The dashed lines represent the target $t_{50\%}$ required for 3-6 months release.

Figure 6.11 shows how changes in the wall thickness and diffusion coefficient affect $t_{90\%}$. At the lower diffusion coefficient values, small changes in K lead to large changes in $t_{90\%}$, especially for values of K below 1.5. For all of the diffusion coefficients, as K reaches values larger than 1.5, $t_{90\%}$ begins to plateau and does not change much as K is increased from 3 to 5. At a fixed value of K of 1.2, $t_{90\%}$ ranged from as low as 10 days to as high as 100 days showing the wide range of release times that can be achieved by changing only the diffusion coefficient. The release is much faster when compared to the 1mm cylinders, which was expected due to the thinner walls and smaller loading volumes. At D = 1.0 x 10^{-10} cm^2/s, $t_{90\%}$ reaches a maximum at 26 days, compared to the 1 mm cylinders which reached a maximum of 112 days.

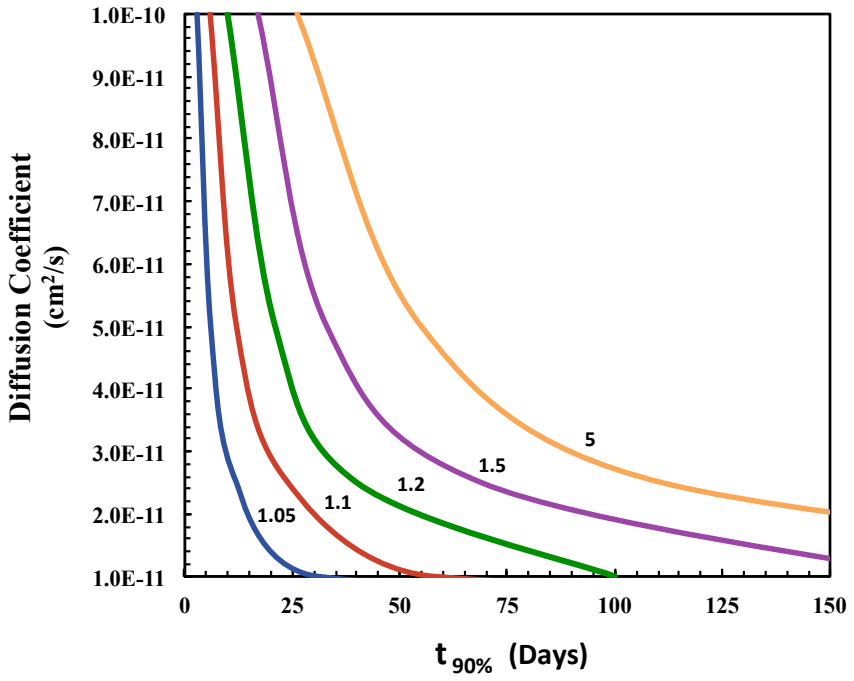

Figure 6.11. The effect of the diffusion coefficient and wall thickness on the release of drugs from a hollow cylinder with an outer diameter of 0.45 mm. Release was measured in terms of $t_{90\%}$, the time it takes for 90% of the loaded drug to be released from the device. The labels indicate the value of K, which is the ratio of the outer to inner radius of the hollow cylinders. (---) = K = 1.05, (---) = K = 1.1, (---) = K = 1.2, (---) = K= 1.25, (---) = K = 5. The dashed lines represent the target $t_{90\%}$ required for 3-6 months release.

The release rate from a 0.45 mm hollow cylinder can be seen in Figure 6.12. The figure follows the same trend that is seen in Figure 6.8 for the 1mm cylinders. As the wall thickness and K increase, the release rate decreases. The largest variations in the release rate occur at values of K below 2 where the walls are the thinnest. As expected, the maximum release rate occurs at the lowest value of K and ranges from 7.1 μg/day all the way up to 52 μg/day. These release rates are roughly 3-20 times higher than the target $r_{t,min}$ which was set at 2.5 μg/day.

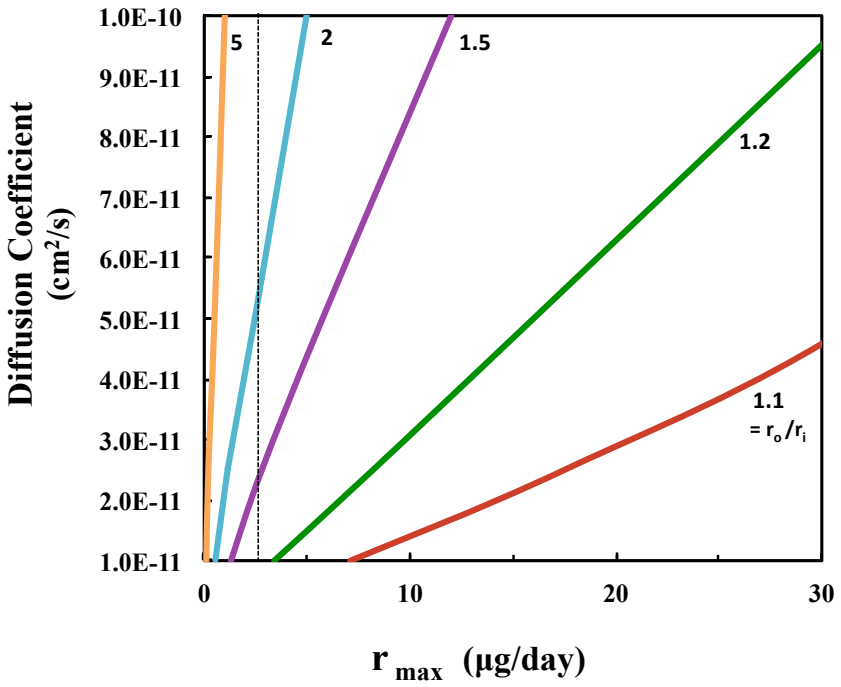

Figure 6.12. The effect of the diffusion coefficient and wall thickness on the maximum release rate of drugs from a hollow cylinder with an outer diameter of 0.45 mm. The labels indicate the value of K, which is the ratio of the outer to inner radius of the hollow cylinders. (---) = K = 1.1, (---) = K = 1.2, (---) = K= 1.25, (---) = K = 2, (---) = K = 5. The dashed line represents the target release rate of 2.5 μg/day that is required in order to reach the therapeutically effective concentration at the retina.

Figure 6.13 displays the duration of action that each cylinder can achieve. While the figure follows the same trends that are seen in Figure 6.8 for the 1mm cylinders, the durations of action are much lower. The longest duration is 28 days at K = 1.1 and D = 1.0 x 10^{-11} cm^2/s. This is less than one full month of release at a rate that is above 2.5 μg/day. In fact, the majority of the cylinders have a duration of action under two weeks. At faster diffusion coefficients (D = 1.0 x 10^{-10} - 5.0 x 10^{-11} cm^2/s) the longest duration does not occur at the lowest values of K and instead reaches a maximum at K values of 1.5. While it may be possible to get a longer duration at a lower diffusion coefficient (D <1.0 x 10^{-11}), doing so would require values of K below 1.1. At these values, the walls become so thin that the cylinders would become impossible to handle without breaking.

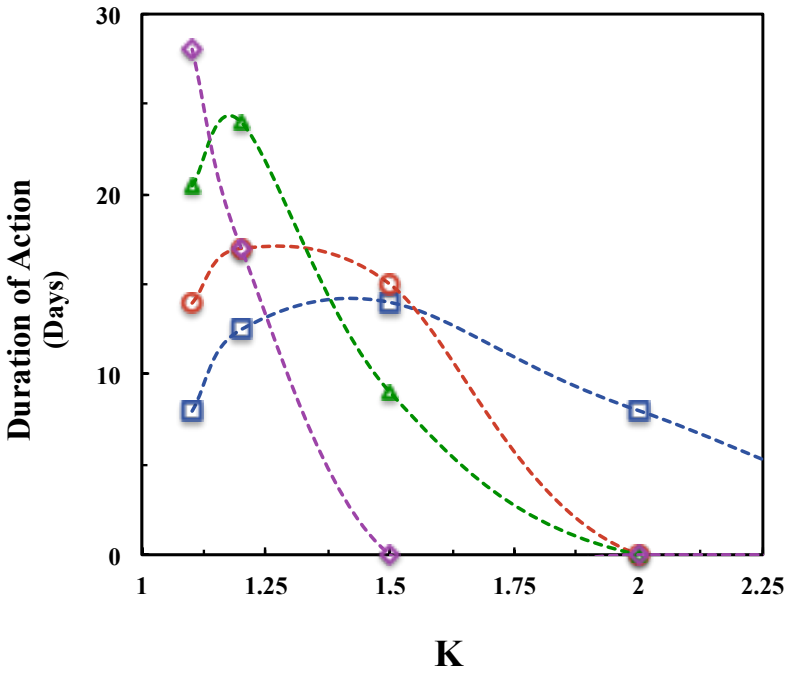

Figure 6.13. The effect of the diffusion coefficient and wall thickness on the duration of action that can be achieved from a hollow cylinder with an outer diameter of 0.45 mm. (□) = D = 1.0 x 10^{-10} cm^2/s, (○) = D = 5.0 x 10^{-11} cm^2/s, (Δ) = D = 2.5 x 10^{-11} cm^2/s, (◇) = D = 1.0 x 10^{-11} cm^2/s

6.4.3. Injectable Hollow Cylinder – 0.21mm O.D.

The release of drug from a 0.21 mm cylinder was also modeled. While the benefits of injecting these cylinders using a 27-gauge needle would be enormous, achieving extended release in a delivery vehicle that small is hindered by a number of challenges. The cylinders are so small that they have very little interior volume available for loading drugs. Table 6.4 shows the physical dimensions, wall thicknesses, inner volume, and the total mass of drug loaded for the cylinders studied. Even at the thinnest wall thickness (K=1.05), the total mass loaded is just over 45 micrograms. Almost five cylinders are needed in order to achieve the same drug loading as one 0.45 mm cylinder, and more than twenty cylinders are needed to equal the loading of a single 1.0 mm cylinder.

Table 6.4. Physical dimensions and loading capacity of 0.21mm hollow cylinders

K **(r_o/r_i)**	**Inner Diameter (mm)**	**Wall Thickness (mm)**	**Inner Volume (µL)**	**M_∞ (µg)**
1.05	0.2	0.005	0.283	45.2
1.1	0.191	0.010	0.258	41.2
1.2	0.175	0.018	0.216	34.6
1.5	0.140	0.035	0.139	22.2
2	0.105	0.053	0.078	12.5
3	0.070	0.070	0.035	5.5
5	0.042	0.084	0.012	2.0

*M_∞ was calculated using 160 mg/mL as the initial loading concentration and assuming 100% release

The thin walls of such a small cylinder also limits the release rates and profiles that can be achieved. In order to achieve extended release, the diffusion coefficient must be lowered to values below D = 1.0 x 10^{-11} cm^2/s. However, at these values, the release rates are much lower than the $r_{t,min}$ which was set at 2.5 µg/day. The duration of action that cylinders of this size can achieve is seen below in Figure 6.14. The longest duration is at K = 1.1 and D = 1.0 x 10^{-11} cm^2/s and is only 7 days of release at a rate that is above 2.5 µg/day. Despite their convenient size, cylinders that can be injected using a 27-gauge needle do not seem to be practical for sustained delivery of therapeutic proteins to the retina.

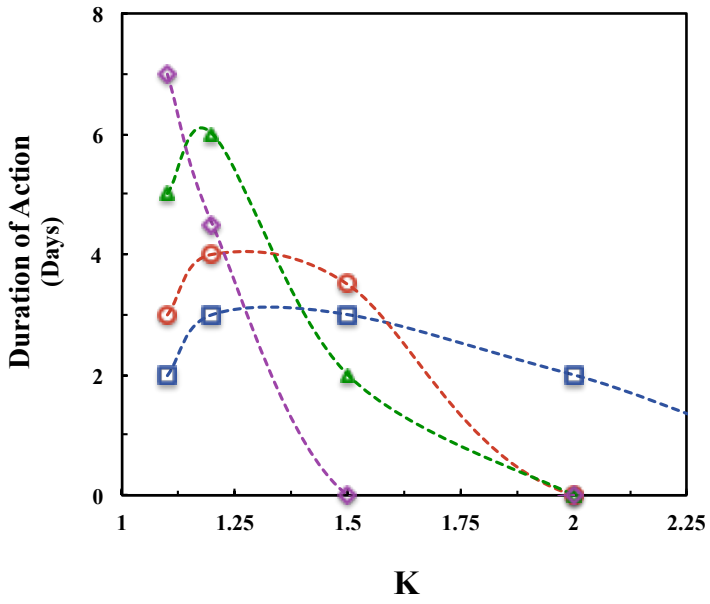

Figure 6.14. The effect of the diffusion coefficient and wall thickness on the duration of action that can be achieved from a hollow cylinder with an outer diameter of 0.21 mm. (□) = D = 1.0 x 10^{-10} cm^2/s, (○) = D = 5.0 x 10^{-11} cm^2/s, (Δ) = D = 2.5 x 10^{-11} cm^2/s, (◇) = D = 1.0 x 10^{-11} cm^2/s

6.5 Analysis

The success and implementation of an intravitreal implant will likely depend on a number of important considerations that were introduced in this chapter. The first is the required release rate and concentration needed at the retina to provide a therapeutic effect. In this chapter, the target release rate was assumed to be 2.5 micrograms a day. If further studies show that a lower concentration is needed at the retina, the duration of action for the implants in this chapter would increase. For example, the microinjected cylinder is capable of releasing for 28 days at a rate of 2.5 micrograms a day. If the target release rate drops to 1 microgram a day, the duration of action increases to 62 days, and if the target release rate drops to 0.5 micrograms a day it increases even further to 93 days. Another consideration is the concentration of the drug that can be achieved in the implant. The concentration used to run the calculations in this chapter was 160 mg/mL. Depending on the drug, it might be possible to achieve higher concentrations that would lead to higher loads and extended durations of action. At the same time, certain drugs may have a lower solubility limit or may not stable for extended periods of time at such a high concentration. This would result in reduced concentrations and would limit the effectiveness of the implant. Furthermore, all of the cylinders in this chapter were assumed to be strong enough to be injected into the eye. Depending on the hydrogel formulation, certain wall thicknesses may not have enough mechanical integrity to be injected and would need to be tested.

One of the goals of this chapter was to understand how the diffusion coefficient of the intravitreal implant impacted the release rates and profiles of the devices. Due to the size of the device, the range of diffusion coefficients that are effective in controlling the release is surprisingly narrow. The cylinders with the longest duration of action had diffusion coefficients between $1.0 \times 10^{-11} – 3.0 \times 10^{-11}$ cm^2/s. When the diffusion coefficient is much larger than this the

release rate becomes so fast that it becomes difficult to achieve extended release. Alternatively, when the diffusion coefficient is much smaller than this the release rate is reduced so much that the device fails to ever reach the target release rate required for therapeutic effect. The results also show how sensitive the release is to the diffusion coefficient as small changes in the diffusion coefficient can lead to drastic changes in both the release rate and the release profile. Additionally, as the cylinders decreased in size the release rate and profile became even more sensitive to changes in the diffusion coefficient. Controlling the diffusion coefficient is critical in developing a successful hydrogel implant and further indicates the importance of understanding the diffusion in hydrogels at the low swelling degrees required to achieve such values.

6.6 Conclusions

In this chapter, the release of therapeutic proteins from hollow cylinders was modeled using the physics software COMSOL for the treatment of retinal diseases. The chapter focused on intravitreal implants with varying dimensions and insertion methods that could be used as an alternative or replacement to the current standard of care. As expected, the largest size cylinders that were studied with a 1mm outer diameter were able to load the largest amount of drug and provide the longest duration of action. These implantable cylinders are capable of delivering over 1 mg of drug and can achieve the target release rate of 2.5 micrograms a day for over 4.5 months. However, a cylinder of that size has to be implanted and involves a surgical procedure that is time consuming, costly, and has a higher risk of complications when compared to the current procedure. Moving to smaller cylinders makes the insertion process faster, safer, and less painful, yet it comes at the expense of smaller drug loading and shorter duration of action. The smaller cylinders that can be inserted using a 22-gauge microinjector can be loaded with a

maximum of 208 micrograms and are capable of releasing at the target rate for almost a full month. Making an even smaller cylinder that can be injected directly into the vitreous humor using a 27-gauge needle severely limits the amount of drug that can be loaded into the device. These cylinders are capable of loading only 45 micrograms of drug, and can achieve the target release rate for only one week.

This chapter also shows the importance of the diffusion coefficient in controlling the release rate and achieving extended release. The small dimensions required for an intravitreal implant leads to a narrow range of diffusion coefficients that are capable of producing an effective delivery device. Creating a hydrogel that can be finely tuned to provide a narrow range of diffusion coefficients is one of the focuses of the next chapter.

REFERENCES

1. Berger M, Shankar V, Vafai A 2002. Therapeutic applications of monoclonal antibodies. Am J Med Sci 324(1):14-30.

2. Schweizer D, Serno T, Goepferich A 2014. Controlled release of therapeutic antibody formats. Eur J Pharm Biopharm 88(2):291-309.

3. Tachikawa M, Ganapathy V, Hosoya K-i. 2011. Systemic route for retinal drug delivery: role of the blood-retinal barrier. Drug Product Development for the Back of the Eye, ed.: Springer. p 85-109.

4. Kauper K, McGovern C, Sherman S, Heatherton P, Rapoza R, Stabila P, Dean B, Lee A, Borges S, Bouchard B, Tao W 2012. Two-Year Intraocular Delivery of Ciliary Neurotrophic Factor by Encapsulated Cell Technology Implants in Patients with Chronic Retinal Degenerative Diseases. Invest Ophthalmol Vis Sci 53(12):7484-7491.

5. Sieving PA, Caruso RC, Tao W, Coleman HR, Thompson DJ, Fullmer KR, Bush RA 2006. Ciliary neurotrophic factor (CNTF) for human retinal degeneration: phase I trial of CNTF delivered by encapsulated cell intraocular implants. Proceedings of the National Academy of Sciences of the United States of America 103(10):3896-3901.

6. Avery RL, Bakri SJ, Blumenkranz MS, Brucker AJ, Cunningham Jr ET, D'Amico DJ, Dugel PU, Flynn Jr HW, Freund KB, Haller JA 2014. Intravitreal injection technique and monitoring: updated guidelines of an expert panel. Retina 34:S1-S18.

7. Rodrigues EB, Grumann A, Penha FM, Shiroma H, Rossi E, Meyer CH, Stefano V, Maia M, Magalhaes O, Farah ME 2011. Effect of Needle Type and Injection Technique on Pain Level and Vitreal Reflux in Intravitreal Injection. J Ocular Pharmacol Ther 27(2):197-203.

8. Carslaw HS, Jaeger JC. 1959. Conduction of heat in solids. ed.: Clarendon Press Oxford.

9. Crank J. 1975. The mathematics of diffusion. ed.: Clarendon press Oxford.

10. Huang I, Yen S 2002. Diffusion in hollow cylinders for some boundary conditions: I. Mathematical treatment. Materials chemistry and physics 74(3):289-299.

11. Ooi E, Ang W-T, Ng E 2007. Bioheat transfer in the human eye: a boundary element approach. Engineering Analysis with Boundary Elements 31(6):494-500.

12. Kotha S, Murtomäki L 2014. Virtual pharmacokinetic model of human eye. Mathematical biosciences 253:11-18.

13. Kushner J, Deen W, Blankschtein D, Langer R 2007. First-principles, structure-based transdermal transport model to evaluate lipid partition and diffusion coefficients of hydrophobic permeants solely from stratum corneum permeation experiments. Journal of pharmaceutical sciences 96(12):3236-3251.

14. Stevenson CL, Santini JT, Langer R 2012. Reservoir-based drug delivery systems utilizing microtechnology. Adv Drug Deliv Rev 64(14):1590-1602.

15. Bagby S, Tong KI, Ikura M 2000. Optimization of protein solubility and stability for protein nuclear magnetic resonance. Methods in enzymology 339:20-41.

16. Arakawa T, Timasheff SN 1985. [3] Theory of protein solubility. Methods in enzymology 114:49-77.

17. Rosenfeld PJ, Brown DM, Heier JS, Boyer DS, Kaiser PK, Chung CY, Kim RY 2006. Ranibizumab for neovascular age-related macular degeneration. New England Journal of Medicine 355(14):1419-1431.

18. Heier JS, Brown DM, Chong V, Korobelnik J-F, Kaiser PK, Nguyen QD, Kirchhof B, Ho A, Ogura Y, Yancopoulos GD 2012. Intravitreal aflibercept (VEGF trap-eye) in wet age-related macular degeneration. Ophthalmology 119(12):2537-2548.

19. Aiello LP, Wong J-S 2000. Role of vascular endothelial growth factor in diabetic vascular complications. Kidney International 58:S113-S119.

20. Ferrara N, Gerber H-P, LeCouter J 2003. The biology of VEGF and its receptors. Nature medicine 9(6):669-676.

21. Oh IK, Kim S-W, Oh J, Lee TS, Huh K 2010. Inflammatory and angiogenic factors in the aqueous humor and the relationship to diabetic retinopathy. Current eye research 35(12):1116-1127.

22. Lowe J, Araujo J, Palma M, Wang Y, Gaudreault J, Yang J, Yu N, Fei D 2003. RhuFab V2 inhibits VEGF-isoforms-stimulated HUVEC proliferation. Investigative Ophtalmology and Visual Science 44(5):1828.

23. Burgos R, Simo R, Audi L, Mateo C, Mesa J, Garcia-Ramirez M, Carrascosa A 1997. Vitreous levels of vascular endothelial growth factor are not influenced by its serum concentrations in diabetic retinopathy. Diabetologia 40(9):1107-1109.

24. Rezende FA, Lapalme E, Qian CX, Smith LE, SanGiovanni JP, Sapieha P 2014. Omega-3 Supplementation Combined With Anti–Vascular Endothelial Growth Factor Lowers Vitreal

Levels of Vascular Endothelial Growth Factor in Wet Age-Related Macular Degeneration. American journal of ophthalmology 158(5):1071-1078. e1071.

25. Aiello LP, Avery RL, Arrigg PG, Keyt BA, Jampel HD, Shah ST, Pasquale LR, Thieme H, Iwamoto MA, Park JE, Nguyen HV, Aiello LM, Ferrara N, King GL 1994. VASCULAR ENDOTHELIAL GROWTH-FACTOR IN OCULAR FLUID OF PATIENTS WITH DIABETIC-RETINOPATHY AND OTHER RETINAL DISORDERS. New England Journal of Medicine 331(22):1480-1487.

Chapter 7: Controlling The Network Structure Of Hyaluronic Acid Hyrogels Through The Use Of Thiol-Ene Chemistry

7.1 Abstract

The excellent physical and biological properties of hyaluronic acid (HA) hydrogels have led to an increase in biomedical applications, including the encapsulation of cells and proteins for drug delivery and tissue engineering.[1,2] While there are a number of reactions that can be used to crosslink HA, a number of these reactions have disadvantages, such as complex functionalization, inadequate efficiency, and harsh reaction environments that limits the ability to encapsulate cells or proteins. The thiol-ene reaction provides an alternative way to crosslink HA, and in this work the many advantages that this reaction provides are investigated. Hyaluronic acid was modified with pentenoic anhydride and crosslinked into hydrogels using the crosslinker DTT. Hydrogels made from pentenoate modified HA (PHA) ranged in weight percent from 2-15%, and in most cases were fully reacted gels in less than 120 seconds, among the fastest that have been seen for a thiol-ene hydrogel in literature while using very low initiator concentrations (0.1 mM - I2959) and light intensities (3 mW/cm^2). The swelling degrees of the PHA hydrogels were easily tuned by controlling the degree of substitution as well as the ratio of thiol groups to ene groups and the resulting hydrogels showed an 85% increase in fracture strain when compared to comparable gels crosslinked using free radical polymerizations, an indication of a more uniform network. Additionally, the model proteins ovalbumin and bovine serum albumin (BSA) were encapsulated into the hydrogel and recovered, with the results indicating that the percent recovery is related to the amount and location of free cysteine residues on the protein. Recovery of up to 78% was seen with ovalbumin.

7.2 INTRODUCTION

In the last decade, hyaluronic acid (HA) hydrogels have become increasingly popular in biomedical applications due to their excellent physical and biological properties.[1,2] HA is a naturally occurring polysaccharide that plays a key role in the extracellular matrix of tissues, where it provides mechanical structure and acts as a scaffold.[3] In tissue engineering applications HA hydrogels can be used to encapsulate cells in an effort to mimic this natural scaffold, taking advantage of the inherent biological functions of HA.[2,4] Drug delivery applications take advantage of the nonimmunogenic properties of HA along with the high water content of hydrogels to safely encapsulate and deliver biopharmaceuticals including proteins and peptides.[5,6] In both applications, controlling the reaction conditions and the diffusion of solutes through the HA hydrogel is necessary for clinical success. In this chapter an alternative crosslinking reaction, the thiol-ene reaction, is investigated for the synthesis of HA hydrogels. This crosslinking reaction is hypothesized to allow for greater control of the hydrogel network structure, an important feature that would be useful for hydrogels in drug delivery and tissue engineering applications for controlling diffusion, while at the same time providing a way to quickly and efficiently tune the mechanical properties of the hydrogel.

While there are a number of reaction methods available to crosslink HA into hydrogels, a number of these reactions have disadvantages, such as complex functionalization, inadequate efficiency, and harsh reaction environments that limits the ability to encapsulate cells or proteins. HA hydrogels can be crosslinked by two different routes: using unmodified or modified HA. The first route is to crosslink unmodified HA directly using difunctional crosslinkers such as divinyl sulfone (Figure 7.1b) or bis-epoxides.[1] Crosslinking HA directly requires no prior modification

of HA, and many of the reactions are straightforward and easy to use. However, most of the reactions are non-specific and will readily react with other labile groups (-COOH, -OH, N-$COCH_3$) that are available on the backbone of HA.[1] As seen in Chapter 5, these reactions often lead to undesired reactions with proteins or cells that are being encapsulated, and in many cases occur under degradative conditions. The second route is to modify HA with any number of chemical groups including bromoacetate[7], hydrazides[8], tyramines[9], thiols[10], and methacrylates.[11] These HA derivatives can then be formed into hydrogels by addition reactions, condensation reactions, and radical polymerizations. One of the more commonly used methods for creating HA hydrogels via chemical modification is the free radical polymerization (Figure 7.1a) of methacrylated HA (MHA).[1,12] This reaction can be controlled temporally and spatially using photoinitiation, and has been used to safely encapsulate cells and proteins.[13,14] However, the crosslinking in these hydrogels occurs via the formation of polymethacrylate chains.[15] These dense, hydrophobic chains are known to produce network heterogeneities in hydrogels.[16]

One promising reaction that avoids these obstacles is the radically-initiated thiol-ene reaction.[17-19] The thiol-ene reaction involves the addition of a thiyl radical (RS•) to a carbon-carbon bond that can be either electron rich or poor[18]. The mechanism of the reaction was first proposed in 1938[76] and can be seen below in Figure 7.2.[20,21] The reaction starts with the initiation step in which a thiol is first activated, either with heat or light, to give a thiyl radical. This thiyl radical then propagates across a carbon-carbon double bond ("ene"), resulting in an intermediate carbon-centered radical. This radical is then able to pull a hydrogen electron off of a second thiol, which gives the final thiol-ene product and in turn generates a new thiyl radical (known as chain transfer) that is able to react with another ene group.

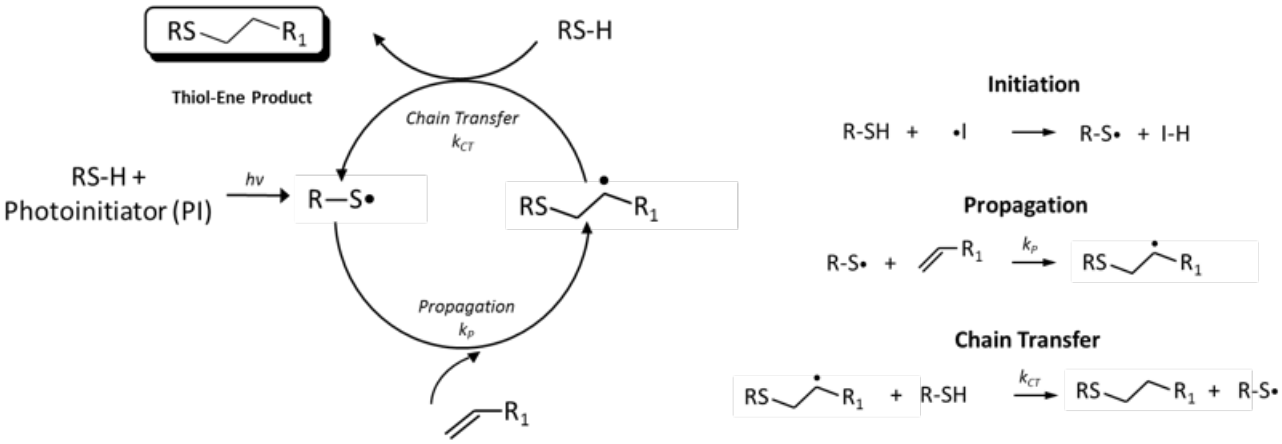

Figure 7.1 The mechanism of the basic thiol-ene reaction including: initiation, propagation, and chain transfer. Adapted from Lowe[21] and Hoyle, Bowman [17]

The thiol-ene reaction is often grouped with a number of reactions termed "click chemistry" that were introduced in 2001 by K.B. Sharpless.[22] Click chemistry is not a single specific reaction, but rather a concept that encompasses a number of possible reactions and mechanisms that allow for the synthesis of new and useful compounds using simple reaction conditions. These reactions proceed to very high yields, are able to be carried out in water and in the presence of oxygen, and give products that are easy to collect and purify. In order to achieve these qualities in a reaction, a high thermodynamic driving force is be needed, and it is this thermodynamic driving force that causes the reaction to be "spring-loaded" and leads to reactions that proceed rapidly and with high selectivity. The thiol-ene reaction has many of these attractive click attributes: it is extremely fast, proceeds to high yields, can be performed in water over a wide range of concentrations, and is insensitive to oxygen.[17] The reaction can take place with virtually any carbon-carbon double bond, including terminal, internal, conjugated,

substituted, and even cyclic alkenes.[23] At the same time, there is a wide range of thiols that can be used, as any thiol is able to react.

The use of the thiol-ene reaction to synthesize HA hydrogels is a more recent development in literature. In 2012 Auzély-Velty and her group attached a pentenoate group onto the backbone of both HA and dextran by esterification of the hydroxyl groups.[24] The motivation behind the work was mostly to functionalize the polysaccharides with hydrophobic groups, peptides, and oligosaccharides, yet they were also able to form hydrogels using the pentenoate modified dextran and a PEG-dithiol. A year later, Burdick and his group also used the thiol-ene reaction to synthesize HA hydrogels, except HA was this time modified with norbornene groups.[25] They crosslinked the modified HA using dithiothreitiol (DTT), a commonly used dithiol molecule, and looked at how the compressive moduli varied with the irradiation time, the ratio of thiols to norbornene, and the weight percent of HA in solution. They were focused on photopatterning the hydrogels to either modify the crosslink density or to couple chemical ligands. They did this by choosing conditions in which after gelation there still existed pendent norbornenes that could undergo further reactions with a variety of thiol containing molecules. In both papers it was evident that the chemistry of the thiol-ene crosslinking reaction provides many advantages including high selectivity and reactivity, mild reaction conditions, and fast reaction times, yet neither paper studied in detail the effects on the mechanical properties.

Another possible advantage that has yet to be investigated in the literature for HA hydrogels is the hypothesis that the thiol-ene reaction is able to form more homogeneous networks than other reactions, allowing for polymers and gels with very uniform network crosslink densities.[17,18] When compared to chain growth reactions, the advantage comes from the fact that thiyl radicals are highly reactive toward ene groups, and, unlike methacrylated HA, the ene groups attached to the HA do not react with one another during the reaction. This results in the addition of a single thiol across a single ene group, and avoids the formation of kinetic chains that increase the heterogeneity of the hydrogel. When compared with Michael addition type reactions (HA-DVS) in which crosslinking can occur at any hydroxyl group along the backbone, the thiol-ene reaction is highly selective and crosslinking can only take place at points along the backbone where an ene group exists. This allows for more control over the location and number of crosslinks and can result in a more uniform hydrogel network. A hydrogel with a more uniform network has many advantages. It has been shown in literature that PEG hydrogels synthesized using the thiol-ene reaction had significantly improved tensile stress and tensile strain when compared to similar hydrogels synthesized by radical chain growth polymerizations at similar crosslink densities.[26] Additionally, it is hypothesized that hydrogels with a more uniform network are able to form hydrogels at lower polymer concentrations.[27]

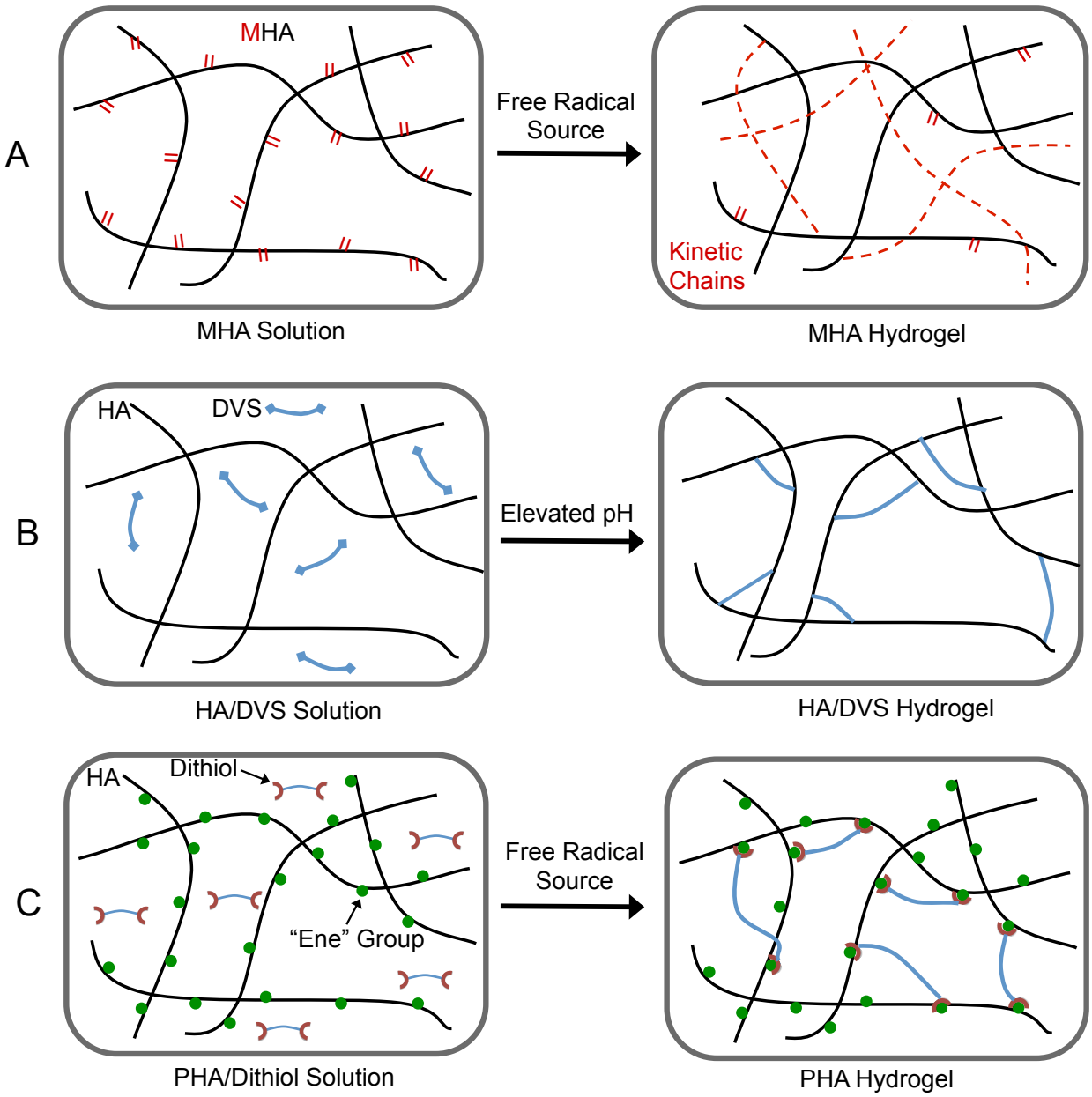

Figure 7.2 Three methods of crosslinking HA that are compared throughout this chapter. (A) The free radical polymerization of methacrylated HA can be controlled spatially and temporally using photoinitiation, however the resulting hydrogel contains kinetic chains that are known to produce network heterogeneities. (B) The crosslinking of HA using the bifunctional crosslinker DVS requires no prior modification of HA and can react with any hydroxyl group on the HA backbone. However, the non-specific nature of the reaction makes it difficult to control the network structure of the hydrogel. Additionally, the reaction only occurs under elevated pH levels, making it difficult to safely encapsulate proteins or cells. (C) The thiol-ene reaction can be controlled spatially and temporally using photoinitiation, occurs under physiological conditions, and is highly selective, occurring only at locations along the HA backbone that contain an "Ene" group. This allows for greater control of the hydrogel network structure. Adapted from Aimetti et al.[28]

The major motivation for this study was the hypothesis that a hydrogel with a more uniform network would have significant effects not only on the mechanical properties but also on the transport of solutes within the hydrogel. While the diffusion models in Chapter 3 focus mainly on the swelling degree of the hydrogel and solute size to predict the diffusion coefficient, the diffusion also depends on the network structure of the hydrogel. This is especially true as the size of the solute approaches the average mesh size of the hydrogel, where the screening effect is hypothesized to occur. It is our theory that a more uniform network will produce a screening effect and lead to a reduction in the diffusion coefficient at higher swelling degrees when compared to hydrogels with more heterogeneous networks. Being able to better control the diffusion of solutes in hydrogels is directly relevant to a number of research fields, including drug delivery and tissue engineering. In drug delivery, understanding the diffusive properties of solutes within a hydrogel is crucial for designing controlled release devices that are able to provide the correct release rate and profile to be therapeutically effective.[29,30] In tissue engineering, the transport of nutrients, proteins, dissolved gases, waste products, and even cells are vital for the successful formation of tissue.[31] In both of these cases, the hope is that the thiol-ene reaction can lead to a more uniform hydrogel in which the diffusion can be better tuned and controlled to produce the required transport properties required.

Another motivation for this study was to compare both the speed and selectivity of HA modified with pentenoate to that of HA modified with norbornene. One of the major benefits of the thiol-ene chemistry is the fact that the reaction is highly selective, which is only true when the reaction proceeds via a pure thiol-ene reaction and there is no homopolymerization that occurs. As seen in Figure 7.3, homopolymerization occurs when the carbon centered radical reacts with another ene group instead of abstracting a hydrogen from another thiol. Homopoylmerization is simply a chain polymerization, reacting the same way in which MHA reacts to form hydrogels.

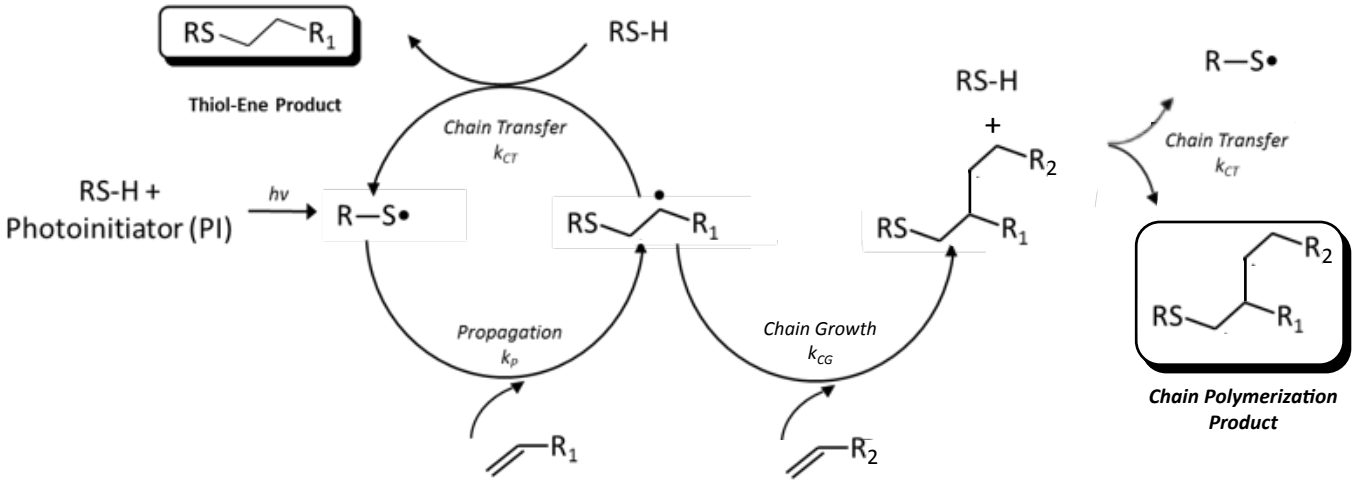

Figure 7.3. The ideal thiol-ene reaction occurs purely via a step crosslinking reaction, and does not include any chain polymerization that occurs between the carbon centered radical and another ene group. "Mixed mode" happens when both occur, affecting the stoichiometry of the reaction and resulting in an increase in heterogeneity. Adapted from Shu et al.[10] and Northrop, Coffey[32]

When homopolymerization of enes does occur, it is considered a mixed-mode reaction as both the thiol-ene crosslinking reaction and radical chain polymerization are occurring simultaneously. The formation of dense, hydrophobic polyvinyl chains that form during homopolymerization increases the heterogeneity of the hydrogel network. Homopolymerization not only affects the network structure of the gels, it also disrupts the stoichiometry of the reaction and can leave a number of thiol groups unreacted. Whether or not the reaction undergoes homopolymerization is largely affected by the relative rates of reaction, which is dependent on the properties of the ene group. One of the reasons that norbornene is often used in thiol-ene reactions is that, due to its bridged cyclic structure, it is unable to undergo chain polymerization and proceeds purely via the thiol-ene reaction. The alleviation of the ring strain of norbornene during the propagation step also provides a high driving force and leads to very fast reaction times. However, it has also been shown that the speed of the thiol-ene reaction increases with increasing electron density of the carbon-carbon double bond[18]. This means that a terminal alkene, such as the HA modified with a pentenoate group used in this chapter, will react faster when compared with the more electron-deficient acrylates and methacrylates, and will lead to less chain polymerization. If reactions involving pentenoate modified HA are shown to compare favorably to norbornene modified HA both in speed and selectivity it would have important implications for future work in this field. The reaction to modify HA with a pentenoate group is simpler and faster when compared to norbornene modified HA, and has been shown so to provide a higher degree of functionalization.

The thiol-ene reaction also has a number of other advantages that would make it useful as a crosslinking method to create HA hydrogels for biomedical applications. In the thiol-ene reaction (Figure 7.1c), a single radical species can cause hundreds and even thousands of reaction events to occur, which allows the overall reaction to occur with much lower initiator when compared with radical chain polymerization, in which radicals are consumed. This low initiator concentration coupled with fast reaction times makes it ideal for *in situ* gelation and protein encapsulation.[28,33] The encapsulation of proteins within hydrogels is an important area of interest in drug delivery, and was one of the motivations for studying the thiol-ene reaction. A number of hydrogel crosslinking methods cannot be performed in the presence of proteins. For example, in Chapters 4 and 5 divinyl sulfone was used to crosslink HA and dextran hydrogels via a Michael addition reaction. While this crosslinking reaction was effective in achieving very low swelling degrees, it only occurs under denaturing conditions and also reacted with proteins diffusing into the hydrogel, covalently attaching them to the hydrogel network. Encapsulating a protein into a hydrogel network using photoinitiation is especially challenging, as exposure to UV light for long periods of time can cause a number of damaging changes to a protein which can lead to loss of activity. Furthermore, the activation of photoinitiators generates free radicals that can cause damage to the protein.[34] Using a thiol-ene reaction to photoencapsulate proteins has two advantages. First, the speed of the reaction minimizes the amount of exposure that the protein has to the UV light. Second, because the thiyl radical is regenerated in the thiol-ene reaction, it requires only small amounts of radical species to complete the reaction, reducing the amount of free radicals that can damage the proteins. Recent research has shown that lysozyme maintains 100% bioactivity after being photoencapsulated in PEG gels using the thiol-ene reaction.[33] Using lithium acylphosphinate (LAP) as an initiator, they showed that this holds true

under a range of initiator concentrations and intensities, and that bioactivity was connected to the total amount of radicals generated during polymerization.

The work in this chapter hopes to advance the literature and build upon the previous work of Burdick and Auzély-Velty by crosslinking pentenoate modified HA using the thiol-ene reaction in an effort to determine the key parameters and synthesis conditions that control the network structure of the resulting hydrogels. The mechanical properties and swelling degrees of these hydrogels will be analyzed in an effort to find evidence of a more uniform hydrogel network when compared to alternative crosslinking methods. A more uniform network structure would allow for better control of the diffusion of solutes within the hydrogel and could lead to a reduction in the diffusion coefficient at higher swelling degrees, both of which would be useful in drug delivery and tissue engineering applications for controlling diffusion. The chapter also extends the knowledge in literature by investigating the encapsulation of proteins within HA hydrogels crosslinked using the thiol-ene reaction, an important area not only for biomedical applications, but also for studying the diffusion within these hydrogels.

7.3 Materials And Methods

7.3.1 General Materials

Hyaluronic acid (51 kDa Mw, pharmaceutical grade from bacterial fermentation) was obtained from Lifecore Biomedicals (Chaska, MN). *N,N*-Dimethylformamide (DMF), 4-pentenoic anhydride (98%), and DL-dithiothreitol (DTT) were obtained from Sigma-Aldrich (St. Louis, MO) along with the proteins bovine serum albumin (BSA, lyophilized powder, ≥ 98%), and ovalbumin (lyophilized powder, ≥ 98%). Pierce™ Coomasie Plus Bradford Reagent was obtained from Thermo Fisher Scientific (Waltham, MA).

7.3.2 Synthesis of Pentenoate Modified Hyaluronic Acid (PHA)

The method described here to synthesize PHA is a modified version of a method used previously in literature.[24] The goal in modifying the previously reported method was to scale up the process while at the same time increasing the yield. First, 0.50 grams of HA (40 kDa) was dissolved in 25 mL of water and kept at 4 °C overnight while being continuously stirred to ensure complete dissolution. 16.66 mL of *N,N*-Dimethylformamide (DMF) was then added dropwise in order to achieve a 3:2 ratio of water:DMF. Pentenoic anhydride was then added to the solution in 1, 1.5, 2, or 5 molar equivalents with respect to the repeating unit of HA. The solution was maintained at a pH between 8 and 9 by adding 0.5M NaOH at regular intervals. The esterification reaction lasted between 2 and 4 hours, depending on the size of the batch, and after the pH had stabilized the reaction was kept at 4 °C overnight to ensure complete reaction. At this point NaCl was added to the reaction mixture to achieve a final salt concentration of 0.5 M and the solution was precipitated into 5 fold excess ethanol. After removal of the supernatant, the precipitate was dissolved in ultrapure water for final purification by diafiltration using

cellulose membrane 10k molecular weight cut-off dialysis tubing. The diafiltration step was performed for 48 hours with the water being changed every 8-12 hours. The remaining solution was then frozen, lyophilized, and stored frozen until used.

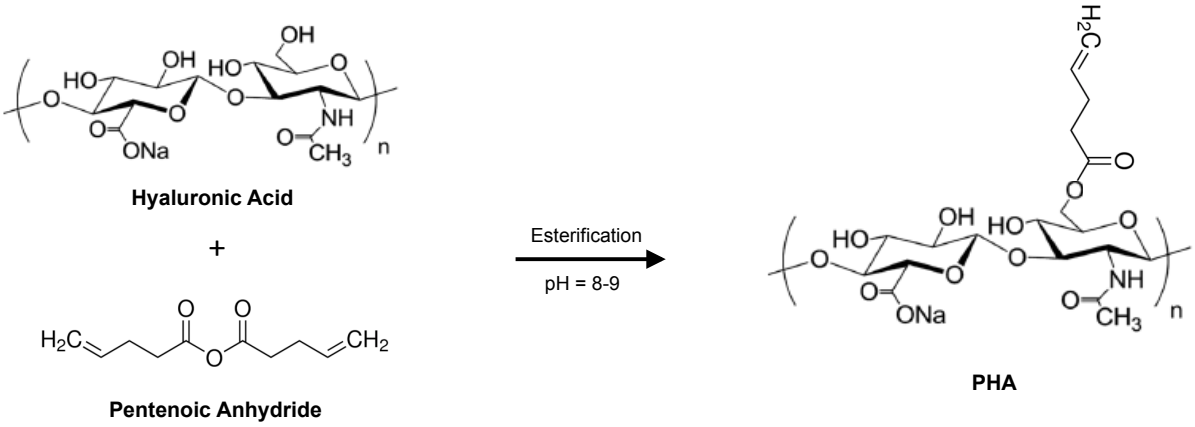

Figure 7.4 Pentenoate groups were added to hyaluronic acid (51 kDa) via an esterification reaction used previously in literature.[24] The degree of substitution (DS), defined as the amount of pentenoate groups per repeating units of HA, was determined by ^{1}H NMR spectroscopy and ranged from 10-55%.

7.3.3 NMR Spectroscopy

In order to determine the degree of substitution (DS), defined as the amount of pentenoate groups per repeating units of HA, the final product was analyzed by ^{1}H NMR spectroscopy. 7 mg of PHA was first dried for 48 hours in the dessicator and then dissolved in 600 µL of deuterium oxide and was analyzed at 25 °C using an Avance AVIII spectrometer operating at 500 MHz. The DS was calculated by comparing the digital integration of the NMR signals that arose from the methylene and double bond protons of the pentenoate group with the signals from the methyl protons of HA.

7.3.4 Synthesis of PHA Hydrogels

PHA hydrogels were synthesized by dissolving PHA and varying amounts of DTT in water containing 0.1 mM 2-hydroxy-1-[4-(2-hydroxyethoxy) phenyl]-2-methyl-1-propanone (Irgacure 2959 – (I2959)). Throughout this work, the weight percent PHA (W_{PHA}%) and the molar ratio of thiol groups to ene groups (X_{DTT}) were systematically varied. The solution was vigorously stirred using a microspatula and then centrifuged to remove any air bubbles before being cast into silicone rubber molds. The molds were 2 mm thick and had precut holes 5 mm in diameter. These molds were clamped between two thin glass plates (1 mm thick) and the hydrogels were irradiated in a Spectrolinker XL-1000 (Spectronics, Westbury, New York) at 312 nm at 3 mW/cm^2 for the desired amount of time. Once formed, the gels were placed into an excess of D.I. water to leach out any unreacted materials.

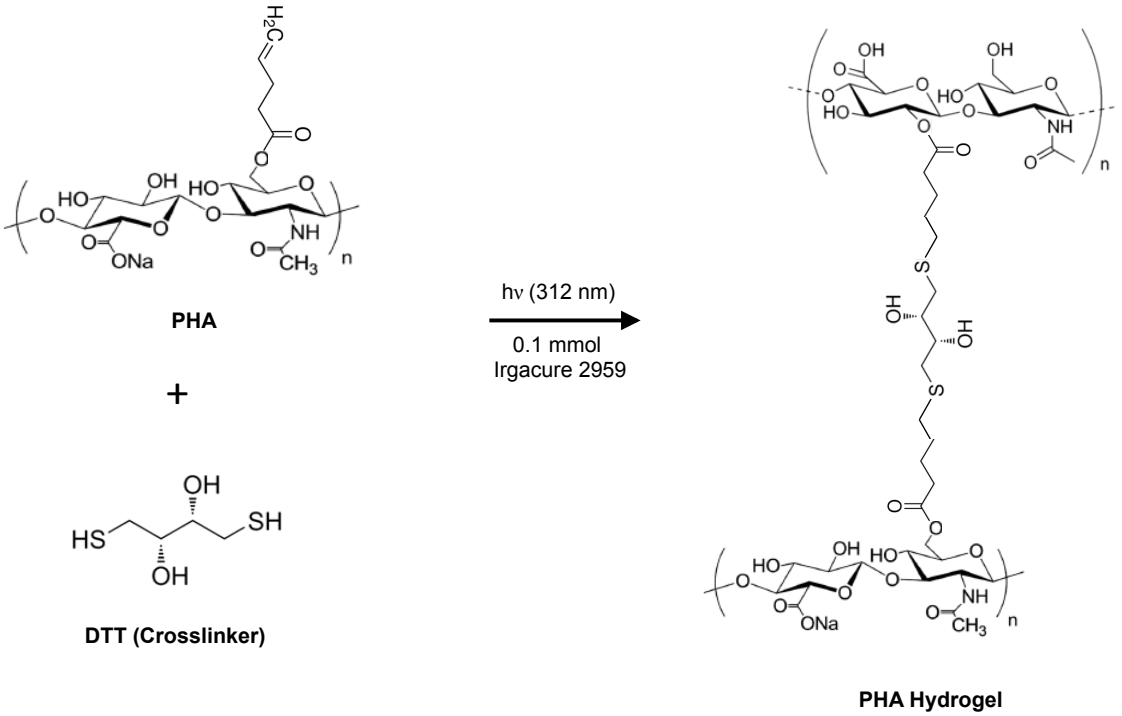

Figure 7.5 The crosslinking of pentenoate modified hyaluronic acid occurs via the thiol-ene reaction using the difunctional thiol DTT as the crosslinker.

7.3.5 Encapsulation and Recovery of Proteins from PHA Hydrogels

The proteins BSA and ovalbumin were encapsulated into the PHA hydrogels using the same synthesis method described earlier (7.3.4), except that protein was also dissolved in the 0.01 M PBS (pH= 7.4) solution at concentrations of 1, 5, and 10 mg/mL. The concentration of I2959 was lowered from 0.1mM to 0.025 mM to prevent the hydrogels from forming before being irradiated with UV light, which was occurring at the 0.1 mM concentration for gels containing 10 mg/mL protein (discussed in Section 7.4.5). The protein was leached from the gels by soaking them in 1 mL of protein free buffer in a shaking incubator at 4° C. At predetermined time points, the gels were placed in 1mL of fresh buffer and the protein content of the leached solution was then determined using a Bradford assay. The predetermined time points were chosen in an effort to maintain sink conditions while still obtaining high enough concentrations to assay accurately. To solve for the diffusion coefficient the analytical solution of diffusion from a disc (Figure 7.6) was used: [35]

$$\frac{M_t}{M_\infty}=1-\frac{8}{h^2r^2}\sum_{m=1}^{\infty}\alpha_m^{-2}\exp(-D\alpha_m^2 t)\times\sum_{n=1}^{\infty}\beta_n^{-2}\exp(-D\beta_n^2 t) \quad (7.1)$$

with

$$J_0(r\alpha_m)=0 \quad (7.2)$$

and

$$\beta_n=\frac{(2n+1)\pi}{2h} \quad (7.3)$$

where M_t is the mass of the solute that has been released from the cylinder at time t, M_∞ is the total mass that has been released from the cylinder at time $t = t_\infty$, r is the radius of the disc, and h is half the thickness of the disc. D is the diffusion coefficient, t is time, and α and β are defined in the above equations, with J_0 being a Bessel function of the first kind of order zero. This equation takes into consideration both radial and axial diffusion, and is valid for discs of all h/r ratios.

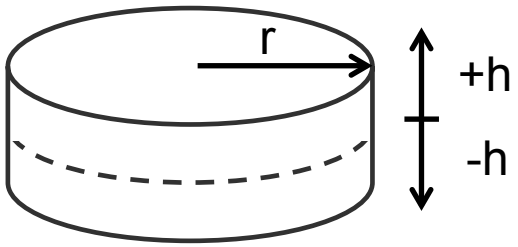

Figure 7.6 The diffusion of a solute from a disc of radius (r) and half thickness (h) can be solved using Equation 7.1 which takes into consideration both the radial and axial diffusion. The equation is valid for discs of all h/r ratios.

7.3.6 Swelling and Mechanical Testing

Fully formed gels were soaked in solutions of D.I. water or 0.01 M phosphate buffer saline (PBS, pH =7.4) until they were swollen to equilibrium and leached of any unreacted polymer or initiator. The wet mass (m_s) was then measured and the gels were placed in a dessicator for 48 hours at room temperature and allowed to dry. The gels that were soaked in PBS were first soaked in excess D.I. water to remove any salt before being placed in the dessicator. The dry mass (m_d) was measured and the swelling degree (q) was defined as:

$$q = \frac{m_s}{m_d} \tag{7.4}$$

The compressive modulus (E) and shear modulus (G) were calculated from stress vs. strain data collected using a RSA-III dynamic mechanical analyzer (TA Instruments, New Castle, DE). Cylindrical gels were tested under uniaxial compression at a rate of 0.05 mm/s and the modulus was calculated from the initial slope of the stress-strain curve as shown below:

$$\sigma = E\varepsilon \tag{7.5}$$

where $\varepsilon = \frac{L_0 - L}{L_0}$ and L and L_0 are the thickness of the deformed and undeformed specimen, respectively. The compressive modulus was calculated by using the data up to strains of 10%.

The shear modulus (G) was calculated using the neo-Hookean model as the slope of the stress (σ) versus the strain function $\left(\lambda - \frac{1}{\lambda^2}\right)$ as shown below:

$$\sigma = G\left(\lambda - \frac{1}{\lambda^2}\right) \tag{7.6}$$

where $\lambda = L/L_0$ and L and L_0 are the thickness of the deformed and undeformed specimen, respectively. The shear modulus was calculated by using the data up to strain function values of 3. The calculation of the shear modulus is based on the assumption that most hydrogels follow Gaussian statistics and behave as ideal elastomers. However certain polyelectrolyte gels, such as HA and methacrylated chondroitin sulfate, do not always exhibit a Gaussian distribution[36], which can lead to errors in the meaningful structural parameters of the hydrogel.[37] Although the data from compression testing fits Equation 7.6 quite well, the Mooney-Rivlin plot confirmed that the hydrogel deviates from neo-Hookean behavior (more detailed analysis can be seen in Appendix A7.4). Because of this, calculations for the parameters that are derived from Equation 7.6, such as the crosslink density and mesh size, are used only for internal comparisons.

The crosslink density (ρ_x) of the hydrogels were calculated using the affine model of rubber elasticity as shown below:

$$\rho_x = \frac{G}{RT\, \upsilon_2^{1/3}\, \upsilon_{2r}^{2/3}} \tag{7.7}$$

where R is the ideal gas constant, T is the absolute temperature, v_2 is the volume fraction of the polymer, and v_{2r} is the polymer volume fraction during hydrogel formation. ρ_x was used to calculate the molecular weight between crosslinks, $\bar{M}_c$, using the equation:

$$\bar{M}_c = \frac{\rho_2}{\rho_x} \tag{7.8}$$

in which ρ_2 is the density of the dry polymer network. The molecular weight between crosslinks was then used in calculating the average mesh size of the gels using the following equation[38]:

$$\xi = \upsilon_2^{1/3} \left[C_n \left(\frac{2\bar{M}_c}{M_r}\right)\right]^{\frac{1}{2}} l \tag{7.9}$$

where C_n is the Flory characteristic ratio for HA, M_r is the molecular weight of the repeating units, and l is the length of bond along the polymer backbone.

7.4 Results And Discussion

In this section, HA macromers modified with pentenoic anhydride were crosslinked into hydrogels using the crosslinker DTT over a wide range of conditions. The reaction conditions were tuned by systematically varying the irradiation time, the weight percent of HA, the degree of substitution, and the ratios of thiol groups to ene groups in an effort to determine how each of these factors affected the swelling degree and mechanical properties of the hydrogel. Additionally, the reaction was carried out in the presence of the model proteins ovalbumin and bovine serum albumin (BSA), encapsulating them into the hydrogels. The amount of protein recovered was measured in order to determine if any side reactions occur during photopolymerization and to determine the diffusion coefficient.

7.4.1 Homopolymerization

The goal of this section was to confirm that the formation of pentenoate modified HA hydrogels occur from a thiol-ene crosslinking reaction and not the chain polymerization that occurs during homopolymerization. To confirm that PHA does not undergo any significant homopolymerization, hydrogels were synthesized using the same procedure described earlier except without the crosslinker DTT. By removing the crosslinker, the only way that the hydrogels can form is from the chain growth reaction between ene groups. The results in Table 7.1 show the difference in swelling degrees between 6% PHA hydrogels that have been synthesized with and without the crosslinker DTT.

Table 7.1. Comparison of the swelling degrees of 6% PHA hydrogels synthesized with and without the crosslinker DTT. The timescale at which the thiol-ene reaction occurs is so much faster than that of the chain growth reaction between ene groups little to no homopolymerization is expected to occur. All hydrogels had a DS=55%, a X_{DTT} =1, and were irradiated at 312 nm (I = 3 mW/cm^2). Mean value ± standard deviation, n ≥ 3.

Time (minutes)	Crosslinked with DTT	No Crosslinker
	q (g/g)	
0.7	38.5 ± 0.9	No Gel
1.3	31 ± 1.2	No Gel
2	30.6 ± 0.5	No Gel
4	29.3 ± 1.2	No Gel
10	32.5 ± 2.7	No Gel
20	-	1180 ± 150
30	-	1000 ± 55
40	-	930 ± 50

When DTT is used as a crosslinker, the solution becomes a gel within 40 seconds, and achieves complete gel formation after only 80 seconds. As the crosslinking reaction comes to a completion, the swelling degree remained unchanged as no new crosslinks are being formed. In comparison, the PHA solution without DTT is unable to form a hydrogel after being irradiated for 10 minutes, and only begins to form after being exposed to UV light for 20 minutes. Even then, the hydrogels formed are very highly swollen, with swelling degrees ranging from 930 ± 50 – 1180 ± 150. The results from Table 7.1 give clear evidence that the reaction between the thiols and enes is faster than the chain reaction between ene groups. This confirms that there is little to no homopolymerization (i.e., chain growth) that occurs during the synthesis of 6% PHA hydrogels and that these hydrogels benefit from the many advantages of a pure thiol-ene reaction.

It should be noted that while the thiol-ene reaction appears to occur much faster than the chain reaction between the ene groups, the results in Table 7.1 are also a result of improved crosslinking efficiency that occurs with the thiol-ene reaction. It is possible that some degree of chain reaction is occurring between the ene groups, but these reactions may not be forming enough elastically effective crosslinks to produce a fully formed gel. For example, MHA hydrogels with similar molecular weights that are reacted via chain polymerization usually only form at concentrations above 10%.[39] This highlights one clear advantage of the thiol-ene reaction: the ability to get a well-defined hydrogel at low polymer concentrations where other crosslinking methods may not be able to form hydrogels.

7.4.2 Kinetics of Hydrogel Formation

The next step in characterizing PHA hydrogels was to determine the time it takes to complete the thiol-ene reaction under the synthesis conditions studied in this chapter. The primary objective was not to perform an in depth kinetics study but rather to determine the time required for the crosslinking reaction to go to completion. This was accomplished by measuring the swelling degrees of 4, 6, and 8% (w/w) PHA hydrogels that had a DS = 55% and an equimolar ratio of thiols to enes after being irradiated with UV light (312 nm) for various amounts of time that ranged from 10-300s. The results can be seen in Figure 7.7, which shows that as the weight percent of PHA increases, the time it takes to form a fully developed hydrogel decreases. The 8% PHA hydrogels reach a plateau in swelling degree (20.8 ± 1.2) after just 40 seconds, while the 4% PHA hydrogels take the longest time to reach a plateau in swelling degree, achieving a final swelling degree of 55 after being exposed to the UV light for 240 seconds.

Figure 7.7 also shows that the swelling degree of PHA hydrogels decreases as the concentration of PHA increases.

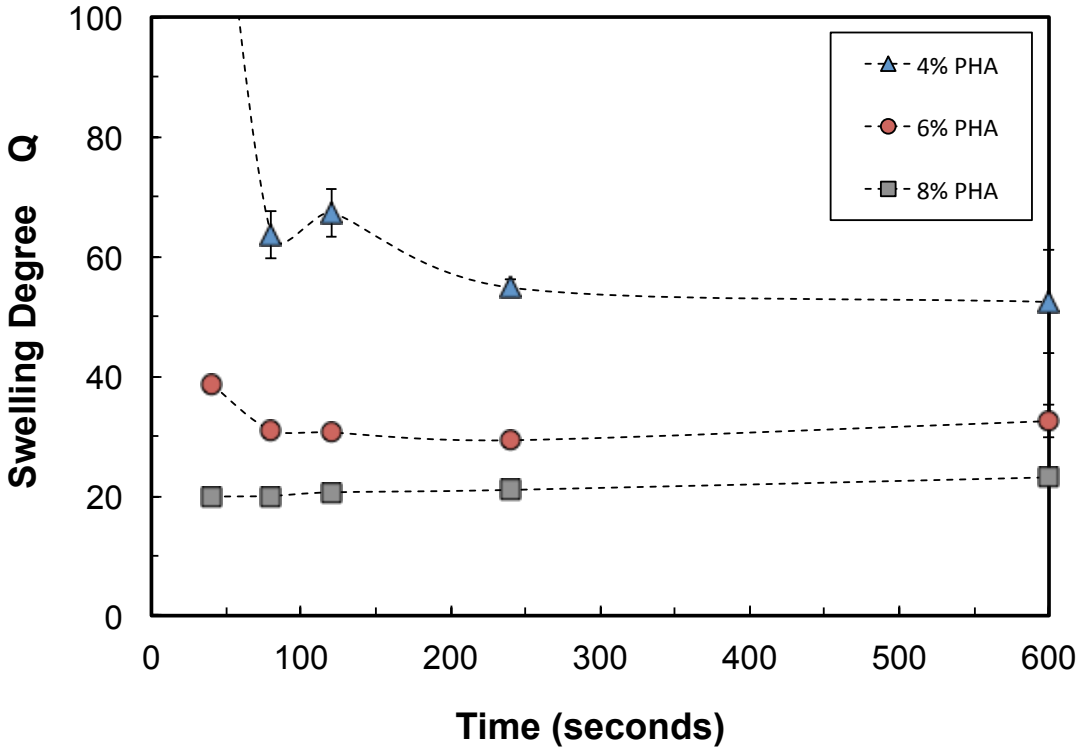

Figure 7.7. Swelling degrees of 4%, 6%, and 8% PHA hydrogels as a function of irradiation time. As weight percent increases, the time it takes to form a fully developed hydrogel decreases. All hydrogels had a DS=55% and were irradiated at 312 nm (I = 3 mW/cm^2). Mean value ± standard deviation, n ≥ 3.

While it is difficult to compare the reaction times of hydrogels in literature due to the many factors that affect gelation kinetics, the speed at which these PHA gels form is among the fastest that have been seen for a thiol-ene hydrogel. The closest comparison in literature comes from hydrogels in which HA was modified with norbornene groups with a DS = 20% and crosslinked with DTT.[1] These 4% HA hydrogels were formed using 10 mW/cm^2 UV light (λ =320-390 nm) and an I2959 initiator concentration of 2.25 mM. While the resulting gels began

to form in the first 60 seconds, they took 20 minutes to reach fully formed gels. The results in Figure 7.2 show that 4% PHA gels take 4 minutes to fully form, using 22 times less initiator and an UV intensity that is 3 times lower. This is direct evidence that HA modified with a pentenoate group can form a hydrogel as fast as HA modified with a norbornene group. Another example of thiol-ene gels in literature is a PEG 4-arm norbornene that was crosslinked with a PEG dithiol.[33] With a 10 wt % monomer solution, the gels were formed using 10 mW/cm^2 UV light (λ = 390 nm) and the initiator lithium acylphosphinate (LAP) at concentrations of 10, 1, and 0.1 mM. The hydrogels with initiator concentrations of 10 and 1 mM were fully formed in less than 10 seconds and hydrogels with an intiator concentration of 0.1 mM required 60s to reach fully formed gels. 8% PHA gels took less time to gel at identical initiator concentrations and with a UV intensity that was 3 times lower. In comparison, MHA hydrogels are often polymerized for 10-30 minutes using 3-10 mW/cm^2 UV light (λ =312-390 nm) and an I2959 initiator concentration of 2.25 mM.[11,14,39]

While the results from Figure 7.7 show the speed at which the thiol-ene reaction can take place, they also display the ability to control the swelling degree of the hydrogel by simply controlling the irradiation time. One of the advantages of having a reaction that is photoinitiated is the ability to control the reaction both spatially and temporally. By controlling the duration of time a gel is irradiated, a hydrogel with a wide range of swelling degrees and mechanical properties can be created and applied to numerous biological applications.[40]

7.4.3 Effect of PHA Concentration

Another hypothesized way of controlling the network structure of the hydrogel is by changing the PHA macromer concentration. Increasing the concentration of PHA in solution is expected to increase the crosslinking density of the hydrogels, leading to lower swelling degrees and higher moduli. To study the effect of monomer concentration on swelling degree, hydrogels with varying weight percent PHA were synthesized. The degree of substitution (55%) and the ratio of thiols:enes (1:1) were kept constant throughout the experiment along with the irradiation time (320s) and intensity. The swelling degrees of the hydrogels are presented in Figure 7.8 and declined continuously as the weight percent of PHA increased. Hydrogels with a 2% PHA concentration are not shown, and had a swelling degree of 300 ± 30. The swelling degrees of PHA hydrogels ranged from a low of 8.8 at a 15% concentration all the way up to a high of 300 at a 2% concentration.

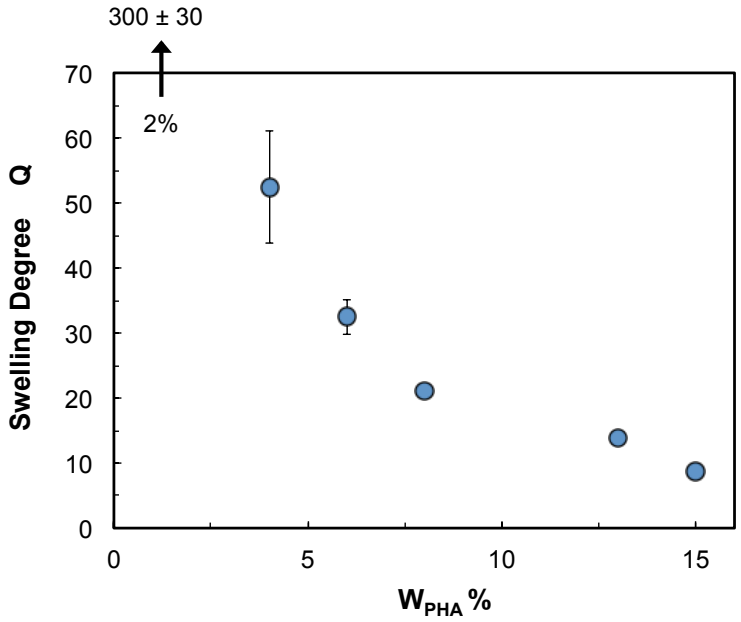

Figure 7.8. Swelling degree as a function of the weight percentage of PHA. As W_{PHA} % increases the swelling degree decreases. All hydrogels had a DS=55% and were irradiated at 312 nm (I = 3 mW/cm^2) for 320 seconds. Mean value ± standard deviation, n ≥ 3.

7.4.4 Effect of Crosslinker Ratios

In the previous sections it was confirmed that two minutes was an adequate time to fully complete the crosslinking reaction and that crosslinking was effective only via the thiol-ene reaction under the conditions used. In this section, the primary goal was to determine how the network structure of the hydrogel can be controlled by changing the ratio of thiol groups to ene groups (X_{DTT}) and the degree of substitution. To study these changes in network structure, PHA hydrogels with a wide range of both X_{DTT} and degree of substitution (15-55%) were synthesized. The weight percent of PHA (6%) was kept constant throughout the experiment along with the irradiation time (320s) and intensity.

The swelling degrees of PHA hydrogels synthesized using varying thiol to ene ratios are presented in Figure 7.9a. A more detailed view of the effect of crosslinking ratio on the swelling degree of PHA hydrogels can be seen in Figure 7.9b. The results from Figures 7.9a and 7.9b indicate that the swelling degree reaches a minimum at X_{DTT} values from 0.6-1.0. This is especially clear for the lower substituted PHA, where a clear minimum range is seen. This is consistent with compressive modulus data seen in Burdick's data on norbornene hydrogels in which the DS = 20%.[25] However, at the highest degree of substitution (55%), instead of a rather sharp change in the swelling, the results indicate that there is no statistically significant change from X_{DTT} = 0.6 - 1.4 ($p > .05$), a result that has never been seen in literature.

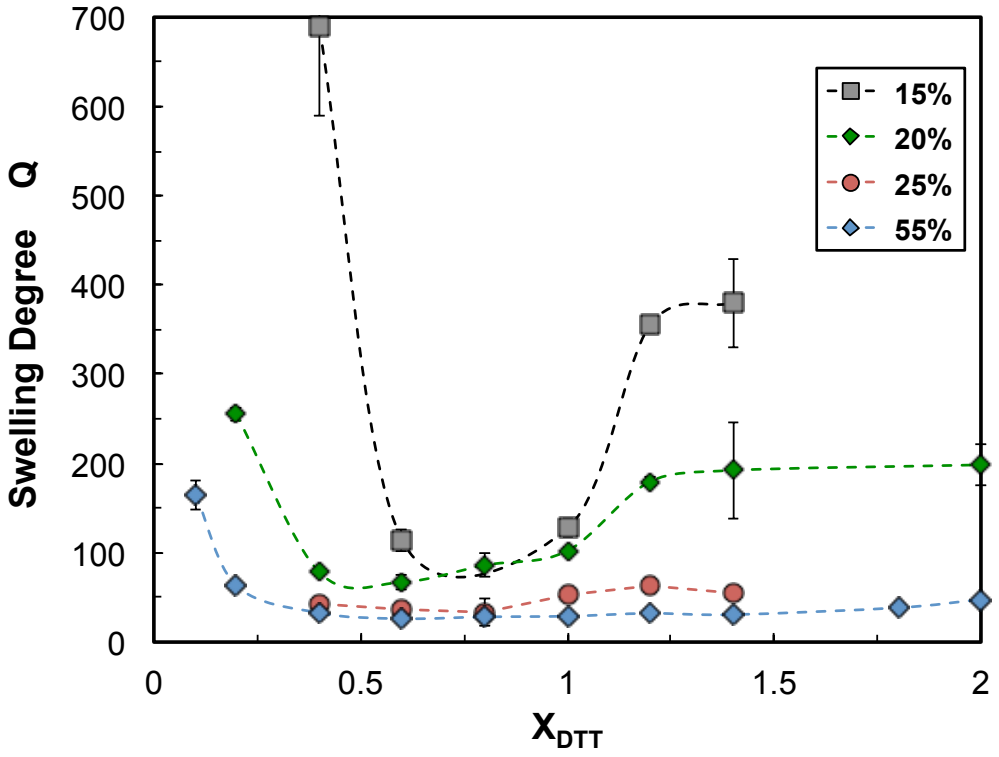

Figure 7.9a. The effect of crosslinking ratio on the swelling degree of 6% (wt/wt) PHA hydrogels. The swelling degrees of the hydrogels are less affected by changes in the X_{DTT} as the degree of substitution (DOS) increases.All hydrogels had a PHA weight percent of 6 and were irradiated at 312 nm (I = 3 mW/cm^2) for 320 seconds. Mean value ± standard deviation, n ≥ 3. The dashed lines serve as a guide to the eye.

As the degree of substitution increases, the swelling degrees of the hydrogels are less affected by the changes in the thiol to ene ratio. For example, with a DS =15%, as the value of X_{DTT} increases from 0.4 to 0.6 the swelling degree drops sharply from 690 ± 100 to 115 ± 13. When the values of X_{DTT} are at 0.6 and1.0, the swelling degrees remain at a value around 120, yet as soon as X_{DTT} increases past 1.0, the swelling degree increases sharply again, reaching a swelling degree of 355 ± 9 at a X_{DTT} value of only 1.2. Alternatively, PHA hydrogels formed with a DS = 55% do not exhibit the same sharp decrease and increase in swelling degrees, and the swelling degree is largely unchanged as the value of X_{DTT} increases from 0.4-1.4. The

reasoning for this is due to the small amount of functional groups that are on the 15% substituted PHA when compared with the 55% substituted HA. At low degree of substitutions, getting the correct ratio of thiols to enes is critical for forming enough crosslinks to form a highly crosslinked hydrogel.

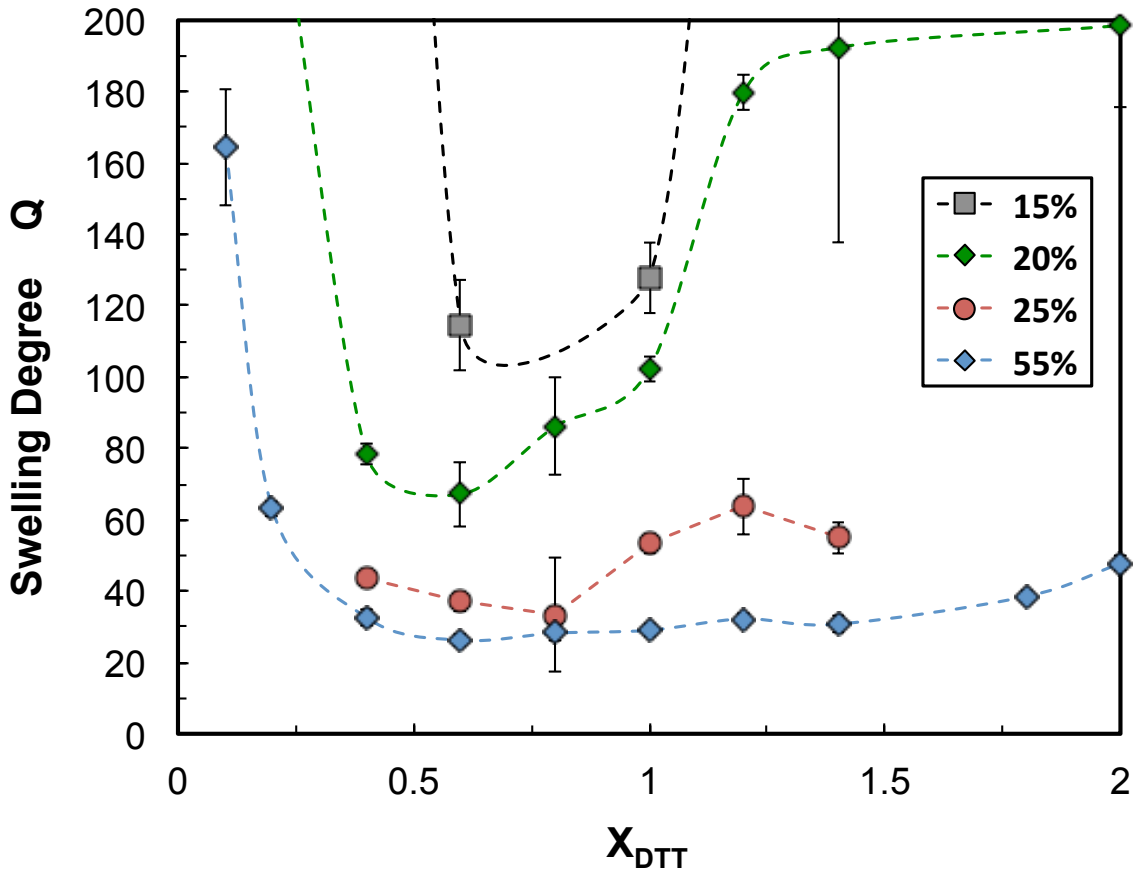

Figure 7.9b. The effect of crosslinking ratio on the swelling degree of 6% (wt/wt) PHA hydrogels for conditions with Q < 200. The swelling degrees of the hydrogels seem to reach a minimum at values of X_{DTT} between 0.6 and 1.0. All hydrogels had a PHA weight percent of 6 and were irradiated at 312 nm (I = 3 mW/cm^2) for 320 seconds. Mean value ± standard deviation, n ≥ 3. The dashed lines serve as a guide to the eye.

Figure 7.10 shows the compressive moduli of 6% PHA gels (DOS=55%) in which the value of X_{DTT} ranged from 0.1 to 2.0. A hydrogel with a higher crosslink density will lead to a higher value of E. The compressive modulus increases as the value of X_{DTT} increases from 0.1 to 0.4. When the value of X_{DTT} increases from 0.4 to 1.4, the resulting gels exhibit only a slight change in modulus. It is only when the values of X_{DTT} increase past 1.4 where the addition of more thiols results in a significant drop in the compressive modulus.

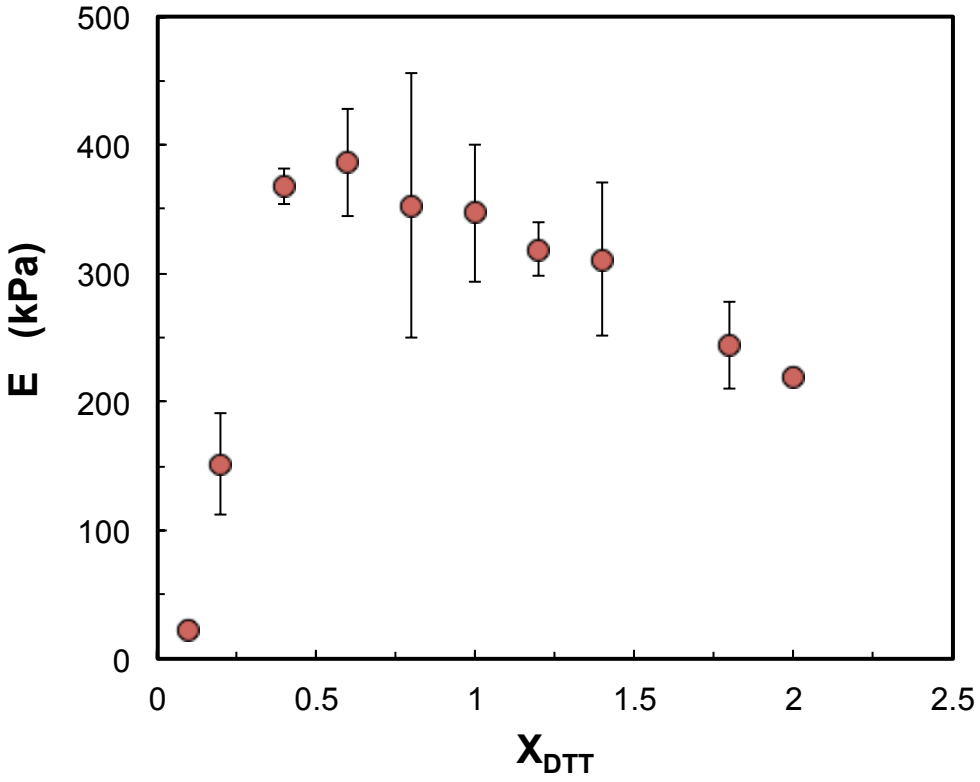

Figure 7.10. The effect of crosslinking ratio on the compressive modulus. The modulus reaches a maximum at X_{DTT} = 0.4-1.4 and decreases as more or less DTT is added. All hydrogels had a DS=55% and were irradiated at 320 nm (I = 3 mW/cm^2) for 320 seconds. Mean value ± standard deviation, n ≥ 3.

The calculated compressive modulus, shear modulus, fracture stress, and fracture strain can be seen in Table 7.2 for 6% PHA hydrogels (DOS = 55%) along with the crosslink density and mesh size. The moduli data and the corresponding calculations of crosslink density and mesh size provide additional evidence that the highest crosslinked gels do not occur precisely at X_{DTT} = 1.0 but rather a range between 0.4-1.0. The shear modulus (G) increases as the value of X_{DTT} increases from 0.1 to 0.4 and then plateaus at around 125 when the value of X_{DTT} ranges from 0.4 to 1.4. A similar trend is seen in both the crosslink density and mesh size of the PHA hydrogels.

Table 7.2 Mechanical properties of 6 wt % PHA hydrogels (DS = 55%)

Gel Formulation		Moduli		Compressive Failure Properties		Crosslink Density	Mesh Size
X_{DTT}	q (w/w)	E (kPa)	G (kPa)	Stress (kPa)	Strain (%)	ρ_x (mol/m^3)	ξ (nm)
0.1	164 ± 16.4	23 ± 6.5	8.0 ± 2.7	8.7 ± 4.2	29.1 ± 5.3	117.5 ± 34.1	85.6 ± 11.3
0.2	63.1 ± 2.1	151 ± 39.5	52 ± 5.5	67.7 ± 27.6	27.6 ± 10.6	552.6 ± 54.6	28.6 ± 1.2
0.4	32.6 ± 2.2	368 ± 14.1	124 ± 16.9	172.5 ± 55.9	32.2 ± 4.4	1057.3 ± 116.0	16.6 ± 0.8
0.6	26.2 ± 1.5	387 ± 42.1	134 ± 8.5	240.2 ± 66.8	36.0 ± 4.7	1062.3 ± 45.2	15.4 ± 0.4
0.8	28.2 ± 2.3	353 ± 103.1	121 ± 26.2	256.1 ± 81.6	39.9 ± 3.1	983.0 ± 172.4	16.4 ± 2.0
1	29.0 ± 1.6	347 ± 53.6	121 ± 14.6	270.8 ± 31.9	41.2 ± 2.3	992.3 ± 98.8	16.5 ± 0.9
1.2	32.2 ± 1.4	319 ± 20.5	105 ± 5.9	172.6 ± 37.6	34.2 ± 3.9	891.6 ± 36.5	18.0 ± 0.4
1.4	30.7 ± 2.4	311 ± 59.6	114 ± 9.2	188.9 ± 32.8	38.3 ± 2.8	952.8 ± 48.4	17.1 ± 0.7
1.8	38.5 ± 1.4	244 ± 34.1	83 ± 11.1	171.3 ± 42.2	38.7 ± 3.8	748.1 ± 89.1	20.9 ± 1.2
2	47.7 ± 2.0	219 ± 5.8	76 ± 7.7	155.1 ± 26.7	38.67± 2.3	735.7 ± 63.3	22.6 ± 1.0

Values are mean ± standard deviation with n = 3

In an ideal system, the maximum crosslink density would occur at $X_{DTT} = 1.0$, the ratio at which every thiol has an ene to react with, and each dithiol that reacts would form an effective crosslink between two different chains. Therefore, hydrogels synthesized at $X_{DTT} = 1.0$ should have the lowest swelling degree and the highest moduli. As Figure 7.11 shows, at X_{DTT} values lower than 1, there are not enough thiol groups to react with the surplus of ene groups, and even though each reaction is expected to form an effective crosslink, the hydrogel will have a lower crosslink density compared to the gels synthesized at $X_{DTT} = 1.0$. At X_{DTT} values greater than 1 there are excess amounts of thiol groups, which saturate the ene groups. Even though all of the ene groups are able to react, the excess amount of thiol groups combined with the speed of the reaction limit the amount of effective crosslinks that can form, which is hypothesized to lead to lower crosslink densities. Additionally, under these conditions, there is expected to be a number of DTT molecules that have been incorporated into the network that contain an unreacted thiol group.

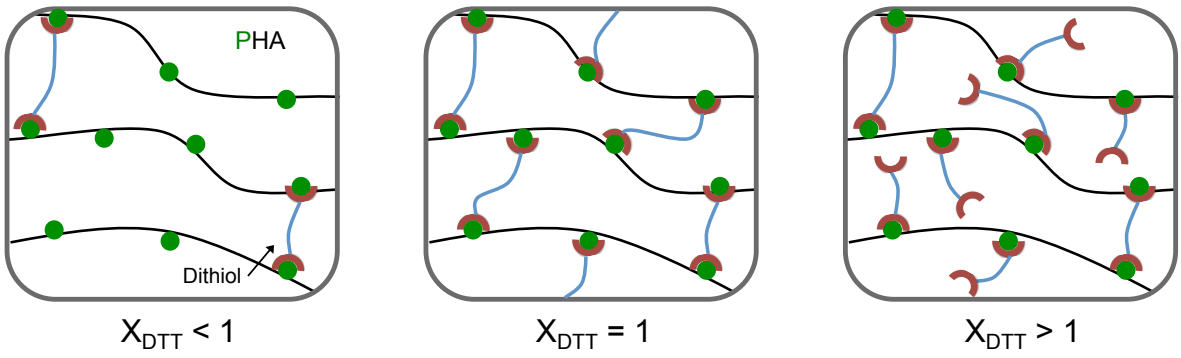

Figure 7.11. Idealized schematic showing how the thiol-ene crosslinking reaction of PHA is affected by the ratios of thiol groups to ene groups (X_{DTT}). The green dots represent the ene groups attached to the HA backbone and the red semicircles represent a thiol.

The results in Figures 9, 10 and Table 7.2 show that hydrogels synthesized at $X_{DTT} = 1.0$ have the lowest swelling degree and the highest moduli. The results indicate that the highest crosslinking density occurs at values X_{DTT} between 0.6 and 1.0. There are a number of possible explanations as to why this is, and they all relate to the potential reactions that can occur that limit the efficiency of the reaction (Figure 7.12). Despite the fact that at $X_{DTT} = 1.0$ there is one thiol for every ene, this does not mean that every thiol will react with an ene to form an effective crosslink. In some cases, thiols can react with two enes that are on the same HA chain, forming an intramolecular loop. This may lead to instances in which only one of the thiols of a DTT molecule reacts with an ene group, leaving a free thiol attached to the HA backbone. This can also be affected by steric constraints as well as structural limitations due to the chain conformations of the HA polymer.

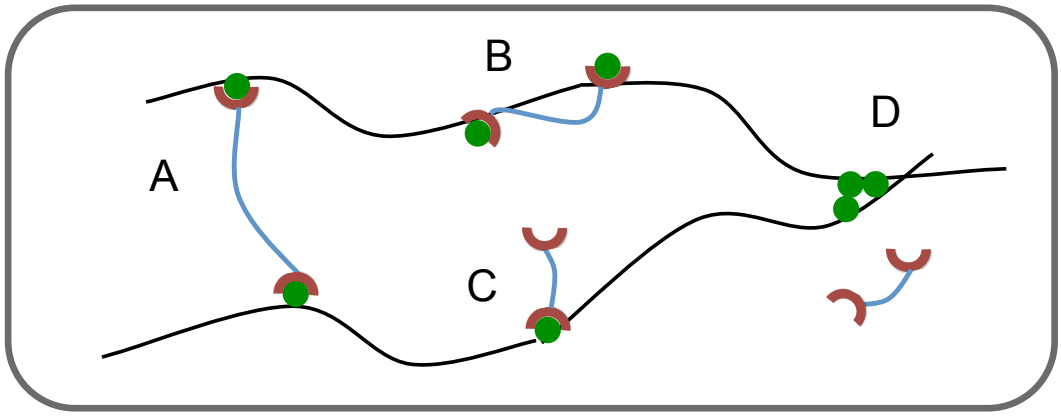

Figure 7.12. Idealized schematic showing potential reactions that can occur at a ratio of thiol groups to ene groups (X_{DTT}) equal to one. (A) Ideal reaction in which each ene group (green dots) reacts with a thiol group (red semicircles), forming an elastically effective crosslink between two separate chains. (B) Two thiols react with enes that are on the same chain, forming an intramolecular loop. (C) Only one thiol is able to react with an ene group, leaving a free thiol group attached to the HA backbone. (D) A chain reaction occurs between ene groups on the HA backbone, reducing the amount of enes available to crosslink.

Additionally, there is a possibility that some degree of homopolymerization is occurring, which would reduce the amount of enes that are available to form crosslinks and lead to a shift in the minimum away from $X_{DTT} = 1$ that is seen in Figures 7.9a and 7.9b. However, this shift was also seen in thiol-ene hydrogels in which norbornene was attached to HA, and norbornene is unable to participate in chain reactions.

One of the hypotheses this chapter set out to prove was the idea that thiol-ene reactions are believed to form much more homogeneous networks than its chain growth counterparts, which allows for polymers and gels with very uniform network crosslink densities. One of the advantages of a more uniform hydrogel network is improved mechanical properties, especially the fracture stress and strain. As gels are placed under strain, the energy is distributed among the elastically effective chains. In heterogeneous hydrogels, there will be regions within the gel that contain a less concentrated amount of chains. Under strain these weaker regions will undergo failure first, which causes multiple fracture events and leads to macroscopic rupture. In a more uniform network, the strain is more evenly spread out across the chains, which results in increased fracture strains. This was demonstrated by Sakai and Shibayama in 2008 through the use of highly uniform tetra-PEG hydrogels.[41]

While it may be difficult to distinguish the differences in network uniformity between the PHA hydrogels listed in Table 7.2 which were all synthesized using the thiol-ene reaction, a comparison of HA hydrogels synthesized using three different crosslinking methods provides clearer evidence. This comparison can be seen in Table 7.3, which displays the fracture stress and strain of 13% (w/w) HA hydrogels synthesized using the thiol-ene reaction, the radical chain polymerization of methacrylated HA[15], and the crosslinking of HA using the bifunctional crosslinker DVS (Chapter 5). While the compressive modulus and fracture stress differs

between the three crosslinking methods, this can be attributed to wide range in swelling degrees that are seen between the three types of hydrogels due to the varying crosslinking densities. In general, as the swelling degree of an HA gel decreases, both the compressive modulus and the fracture stress increase. However, the fracture strain of a HA gel has been shown to not be strongly dependent on the swelling degree and crosslinking density, as can be seen in Table 7.2, Table 5.1, and in work with MHA hydrogels.[15] The fracture strains of PHA hydrogels are on average 85% higher than the fracture strains of MHA hydrogels. For MHA hydrogels, the low fracture strain was hypothesized to be a result of the stiff chain conformation of HA which could possibly lead to network deformations. The fracture strains of PHA are still relatively low, most likely due to the chain conformation of HA, yet they are much higher than MHA hydrogels. This suggests that the PHA networks are less heterogeneous and provides evidence that the hydrogel networks of HA hydrogels crosslinked via the thiol-ene reaction are more uniform than the networks of MHA hydrogels. Additionally, these trends can be observed over a wide range of formulations, as 6% PHA hydrogels also had very high fracture strains of 36 ± 4%. PHA hydrogels were synthesized at the same concentration and with similar degrees of functionalization as the MHA hydrogels, yet the MHA gels have swelling degrees that are almost three times higher and have compressive moduli that are more than half that of PHA hydrogels. While this does not provide further evidence of a more uniform network, it does provide evidence of a much more efficient crosslinking reaction.

Table 7.3. How the type of crosslinking reaction affects the fracture stress and strain.

Hydrogel	Crosslinking Reaction	q (w/w)	E (kPa)	Fracture Stress (kPa)	Fracture Strain (%)
13% PHA*	Thiol-ene	10.5 ± 0.5	1090.6 ± 76	523.4 ± 91	30.1 ± 1.9
13% MHA[#]	Chain growth	27.5 ± 0.22	476 ± 63	75.1 ± 9.7	16.28 ± 0.61
13% HA-DVS[a]	Michael addition	6.6 ± 0.19	2230 ± 160	730 ± 230	26.6 ± 6.5

Values are mean ± standard deviation

*Degree of substitution = 55%, X_{DTT} = 1.0, n=4

[#] Degree of methacrylation = 47%, n =5

[a] HA:DVS ratio = 3:1, n=5

The fracture strains between the PHA and HA-DVS hydrogels were not statistically significant (p=0.338), and therefore no conclusions could be made about differences in network structure between the gels. The benefit of the thiol-ene reaction is that crosslinking can only occur on the HA backbone where ene groups are present, which allows for more control of the network structure. Further work is needed to investigate the hypothesis that PHA hydrogels would have a more uniform network structure than HA-DVS hydrogels.

7.4.5 Encapsulation of Proteins into a PHA Hydrogel

The results of the previous sections investigated a number of variables that can be used to control the network structure of the hydrogel including the irradiation time, the polymer concentration, the degree of substitution, and the ratio of thiols to enes. The results also provided evidence of a more uniform network structure. The major motivation behind this work was to test the hypothesis that a hydrogel with a more uniform network could have significant effects on the transport of solutes within the hydrogel. Another motivation for using the thiol-ene reaction was to encapsulate proteins within hydrogels, taking advantage of the speed and selectivity of the thiol-ene reaction, along with the mild reaction conditions. If proteins could be successfully encapsulated, it would represent a major improvement when compared to the Michael addition reaction used in Chapters 4 and 5 in which divinyl sulfone was used to crosslink HA and dextran hydrogels. Not only did this reaction occur under denaturing conditions, it also reacted with proteins diffusing into the hydrogel and covalently attached them to the hydrogel network.

To study the photoencapsulation and release of proteins in PHA hydrogels, the model proteins BSA and ovalbumin were encapsulated into PHA hydrogels with the concentration of protein in the hydrogels ranging from 1 mg/mL to 10 mg/mL. These proteins were chosen due to the fact that they have similar sizes yet differed in the amount of free thiols that might participate in the reaction during encapsulation. BSA is known to have a free cysteine residue that is on the surface of the protein, and this thiol can react with the ene groups on the HA backbone.[42] On the other hand, while ovalbumin has 4 total cysteine residues, 2 are in a dithiol bond and the other two have been shown to be buried in the hydrophobic regions of the deeply folded protein, and only accessible after denaturation.[43] These buried free thiols are not expected to react with the

ene groups on the HA backbone, which should lead to much higher recoveries when compared to BSA.

To test this hypothesis, ovalbumin and BSA were encapsulated under identical conditions. The weight percent of the PHA hydrogels was increased to 13% and X_{DTT} was set equal to 1.0 in order to lower the swelling degree and the diffusion coefficient in an effort to extend the release. The release of ovalbumin from 13% PHA hydrogels can be seen in Figure 7.13. After 700 minutes, 90% of the ovalbumin had diffused of the gel. The release profile follows Fickian diffusion, as seen by the dashed line that represents the analytical solution described in Equation 7.1. The discs released 71.5 ± 10.9% of the total protein that was loaded. Using the dimensions of the discs and Equation 7.1, a diffusion coefficient was fit to each curve (n=3) by minimizing the sum of squared residuals. The three values were then averaged together to give a final diffusion coefficient of $8.70 \pm 1.1 \times 10^{-8}$ cm^2/s. Unfortunately, the high swelling degrees (q=10.5) of these PHA hydrogels makes it difficult to compare diffusion coefficients with the HA-DVS hydrogels (q<6) studied in Chapter 5. However, using the projections based on the free volume theory presented in Figure 5.3 for BSA, a HA hydrogel with a swelling degree of 10.5 is predicted to have a diffusion coefficient of 8.30×10^{-8} cm^2/s. This is noteworthy because the similarity in the predicted and measured diffusion coefficients signifies that, despite some evidence of a more uniform network structure in PHA hydrogels found in the previous section, there is no dramatic change in the diffusion coefficient. However, it may be that the swelling degree is too high to notice any impacts the network structure might have on the diffusion coefficient due to the hypothesized screening effect, and any possible deviations from the predictions may only occur at lower swelling degrees or with larger solutes.

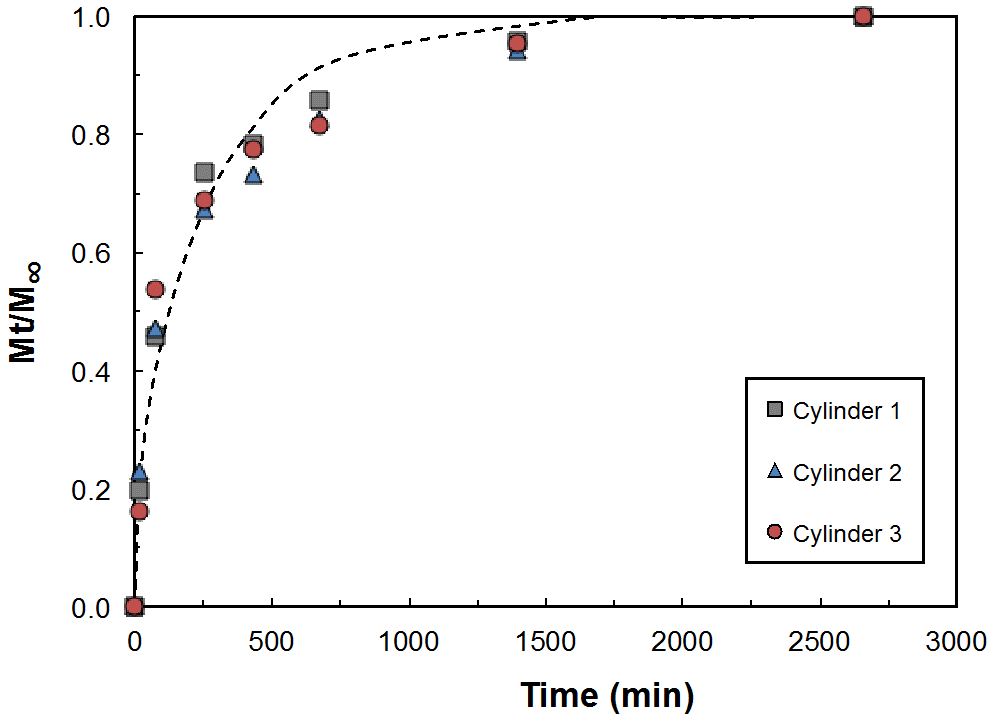

Figure 7.13. The release of ovalbumin from 13% PHA hydrogels exhibits Fickian release. Dashed line represents a D = 8.70 ± 1.1 x 10^{-8} cm^2/s. Gels were loaded with 10 mg/mL ovalbumin and released 71.5 ± 10.9% of the total protein loaded. All hydrogels had a DS=55% and were irradiated at 312 nm (I = 3 mW/cm^2) for 320 seconds. Q = 10.5

One unexpected observation of the encapsulation study was that the addition of 10 mg/mL BSA caused the solution to gel before being irradiated with UV light. This prevented them from being formed into discs, making it difficult to accurately measure the release. The early gelation also resulted in an increase in swelling degree when compared with the PHA hydrogels encapsulated with 10 mg/mL ovalbumin. To further investigate the effects of protein concentration on the swelling, equilibrium experiments were performed.

For these equilibrium experiments, the release of protein from PHA discs was only measured after 24, 48, and 72 hours to confirm complete release. The swelling degrees and the

amount of protein recovered after release are presented in Table 7.4. Hydrogels synthesized without encapsulated proteins had an equilibrium swelling degree of 10.50 ± 0.03. When proteins were encapsulated during hydrogel formation at concentrations below 5 mg/mL the swelling degree remained unchanged and stayed at 10.5 for all of the formulations, evidence that protein is not interfering is not altering the network structure of the PHA hydrogels

Table 7.4. Swelling degree and protein recovery from 13% PHA hydrogels. The swelling degree of the PHA hydrogels remains unchanged for all formulations except 10mg/mL BSA. Ovalbumin has a higher % recovery when compared to BSA. All hydrogels had a DS = 55% and were irradiated at 312 nm (I = 3 mW/cm^2). Mean value ± standard deviation, n ≥ 3. (n=2 for 10mg/ml BSA hydrogels) *Data taken from previous release experiments (shown in Fig 7.13)

Protein	Protein Concentration (mg/mL)	Swelling Degree (g/g)	Protein Loaded (mg)	% Released
No Protein	0	10.50 ± 0.03	0	-
BSA	1	10.49 ± 0.16	0.031	29.9 ± 3.7%
	5	10.58 ± 0.14	0.157	49.7 ± 1.3%
	10	13.24 ± 0.44	0.314	66.8 ± 4.0%
Ovalbumin	5	10.58 ± 0.31	0.157	77.8 ± 1.6%
	10*	10.56 ± 0.82	0.314	71.5 ± 10.9%

However, when the concentration of protein was increased to 10 mg/mL, the protein began to have an effect on the thiol-ene reaction. Hydrogels containing both BSA and ovalbumin were synthesized at 10 mg/mL concentrations and began to gel in minutes, even before being placed into molds and exposed to UV light. The solution containing 10 mg/mL ovalbumin completely gelled and was not able to be molded and for that reason was not included in Table

7.4. This contradicts the results seen in the previous release studies (shown in Figure 7.13) in which 10 mg/mL ovalbumin was successfully encapsulated and released from PHA hydrogels and had no effect on the swelling degree. The solution containing 10 mg/mL BSA only partially gelled, and the remaining solution was able to be placed into molds and irradiated. The swelling degree of these hydrogels encapsulated with 10 mg/mL BSA increased to 13.24 ± 0.44.

The reason these solutions gelled before being exposed to UV light is unknown. Perhaps an impurity in the lyophilized protein introduced a free radical into the solution that started the reaction at high concentrations. Another possibility is that the protein itself is absorbing light and causes the thiol-ene reaction to start. Tryptophan, tyrosine, and phenylalanine are known to absorb light in the near UV range, which could lead to an excitation followed by a relaxation that could produce a radical species[44]. It has already been mentioned earlier that in the thiol-ene reaction a single radical species can cause hundreds and even thousands of reaction events to occur due to the regeneration of the thiyl radical. The fact that these gels partially formed before being exposed to UV light could explain the increase in swelling degree. Another theory for the change in swelling degree is that the high concentration of proteins in the solution affects the thiol-ene reaction. If BSA prevents DTT from reacting with PHA or if BSA reacts itself with the PHA it would reduce the amount of effective crosslinks and increase the swelling degree.

Table 7.4 also displays the percentage of protein released from PHA hydrogels. When 1 mg/mL of BSA is encapsulated, 30% of the protein is recovered. When the concentration of BSA is increased to 5 mg/mL, 50% of the protein is recovered. While there are a number of possible explanations for this, the most likely is that a finite amount of BSA, which is known to have a free cysteine residue, has reacted with ene groups on the HA backbone and are covalently attached to the network. One piece of evidence that supports this theory is the fact that almost 80%

of the ovalbumin, whose free cysteines are buried in the folded protein, is recovered from PHA hydrogels. More experiments are needed to fully understand how the proteins are being affected by the thiol-ene reactions and to investigate the effects that encapsulated proteins have on the swelling degree and initiation kinetics of PHA hydrogels. This is especially important for drug delivery applications where expensive drugs such as antibodies need to be delivered and a high recovery is necessary in order to reduce costs. More importantly, many antibodies rely on internal disulfide bridges to maintain their structure and any reactions that alter or affect this structure may reduce the binding capability and effectiveness of the antibody.

7.5 Conclusions

Overall, the results in this chapter illustrate a simple yet versatile way to synthesize HA hydrogels and take advantage of the benefits offered by the thiol-ene reaction. Using this reaction, PHA gels are able to form complete gels in less than 120 seconds, among the fastest that have been seen for a thiol-ene hydrogel in literature at very low initiator concentrations (0.1 mM - I2959) and light intensities (3 mW/cm^2). Not only does the speed of this reaction compare favorably with reactions seen in literature that use norbornene, the results also confirmed that there is little to no homopolymerization that occured during the synthesis of PHA hydrogels, evidence of the high selectivity of the reaction. The results also expand the literature knowledge of the effects of X_{DTT} on the swelling and mechanical properties of HA hydrogels. The results indicate that the highest crosslinking density occurs at values X_{DTT} between 0.6 and 1.0, while also showing for the first time that a low degree of substitution increases the sensitivity of this effect. The results also provided evidence of a more uniform network structure when compared to similar MHA hydrogels crosslinked via radical chain polymerization, as evidenced by an

increase in fracture strain of 85%. Lastly, it was shown that proteins could be encapsulated into PHA gels and released. The amount of protein released was revealed to be influenced by the amount and location of free cysteine residues on the protein, and recovery of up to 78% was seen with ovalbumin.

REFERENCES

1. Burdick JA, Prestwich GD 2011. Hyaluronic Acid Hydrogels for Biomedical Applications. Adv Mater 23(12):H41-H56.

2. Leach JB, Bivens KA, Patrick CW, Schmidt CE 2003. Photocrosslinked hyaluronic acid hydrogels: natural, biodegradable tissue engineering scaffolds. Biotechnology and bioengineering 82(5):578-589.

3. Garg HG, Hales CA. 2004. Chemistry and biology of hyaluronan. ed.: Elsevier.

4. Sahoo S, Chung C, Khetan S, Burdick JA 2008. Hydrolytically degradable hyaluronic acid hydrogels with controlled temporal structures. Biomacromolecules 9(4):1088-1092.

5. Kurisawa M, Chung JE, Yang YY, Gao SJ, Uyama H 2005. Injectable biodegradable hydrogels composed of hyaluronic acid–tyramine conjugates for drug delivery and tissue engineering. Chemical communications (34):4312-4314.

6. Luo Y, Kirker KR, Prestwich GD 2000. Cross-linked hyaluronic acid hydrogel films: new biomaterials for drug delivery. J Control Release 69(1):169-184.

7. Serban MA, Prestwich GD 2007. Synthesis of hyaluronan haloacetates and biology of novel cross-linker-free synthetic extracellular matrix hydrogels. Biomacromolecules 8(9):2821-2828.

8. Prestwich GD, Marecak DM, Marecek JF, Vercruysse KP, Ziebell MR 1998. Controlled chemical modification of hyaluronic acid: synthesis, applications, and biodegradation of hydrazide derivatives. J Control Release 53(1-3):93-103.

9. Darr A, Calabro A 2009. Synthesis and characterization of tyramine-based hyaluronan hydrogels. J Mater Sci-Mater Med 20(1):33-44.

10. Shu XZ, Liu YC, Luo Y, Roberts MC, Prestwich GD 2002. Disulfide cross-linked hyaluronan hydrogels. Biomacromolecules 3(6):1304-1311.

11. Burdick JA, Chung C, Jia XQ, Randolph MA, Langer R 2005. Controlled degradation and mechanical behavior of photopolymerized hyaluronic acid networks. Biomacromolecules 6(1):386-391.

12. Burdick JA, Chung C, Jia X, Randolph MA, Langer R 2005. Controlled degradation and mechanical behavior of photopolymerized hyaluronic acid networks. Biomacromolecules 6(1):386-391.

13. Bae KH, Yoon JJ, Park TG 2006. Fabrication of hyaluronic acid hydrogel beads for cell encapsulation. Biotechnology Progress 22(1):297-302.

14. Erickson IE, Huang AH, Sengupta S, Kestle S, Burdick JA, Mauck RL 2009. Macromer density influences mesenchymal stem cell chondrogenesis and maturation in photocrosslinked hyaluronic acid hydrogels. Osteoarthritis and Cartilage 17(12):1639-1648.

15. Khanlari A, Schulteis JE, Suekama TC, Detamore MS, Gehrke SH 2015. Designing crosslinked hyaluronic acid hydrogels with tunable mechanical properties for biomedical applications. Journal of Applied Polymer Science 132(22).

16. Lin-Gibson S, Jones RL, Washburn NR, Horkay F 2005. Structure-property relationships of photopolymerizable poly (ethylene glycol) dimethacrylate hydrogels. Macromolecules 38(7):2897-2902.

17. Hoyle CE, Bowman CN 2010. Thiol-Ene Click Chemistry. Angewandte Chemie-International Edition 49(9):1540-1573.

18. Hoyle CE, Lee TY, Roper T 2004. Thiol-enes: Chemistry of the past with promise for the future. J Polym Sci Pol Chem 42(21):5301-5338.

19. Lowe AB 2010. Thiol-ene "click" reactions and recent applications in polymer and materials synthesis. Polymer Chemistry 1(1):17-36.

20. Kharasch M, MAY EM, MAYO FR 1938. The peroxide effect in the addition of reagents to unsaturated compounds. Xviii. The addition and substitution of bisulfite*. The Journal of Organic Chemistry 3(2):175-192.

21. Lowe AB 2010. Thiol-ene “click” reactions and recent applications in polymer and materials synthesis. Polymer Chemistry 1(1):17-36.

22. Kolb HC, Finn MG, Sharpless KB 2001. Click chemistry: Diverse chemical function from a few good reactions. Angew Chem-Int Edit 40(11):2004-+.

23. Roper TM, Guymon CA, Jonsson ES, Hoyle CE 2004. Influence of the alkene structure on the mechanism and kinetics of thiol-alkene photopolymerizations with real-time infrared spectroscopy. J Polym Sci Pol Chem 42(24):6283-6298.

24. Mergy J, Fournier A, Hachet E, Auzely-Velty R 2012. Modification of polysaccharides via thiol-ene chemistry: A versatile route to functional biomaterials. J Polym Sci Pol Chem 50(19):4019-4028.

25. Gramlich WM, Kim IL, Burdick JA 2013. Synthesis and orthogonal photopatterning of hyaluronic acid hydrogels with thiol-norbornene chemistry. Biomaterials 34(38):9803-9811.
26. Malkoch M, Vestberg R, Gupta N, Mespouille L, Dubois P, Mason AF, Hedrick JL, Liao Q, Frank CW, Kingsbury K, Hawker CJ 2006. Synthesis of well-defined hydrogel networks using Click chemistry. Chemical Communications (26):2774-2776.
27. Malkoch M, Vestberg R, Gupta N, Mespouille L, Dubois P, Mason AF, Hedrick JL, Liao Q, Frank CW, Kingsbury K 2006. Synthesis of well-defined hydrogel networks using click chemistry. Chemical Communications (26):2774-2776.
28. Aimetti AA, Machen AJ, Anseth KS 2009. Poly(ethylene glycol) hydrogels formed by thiol-ene photopolymerization for enzyme-responsive protein delivery. Biomaterials 30(30):6048-6054.
29. Lin C-C, Metters AT 2006. Hydrogels in controlled release formulations: network design and mathematical modeling. Advanced drug delivery reviews 58(12):1379-1408.
30. Hoare TR, Kohane DS 2008. Hydrogels in drug delivery: progress and challenges. Polymer 49(8):1993-2007.
31. Drury JL, Mooney DJ 2003. Hydrogels for tissue engineering: scaffold design variables and applications. Biomaterials 24(24):4337-4351.
32. Northrop BH, Coffey RN 2012. Thiol–ene click chemistry: computational and kinetic analysis of the influence of alkene functionality. Journal of the American Chemical Society 134(33):13804-13817.
33. McCall JD, Anseth KS 2012. Thiol-Ene Photopolymerizations Provide a Facile Method To Encapsulate Proteins and Maintain Their Bioactivity. Biomacromolecules 13(8):2410-2417.
34. Lin CC, Sawicki SM, Metters AT 2008. Free-radical-mediated protein inactivation and recovery during protein photoencapsulation. Biomacromolecules 9(1):75-83.
35. Fu J, Hagemeir C, Moyer D, Ng E 1976. A unified mathematical model for diffusion from drug–polymer composite tablets. Journal of biomedical materials research 10(5):743-758.
36. Waters J, Leiske D 2005. Characterization of hyaluronic acid with on-line differential viscometry, multiangle light scattering, and differential refractometry. LC GC Magazine-North America-Solutions for Separation Scientists 23(3):302-311.

37. Khanlari A, Suekama TC, Detamore MS, Gehrke SH 2015. Structurally diverse and readily tunable photocrosslinked chondroitin sulfate based copolymers. Journal of Polymer Science Part B-Polymer Physics 53(15):1070-1079.

38. Peppas NA, Merrill EW 1976. Poly (vinyl alcohol) hydrogels: Reinforcement of radiation-crosslinked networks by crystallization. Journal of Polymer Science: Polymer Chemistry Edition 14(2):441-457.

39. Khanlari A, Schulteis JE, Suekama TC, Detamore MS, Gehrke SH 2015. Designing crosslinked hyaluronic acid hydrogels with tunable mechanical properties for biomedical applications. Journal of Applied Polymer Science 132(22):7.

40. Bowman CN, Kloxin CJ 2008. Toward an Enhanced Understanding and Implementation of Photopolymerization Reactions. Aiche Journal 54(11):2775-2795.

41. Sakai T, Matsunaga T, Yamamoto Y, Ito C, Yoshida R, Suzuki S, Sasaki N, Shibayama M, Chung U-i 2008. Design and fabrication of a high-strength hydrogel with ideally homogeneous network structure from tetrahedron-like macromonomers. Macromolecules 41(14):5379-5384.

42. He XM, Carter DC 1992. Atomic-Structure and chemistry of human serum-albumin. Nature 358(6383):209-215.

43. Ibrahim H 1996. Insights into the structure-function relationships of ovalbumin, ovotransferrin, and lysozyme. Hen eggs Boca Raton, Florida:37-56.

44. Neves-Petersen MT, Gajula GP, Petersen S. 2012. UV light effects on proteins: from photochemistry to nanomedicine. ed.: INTECH Open Access Publisher.

Chapter 8: Concluding Remarks And Future Work

In the last decade the use of antibodies to treat cancer, autoimmune diseases, viral infections, and even asthma has increased, causing an increase in the study of ways to extend the release of therapeutic proteins. Parenteral delivery routes often lead to an increase in systemic exposure while requiring frequent injections, and in many cases, long term, local delivery systems are preferred. In ocular drug delivery this is particularly true, due to retinal diseases such as age related macular degeneration and diabetic macular edema that require frequent injections into the vitreous in order to deliver drugs to the retina and prevent major vision loss. While there are a number of drug delivery methods and materials that are being developed in an effort to provide long-term, sustained release to the retina, for this application hydrogels have received very little attention. Hydrogels can exhibit a wide range of permeabilities while also having the ability to be synthesized using a variety of biocompatible materials, making them a favorable option for ocular delivery vehicles. The difficulty in developing an effective ocular delivery device is in controlling the diffusion of proteins within a hydrogel in order to provide the correct release rate and profile. The objective of this dissertation, therefore, was to investigate the permeability of therapeutic proteins in hydrogels to aid the development of long-term drug delivery vehicles.

While one of the aims addressed in this dissertation was the development of a hydrogel implant that can be used specifically for treating ocular delivery, the major aim was to develop a better understanding of how solutes diffuse through hydrogels when the diffusion coefficient is very small. The review in Chapter 3 highlighted the need for this, and showed that even though there is a large amount of work in literature that has advanced the understanding of the important variables that govern diffusion in hydrogels, very little has been done at diffusion coefficients

below 10^{-10} cm^2/s. These low values are achieved as the polymer volume fraction of the gel increases or as the size of the solute increases, and under these conditions it has been hypothesized in literature that a dramatic reduction in the diffusion coefficient will be seen, which is referred to as the screening effect. However, there is very little evidence in literature that supports the hypothesis that such a phenomenon exists due to the difficulty in measuring diffusion coefficients at such low values in hydrogels. The majority of the work in the chapter was concentrated on a number of the established theories that describe the diffusion of solutes within hydrogels, specifically focusing on how models based on these theories predict the diffusion of large solutes in hydrogels with low swelling degrees where the screening effect is hypothesized to occur. Of these models, those based on the free volume theory are the only ones that contain a specific parameter (the sieving factor) that can cause a dramatic drop in the predicted diffusion coefficient. However, these models rely heavily on the accuracy of measured gel parameters such as the molecular weight between crosslinks ($\bar{M}_c$), the network mesh size (ξ), and on undefined fitting parameters. The other models based on the obstruction theory and the hydrodynamic theory do not predict a dramatic reduction in the diffusion coefficient at low swelling degrees. Overall this analysis showed the need for additional research and data in order to rigorously test the models and see how they perform under a wide range of hydrogels and solutes.

The permeability of solutes within hydrogels was a central theme throughout this dissertation, and played a large role in Chapter 4, where a method for loading therapeutic proteins into hydrogels using the thermodynamic principles of aqueous two-phase extraction was developed. While the loading method was first developed by Gehrke et al.[1] with proteins on the order of 50 kDa in dextran hydrogels, it was hypothesized that the thermodynamic principles of

this method could be generalized to any type of hydrogel and that it could work even for proteins as large as monoclonal antibodies. The results in Chapter 4 supported this hypothesis. The model protein ovalbumin was shown to diffuse into both PEG and dextran hydrogels, and the partition coefficients were manipulated by using salts in a manner that was predicted by heuristics both above and below the isoelectric point. The partition coefficient of ovalbumin was even shown to increase with PEG hydrogels by using a polymer-salt loading system, something that has never been shown in literature before and further demonstrated the generality of the concept. The results expand the options for hydrogel drug delivery and allow for systems that can be chosen that maximize both the partition coefficient and the swelling degree and have a polymer that is best suited for a given application. The second hypothesis was also confirmed, as the antibody IgG was successfully loaded into both PEG and dextran hydrogels. Partition coefficients of up to 18 were reached for IgG in dextran hydrogels with the addition of only 6% PEG after being almost completely excluded when loaded in buffer alone. The results showed promise as a drug loading method, but also brought the importance of the diffusion of solutes within hydrogels to light. The diffusion of IgG was significantly slower than ovalbumin and required extended loading times, which limits the practical ability of the method to load monoclonal antibodies into hydrogels with dimensions other than microgels.

The diffusion time was also a consideration in developing a prototype ocular implant using a hydrogel that could provide 3-6 months release of anti-vascular endothelial growth factors to the retina, the main objective in Chapter 5. Postloading a monolithic implant using diffusion (similar to the loading method used in Chapter 4) would not only take 3-6 months, it would also require either very large partition coefficients or a very high loading concentration (most likely above the solubility limit) in order to provide the dosage required in a device small enough to be

implanted in the vitreous. Since this was not feasible, the focus on the chapter was in developing a hollow cylinder made from a hyaluronic acid (HA) hydrogel that could be filled with a concentrated drug solution and then capped. The main challenge was in producing a HA hydrogel that had a diffusion coefficient low enough to achieve extend release. Using the cylinder dimensions and Fick's law, a target diffusion coefficient was calculated. Using the models in Chapter 3, the swelling degree needed to achieve this target diffusion coefficient was predicted to be between 3.5 and 5.8. In order to achieve such low swelling degrees, the cylinders were made from (HA) hydrogels that were highly crosslinked using the difunctional crosslinker divinyl sulfone (DVS). The resulting hydrogels had swelling degrees as low as 2.7 using HA concentrations that ranged from 15-30% (w/w) and HA:DVS ratios that ranged from 3:1–1:1. Using a custom machined mold, a prototype hollow cylinder was successfully fabricated, loaded with drug, and capped. The model protein bovine serum albumin (BSA) exhibited steady release from the hollow cylinders for over 140 days. While the release slowed over time, the release rate stayed at or above 2.5 micrograms per day for over 50 days when loaded with a 250 mg/mL solution. Additionally, the cylinders exhibited a much lower diffusion coefficient than predicted (3×10^{-11} vs. 9×10^{-9} cm^2/s) for a hydrogel with a swelling degree of 6.5, which suggests the possibility of screening effects playing a role in the diffusion. The release of an antigen-binding fragment (Fab) was also examined and the results demonstrated that these cylinders are capable of delivering Fabs for 3 months. The release was slightly faster when compared to that of BSA, which is to be expected given the smaller size of the Fab and was reflected in the measured diffusion coefficient of $5.5 \pm 1.5 \times 10^{-11}$ cm^2/s, about twice as large as the diffusion coefficient of BSA in the same cylinders. The results demonstrated that these HA-DVS hollow cylinders are

suitable implants that can provide extended release and could be further investigated for the treatment of retinal diseases.

However, the results also revealed some of the difficulties in developing injectable hollow cylinders from an HA-DVS hydrogel. The small size of the cylinders and the crude capping method led to a few punctures, cracks, and leaks after repeated handling during measurements and led to a smaller number of cylinders being tested. This contributed to the high variability that was seen in the data. Furthermore, due to poor crosslinking efficiency, the hydrogel required a high concentration of DVS in order to get the low swelling degrees that were required for extended release. This led to an excess amount of vinyl sulfone groups that were attached to the HA backbone which required ethylene glycol capping to eliminate unwanted side reactions with the solutes. This, along with the high functionalization required to reduce the swelling degree, may lead to a decrease in biocompatibility.

One of the advantages of a hydrogel implant is that it can be molded and shaped into any size and therefore, for any given application, the release profile and rate can be controlled by tuning the wall thickness, hydrogel formulation, and concentration of protein within the hollow cylinder. In Chapter 6, the diffusion of drugs through intravitreal hollow cylinder hydrogel implants were modeled using COMSOL Multiphysics© software in order to determine the range of diffusion coefficients and cylinder dimensions that would produce a therapeutically effective ocular delivery device. Once this range in diffusion coefficients was determined, a corresponding gel formulation could be developed. Hydrogel implants with three different outer diameters were modeled in order to compare devices that would need to be implanted, inserted using a microinjector, or injected using a 27-gauge needle. Implantable cylinders with 1mm outer diameters were shown to be capable of delivering over 1 mg of drug and achieving a release of

2.5 micrograms per day for 4.5 months. While these larger cylinders are able to provide the longest duration of action, their size requires them to be surgically implanted in a procedure that is time consuming, costly, and can lead to complications. While a smaller cylinder makes the insertion process safer, less painful, and faster, the results showed that these smaller cylinders are limited in their ability to deliver high loads and achieve extended release. Cylinders with outer diameters of 0.45 mm were found to be capable of delivering only 208 micrograms of drug and could achieve a release of 2.5 micrograms a day for only 28 days, roughly five times shorter than the larger cylinders. The cylinders with an outer diameter of 0.21 mm, while able to be injected directly using a 27-gauge needle, was severely limited in the amount of drug that could be loaded and released. The cylinders achieved a release of 2.5 micrograms a day for only one week.

The results showed just how challenging it can be to develop an effective intravitreal implant. The size dimensions that are required for ocular delivery leads to a narrow range of diffusion coefficients that are capable of producing an effective delivery device. The hollow cylinders were most effective at diffusion coefficients between 1.0×10^{-11} and 3.0×10^{-11} cm^2/s, a very narrow range that highlights the importance of being able to tune the diffusion coefficient of hydrogels. The results also show that hollow cylinders are a viable option for ocular drug delivery. While the dimensions for an intravitreal implant will always be limited to the sizes in Chapter 6, the target release rate and initial concentration within the cylinder may vary depending on the desired application. This could result in cylinders that are capable of longer release times, and might shift the range of diffusion coefficients that is most effective in achieving both the release rate and duration. Regardless, given the size requirements for ocular delivery, any application will require tight control of the diffusion coefficient in order to be therapeutically effective.

Creating a hydrogel that can be finely tuned to provide a narrow range of diffusion coefficients was one of the main focuses of Chapter 7. In this chapter, HA was modified with pentenoic anhydride and crosslinked into hydrogels via the thiol-ene reaction. The thiol-ene reaction was hypothesized to produce hydrogels that not only consisted of a more homogeneous network structure, but could also be easily tuned by controlling the ratio of thiols to enes. The thiol-ene reaction was also investigated due to its many advantages, which include fast reaction times, high efficiency, insensitivity to oxygen, and a wide range of possible crosslinkers. Using this reaction, PHA gels were able to form fully crosslinked gels in less than 120 seconds while using very low initiator concentrations (0.1 mM - I2959) and light intensities (3 mW/cm^2). This was among the fastest that have been seen for a thiol-ene hydrogel in literature. The results also confirmed that there is little to no unwanted side reactions that occur between the ene groups during the synthesis of PHA hydrogels, evidence of the high selectivity of the reaction. The results also expand the literature knowledge of the effects of X_{DTT} on the swelling and mechanical properties of HA hydrogels. The results indicate that the highest crosslinking density occurs at values X_{DTT} between 0.6 and 1.0, while also showing for the first time that a low degree of substitution increases the sensitivity of this effect. Evidence of a more uniform network structure was also observed when compared to similar MHA hydrogels crosslinked via radical chain polymerization, as the fracture strain of PHA hydrogels were approximately double that of MHA.

The results also showed that proteins could be encapsulated into PHA gels and released. Studies comparing the release of BSA and ovalbumin revealed that the percent recovery of encapsulated proteins was affected by the amount and location of free cysteine residues on the protein. Recovery of up to 78% was seen with ovalbumin, while the recovery of BSA ranged

from 30-50%, providing evidence of a possible reaction between the PHA and free thiols on BSA. One of the benefits of being able to encapsulate proteins is the ability to measure the release from PHA hydrogels. The release of ovalbumin from PHA hydrogels (q=10.5) exhibited Fickian release with a calculated diffusion coefficient of 8.7×10^{-8} cm^2/s. Based on the free volume theory presented in Figure 5.3 for BSA, a HA hydrogel with a swelling degree of 10.5 is predicted to have a diffusion coefficient of 8.30×10^{-8} cm^2/s. This is significant because it signifies that, despite some evidence of a more uniform network structure in PHA hydrogels, there was no dramatic change in the diffusion coefficient when compared with predictions. Possible deviations from the predictions may only occur at lower swelling degrees or with larger solutes. More work is required in order to determine if the network structure of PHA hydrogels can actually lead to differences in the diffusion coefficients when compared to gels with similar swelling degrees crosslinked via other reactions. This is discussed in the future work section later in this chapter.

As a whole, this dissertation advances the current knowledge on the permeability of proteins in hydrogels for drug delivery applications. The work presented demonstrates that hydrogel delivery vehicles are capable of achieving extended release of therapeutic proteins. The work also highlights the need in literature for more data at very low diffusion coefficients where the diffusion models were demonstrated not to work. The dissertation also introduced the development of a hydrogel system that may not only be suitable for practical applications such as ocular delivery, but also provides a framework for further systematic scientific investigation.

RECOMMENDATIONS FOR FUTURE WORK

1. Further investigation of the screening effect in hydrogels

One of the main goals of this dissertation was to investigate the diffusion of solutes in hydrogels where the diffusion coefficient is very small, with values below 10^{-10} cm^2/s. It was hypothesized that as the size of the solute approaches the average mesh size of the hydrogel, a dramatic reduction in the diffusion coefficient would occur due to a screening effect, and that these low values can be achieved achieved as the polymer volume fraction of the gel increases or as the size of the solute increases. While the diffusion of BSA in HA-DVS hydrogels provided some evidence of this screening effect in Chapter 5, more work is needed to confirm that the experimental diffusion coefficients strayed significantly from the values predicted by a number of the diffusion models because of this screening effect and not due to errors in the models' prediction due to extrapolation.

The work in Chapter 7 set the foundation for answering this question by developing a hydrogel that has a more uniform network. It is hypothesized that a more uniform network will produce a screening effect and lead to a reduction in the diffusion coefficient at lower polymer volume fractions when compared to hydrogels with more heterogeneous networks. For example, a 10% PHA hydrogel would be expected to have more of a screening effect when compared with a 10% methacrylated HA hydrogel or a 10% hydrogel synthesized using the crosslinker DVS. Despite evidence of a more uniform network structure, the results in Chapter 7 revealed that

diffusion of BSA in PHA hydrogels with a swelling degree of 10.6 were not significantly different than the predictions based on the free volume theory presented in Chapter 5. However, it may be that the swelling degree was too high to notice any impacts the network structure might have had on the diffusion coefficient, and any possible deviations from the predictions may only occur at lower swelling degrees or with larger solutes.

Future work that focused on the diffusion of large solutes such as IgG or BSA in PHA, MHA, and HA-DVS hydrogels of similar swelling degree would provide greater insight into the role that the network structure plays on the diffusion coefficient and would be helpful in determining whether or not the screening effect is real. If it can be shown that the diffusion in PHA hydrogels is significantly slower than that of MHA and HA-DVS hydrogels it would impact the way we think about diffusion. Most of the diffusion models focus mainly on the swelling degree and solute size to predict the diffusion coefficient. While many of the models include parameters that try to take into account differences in network structure, they all vary in how the diffusion is predicted at very low diffusion coefficient values. The results would provide actual evidence that the crosslinking method and network structure need to be considered when determining the diffusion of a solute within a gel and would also provide the much needed data needed to evaluate the accuracy of the models. If the results showed significantly different diffusion coefficients at similar swelling degrees, it would also have an immediate impact on drug delivery applications. A specific example is the need for extended release from an ocular delivery system that has been the focus of chapters 5 and 6 in this dissertation. The screening effect and dramatic decrease in the diffusion coefficient can be used as an advantage, giving the desired release rate and profile at higher swelling degrees. This would require less polymer

modification and could lead to increased biocompatibility and a reduction in interactions between the crosslinker and the diffusing solute.

While the results would have a significant impact, the research in this dissertation highlights some of the reasons why there are very few studies with hydrogels that display these screening effects: the experiments are very long and present many challenges. These challenges include the inability to produce hydrogels with a polymer volume fraction that is high enough to observe the screening effect, and the difficulty in actually measuring the diffusion coefficients at such low values in hydrogels due to concentrations that are often below the detection limit[2] or take too long to build up to the detection limit within the time period studied. A successful experiment would have to overcome both of these challenges. A PHA hydrogel would have to be made with a low enough swelling degree (which correlates with a smaller average mesh size) in order to observe any hypothesized screening effect. If that can be achieved and MHA and HA-DVS hydrogels can be made with similar swelling degrees, the diffusion coefficient also has to be accurately measured. While there are some issues that would need to be resolved, an experiment using fluorescently labeled proteins measured with confocal microscopy is still a promising option. Despite the limited amount of results presented in Chapter 5, a large amount of work and effort went in to developing the confocal microscopy methods needed to measure diffusion coefficients. The time and energy spent establishing the procedures and protocols will help speed up future progress and will help provide more immediate returns.

While the results of this study rely heavily on the assumption that the PHA hydrogels do in fact have a highly uniform network structure, there are alternative hydrogels that could be used to test the overall theory. While the synthesis method is different (polymerization of monomers vs. crosslinking of polymers) there are a number of PEG based hydrogels that have

been synthesized using thiol-ene chemistry which have been shown to have very well defined network structures and would be an excellent substitute to PHA[3-6]. Additionally, PEG hydrogels are cheap, readily available, and easy to work with and would provide an alternative to the costly HA.

2. Synthesizing HA hydrogels via the thiol-yne reaction

Chapter 7 showed the many advantages the thiol-ene reaction offers when used to make HA hydrogels. If there is one downside to radical initiated thiol-ene reactions it is that the gels are more limited in terms of crosslink density when compared to some of the more common HA polymerization methods, especially the crosslinking of unmodified HA directly using bifunctional crosslinkers such as divinyl sulfone or bisepoxides. The difficulty is that the crosslink densities of a thiol-ene gel are ultimately determined by the degree of substitution. In Chapter 7, the degree of substitution of HA with ene groups plateaued at around 60%, and further attempts to add more functional groups were unsuccessful due to the inaccessibility of the remaining hydroxyl groups. One possible way around this is to replace the "ene" groups with "yne" groups, changing the reaction to a thiol-yne reaction.[7,8]

Thiol-yne reactions have been around since the middle of the 1900's, [9-11] yet it wasn't until the last couple of years that researchers have started to use the reaction to create and modify polymer networks [7,12,13]. The reaction is shown in Figure 8.1 and proceeds similarly to a thiol-ene reaction. First a thiyl radical reacts with the alkyne to produce a carbon-centered radical. This carbon-centered radical then abstracts a hydrogen from a nearby thiol, forming a vinyl sulfide and generating another thiyl radical. This vinyl sulfide is then capable of reacting with another thiyl radical, eventually forming a dithioether. The benefit of this reaction is that each yne moiety can

react with two thiols, increasing the functionality and therefore the amount of crosslinks that can theoretically occur.

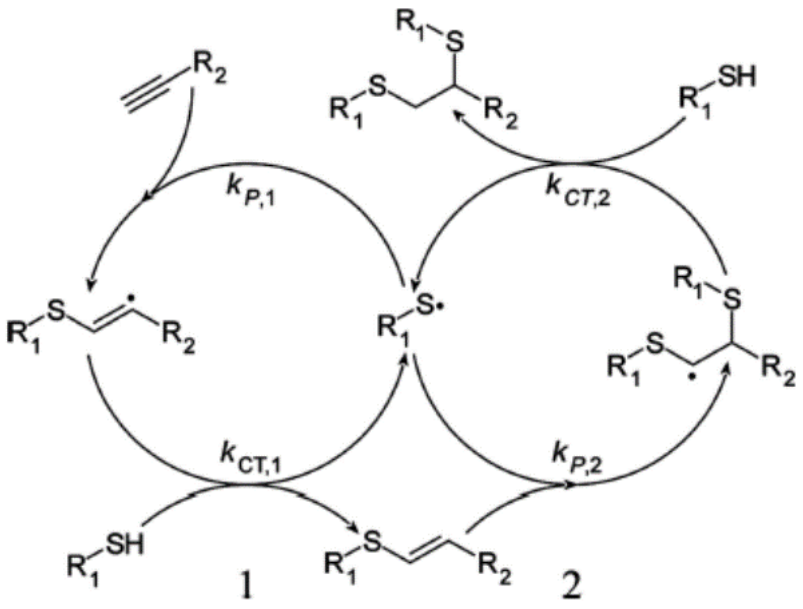

Figure 8.1 The mechanism of the thiol-yne reaction. Reproduced from Fairbanks et al.[7]

To the best of our knowledge, the use of the thiol-yne reaction to crosslink HA would demonstrate for the first time the use of radical thiol-yne chemistry to form hydrogels from disaccharides. In fact, the only other instance in literature on hydrogels and thiol-yne chemistry is when poly-(diethylacrylamide) was modified with alkynes and reacted with a multithiol to form thermoresponsive hydrogels[8]. The alkyne group can be attached to HA using the same esterification chemistry described in Chapter 7 except propiolic anhydride is used instead of pentenoic anhydride, virtually the same molecule except instead of an alkene group it contains an alkyne group. If for some reason the esterification reaction does not work, an alternative method

developed by Crescenzi et al. can be used in which an amine group is reacted with the carboxyl group.[14]

When added to the HA backbone, the additional functionality of the alkyne will provide a number of advantages not only in increasing the crosslink density, but also for postmodification. Since two thiols are able to react with each yne group, it is possible to form an HA hydrogel with double the amount of crosslinks when compared to an HA gel that has been functionalized with the same amount of ene groups. However, this does assume that the addition of a second thiol group would produce an effective crosslink. As Figure 8.2 shows, it is very possible that the second thiol would react with the same yne group that the first thiol group did, forming essentially one large crosslink that would not significantly affect the mechanical properties or the diffusion of solutes within the hydrogel.

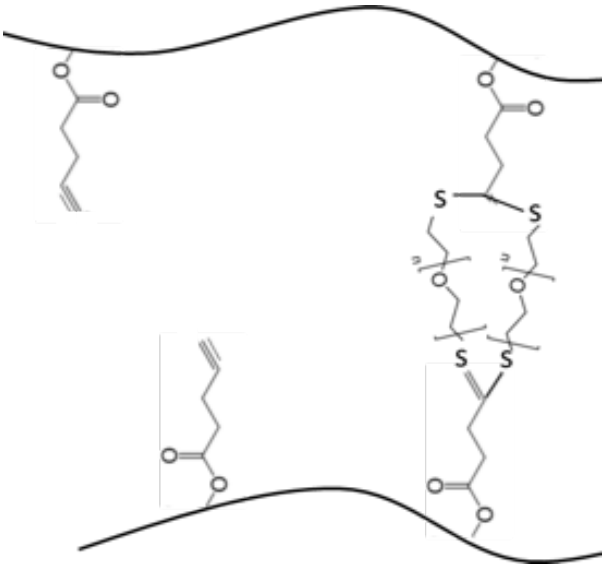

Figure 8.1 The addition of two dithiol groups to the same yne groups would not significantly affect the mechanical properties or the diffusion of solutes within the hydrogel when compared to the thiol-ene gels produced in Chapter 7.

This would have to be tested, and could be further influenced by the molecular weight of the dithiol crosslinker. For example, a larger dithiol such as a PEG-dithiol could be used initially to form the hydrogel using a 1:1 thiol:yne ratio, which would form a hydrogel while at the same time leaving ene groups on the backbone. Then, the hydrogel could be soaked in a solution containing a smaller dithiol, such as DTT and reacted again. This would reduce the probability of two dithiols reacting with the same yne groups.

The other added benefit is that unreacted ene groups can undergo secondary modifications, which can be used to introduce chemical groups other than crosslinkers. These modifications can be performed with any chemical that has a terminal thiol, making it useful for a wide variety of applications from tissue engineering to drug delivery. Burdick and his group have demonstrated this use of secondary modification and photopatterning using the norbornene modified HA described earlier.[15] However, they use a thiol-ene gel, and in order to perform secondary reactions they had to leave unreacted vinyl groups attached to HA which reduced the compressive modulus of the gel relative to a fully crosslinked hydrogel. By using thol-yne chemistry, highly crosslinked gels can be obtained while still leaving functional groups available to perform secondary reactions.

REFERENCES

1. Gehrke SH, Uhden LH, McBride JF 1998. Enhanced loading and activity retention of bioactive proteins in hydrogel delivery systems. Journal of controlled release 55(1):21-33.

2. Cruise GM, Scharp DS, Hubbell JA 1998. Characterization of permeability and network structure of interfacially photopolymerized poly (ethylene glycol) diacrylate hydrogels. Biomaterials 19(14):1287-1294.

3. Malkoch M, Vestberg R, Gupta N, Mespouille L, Dubois P, Mason AF, Hedrick JL, Liao Q, Frank CW, Kingsbury K 2006. Synthesis of well-defined hydrogel networks using click chemistry. Chemical Communications (26):2774-2776.

4. Fairbanks BD, Schwartz MP, Halevi AE, Nuttelman CR, Bowman CN, Anseth KS 2009. A Versatile Synthetic Extracellular Matrix Mimic via Thiol‐Norbornene Photopolymerization. Advanced Materials 21(48):5005-5010.

5. Anderson SB, Lin C-C, Kuntzler DV, Anseth KS 2011. The performance of human mesenchymal stem cells encapsulated in cell-degradable polymer-peptide hydrogels. Biomaterials 32(14):3564-3574.

6. Cui J, Lackey MA, Madkour AE, Saffer EM, Griffin DM, Bhatia SR, Crosby AJ, Tew GN 2012. Synthetically simple, highly resilient hydrogels. Biomacromolecules 13(3):584-588.

7. Fairbanks BD, Scott TF, Kloxin CJ, Anseth KS, Bowman CN 2009. Thiol-Yne Photopolymerizations: Novel Mechanism, Kinetics, and Step-Growth Formation of Highly Cross-Linked Networks. Macromolecules 42(1):211-217.

8. Lowe AB, Hoyle CE, Bowman CN 2010. Thiol-yne click chemistry: A powerful and versatile methodology for materials synthesis. Journal of Materials Chemistry 20(23):4745.

9. Behringer H 1949. *ZUR KENNTNIS DER THIOSAUREN .1. UBER DIE ANLAGERUNG VON THIOSAUREN AN ACETYLEN-ABKOMMLINGE UND DIOLEFINE. Annalen Der Chemie-Justus Liebig 564(3):219-234.

10. Blomquist AT, Wolinsky J 1958. ADDITION OF ETHYL MERCAPTAN TO ACETYLENIC COMPOUNDS. Journal of Organic Chemistry 23(4):551-554.

11. Griesbau.K 1970. PROBLEMS AND POSSIBILITIES OF FREE-RADICAL ADDITION OF THIOLS TO UNSATURATED COMPOUNDS. Angewandte Chemie-International Edition 9(4):273-&.

12. Chan JW, Hoyle CE, Lowe AB 2009. Sequential Phosphine-Catalyzed, Nucleophilic Thiol-Ene/Radical-Mediated Thiol-Yne Reactions and the Facile Orthogonal Synthesis of Polyfunctional Materials. Journal of the American Chemical Society 131(16):5751-+.

13. Chan JW, Zhou H, Hoyle CE, Lowe AB 2009. Photopolymerization of Thiol-Alkynes: Polysulfide Networks. Chemistry of Materials 21(8):1579-1585.

14. Crescenzi V, Cornelio L, Di Meo C, Nardecchia S, Lamanna R 2007. Novel hydrogels via click chemistry: Synthesis and potential biomedical applications. Biomacromolecules 8(6):1844-1850.

15. Gramlich WM, Kim IL, Burdick JA 2013. Synthesis and orthogonal photopatterning of hyaluronic acid hydrogels with thiol-norbornene chemistry. Biomaterials 34(38):9803-9811.

Appendix For Chapter 5

A5.1 HA-DVS Hollow Cylinder Dimensions

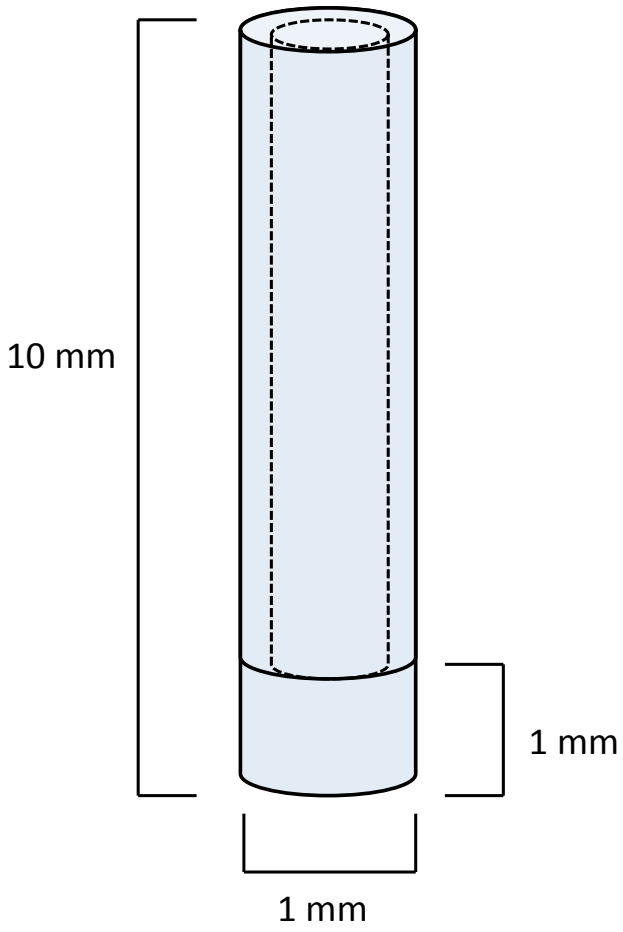

The inner diameter can be varied to control the inner volume as well as the wall thickness

We currently have molds with an inner diameter of :
0.460 mm = Wall thickness of 0.27 mm
0.635 mm = Wall thickness of 0.183 mm

Inner Diameter of .460 mm = .00150 mL volume
Inner Diameter of .635 mm = .00285 mL volume

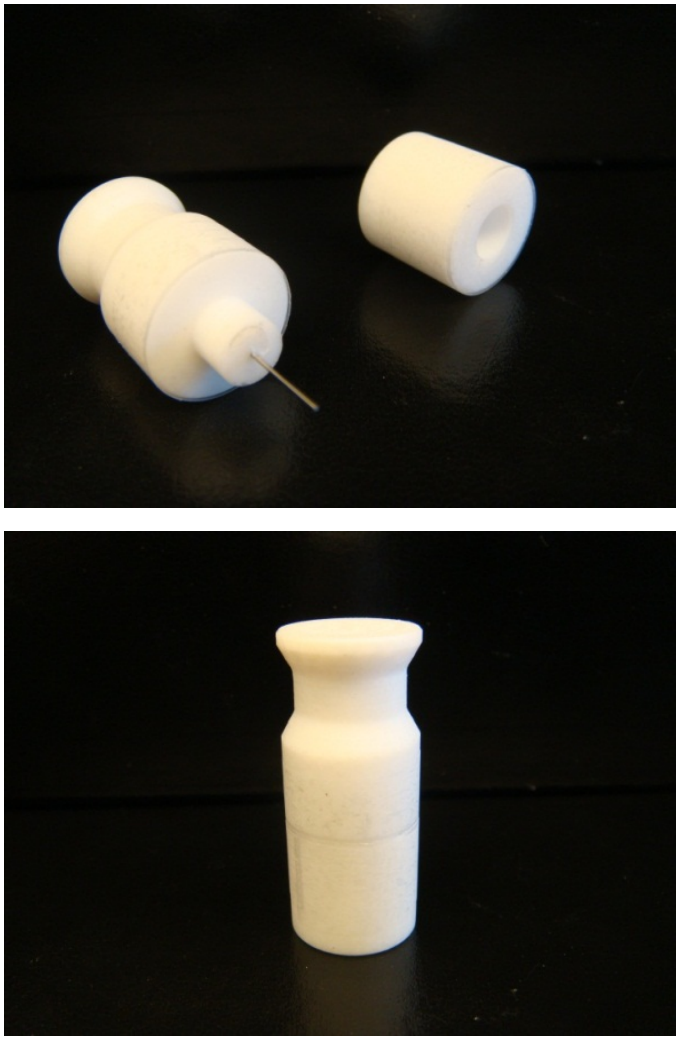

Hollow Cylinder Molds

A5.2 HA-DVS Hollow Cylinder Pictures

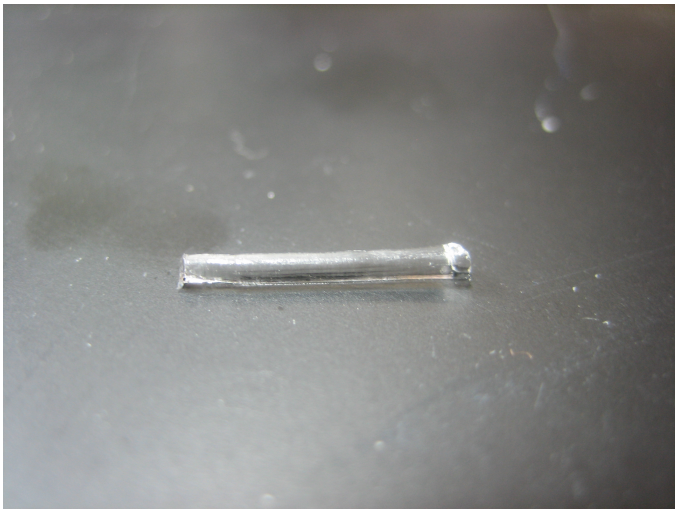

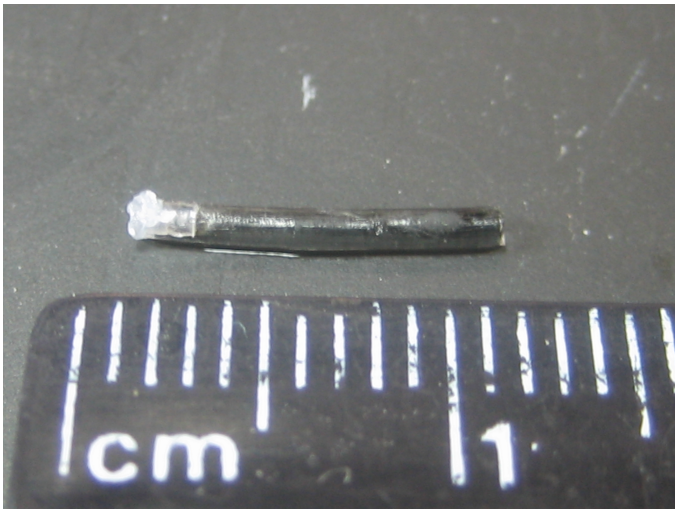

A5.3 HA-DVS Sulfur Content

Reaction:

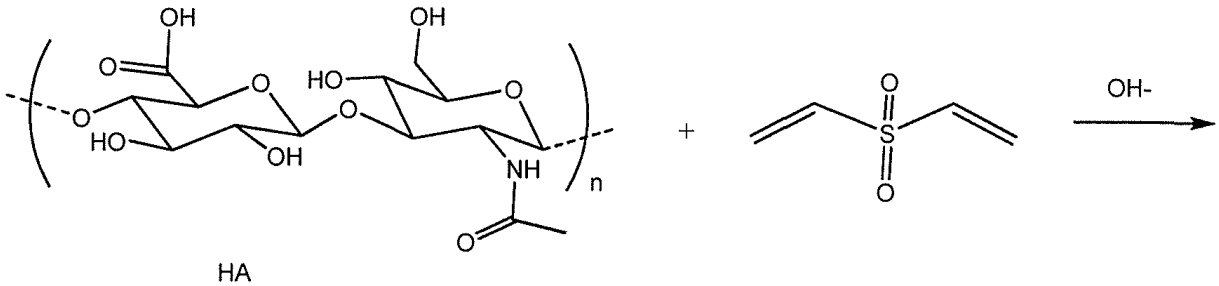

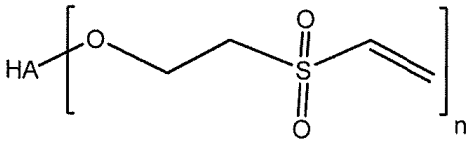

Weight Percentages:

Hyaluronic Acid (MW = 379.32) : $C_{14}H_{20}O_{11}N_1$
Carbon = 44.3%
Hydrogen = 5.6%
Oxygen = 46.4%
Nitrogen = 3.7%

Divinyl Sulfone (MW = 118.15) $C_4H_6O_2S_1$
Carbon = 40.7%
Hydrogen = 5.1%
Oxygen = 27.1%
Sulfur = 27.1%

# of DVS on HA Repeating Unit	Carbon	Hydrogen	Oxygen	Nitrogen	Sulfur	Total Weight
0	14	21	11	1	0	379.318
1	18	27	13	1	1	497.473
2	22	33	15	1	2	615.628
3	26	39	17	1	3	733.783
4	30	45	19	1	4	851.938
5	34	51	21	1	5	970.093
1.5	**20**	**36**	**14**	**1**	**1.5**	**562.5985**

# of DVS on HA Repeating Unit	Carbon	Hydrogen	Oxygen	Nitrogen	Sulfur	Ratio S/N
0	44.3%	5.6%	46.4%	3.69%	0.00%	0.00
1	43.5%	5.5%	41.8%	2.82%	6.45%	2.29
2	42.9%	5.4%	39.0%	2.28%	10.42%	4.58
3	42.6%	5.4%	37.1%	1.91%	13.11%	6.87
4	42.3%	5.3%	35.7%	1.64%	15.06%	9.16
5	42.1%	5.3%	34.6%	1.44%	16.53%	11.45
1.5	42.7%	6.5%	39.8%	2.49%	8.55%	**3.43**

Hydrogel Synthesis and Characterization:

30% HA-DVS 1:1 Ratio = 3.2 Molecules of DVS for every repeat unit of HA
30% HA-DVS 2:1 Ratio = 1.6 Molecules of DVS for every repeat unit of HA
30% HA-DVS 3:1 Ratio = 1.07 Molecules of DVS for every repeat unit of HA

HA	Swelling Degree Q	Shear Modulus G	Crosslink Density ρ_x	M_c	Mesh Size ξ
15% HA 3:1	6.6	681.4	0.001852	647.9	7.36
15% HA 2:1	5.86	758.7	0.001982	605.42	6.84
15% HA 1:1	4.54	841.2	0.002018	594.53	6.23
30% HA 3:1	3.55	2367.2	0.003296	364.03	4.49
30% HA 2:1	2.73	3710.9	0.004734	253.46	3.43
30% HA 1:1	2.87	3054.9	0.003963	302.8	3.81

Sample ID	% Carbon	% Hydrogen	% Oxygen	% Nitrogen	% Sulfur	Ratio S/N	# of DVS on HA Repeating Unit	Reaction Efficiency
30% HA-DVS 1:1	38.98	5.65	45.04	2.33	8.0	3.43	1.5	47%
30% HA-DVS 2:1	39.08	5.9	44.36	2.46	8.2	3.33	1.45	91%
30% HA-DVS 3:1	39.1	5.98	45.87	2.49	6.56	2.63	1.15	107%
15%HA-DVS 1:1	39.73	5.16	42.78	2.29	10.04	4.38	1.91	60%
15%HA-DVS 2:1	39.21	5.79	45.17	2.49	7.34	2.95	1.29	81%
15%HA-DVS 3:1	39.29	5.59	46.77	2.78	5.57	2.00	0.87	81%

A5.4 HA-DVS Ethylene Glycol Capping

*****Special thanks to Dr. Berkland and Jian Kian for their help in producing these figures*****

Protein diffusing through the hydrogel network would be able to react with any DVS groups that had only singly-reacted with HA:

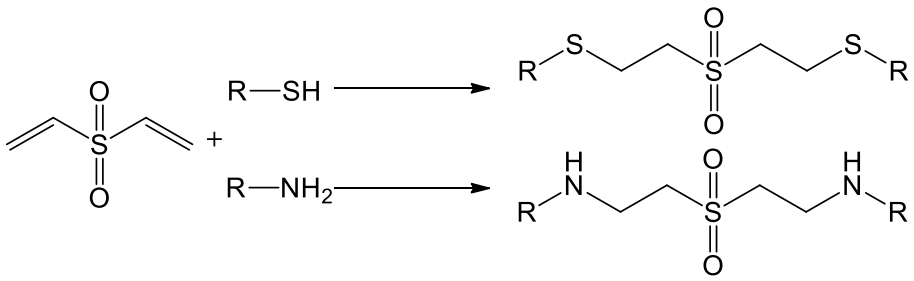

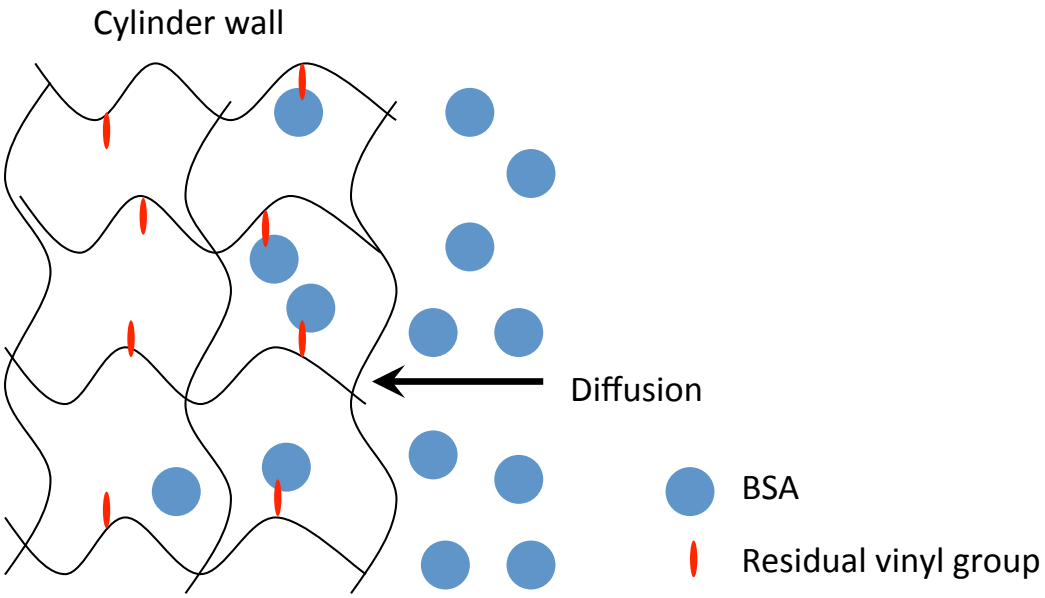

A simple calculation (HA:DVS 3:1):

The feed amount of DVS in a cylinder gel:
~2.2 umol
Total Protein loaded:
~450 mg, 0.0068 umol

Theoretically, only 0.3% residual vinyl groups could react with all the proteins.

Coomassie staining indicated that Fab appears to be binding with cylinder wall:

Cylinder
Fab loaded into 15% HA 1:1 Cylinder
(32 Days)

15% HA 1:1 Cylinder
No Protein loaded

SDS-PAGE indicates no protein aggregation in cylinders up to 64 days; Fab missing after 32 days:
BSA Controls = Fresh 0.5 mg/ml solution + 0.5 mg/ml solution that has been stored in fridge for 64 days

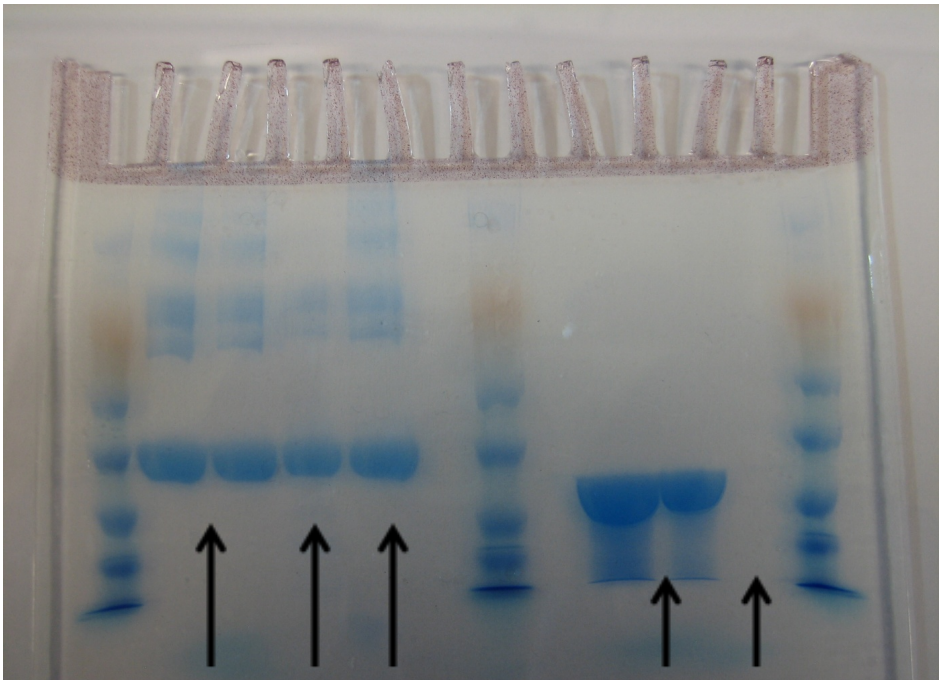

BSA Controls | **Cylinder D (64 Days)** | **Cylinder G (46 Days)** | **mAb Controls** | **Cylinder mC (32 Days)**

Cylinder D = BSA from 30% HA 3:1 (64 days in cylinder)
Cylinder G = BSA from 15% HA 1:1 (46 days in cylinder)
mAb controls = Fresh 0.5 mg/ml solution + 0.5 mg/mL solution that was stored in fridge for 32 days
Cylinder mC = mAb from 15% HA 1:1 (32 days in cylinder)

In order to eliminate any unwanted side reactions that might occur between the DVS and the proteins diffusion through the hydrogel network, the cylinders were treated with ethylene glycol to eliminate any residual vinyl groups:

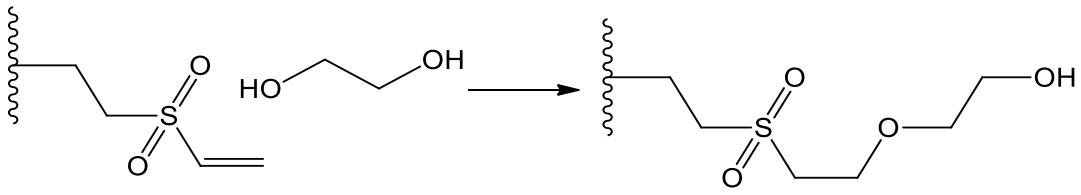

This did not significantly affect the swelling degree of the hydrogels:

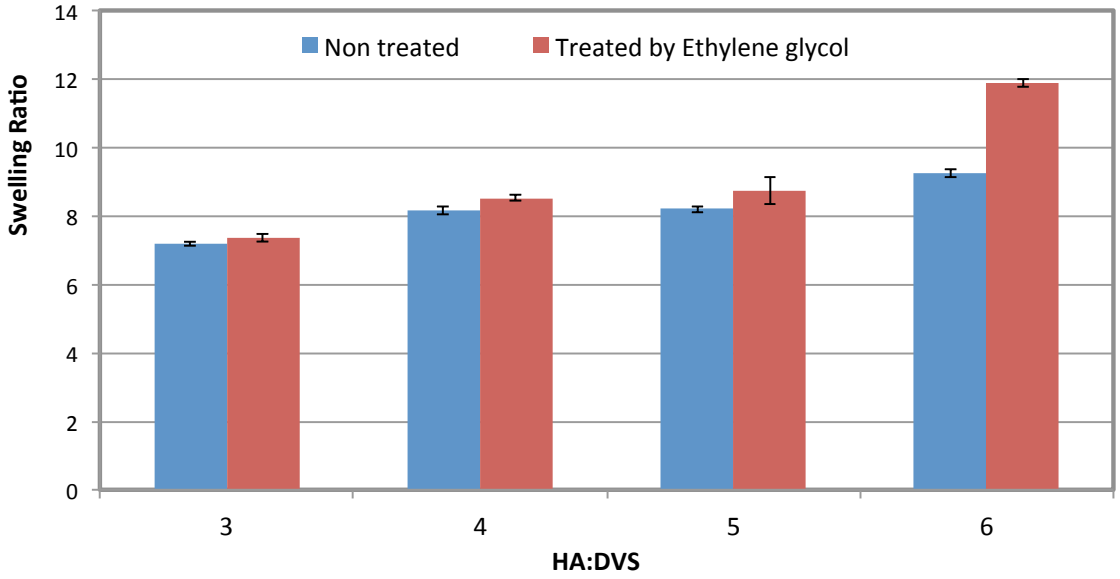

APPENDIX FOR CHAPTER 7

A7.1 Pentenoate Modified Hyaluronic Acid (PHA) Synthesis

Purpose: To make a pentenoate modified HA that can be used to make gels via thiol-ene click chemistry. The synthesis is relatively simple, and the most difficult part is the precipitation/purification step. Each batch takes about 2-3 days to make, however the total work time required is about 4-6 hours. The batch size has been successfully increased from 0.3 g to 0.5 g to 1.0 g. The degree of substitution (DOS) of PHA can range from about 6% to 60% depending on the ratio of pentenoic anhydride to HA during synthesis. The DOS is calculated by spectral integration of the 1H NMR (accuracy ~10%) and is defined as the amount of ene groups per repeat unit.

Materials Needed:

- Hyaluronic Acid (51 kDa)
- DIUF Water
- Pentenoic Anhydride
- 0.5M or 1.0M NaOH
- DMF
- NaCl
- Dialysis Tubing (10k MWCO)

Procedure:

1.) HA (0.50 g, 0.75 mmol) is dissolved in ultrapure water (25 mL) at 4C, and the resulting mixture is kept at 4C under continuous stirring overnight for complete dissolution. Can be scaled up. Ratio = 5 mL of water for every 0.1 g of HA.

2.) DMF (16.66 mL) is then added dropwise in order to have a water/DMF ratio of 3/2 (v/v).

3.) Pentenoic anhydride (1.2g) is added (= 5 molar equivalents with respect to the repeating unit of HA) while maintaining the pH between 8 and 9 (by adding 0.5M or 1.0 M NaOH) for 3-6 h. Reaction is carried out in the fume hood and hooked up to a pH meter to read continuously at room temperature. At first, NaOH is added about every 5 minutes, but by the end of the reaction it slows down to every 20-30 minutes. The pentenoic anhydride will look like small brown immiscible droplets, and they should slowly disappear as the reaction proceeds.

4.) When the pH stabilizes, the reaction is kept at 4C overnight under continuous stirring to ensure complete reaction.

5.) After this time, NaCl isadded to the reaction mixture to have a NaCl concentration of 0.5M

6.) The polymer is precipitated by addition of cold ethanol (with a water/EtOH (v/v) ratio of at least 1/5).

7.) The solution is then centrifuged and the supernatant is removed, the precipitate is redissolved in ultrapure water for a final purification by diafiltration with ultrapure water (10k MWCO). Diafiltration lasts for 48 hours, changing the water every 8-12 hours.

8.) The purified product is recovered by freeze-drying and characterized by 1H NMR spectroscopy.

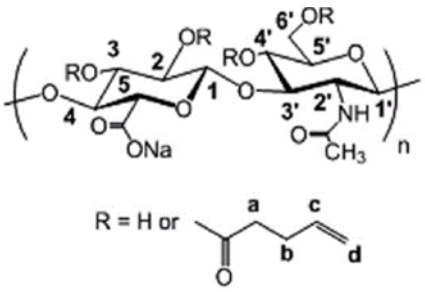

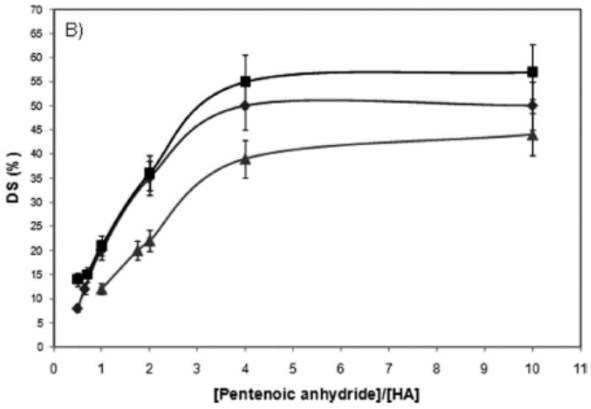

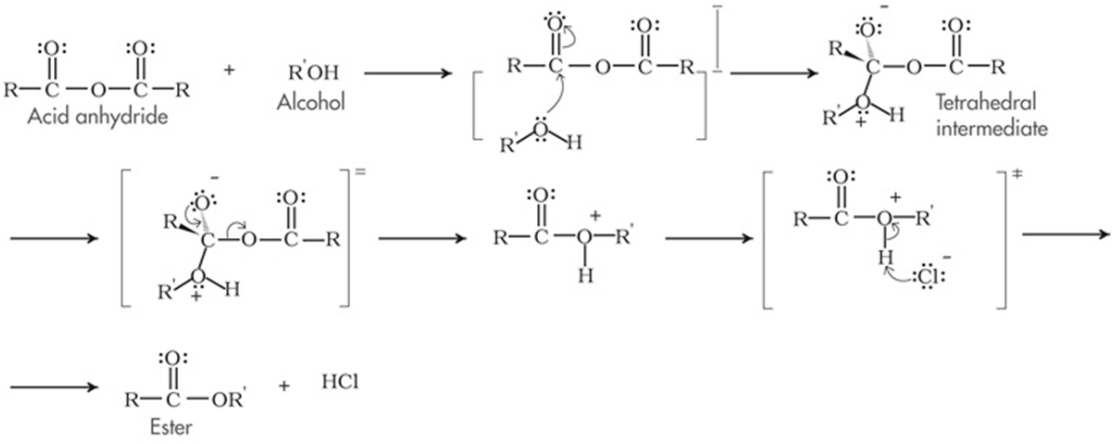

A7.2 Pentenoate Modified Hyaluronic Acid (PHA) Hydrogel Synthesis

Purpose: To synthesize PHA hydrogels

Materials Needed:

- Pentenoate modified Hyaluronic Acid (PHA)
- DIUF Water
- Dithiothreitol (DTT)
- Irgacure 2959
- Gel Molds

Procedure:

1.) A solution of 0.1 mmol Irgacure 2959 is made. This is a very low initiator concentration, so it is best to make in large quantities. Due to the sensitivity of the reaction to free radicals, a fresh Irgacure 2959 solution should be made with each batch of PHA gels.

2.) In one vial, the amount of PHA needed for hydrogel synthesis is measured out. PHA hydrogels have been made with the concentration of PHA ranging from 2-16%.

3.) In another vial, the amount of crosslinker needed is measure out. While the majority of the PHA hydrogels in this dissertation were crosslinked with DDT, the advantage of the thiol-ene chemistry is that any soluble difunctional thiol will work as a crosslinker.
The key here is how many thiol groups are added relative to the amoung of ene groups that are functionalized on the HA. Depending on the application, the ratio of thiol groups to ene groups (X_{DTT}) can be varied. In most cases, the hydrogels are synthesized with a 1:1 ratio.

4.) Then amount of Irgacure solution needed to make your gels (2% to 16% PHA) is then calculated. This solution is then pipetted into the vial with the crosslinker and stirred to make sure it is fully dissolved. This solution is then pipetted into the vial that contains the PHA.

5.) The final solution is stirred thoroughly, centrifuged to remove any bubbles (40-60s), and pipetted into molds.

6.) The molds are then irradiated at 312 nm. The time required for complete hydrogel formation is dependent on the concentration of PHA.

7.) After 5-10 minutes the hydrogels are removed from the molds and placed into an excess of D.I. water to remove any unreacted materials.

A7.3 Irgacure 2959 vs. Lithium Acylphospinate

Irgacure 2959:

- The most commonly used Type 1 photoinitiator (cleavage type)
- Among the most water soluble of the commercially available Type 1 photoinitators
  - Solubility limit in water at ambient conditions is less than 2%
  - However, even 0.5 % (w/w) solutions require substantial agitation/heating to dissolve
- The bigger drawback is the low molar extinction coefficient at 365 nm. (4 M^{-1} cm^{-1})
  - Above 370 nm the extinction coefficient is effectively zero (see next page)

LAP:

- Water solubility is much better (up to 8.5 wt%)
- Molar extinction coefficient at 365 is substantially higher (218 M^{-1} cm^{-1})
- Major benefit comes from the fact that when the LAP is photoinitiated and cleaved, there is a significant reduction in light absorption

-Can play a significant role in cases where the gel is not optically thin. As initiator on the surface is consumed, the light is able to reach greater depths and increase the cure depths that can be achieved.

Impact on our Thiol-Ene Research:

- If we were initiating at 365 nm it would have a huge impact, but as the graphs on the next page show, both LAP and I2959 have very high extinction coefficients at 312 nm. Since the rate of initiation is:

$$R_i = \frac{2\phi\varepsilon f I C_i}{N_A h\upsilon}$$

if we use I2959 vs LAP at 312, both H,v, Na, f, ϕ and I will all be roughly the same. The only difference could be ε (which we already said was high for both at 312) and the concentration.
Also, at 312 nm we have to worry about light attenuation since both LAP and I2959 absorb a ton of light at 312 nm even after initiation.

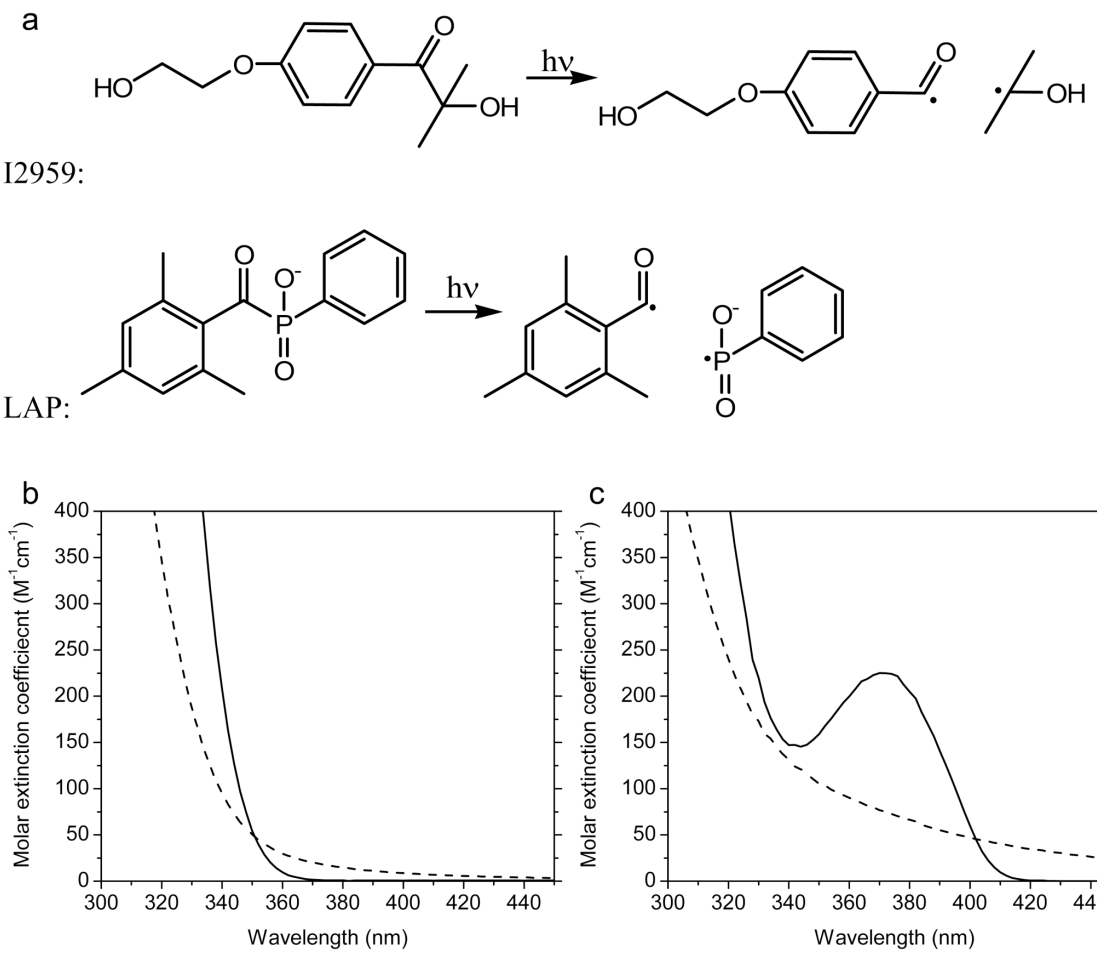

(a) Cleavage of I2959 and LAP into substituent radicals following photon absorption. (b) Molar absorptivities of the I2959 (solid line)and cleavage products (dashed line). (c) Molar absorptivities of LAP (solid line) and cleavage products (dashed line).

Cost to Produce LAP:

- Dimethyl phenylphosphonite (5g - $60)
- 2,4,6-trimethylbenzoyl chloride (5g - $205)
- lithium bromide (100 g - $53)
- 2-butanone (500 mL - $48)

TOTAL = $366 to produce roughly 2 x 5g. Which given how little we need to use (0.03 wt% to .3 wt%) would probably last for quite some time.

Initial reaction is under argon = Glove box

A7.4 Pentenoate Modified Hyaluronic Acid (PHA) Mechanical Testing and Mooney Rivlin

6% PHA Hydrogels – Thiol:Ene Ratio =1.0

Summary of 6% PHA 1.0 (last data preceding break, E, G, and E/G)

	Stress(kPa)	Strain(%)	Strain Fcn	E	G	E/G
	280.7	41.9	2.4	349.2	121.4	2.9
	296.5	41.2	2.3	399.7	135.8	2.9
	229.7	41.0	2.3	292.6	107.1	2.7
Average	269.0	41.36	2.322	347.2	121.5	2.9
StDev	34.9	0.5	47.8	53.6	14.4	0.1

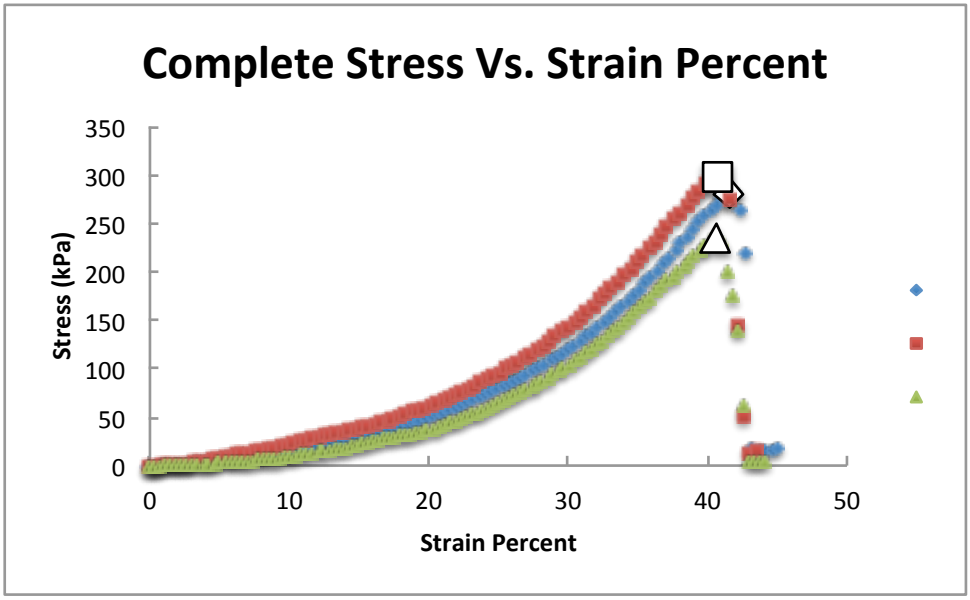

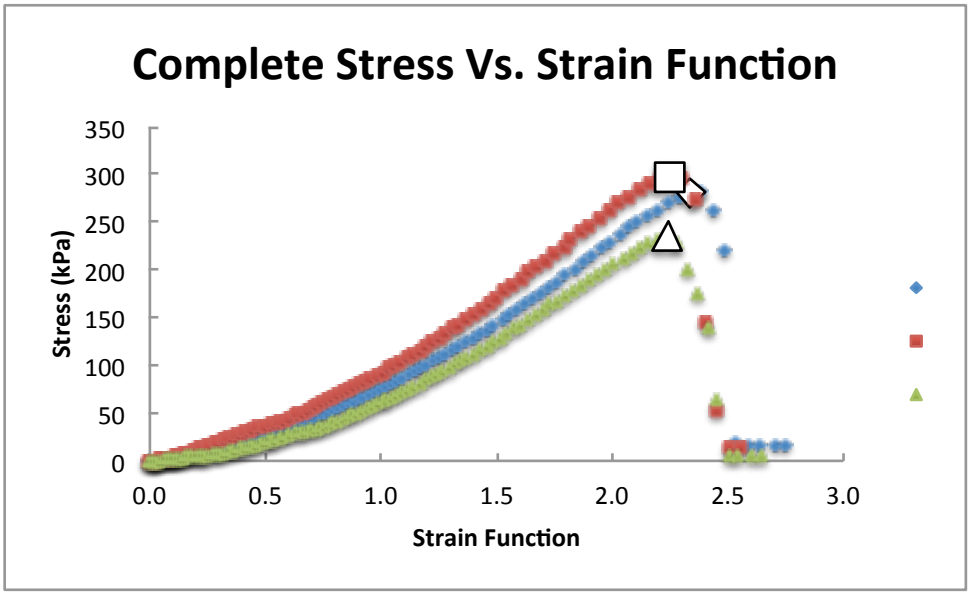

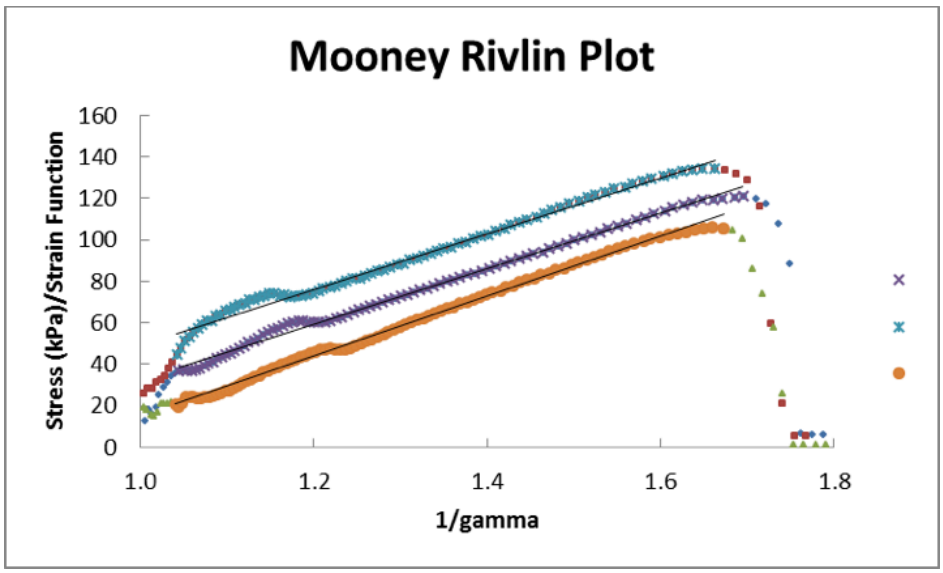

Summary of 6% PHA 1.0 Mooney Rivlin Data(between specified data points)

~[f*]=2C1+2C2*(1/lambda)

	Intercept (G)	Slope	C1	C2	R-Squared	Best Fit Start (x-value)	Best Fit End (x-value)
	-100.6	133.370	-50.3	66.7	0.995	1.044	1.695
	-85.3	134.668	-42.7	67.3	0.989	1.042	1.663
	-129.5	144.500	-64.8	72.2	0.996	1.040	1.673
Average	-105.1	137.51258	-52.57025	68.8			
StDev	22.4	6.1	11.2	3.0			

13% PHA Hydrogels – Thiol:Ene Ratio =1.0

Summary of 13% PHA X_{DTT}=1- In Water (last data preceding break, E, G, and E/G)

	Stress(kPa)	Strain(%)	Strain Fcn	E	G	E/G
	450.0	29.5	1.3	1017.2	355.1	2.9
	516.4	29.6	1.3	1165.0	432.2	2.7
	473.9	28.4	1.2	1033.1	384.9	2.7
	653.5	32.8	1.5	1147.3	445.2	2.6
Average	523.4	30.1	1.4	1090.6	404.3	2.7
StDev	90.9	1.9	33.2	76.3	41.8	0.1

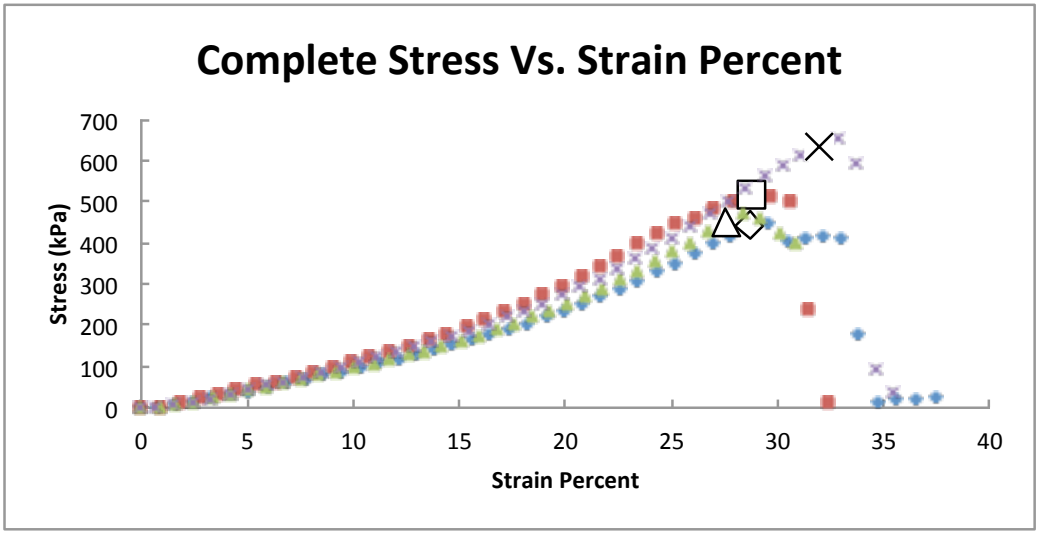

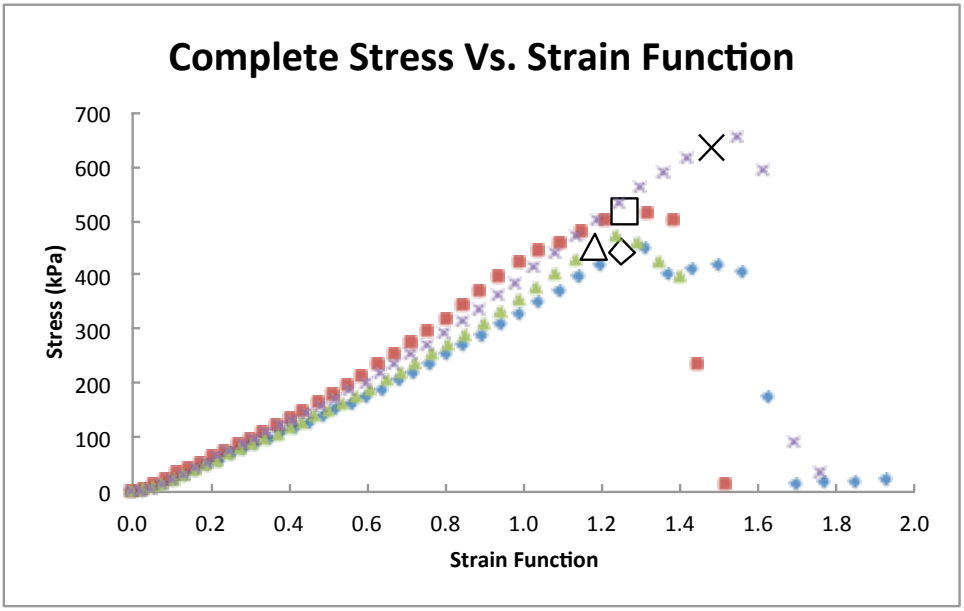

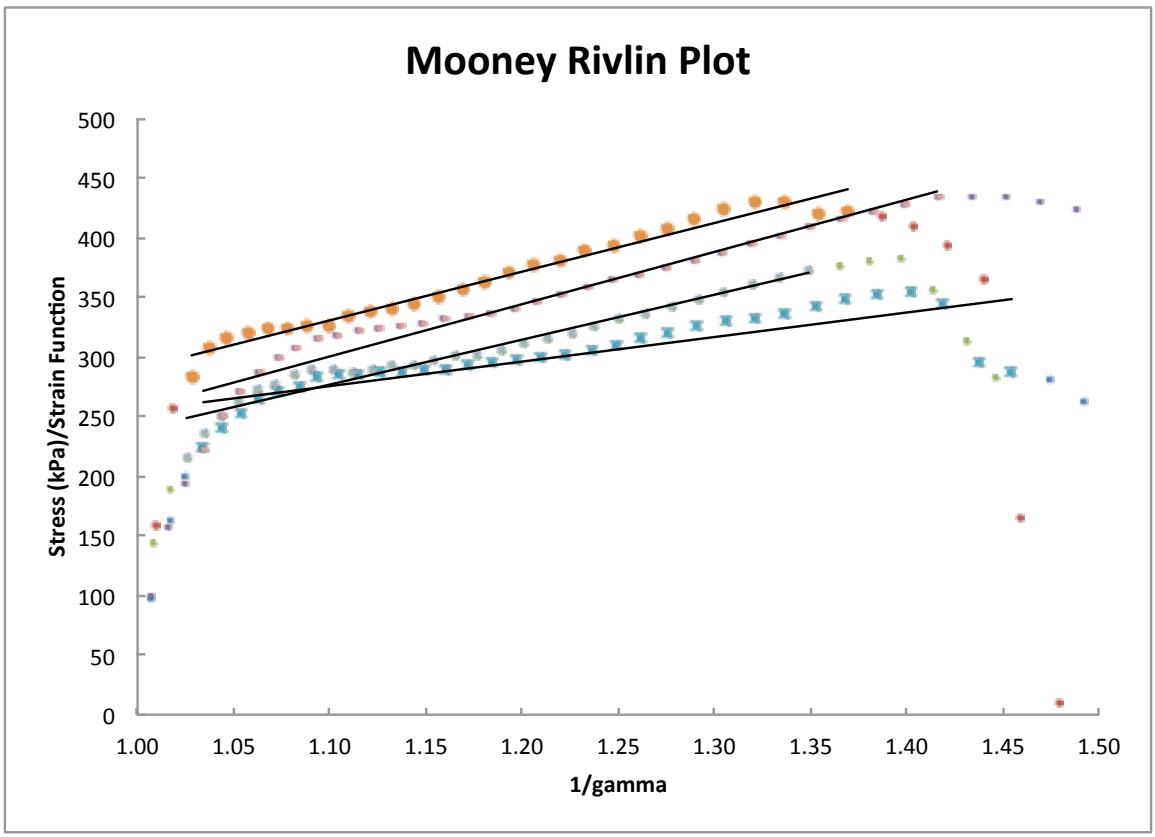

Summary of 13% PHA In Water Mooney Rivlin Data(between specified data points)
~[f*]=2C1+2C2*(1/lambda)

	Intercept (G)	Slope	C1	C2	R-Squared	Best Fit Start (x-value)	Fit End (x-value)
	49.2	205.74	24.6	102.9	0.673	1.034	1.454
	-118.3	408.15	-59.1	204.1	0.971	1.028	1.369
	-137.7	376.82	-68.9	188.4	0.942	1.025	1.349
	-181.7	438.28	-90.8	219.1	0.943	1.034	1.416
Average	-97.12	357.25	-48.56	178.6			
StDev	101.1	104.1	50.5	52.0			

A7.5 PHA Hydrogels in Various Salt Solutions

NaCl Concentration	Q	Compressive Modulus (kPa)	Fracture Stress (kPa)	Fracture Strain (%)
0	13.9 ± 0.5	1090.6 ± 76.3	523.4 ± 90.9	30.1 ± 1.9
0.1	12.08 ± 1.3	627.7 ± 61.5	769.4 ± 187	44.5 ± 3.5
0.3	9.01 ± 0.6	523.5 ± 135	592 ± 85.7	44.9 ± 1.2
1	7.41 ± 0.5	316.9 ± 41.7	544.8 ± 90.7	49.1 ± 2.6
1.5	6.17 ± 0.4	467 ± 50.2	1049.6 ± 211.8	53.2 ± 3.3
3	4.32 ± 0.2	434.5 ± 56.0	960.4 ± 231.3	52.3 ± 3.2

CaCl Concentration	Q	Compressive Modulus (kPa)	Fracture Stress (kPa)	Fracture Strain (%)
0	13.9 ± 0.5	1090.6 ± 76.3	523.4 ± 90.9	30.1 ± 1.9
0.033	9.94 ± 1.45	545.1 ± 56.4	711.2 ± 78.9	47.5 ± 0.6
0.1	8.57 ± 0.83	506.1 ± 37.1	801.0 ± 104.8	48.6 ± 1.1
0.3	7.00 ± 0.55	284.8 ± 122.1	833.61 ± 377.4	56.3 ± 2.1
0.5	6.41 ± 0.17	206.2 ± 125.3	845.5 ± 347.3	59.7 ± 4.6
1	4.98 ± 0.22	104.9 ± 93.2	688.8 ± 46.6	64.3 ± 7.0

A7.6 Synthesizing PHA Hydrogels using EDTT instead of DTT

Hydrogels were orginally made using the crosslinker 2,2′-(Ethylenedioxy)diethanethiol (EDTT). This is a very cheap dithiol that is in liquid form and was used to make the Dextran gels in the Mergy/ Auzely Velty paper.

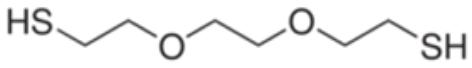

Figure A7.6.1. Structure of 2,2′-(Ethylenedioxy)diethanethiol (EDTT)

Early obersvations indicated that when adding the crosslinker the solution was always cloudy. After testing the solubility, it was found that EDTT was mostly immiscible in water, causing cloudiness in the solutions. However, we were still able to get hydrogels after irradiating for only 20 seconds (10s on both sides of the molds = 20 seconds total). From this point on the crosslinker used was dithiothreitol (DTT) which is very soluble. The swelling degrees of the hydrogels made with the two different crosslinkers were very similar.